MODELING ADSORPTION DATA OF HYDROCARBONS ON 13X ZEOLITE USING THE GAUSSIAN ADSORPTION ISOTHERM MODEL

by

Salam Mazen Taji

A Thesis Presented to the Faculty of the
American University of Sharjah
College of Engineering
in Partial Fulfillment
of the Requirements
for the Degree of

Master of Science in
Chemical Engineering

Sharjah, United Arab Emirates

January 2013

Approval Signatures

We, the undersigned, approve the Master's Thesis of Salam Mazen Taji.

Thesis Title: Modeling Adsorption data of Hydrocarbons on 13X zeolite using the Gaussian adsorption isotherm model.

Signature	**Date of Signature**
_____	_____
Dr. Kevin Francis Loughlin Professor, Department of Chemical Engineering Thesis Advisor	
_____	_____
Dr. Dana Abouelnasr Associate professor, California State University, Bakersfield Department of Chemical Engineering Thesis Co-Advisor	
_____	_____
Dr. Rachid Chebbi Professor, Department of Chemical Engineering Thesis Committee Member	
_____	_____
Dr. Fawwaz Jumean Professor, Department of Biology, Chemistry and Environment Thesis Committee Member	
_____	_____
Dr. Naif Darwish Head, Department of Chemical Engineering	
_____	_____
Dr. Hany El-Kadi Associate Dean, College of Engineering	
_____	_____
Dr. Yousef Al-Assaf Dean, College of Engineering	
_____	_____
Dr Khaled Assaleh Director of Graduate Studies	

Acknowledgements

In the name of Allah most Merciful, most Gracious.

I have been indebted in the preparation of this thesis to my advisors, Dr. Kevin Loughlin of the American University of Sharjah, and Dr. Dana Abouelnasr of California State University. Their patience and constant support, as well as their academic experience, have been invaluable to me. I am extremely grateful to my committee members, Dr. Fawwaz Jumean from the Department of Biology, Chemistry and Environment and Dr. Rachid Chebbi from the Chemical Engineering Department for their constructive criticism and their professional help that contributed significantly to the completion of this work. I must also acknowledge my laboratory instructor, Engineer Essam Al-Zubaidy for his time, technical support and the huge effort made by his side throughout my graduate years.

My parents Dr. Mazen Taji and Dr. Samar Gheibeh have always been my continuous source of inspiration and support of my intellectual aspirations. This thesis would not have existed without their emotional, moral and financial support. Special thanks to my friends and colleagues, Laura and Noha for making my years at graduate school unforgettable.

Abstract

Subcritical and supercritical adsorption data available in the literature for alkanes, alkenes and aromatics on 13X zeolite are correlated using the Gaussian adsorption model. This model is specified by three parameters: q_{max}, the saturation loading; P_{50}, adsorption pressure at 50% of the maximum loading; and σ, the standard deviation. A semi log plot of pressure vs. the inverse of the Gaussian cumulative distribution function produces a linear relation with a slope equal to the standard deviation of the isotherm and an intercept equal to the logarithm of the pressure at 50% of the maximum loading.

The model is applied to 138 alkane isotherms, 17alkene isotherms and 44 aromatic isotherms from the literature on 13X zeolite. The isotherms are collected from 17 different studies and fitted to the model using a pre-specified maximum saturation loading value for the supercritical isotherms and a calculated value using crystallographic zeolite data and the Rackett or modified Rackett equation for the subcritical isotherms. The mean standard deviation is found to be equal to 1 for reduced temperatures greater than 0.65 and greater than three for reduced temperatures less than 0.65.

Plots of the pressure at 50% of the maximum loading vs. the inverse of the temperature are constructed. The slopes of the generated lines are used to calculate the values of the heat of adsorption at 50% loading for each species. The values are either equal or less than the values published in literature at 0% loadings for isotherms with a sigma value of (0.5 to 1) and are remarkably higher for isotherms with a sigma value above 3. The Gaussian model is found to be a better fit for supercritical data than for subcritical data especially for reduced temperatures below 0.75 where some inconsistencies are encountered.

Keywords: Isotherm**,** Gaussian model**,** alkanes, alkenes, aromatics, 13X zeolite.

Table of Contents

List of Figures

List of Tables

Nomenclature

a	pre-exponential factor for isostere
a	amount adsorbed, mole/cc
b	affinity constant, kPa^{-1}
b_0	affinity constant at some reference temperature, kPa^{-1}
b_∞	affinity constant at infinite temperature, kPa^{-1}
c	free species concentration mole/cc of gas
C	constant in BET equation (Eq. 2.20)
C_μ	adsorbed concentration, mole/cc solid
$C_{\mu s}$	maximum adsorbed concentration, mole/cc solid
E_d	activation energy for desorption, joule/mole
j_g	the internal partition function of gas phase
j_s	internal and vibrational partition function
K, K′	Henry's law constant (Eq. 2.21)
K_0, K'_0	Henry's law constant at infinite temperature (Eq. 2.23)
k	Boltzman constant (Eq. 2.15), joule/mole/K
k_d	rate constant for desorption, dimensionless
$k_{d\infty}$	rate constant for desorption at infinite temperature, dimensionless
K(T)	Henry's law constant (Eq. 2.6), g/100g Z/kPa
K_H	Henry's constant, g/100g Z/kPa
M	molecular weight, g/mole
n	carbon number or number of moles in equation 2.5
P	pressure, kPa
P_0	vapor pressure, kPa
P_C	critical pressure, kPa
P_{LM}	log mean pressure for the entire isotherm, kPa
P_{50}	pressure at 50% loading, same value as P_{LM}, kPa
P_r	reduced pressure, dimensionless
$P_{r,50}$	reduced pressure at 50% loading, dimensionless

R, R_g	Gas constant, joule/mole/K
R_a	rate of adsorption, mole/sec
R_d	rate of desorption, mole/sec
R_s	rate of surface striking, mole/cm^2/s
Q	heat of adsorption, joule/mole
q	zeolite loading, g/100 gZ
q_{max}	maximum zeolite loading, g/100 gZ
T	temperature, K
T_C	critical temperature
T_{CAR}	critical adsorbate reduced temperature
T_r	reduced temperature
u	pair wise adsorbate-adsorbate interaction energy, joule/mole
V	volume of gas adsorbed, cc
V_m	volume of gas adsorbed to fill a monolayer, cc
w	adsorbate-adsorbate interaction energy, joule/mole
x_v	mole fraction of species v.
Z	standard normal probability distribution variable
z	coordination number

Greek Letters

α	sticking coefficient
γ_v	activity coefficient of species v
ε	adsorption energy per molecule for adsorbate-adsorbent interaction, joule/mole
π	pi or spreading pressure, joule/m^3
θ	fractional loading, (=q/q_{max})
σ	standard deviation for an isotherm
σ	area per unit molecule (Eq. 2.10), cm^2/mole
σ_0	minimum area per unit molecule (Eq. 2.10), cm^2 /mole
σ_v	partial molar surface are of species v (Eq. 2.16)
$(-\Delta H_0)$	heat of adsorption at 0% loading, kcal/mole
$(-\Delta H_{50})$	heat of adsorption at 50% loading, kcal/mole

ΔF	difference in Helmholtz free energy, joule/mole
ΔH_0	difference in enthalpy, joule/mole
ΔU_0	difference in internal energy, joule/mole
ΔS	difference in entropy, joule/mole/K
Φ	cumulative distribution function
Φ^{-1}	inverse cumulative distribution function
ζ	parameter relating to the flexibility and the symmetry of a molecule
Λ	the thermal de Broglie wavelength, cm
Λ_{IV}, Λ_{VI}	constants in equation 2.17

CHAPTER 1: Introduction

1.1 Background

1.1.1 Definition

The first notion of adsorption came alive as early as the 18th century when the uptake of gases by charcoal was first described by Scheele in 1773 and by Fontana in 1777. In 1785, Lowitz discovered that charcoal took the coloring matter out of solutions [1]. In 1814, de Saussure carried out the first systematic investigations to measure the adsorption of different gases on a variety of adsorbents [1]. His findings outline our basic principles of adsorption.

According to Hill [2], "Adsorption is the preferential concentration of a species at the interface between two phases." When a gas comes in contact with a porous solid, it gets taken (adsorbed) into the pores of that solid. Adsorption occurs at the surface due to the difference in concentration of the sorbate inside the pores of the adsorbent and the gas or vapor that holds the sorbate. Like all transport phenomena adsorption occurs in order to achieve equilibrium.

1.1.2 Classification

It is possible to classify this process into two categories: physical adsorption (physisorption) and chemical adsorption (chemisorption). Physical adsorption occurs due to intermolecular forces such as Van der Waals, permanent dipole, induced dipole and quadrupole interactions. The forces involved in chemical adsorption, on the other hand, are the much stronger valence forces. These forces involve chemical reactions and the transfer of electrons between the adsorbent and the adsorbate. The differences between the two adsorption types are summarized in Table 1.1.

Table 1.1: Physical vs. chemical adsorption [3]

Physical adsorption	Chemisorption
Low heat of adsorption (1 to 1.5 times latent heat of evaporation).	High heat of adsorption (> 1.5 times latent heat of evaporation).
Non specific.	Highly specific.
Monolayer or multilayer.	Monolayer only.
No dissociation of adsorbed species.	May involve dissociation.
Only significant at relatively low temperatures.	May occur at a wide range of temperatures.
Rapid, nonactivated, reversible.	Activated, may be slow and irreversible.
No electron transfer, polarization of sorbate may occur.	Electron transfer leading to bond formation between sorbate and surface.

Whether adsorption is chemical or physical, it is accompanied by a decrease in the free energy of the system undergoing adsorption which makes it a spontaneous process. This decrease is due to the saturation of the unbalanced forces on the surface of the adsorbent. Moreover, adsorption is accompanied with a decrease in entropy because the adsorbed gas molecule is transformed from a three dimensional movement to being attached rigidly or with limited movement on the surface of the adsorbent. The decrease in the free energy and in the entropy of the adsorption process means that the heat change in the system is also negative, according to equation 1.1. Therefore the adsorption process in general is an exothermic process. (-ΔH) in the case of adsorption is referred to as the heat of adsorption [3].

$$\Delta H = \Delta F + T\Delta S \qquad 1.1$$

1.1.3 Adsorption isotherms

When an evacuated solid is brought in contact with a gas or vapor at a certain temperature and pressure, adsorption takes place until equilibrium is established. At this specific temperature and pressure the amount of gas that is adsorbed is a function of the nature of the adsorbent and the adsorbate [1]. The adsorbent's nature is defined by its physical structure (e.g. size, shape, surface area, pore distribution) and its chemical constitution. While for the adsorbed gas the nature is defined by its physical and chemical properties.

For a given gas per unit weight of adsorbent, the amount of gas adsorbed is a function of the final temperature and pressure at equilibrium [1].

$$a = f(T, P) \qquad 1.2$$

where a represents the amount of gas adsorbed per unit mass of adsorbent, and T and P are the final temperature and pressure respectively. When studying adsorption, either the temperature or the pressure is varied while keeping the other constant; however, it is more common to keep the temperature constant and vary the pressure.

A plot of the amount adsorbed per unit weight of the adsorbent vs. the pressure of the system at equilibrium is called the adsorption isotherm.

$$a = f(P),\ Tisconstant \qquad 1.3$$

while on the other hand, varying the temperature and keeping the pressure constant will generate the adsorption isobar.

$$a = f(T),\ Pisconstant \qquad 1.4$$

Brunauer et al. [4] classified the adsorption isotherms into five categories. Figure 1.1 shows the five different isotherm shapes where the amount adsorbed is plotted against the normalized pressure, P/P_0, P_0 being the saturation pressure at the given isotherm temperature.

Type I is referred to as the Langmuir type adsorption. The curve reaches a maximum saturation point where adsorption no longer occurs. This happens when the adsorbent pore size is comparable to the molecular diameter of the sorbate causing complete filling of the micropores and hence a definite saturation limit. Large intermolecular attraction effects result in an isotherm of type V. Type IV isotherm is encountered in the case where there is multilayer adsorption either on a plane surface or on the wall of pore that is wider than the molecular diameter of the sorbate. Types II and III are observed in adsorbents in which there is a wide range of pore sizes. With increased loading, adsorption develops continually from monolayer to multilayer and then to pore condensation. Capillary condensation occurs because the vapor pressure of the adsorbate inside the pores of the adsorbent is lower than that in the bulk phase due to the capillary forces exerted by the pore walls of the adsorbent.

Pores with smaller size fill first at lower pressures and as the pressure increases all of the pores are filled with liquid at the saturation pressure. According to the capillary condensation theory, adsorption at sufficiently high pressures is due to condensation in the mesopores [5].

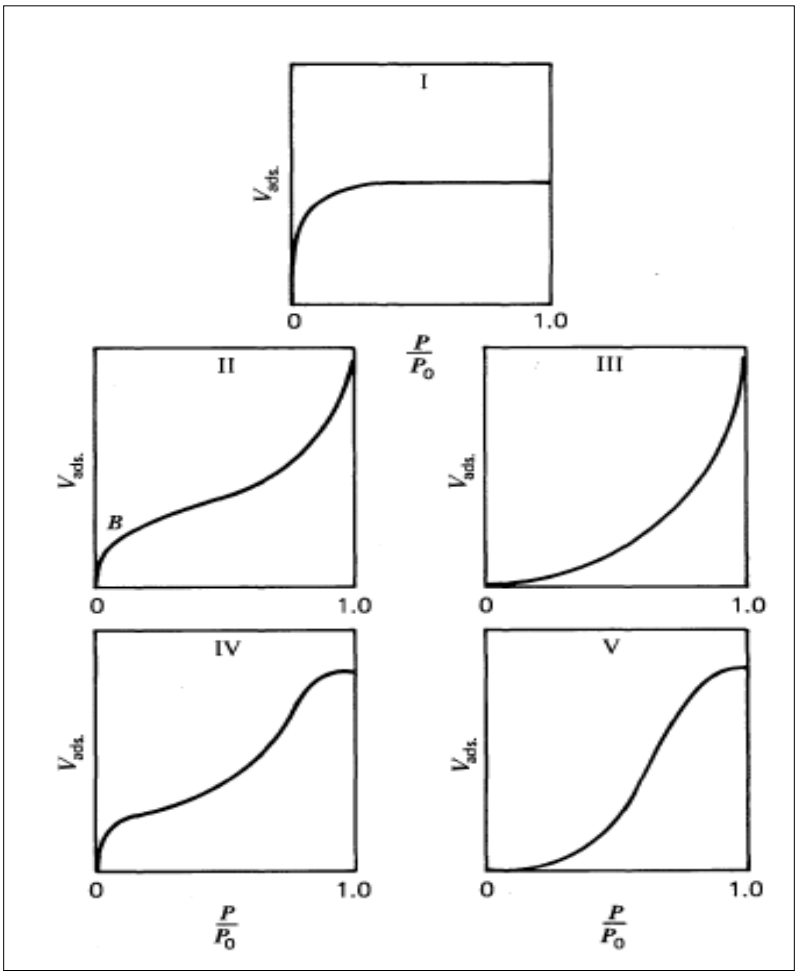

Figure 1.1: The five isotherm categories according to Brunauer et al. [4].

1.1.4 **Applications**

Besides being a natural phenomenon that is worth understanding, adsorption found a variety of important industrial applications. The most important ones are [1]:

1. Gas purification:
    a. The purification of carbon dioxide coming from fermenting vats to make it usable for carbonated water.
    b. The purification of hydrogen before catalytic hydrogenation.
    c. The refining of helium.
    d. The drying of air and other gases.
    e. The purification of air in submarines.
    f. The deodorizing of refrigerating rooms.
    g. The use of adsorbents for protection in gas masks.
2. Separation and recovery of gases.
    a. Separation of the rare gases.
    b. Extraction of gasoline from natural gas.
    c. Recovery of benzene and light oil from illuminating gas.
    d. Recovery of acetone, alcohol, and butanol from the waste gases of fermenting vats.
    e. Recovery of volatile solvent vapors in dry cleaning.
    f. Manufacturing of artificial silk, celluloid, rubber.
3. Catalysis.

    Catalysts are microporous structures which increase the rate of the reaction. Gases get adsorbed into the catalyst pores where they react on the surface, form products and then desorb. Adsorption on catalysts is very complex and unpredictable due to the non-uniform catalyst surface, that is, energy, crystal structure and chemical composition vary from one point to another on that surface [2].

1.1.5 **Adsorbents**

Adsorbents used in commercial separation processes must have some unique qualities that would make the process technically effective. The porosity of the adsorbent material is an important characteristic of its effectiveness. A highly porous adsorbent material with a high internal volume makes it more accessible for the components being removed. Mechanical strength and resistance to attrition especially under severe conditions, high temperatures during regeneration, are also important measures of effectiveness. The adsorbent must be able to preserve its adsorptive capability and efficiency in transferring adsorbing molecules rapidly to the adsorption sites. An important aspect also is the cost of raw materials and the methods of producing the adsorbent in order for the separation process to be economically feasible and more efficient compared to other separation processes.

Activated carbon. Activated carbons are commonly used adsorbents in the industry. Their wide range of uses include decolorizing sugar solutions, personnel protection, solvent recovery, volatile organic compound control, hydrogen purification, and water treatment [6].

They are formed out of elementary microcrystallites stacked in random orientation. The manufacturing process consists of the thermal decomposition of carbonaceous raw materials such as hard and soft woods, rice hulls, refinery residuals, peat, lignin, coals, coal tars, pitches, carbon black and nutshells, such as coconut, and which is followed by an activation process [6]. The activation process can be done through a gas or through chemical activation.

Activation with a gas involves heating in the absence of air at temperatures around 400-500 °C to get rid of all volatile materials and form small pores [6]. Afterwards, steam at 800-1000 ° C, or other gases such as carbon dioxide or flue gases, is used for activation. In chemical activation, chemicals such as zinc chloride or phosphoric acid are used directly with the raw materials to produce activated carbon [6].

Packed beds have granular material of particle size in the range of 0.4-2.4 mm. Activated carbon cloths are made from cellulose-based woven cloth. They have high external and internal surface areas and compare to the granular form they have higher capacity and better kinetic properties [6].

Table 1.2 displays the full range of pore sizes of activated carbon. The pore size and the pore size distribution can be controlled while manufacturing to yield a wide range of adsorbents with different selectivities and applications. For instance, liquid phase applications need bigger pore sizes than gas phase applications [6].

Table 1.2: Pore sizes in typical activated carbons [7].

	Micropores	Mesopores or transitional pores	Macropores
Diameter (nm)	<2	2-50	>50
Pore volume (cm^3 /g)	0.15-0.5	0.02-0.1	0.2-0.5
Surface area (m^2 /g)	100-3000	10-100	0.5-0.2
(Particle density 0.6-0.9 g/cm^3; porosity 0.4-0.6)			

Carbon molecular sieves (CMS). Carbon molecular sieves are produced from activated carbon by coating the pore mouths with a carbonized or coked thermosetting polymer.

This special manufacturing procedure converts amorphous carbons with a very narrow distribution of pore sizes to effective diameters ranging from 0.4-0.9 nm [6]. Figure 1.2 shows the pore structure of carbon molecular sieves. Chemicals like polyvinylidene dichloride and phenolic resin or naturally occurring materials such as anthracite or hard coal are used as raw materials in the manufacturing of these adsorbents [6]. Even though the adsorptive capacity of CMS is lower than activated carbon, this modification on activated carbon results in better kinetic properties which lead in turn to better kinetic selectivity. Carbon molecular sieves are mainly used in the production of high purity nitrogen from air by pressure swing adsorption.

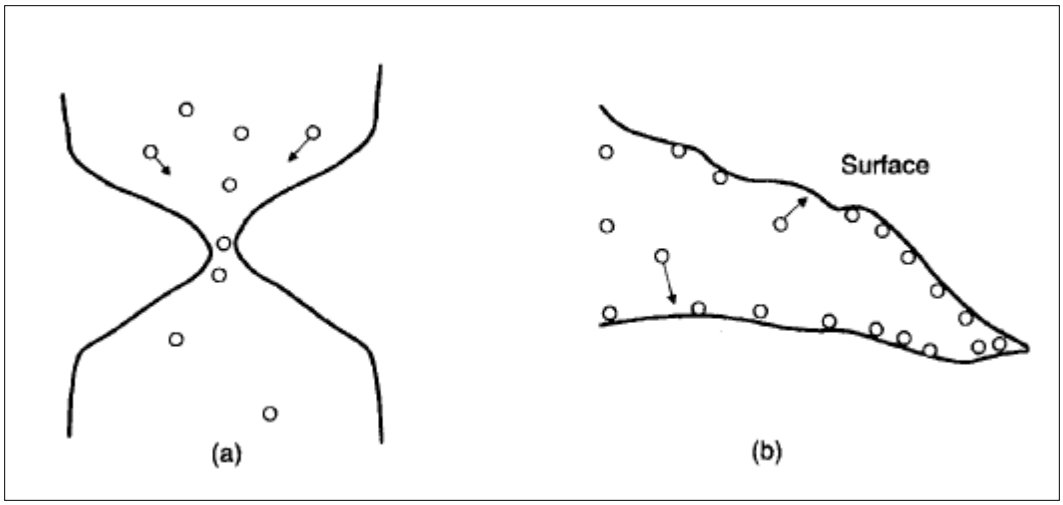

Figure 1.2: Molecular sieve carbons (a) Type CMSN2 with bottlenecks near 0.5 nm formed by coke deposition on the pore mouth; (b) Type CMSH2 formed by steam activation [6].

Carbonized polymers and resins. Pyrolising resins such as formaldehyde and highly sulphonated styrene/divinyl benzene macroporous ion exchange resins result in carbonaceous adsorbents with macro-, meso-, and micro porosity and surface areas up to 1100 m^2/g [6]. Their main application is the removal of organic compounds from water because these adsorbents are more hydrophobic than granular activated carbon.

Polymeric adsorbents. These synthetic non-ionic polymers are practical for analytical chromatography applications. The polymer matrix is formed from monomers that are emulsions polymerized in the presence of a solvent which dissolves the monomers without swelling the polymer [6].

Their surface areas may reach up to 750 m^2 /g. The structure of these polymers along with the controlled distribution of pore sizes, the high surface areas and the chemical nature of the matrix all contribute to the selective properties of these adsorbents.

One of the applications of polymeric adsorbents is solute recovery from the aqueous phase including phenol, benzene, toluene, chlorinated organics, PCB's, pesticides, antibiotics, acetone, ethanol, detergents, emulsifiers, dyes, steroids, amino acids, etc. [6].

Silica Gel. Silica gel is a partially dehydrated polymeric form of colloidal silicic acid with the formula $SiO_2.nH_2O$. Spherical particles with a diameter of 2-20 nm aggregate to form an adsorbent with pore sizes in the range of 6-25 nm and surface areas in the range of 100-850 m^2/g [6].

Its polar surface consists of mainly SiOH and SiOSi groups. Silica Gel can be used to adsorb water, alcohols, phenols, amines, etc. by hydrogen bonding mechanisms. Additionally, it is used in the separation of aromatics from paraffins and the chromatographic separation of organic molecules [6]. Silica gel has higher adsorption capacities at low temperatures and moderate water vapor pressure. It may lose activity through polymerization which involves the surface hydroxyl groups. Table 1.3 shows the typical properties of adsorbent-grade silica gel.

Table 1.3: Typical properties of silica gel [8].

	Physical properties
Surface area (m^2/g)	830
Density (kg/m^3)	720
Reactivation temperature (°C)	130-280
Pore volume (%of total)	50-55
Pore size (nm)	1-40
Pore volume (cm^3 /g)	0.42
Adsorption properties	Percent by weight
H_2O capacity at 4.6 mmHg. 25°C	11
H_2O capacity at 17.5 mm Hg. 25 °C	35
O_2 capacity at 100 mmHg. -183°C	22
CO_2 capacity at 250mm Hg. 25°C	3
n-C_4 capacity at 250 mm Hg. 25°C	17

Activated alumina. Activated alumina is a high porous form of aluminum oxide with the formula $Al_2O_3.nH_2O$. The surface of activated alumina is both acidic and basic given the amphoteric nature of aluminum. Compared to silica gel, activated alumina's surface is higher in polarity with an area in the range of 250-350 m^2/g [6]. Also, at elevated temperatures alumina has a higher capacity for water; therefore, it is used as a desiccant for warm gases such as air, argon, helium, hydrogen, low molecular weight alkanes (C_1-C_3), chlorine, hydrogen chloride, sulphur dioxide, ammonia and fluoroalkanes [6]. Activates alumina is also used in drying of some liquids like kerosene, aromatics, gasoline fractions and chlorinated hydrocarbons and in chromatography [6].

Clay materials. Clays are synthesized from natural deposits. They are formed of layer silicates which adsorb guest molecules between their siliceous layers causing their crystals to swell. Fuller's earth is an activated natural montmorillonite. Acid treatment can increase its surface area to 150-250 m^2/g. Clay materials are used for re-refining edible and mineral oils, adsorbing toxic chemicals, removing pigments, etc. [6]. The cationic forms can adsorb a range of polar and non-polar molecules in the presence of water. Those layers can be enlarged through ion exchange to form pillared interlayered clays. The charge compensation cations are replaced by polynuclear metal ion hydro-complexes which are formed in hydrolyzed solutions of polyvalent metal ions such as Al(III) or Zr(IV) [6]. The polynuclear cations dehydrate on calcination to create metal oxide clusters which act as pillars between the clay layers and create spaces of molecular dimensions [6]. Those pillared clays are used in the separation of oxygen and nitrogen, and the separation of isomers.

Zeolites. Zeolites are crystalline alumino-silicates. They are called molecular sieves because they have the ability to separate molecules by their size. There is a huge variety of natural and synthetic zeolites. Synthetic types A and X, synthetic mordenite along with their ion exchange varieties are the most used commercially. The zeolite framework consist of an assemblage of SiO_4 and AlO_4 tetrahedra joined together in different regular arrangement with a shared oxygen atom, to form an open crystal lattice containing pores of molecular dimensions into which sorbate molecules can penetrate [7]. The uniform micropore structure produced by the crystal lattice makes zeolites different than other microporous adsorbents.

The zeolite framework consists of several tetrahedrals joined together in different polyhedral arrangements to form secondary units. Figure 1.3 shows some secondary building units with commonly occurring polyhedral. Each vertex represents a Si or Al atom while the lines represent the diameters of the oxygen atoms or ions. Each aluminum atom contributes to a negative charge which must be balanced by a cation through ion exchange. Those exchangeable cations play a very important role in determining the adsorptive properties. Si atoms are always more than Al atoms in a given zeolite framework. The Si/Al ratio determines the adsorptive properties of zeolites.

Aluminum rich sieves have higher affinities for water and other polar molecules while microporous silicas are hydrophobic and adsorb n-paraffins in preference to water.

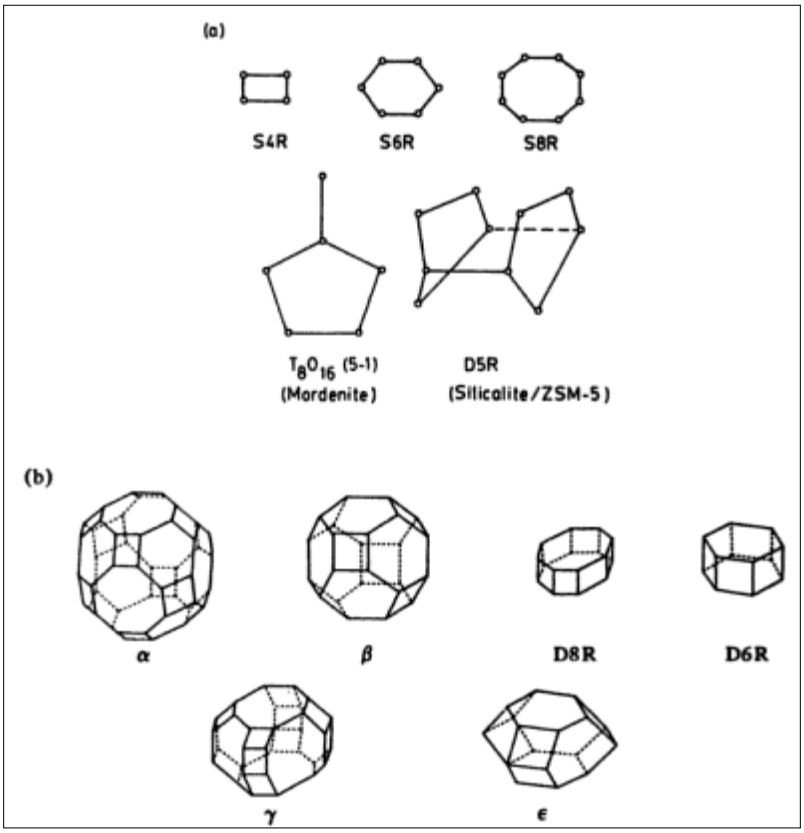

Figure 1.3: (a) secondary building units. (b) Commonly occurring polyhedral units in zeolite framework structures [7].

Zeolite A. Figure 1.4 shows a schematic diagram of the zeolite A structure. As described by Ruthven [7] the structure of a pseudo cell of a zeolite consists of eight unit cells of type ß (shown in Figure 1.3) located at the corners of a cube and connected through four membered oxygen rings. This arrangement assembles a large polyhedral α cage with a free diameter of 11.4 Å. These cells stack together in a cubic lattice to form three dimensional isotropic channel structure, constricted by eight-membered oxygen rings. Each pseudo cell contains 24 tetrahedral AlO_2 or SiO_2 and since the Si/Al ratio is always close to 1, there are 12 univalent exchangeable cations per cell. Exchanging with different cations produces zeolites with different selectivities and adsorptive properties. For example 5A zeolites, produced from exchanging with Ca^{2+} or Mg^{2+}, can accommodate larger molecules than 3A zeolites obtained by potassium exchange.

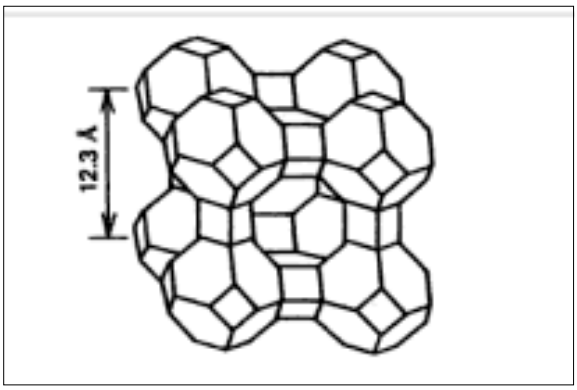

Figure 1.4: Framework structures of zeolite A [7].

Zeolite X and Y. Their structures, as shown in Figure 1.5 below, are formed by a group of tetrahedrons with the aluminum and silicon atoms at the center and four oxygen atoms at the vertexes [9]. Groups of tetrahedrons form regular structures of stumped octahedrons or a sodalite cage, which has 8 hexagonal sides (formed by 6 tetrahedrons) and 6 square sides (formed by 4 tetrahedrons) [9]. The shape of a sodalite cage is shown in the Figure 1.6.

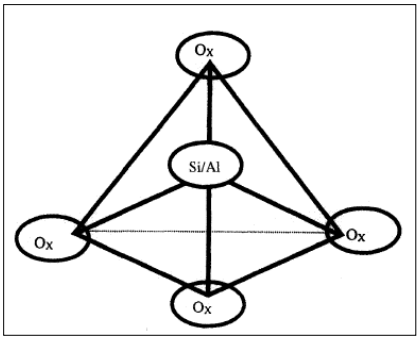

Figure 1.5: Tetrahedron [9]

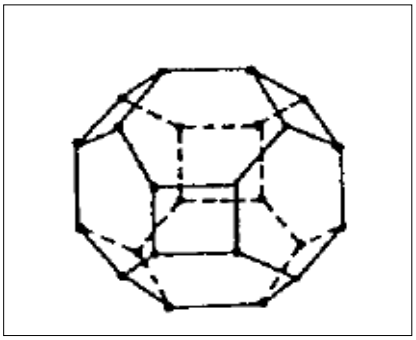

Figure 1.6: Sodalite cage. [9]

The basic element of these zeolites X and Y consists of 6 sodalite cages with the hexagonal faces connected through prisms, Figure 1.7. A network of very small pores, with an internal diameter of around 7.5Å, leads to cavities inside the zeolite with a mean diameter of 13Å (Raseev [9]). The internal surface area of the pores is around 600 m^2/g [10].

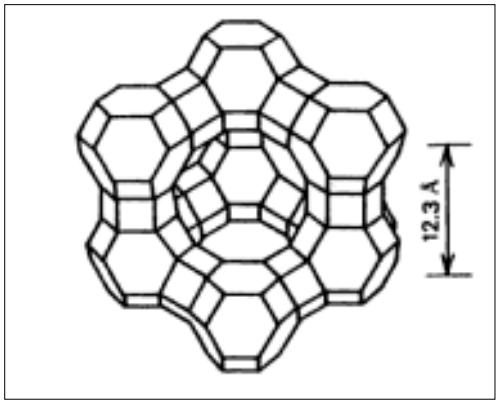

Figure 1.7: Framework structures of zeolite X and Y [7].

Zeolite X and Y have the following common formula [9]:

$$Na_n[(Al_2O_3)_n(SiO_2)_{192-n}].mH_2O$$

$$m \approx 250\text{-}260$$

$$n \approx 48\text{-}76 \text{ for zeolite Y}$$

$$\approx 77\text{-}96 \text{ for zeolite X}$$

The difference between type Y and X zeolites is the Si/Al ratio. Having lower Si/Al ratio, X zeolites are also less thermally and hydrothermally stable. Each silicon and aluminum atom is connected to four oxygen atoms. That leaves the silicon atom neutral while placing a negative charge on the aluminum atom as shown below.

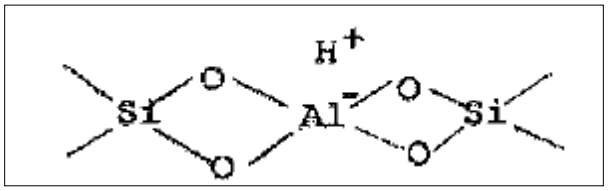

Figure 1.8: Chemical structure of zeolite X and Y [9].

1.1.6 **Pelletization**

Commercial molecular sieve zeolite crystals are small in size and, on their own, cannot withstand severe conditions and mechanical attrition. Therefore they are produced in forms of macroporous pellets of suitable size, porosity and mechanical strength. Nevertheless, the pellet form gives rise to two kinds of resistances: micropore diffusional resistance of the zeolite crystal itself and the macropore diffusional resistance of the intracrystalline pores. Reducing the crystal size reduces intracrystalline resistance but it may also, in turn, increase the diameter of intercrystalline macropores causing the diffusivity to drop to undesired levels. Reducing the gross particle size reduces macropore resistance but if the particles are too small, pressure drop might also become unacceptable. That is why an optimum pellet design balances between macro- and micro-pore resistances depending on the system designed.

Pellets may be formed in different ways. The most common processes are: extrusion to form cylindrical pellets, granulation to form spherical particles, and combined processes of extrusion followed by rolling to form spheres.

A clay material is sometimes added to the pellet in order to bind the crystals and supply the desired mechanical strength. The binder usually accounts for 10-20% of the final pellet and sometimes it would be much less than that.

Care must be taken in choosing the binder material as some might have adsorptive properties and might, as a result, reduce the selectivity as compared to unaggregated crystals.

1.1.7 Adsorbent selection

A wide variety of adsorbent are available in today’s industry. Choosing the most appropriate and effective one depends on the properties of this adsorbent compared to the separation or purification process desired. In order to know whether a certain adsorbent is suitable for a given separation or purification process, one should first look at the equilibrium data at the temperature and pressure of interest.

Equilibrium isotherms can be obtained experimentally or can be supplied by the vendor. Once equilibrium data are interpreted, the kinetic properties of that adsorbent should be studied.

If both equilibrium data and kinetic properties indicate that the given adsorbent can achieve the desired purity then the next step is to establish a method of regenerating the adsorbent. Finally the adsorbent should have suitable physical and mechanical properties to withstand all the process condition including the regeneration step.

1.1.8 Measurement techniques

The following is a brief description of two of the most basic methods of measuring gas adsorption equilibria on a solid phase [11].

Volumetry/ Manometry. Volumetry was the first method invented to measure the adsorption of gases on solids. Its basic principle is subjecting a known amount of gas to an evacuated solid where the sorbate become adsorbed on the surface of the adsorbent until equilibrium is reached. The amount adsorbed can then be calculated through mass balance done on the system. The void volume of the adsorbent, the volume that doesn't contain any adsorbent, as well as the dead volume in the cell must be taken into account.

Figure 1.9 shows the experimental setup for volumetric measurements of pure gas adsorption equilibria. It consists of a gas storage vessel connected to an adsorption chamber through a tube bearing a valve.

A thermostat is setup within both vessels in order to control the temperature. Tubes are connected to the vessels to supply and evacuate gases as needed. Both temperature and pressure are monitored through thermometers and manometers respectively. The adsorbent material being tested should be activated at high temperatures in vacuum to make sure all pre-adsorption gases are evacuated. The gas chamber is evacuated and a known amount of gas is loaded. The expansion valve is then opened to allow the gas to expand to the adsorption chamber where it gets adsorbed on the surface of the adsorbent.

The achievement of constant temperature and pressure indicates that thermodynamic equilibrium has been reached. From the pressure and temperature the amount of gas adsorbed can be calculated using an appropriate equation of state.

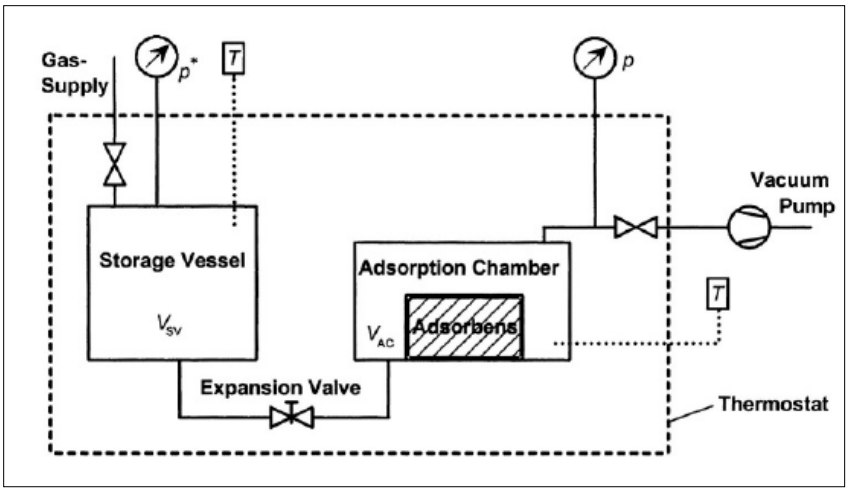

Figure 1.9: Experimental setup for volumetric measurement of pure gas adsorption equilibria [11].

Gravimetry. It is one of the new methods of measuring gas adsorption equilibria that was made possible due to the development of highly sensitive balances that are able to measure small relative changes in the weight of the adsorbent sample. The two beam microbalance is one of the gravimetric techniques used to measure the adsorption of pure non-corrosive gases on a solid. The schematic diagram shown in Figure 1.10 is the experimental setup used. Two vessels, one contains the sample and the other contains ballast, are mounted under the balance and are placed in a thermostat. Gas is supplied and evacuated through tubes connected to the vessels. A thermostat and a manometer are mounted on both vessels as well to monitor the temperature and pressure respectively. The adsorbent sample is mounted inside the microbalance to be activated by evacuation, heating and flushing with helium. Next the balance must be evacuated before measuring the adsorbent sample initial weight. After that the gas is administered to the adsorbent vessel which causes the balance recording to change. This change is not only due to the adsorption of gas on the sorbent's surface but also due to the buoyancy effects of the sample in the surrounding gas. In gravimetry, one can identify the approach to equilibrium through the data display on the balance. If the mass change is less than some predefined value in a defined time interval then equilibrium can be assumed.

Temperature, pressure and the final sample weight is recorded. After that the pressure in increased in sequential steps and the procedure is repeated to get the amount adsorbed at each pressure. Buoyancy effects must be accounted for.

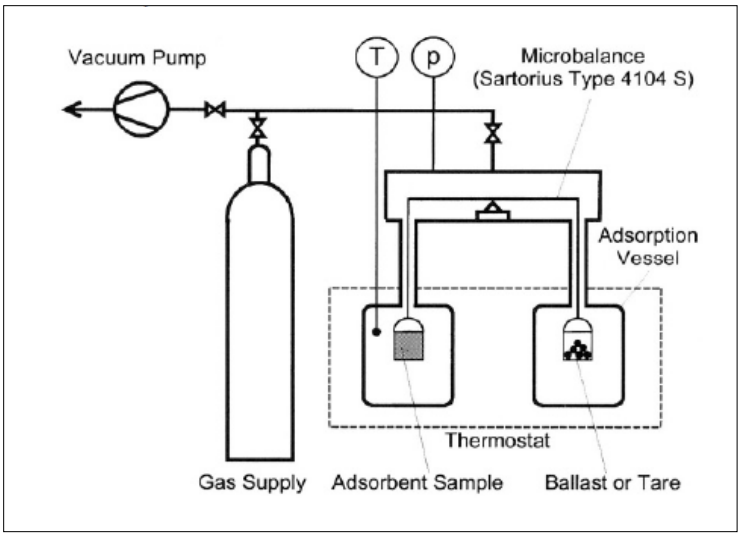

Figure 1.10: Experimental setup for gravimetric measurements of pure gas adsorption equilibria using a two beam balance [11].

In case of corrosive gases like NH_3 or SO_2, a single beam balance setup is used, shown in Figure 1.11, instead of the double beam one. To prevent the corrosive gas from touching the microbalance, the sorbent is loaded on a suspension rod that hangs freely inside the adsorbent vessel due to the magnetic field coming from above. Other than that the procedure of measuring the sample weight is similar to what have been discussed earlier in the two beam microbalance.

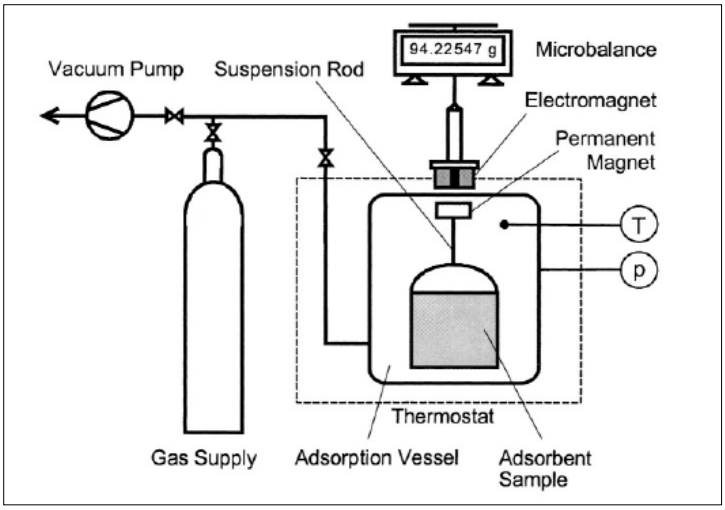

Figure 1.11: Experimental setup for gravimetric measurements of pure gas adsorption equilibria using a single beam balance [11].

1.2 Literature Review

A number of studies exist in literature on the adsorption of hydrocarbons on 13X zeolites. Those studies contain information on the measurement techniques, adsorption isotherms and heats of adsorption. For the purpose of this study, adsorption data were collected from 22 different studies that measured the adsorption of some selected alkanes, alkenes and aromatics. This section includes a brief description of each of the studies that were used to get the adsorption data.

Barrer and Sutherland [12] investigated the occlusion of paraffins, including (nC_1-nC_8), i-C_4, i-C_5, neo-C_5 and i-C_8, and some permanent gases within the crystal lattice of dehydrated synthetic faujasite ($Na_2O.Al_2O_3.2.67SiO_2.mH_2O$).Adsorption measurements were quantified through a sorption apparatus that comprised both gravimetric and volumetric sections. Isotherms of the studied species were constructed by plotting the amount adsorbed vs. the pressure and the differential heats of sorption were evaluated.

Barrer et al. [13] studied the properties of the inclusion complexes of cyclic hydrocarbons in the structures of faujasites. The adsorption of toluene, benzene, cyclopentane and cyclohexane were measure and their isotherms were constructed. Thermodynamic data such as the heat of adsorption and the entropy change were also measured for the selected hydrocarbons.

Zhdanov et al. [14] measured the adsorption of benzene and n-hexane and their binary solutions on 10X and 13X zeolites.

Ruthven and Doetsch [15]measured the diffusivity of four hydrocarbons, nC_7H_{16}, C_6H_{12}, C_6H_6 and $C_6H_5.CH_3$, on 13 X zeolite by the gravimetric technique. The purpose of the study was to investigate the dependence of diffusivity on concentration and temperature in such systems. Equilibrium isotherms, Henry's constant and heats of adsorption were also measured for these hydrocarbons.

Rolniak and Kobayashi [16] measured the adsorption of pure methane and several methane-carbon dioxide mixtures on 5A and 13X molecular sieves at elevated pressures and near ambient temperatures by applying the principles of tracer perturbation chromatography. The data were correlated by applying the statistical mechanical model of Ruthven.

Hyun and Danner [17] used the static volumetric method to determine the adsorption equilibria of C_2H_4, C_2H_6, i-C_4H_{10} and CO_2 and their binary mixtures on 13X molecular sieves at various temperatures between 273 and 373 K.

Loughlin et al. [18] reported the pure and multi-component adsorption data for the adsorption of the light n-alkanes, (nC_1-nC_4), on Linde 5A and 13X pellets in the temperature range 275-350 K. The intrinsic Henry's law constant and the heats of adsorption were extracted from the data using virial isotherm techniques.

Ruthven and Tezel [19] studied the sorption of benzene on NaX zeolites where they reported an unusual hysteresis effect that was observed from the adsorption measurements. Measurement studied in this paper was done gravimetrically using a vacuum microbalance system on a sample of unaggregated NaX crystals.

Ruthven and Kaul [20] measured the equilibrium isotherms and isobars of a series of aromatic hydrocarbons (benzene, toluene, tetramethylbenzene, dimethylnaphthalene, and anthracene) on NaX crystal zeolites. Henry's constants and the heats of adsorption were also reported in the study.

Salem et al. [21] measured the adsorption equilibria of argon, nitrogen and methane on 13X molecular sieves and activated carbon using a microbalance at five temperatures over a wide pressure range. The equilibrium isotherm data were used to calculate the absolute isotherms using equations of state for a real gas.

Da Silva and Rodrigues [22] measured the single adsorption equilibrium isotherms of propylene and propane and their mass-transfer kinetics on 13X and 4A zeolite pellets using gravimetry and zero length column techniques, respectively. The experimental equilibrium isotherm data obtained were fitted by the Toth isotherm equation.

Wang et al. [23] measured the adsorption of some organic compounds, benzene, toluene, o-xylene, p-xylene, and m-xylene, on the activated carbon, silica gel and 13X zeolite by the gravimetric adsorption method. The equilibrium isotherm data obtained were fitted by the Freundlich equation.

Pinto et al. [24] studied the adsorption of toluene and nitrogen on different composite adsorbent materials to study the effect of the supporting process in the

adsorption capacity of those materials. Three activated carbons, one zeolite and one pillared clay were supported in polyurethane foam to form the composite material.

Lamia et al. [25] measured the adsorption equilibrium isotherms of propylene, propane, and isobutane on 13Xzeolite pellets over a temperature range from 333 K to 393 K and pressure up to160 kPa using the gravimetric method. The adsorption equilibrium isotherm data were fitted by the Toth equation. The aim of this study was to investigate the ability of iso-butane to act as a desorbent of the propane/ propylene mixture over 13X zeolite in a simulated moving bed. The heats of adsorption at zero coverage for propylene, propane, and iso-butane were also measured.

Lamia et al. [26] measured the adsorption equilibrium of 1-butene over 13X zeolite by the gravimetric method at temperature of 333, 353, 373 and 393 K. The experimental adsorption data were fitted by the Toth equation. The heat of adsorption at zero coverage and the maximum loading capacity of 1-butene were also measured.

1.3 Deliverables

Modeling experimental adsorption equilibrium data is a way of theoretically predicting unmeasured adsorption equilibrium data for materials of the same species. The most commonly used models in adsorption equilibria use the concept of surface coverage or micropore volume filling and were either derived from a kinetic or a thermodynamic point of view. A new idea was put forward to model adsorption data that is different from all traditional models. Abouelnasr and Loughlin [27] proposed a model based on the Gaussian cumulative frequency distribution principles, which has been used before to model energy sites rather than adsorption sites [27].

In this study, the Gaussian model is used to model data on the adsorption of hydrocarbons on 13X zeolites; the data has been collected from previous published work in literature. The scope will cover selected sorbates from alkanes, alkenes and aromatics. The parameters of the model will be determined for each group of hydrocarbons by fitting the experimental data by the Gaussian equation. Heats of adsorption at a constant θ of 50% will be determined for each species.

1.4 Thesis Outline

- Chapter1: thesis introduction. Includes background information, literature review and thesis deliverables.
- Chapter 2: theoretical background and model derivation.
- Chapter 3: modeling the adsorption of alkanes over 13X zeolite by the Gaussian model.
- Chapter 4: modeling the adsorption of alkenes over 13X zeolite by the Gaussian model.
- Chapter 5: modeling the adsorption of aromatics over 13X zeolite by the Gaussian model.
- Chapter 6: Conclusion.

CHAPTER 2: Theoretical Background and Model Derivation

2.1 Adsorption Equilibrium Theory

2.1.1 Langmuir theory

Adsorption equilibria have been studied since the beginning of the 20th century. The first basic theory of adsorption was derived by Langmuir back at 1918. This theory assumes an ideal surface on which surface adsorption occurs, and it is deduced from a kinetic point of view. Three main assumptions of this theory are [5]:

1- Homogenous surface, meaning that the adsorption energy is constant across the surface on each site.
2- One molecule only can be adsorbed on each site.
3- Adsorption occurs on definite, localized sites.

The well known Langmuir isotherm,

$$\theta = \frac{bP}{1+bP} \qquad 2.1$$

is derived originally from equating the rate of adsorption on an occupied site, eq. 2.2, to the rate of desorption on an occupied site, eq. 2.3:

$$R_a = \frac{\alpha P}{\sqrt{2\pi M R_g T}}(1-\theta) \qquad 2.2$$

$$R_d = k_d\theta = k_{d\infty}e^{-(\frac{E_d}{R_g T})}\theta \qquad 2.3$$

The term $\left(\frac{P}{\sqrt{2\pi M R_g T}}\right)$ in equation 2.2 is the rate of striking the surface, Rs, in mole per unit time per unit area, obtained from the kinetic theory of gases [5]. This term is multiplied by a sticking coefficient, α, to account for non ideal sticking on a non ideal surface. The term is also multiplied by (1-θ) which is the fraction of empty sites to finally yield the rate of adsorption given by equation 2.2.

The rate of desorption in equation 2.3 is the equal to k_d, the rate of desorption from a fully covered surface, multiplied by θ, the percent coverage. E_d is the activation energy

for desorption, $k_{d\infty}$ is the rate constant for desorption at infinite temperature and b is the Langmuir constant given by:

$$b = \frac{\alpha \exp(Q/R_g T)}{k_{d\infty}\sqrt{2\pi M R_g T}} \qquad 2.4$$

Here Q is the heat of adsorption and is equal to the activation energy for desorption, E_d.This equality follows the assumption that at equilibrium, the rate of bombardment of molecules onto the surface is equal to the rate of desorption of molecules from the surface and, hence, zero accumulation occurs at equilibrium.

2.1.2 Gibbs thermodynamic theory [5]

Another theory was proposed from a thermodynamic point of view. Gibbs used the principles of classical thermodynamics of the bulk phase and applied it to the adsorbed phase.

In this analogy the volume is replaced by the area and the pressure is replaced by what is called the spreading pressure, π. The result is the Gibbs isotherm equation:

$$\left(\frac{d\pi}{dlnP}\right)_T = \frac{n}{A} R_g T \qquad 2.5$$

Given an equation of state that relates the spreading pressure to the number of moles in the adsorbed phase, an isotherm can be produced that expresses the number of moles adsorbed in terms of pressure. Two examples are the linear isotherm and the Volmer isotherm.

Linear isotherm:

$$\frac{n}{A} = K(T)P \qquad 2.6$$

$$K(T) = \frac{C(T)}{R_g T} \qquad 2.7$$

where C (T) is some function of temperature and K (T) is called Henry's constant.

Volmer isotherm:

$$b(t)P = \frac{\theta}{1-\theta}\exp\left(\frac{\theta}{1-\theta}\right) \qquad 2.8$$

$$b(T) = b_\infty exp\left(\frac{Q}{R_g T}\right) \qquad 2.9$$

The linear isotherm is applied to dilute systems where the adsorbed molecules act independently from each other. The Volmer isotherm on the other hand takes into account a finite size of the adsorbed molecules. Nevertheless, the Volmer isotherm still does not take into account the mobility of the adsorbed molecules. This factor can be included by using a different equation of state, one that includes the co-volume term and the attractive force term.

An example is the following van der Waals equation:

$$\left(\pi + \frac{a}{\sigma^2}\right)(\sigma - \sigma_0) = R_g T \qquad 2.10$$

σ is the area per unit molecule adsorbed.

The resulting isotherm is:

$$bP = \frac{\theta}{1-\theta} exp\left(\frac{\theta}{1-\theta}\right) \exp(-c\theta) \qquad 2.11$$

$$b = b_\infty exp\left(\frac{Q}{R_g T}\right) \qquad 2.12a$$

$$c = \frac{2a}{R_g T \sigma_0} = \frac{zw}{R_g T} \qquad 2.12b$$

where z is called the coordination number and is given the values 4 or 6 depending on the packing of molecules, and *w* is the interaction energy between the adsorbed molecules.

This isotherm is called the Hill-deBoer Isotherm and is used in cases where there is mobile adsorption and lateral interaction among adsorbed molecules. Eliminating the first exponential factor from this isotherm presents the case where there is no lateral interaction among molecules to result in what is called the Fowler Guggenheim equation or the quasi approximation isotherm:

$$bP = \frac{\theta}{1-\theta} \exp(-c\theta) \qquad 2.13$$

2.1.3 Statistical thermodynamic theory

In a similar manner different isotherms were proposed from different equations of state. Each of these isotherms describes a unique type of adsorption depending on the equation of state used.

Models were also derived using statistical thermodynamics. Multisite occupancy model of Nitta et al. [28] is an example:

$$nbP = \frac{\theta}{(1-\theta)^n} exp\left(-\frac{nu}{kT}\theta\right) \qquad 2.14$$

$$b = \frac{j_s \xi}{j_g} \frac{\Lambda^3}{kT} \exp\left(\frac{\varepsilon}{kT}\right) \qquad 2.15$$

where b is the affinity constant given by the previous equation, Λ is the thermal de Broglie wavelength, j_s is the internal and vibrational partition functions of an adsorbed molecule, j_g is the internal partition function of gas phase, ε is the adsorption energy per molecule for adsorbate-adsorbent interaction, and u is the molecular interaction parameter for adsorbate– adsorbate interaction.

One of the important models of adsorption also, developed by Suwanayuen and Danner [29], is the vacancy solution model. The system is assumed to consist of two solutions, the gas phase and the adsorbed phase, where both differ in their densities. The isotherm equation was derived by substituting the following equation of state (for species v) into the Gibbs isotherm equation:

$$\pi = -\frac{R_g T}{\sigma_v} \ln(\gamma_v x_v) \qquad 2.16$$

where γ is the activity coefficient and x is the mole fraction.

The result is the following isotherm:

$$P = \left[\frac{C_{\mu s}}{K} \frac{\theta}{1-\theta}\right] \left[\Lambda_{\mathrm{Iv}} \frac{1-(1-\Lambda_{\mathrm{vI}})\theta}{\Lambda_{\mathrm{Iv}}+(1-\Lambda_{\mathrm{Iv}})\theta}\right] exp\left[-\frac{\Lambda_{vI}(1-\Lambda_{vI})\theta}{1-(1-\Lambda_{vI})\theta} - \frac{(1-\Lambda_{\mathrm{Iv}})\theta}{\Lambda_{\mathrm{Iv}}+(1-\Lambda_{\mathrm{Iv}})\theta}\right] \qquad 2.17$$

where K is the Henry constant; $C_{\mu s}$ is the maximum adsorbed concentration.

$$\theta = \frac{C_\mu}{C_{\mu s}} \qquad 2.18$$

2.1.4 Empirical isotherm equations

Equations that were found to best describe data of hydrocarbon adsorption are empirical isotherm equations [5]. The earliest of these isotherms was used mostly by Freundlich (1932), hence was called by his name:

$$C_{\mu} = KP^{1/n} \qquad 2.19$$

where C_{μ} is the concentration of the adsorbed species; K and n are temperature dependent.

More empirical equations were found later such as the Sips equation (Freundlich-Langmuir), Toth equation, Unilan equation, Keller et al., Dubinin-Radushkevitsh, Javonovish equation and Temkin. Braunauer; Emmett and Teller developed an empirical equation that describes sub-critical adsorbates where multi-layer adsorption takes place. The BET theory was published in 1938 and was modified later on by other researchers. Nevertheless the original BET theory remained the most important equation to describe mesoporous solids adsorption [5].

$$\frac{V}{V_m} = \frac{CP}{(P_0 - P)[1 + (C-1)(P/P_0)]} \qquad 2.20$$

2.2 Henry's Law

Physical adsorption does not involve association or dissociation of molecules hence the molecular state of the adsorbent is preserved. If physical adsorption is to occur on a uniform surface at sufficiently low concentrations of the adsorbed phase the molecules will act as if they are isolated from their nearest neighbor. As a result, the relationship between the adsorbed and fluid phase concentrations will be linear. The constant of proportionality is the adsorption equilibrium constant and it is analogous to Henry's constant. Similarly, the equilibrium relation is analogical to Henry's Law. As shown in the following equation the adsorption equilibrium constant (Henry's constant) can be expressed in terms of pressure or concentration:

$$q = Kc \quad or \quad q = K'P \qquad 2.21$$

where q and c are the adsorbed and fluid phase concentrations, respectively.

Henry's constant obeys the vant Hoff equation for temperature dependence:

$$\frac{dlnK'}{dT} = \frac{\Delta H_0}{RT^2}, \qquad \frac{dlnK}{dT} = \frac{\Delta U_0}{RT^2} \qquad 2.22$$

where ΔH_0 and ΔU_0 are the differences in enthalpy and internal energy, respectively, between adsorbed phase and gaseous phase. The previous equations can be integrated, with the assumption that the heat capacity between the phases is negligible, to yield:

$$K' = K_0' e^{-\Delta H_0/RT}, \qquad K = K_0 e^{-\Delta U_0/RT} \qquad 2.23$$

2.3 The Gaussian model

A new idea was put forward to model adsorption data that is different from all traditional above. Abouelnasr and Loughlin [27] proposed a model based on the Gaussian cumulative frequency distribution principles, which has been used before to model energy sites rather than adsorption sites.

According to Abouelnasr and Loughlin [27], adsorption phenomena should be very well described by the Gaussian normal probability distribution function. This is because adsorption is the probability that a molecule gets adsorbed on a surface and it depends upon the following probabilities:

1- The molecule collides with a site on that surface.
2- The site is available.
3- The kinetic energy of the molecule is low enough to prevent it from escaping.

In their paper, Abouelnasr and Loughlin [27] used the adsorption data of methane on 5A zeolite to test the model. The data were collected from six studies to get a total of 24 isotherms that were fitted to the new model.

Figure 2.1 shows the similarity between the shape of adsorption isotherm of methane on 5A zeolite, θ vs. P, and the Gaussian cumulative frequency distribution function [27]. This similarity establishes that the adsorption process follows the Gaussian cumulative distribution [27].

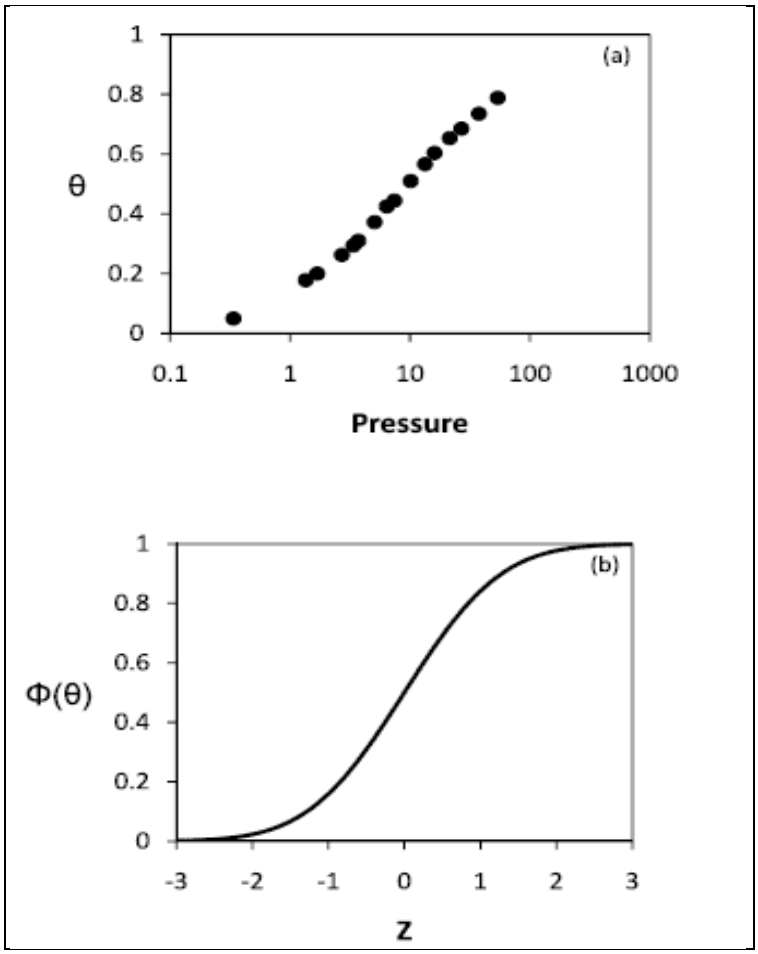

Figure 2.1: (a) Isotherm for methane on 5A zeolite at 194.5 K. data are from Stroud et al. [30] a value for q_{max} of 9 g/100 gZ is used in calculating θ. (b) cumulative distribution function for the standard normal distribution [27].

Abouelnasr and Loughlin [27] stated the following assumptions for the new isotherm:

1. Molecules in the gas phase have a Maxwell-Boltzmann distribution of velocities and energies.
2. All adsorption sites are equivalent.
3. The adsorbed phase inside the micropores is assumed to be a condensed liquid state even though it might have different properties.
4. Adsorption sites are filled to saturation at maximum adsorption.
5. There is no interaction between molecules that are adsorbed on adjacent sites.

2.3.1 Model derivation

First a normal distribution variable, Z, is defined as:

$$Z = \frac{\log(P) - \log(P_{LM})}{\sigma} \qquad 2.24$$

where P_{LM} is the log mean pressure which is defined in this case as the pressure at 50% of the maximum loading or P_{50} and σ is the standard deviation for the entire isotherm. Note, since this chapter is a literature review, log base 10 is used as the original papers were written in this fashion. However, from chapter 3 onwards in this thesis, all calculations are done using ln base e as this is the logical interpretation of the Gaussian isotherm. *Φ (Z)* is the cumulative distribution function for the standard normal distribution where it represents the area to the left of *Z* under the bell shaped curve [31]. The function, *Φ (Z)*, is defined by:

$$\Phi(Z) = \frac{1}{\sqrt{2\pi}} \int_{-\infty}^{Z} e^{-Z^2/2} dZ \qquad 2.25$$

Rearranging equation 2.24 yields:

$$Z = log\left(\frac{P}{P_{50}}\right)^{\frac{1}{\sigma}} \qquad 2.26$$

In this model the cumulative distribution function, *Φ (Z)*, corresponds to θ or q/q_{max}.

$$\Phi\left[\frac{\log(P) - \log(P_{LM})}{\sigma}\right] = \theta \qquad 2.27$$

From the definition of *Φ (Z)*, θ can be written as:

$$\theta = \frac{q}{q_{max}} = \frac{1}{\sqrt{2\pi}} \int_{-\infty}^{\log\left(\frac{P}{P_{50}}\right)^{1/\sigma}} e^{-Z^2/2} dZ \qquad 2.28$$

Equation 2.28 is the Gaussian isotherm model equation. The value of this integral is tabulated for different values of Z. NORMSDIST and NORMSINV are functions in EXCEL that may be used to calculate *Φ* and Φ^{-1}. From equation 2.28 we can see that three parameters, q_{max}, the standard deviation σ and the 50% adsorbate loading pressure P_{50} are needed to specify the isotherm.

Taking the inverse of the cumulative equation, equation 2.27, gives:

$$\left[\frac{\log(P) - \log(P_{50})}{\sigma}\right] = \Phi^{-1}(\theta) \qquad 2.29$$

Rearranging equation 2.29 gives:

$$\log(P) = \sigma\Phi^{-1}(\theta) + \log(P_{50}) \qquad 2.30$$

A plot of *log (P)* vs. Φ^{-1} should give a straight line with a slope equal to the standard deviation and a y-intercept equal to *log* (P_{50}).

The isostere relation at constant loading describes the relation between the pressure at 50% of the maximum loading and the temperature [32]:

$$P_{50} = a\sqrt{T}e^{-\Delta H_{50}/RT} \qquad 2.31$$

Here, a represents the pre exponential factor and $(-\Delta H_{50})$ is the heat of adsorption at 50% loading. The effect of the square root may be neglected so that the plot of *ln P* vs. *1/T* should yield a straight line with $(-\Delta H_{50}/R)$ as the slope.

At low adsorption loadings, Henry's law region is:

$$K_H = \lim_{p\to 0}\left(\frac{dq}{dP}\right) \qquad 2.32$$

K_H is Henry's law constant.

Given that the adsorption is homogenous, q may be replaced by (θq_{max}) and P by P_{50}* (P/P_{50}) to give:

$$K_H = \frac{q_{max}}{P_{50}}\lim_{P\to 0}\frac{d\theta}{d(P/P_{50})} \qquad 2.33$$

Methane adsorption on 5A zeolite is considered to be homogenous and hence K_H may be calculated from the slope of the plot of θ vs. P/P_{50}.

As stated earlier, the model was tested by collecting data for methane-5A zeolite from six different studies, shown in the Table 2.1. A total of 24 isotherms were used with a temperature range of 185 to 308 K.

Table 2.1: Adsorption studies of methane on 5A zeolite [27].

Reference	**Adsorption Temperature (K)**
Loughlin [33]	185, 230, 273
Loughlin et al. [18]	275, 300, 325, 350
Mentasty et al. [34]	258, 273.3, 283, 298
Rolnaik and Kobayashi [16]	288, 298, 308
Stroud et al. [30]	194.5, 218, 233, 253, 273, 288, 300
Zeuch et al. [35]	273, 298, 308

A previous study done by Loughlin and Abouelnasr [36] found that q_{max}, the maximum zeolite loading, was found to be 8±1 g/100g Z at reduced temperatures above a T_r of 0.83. The latter value is the reduced critical temperature for the adsorbed phase also found from the same study.

Using a value of 9 g /100 gZ for q_{max}, the following results were achieved:
Figure 2.2 shows the linearized isotherms for this system according to equation 2.30. The parallel straight lines indicate an agreement with the linear fit.
The slopes range from 0.83 to 1.13 with a mean of 0.98 and a standard deviation of 0.088. The standard deviation, σ, represented by the slopes is taken to be 1 for all isotherms.

In Figure 2.3, $log\ (P/P_{50})^{1/\sigma}$ is plotted against Φ^{-1}according to equation 2.26. All 24 normalized isotherms are overlaid on a single line taking P_{50} and σ separately for each isotherm. Data are clearly well represented by this straight line as can be seen in the figure.

Another representation for all the data in the 24 isotherms are shown in the S shaped curve on Figure 2.4. The plot is similar to the plot in Figure 2.1 which is for one isotherm at 194.5 K. all data fall perfectly on the S shaped curve in agreement with equation 2.27.

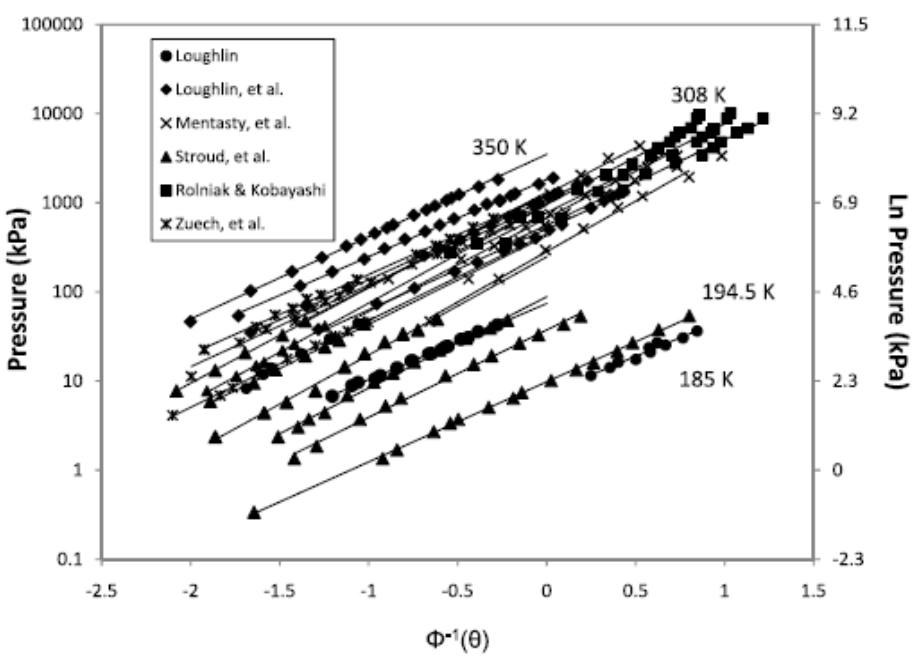

Figure 2.2: Linearized isotherms for methane adsorption on 5A zeolite [27].

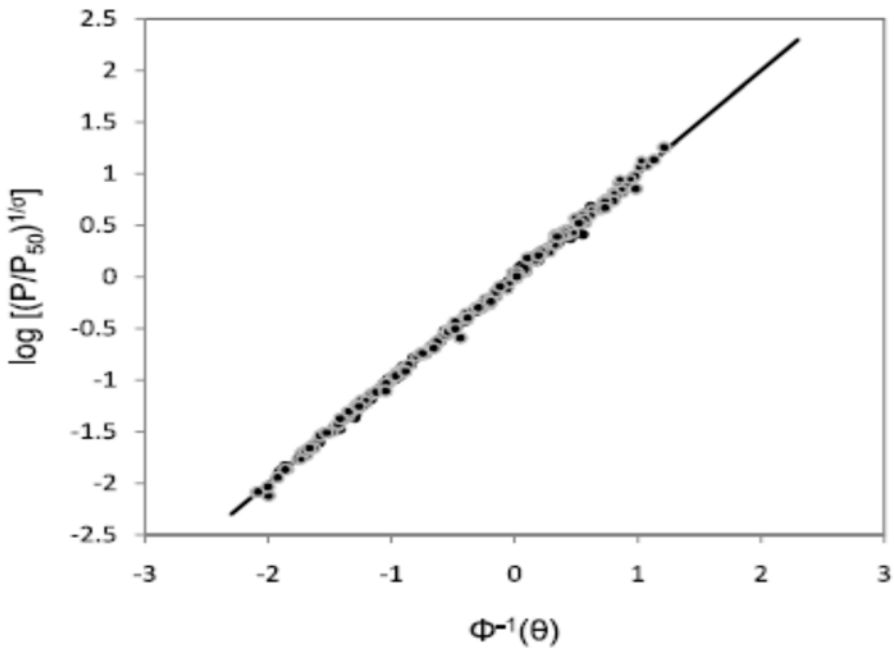

Figure 2.3: Data from 24 methane isotherms overlaid on a single normalized linear isotherm [27].

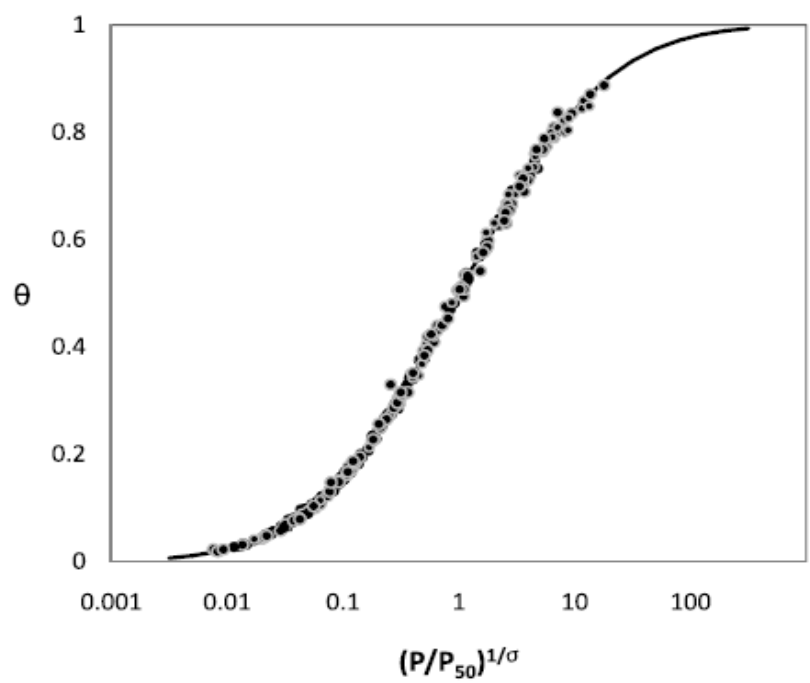

Figure 2.4: Data from 24 methane isotherms, overlaid on a single normalized isotherm graph [27].

According to equation 2.31, neglecting the square root effect, a plot of $\ln P_{50}$ vs. 1/T should have a slope equal to $(-\Delta H_{50}/R)$, the heat of adsorption at 50% loading providing q_{max} is constant as in the case of methane. Abouelnasr and Loughlin found a value of 4.97 kcal/mole for the heat of adsorption [27] and compared it to values reported in a previous study by Loughlin et al. [18]. The values reported were in the range of 4.5-5.12 kcal /mole, which is quiet close to the one calculated by the Gaussian model.

In their paper, Abouelnasr and Loughlin [27] also compared the Gaussian isotherm to two other isotherms, the Langmuir and multi-site Langmuir. Two isotherms were chosen, at 194.5 K and 308 K, from the 24 ones used in this study. Figure 2.5 displays the two isotherms each plotted with the three models. The figures suggests that at 194.5 K both the Langmuir and the MSL models over predict q at high pressures and under predict q at low pressures. At 308 K, both the Gaussian and the MSL model agree with the experimental data unlike the Langmuir model which falls off the models and the data. Figure 2.6 displays the predictions from the Gaussian model and the experimental data from all 24 isotherms, each plotted separately. The Gaussian model seems to be in a very good agreement with the data for most of the isotherms.

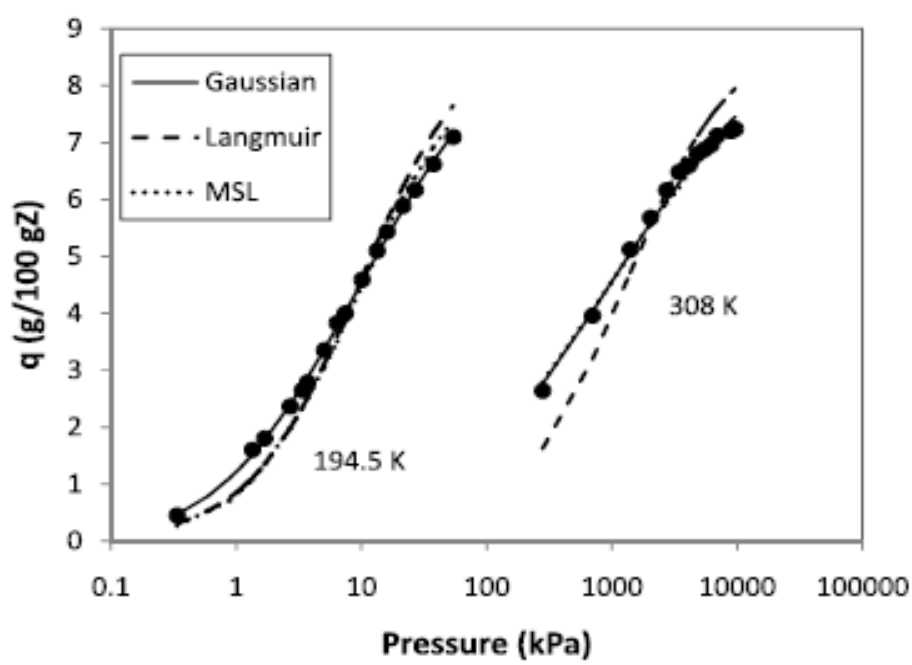

Figure 2.5: Two isotherms of methane adsorption, (194.5K from [30]and 308 K from [35]) [27].

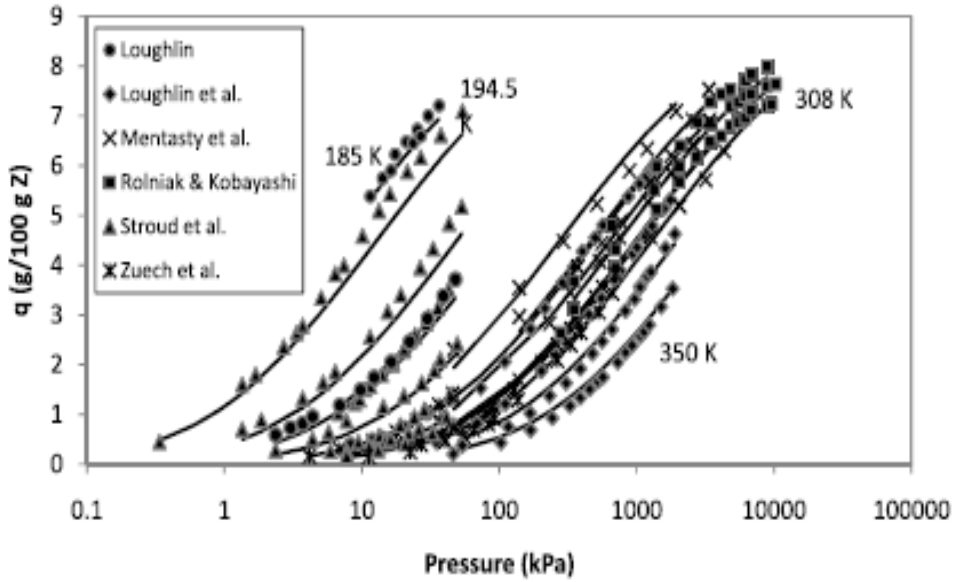

Figure 2.6: Experimental data for 24 isotherms, compared to prediction from Gaussian model [27].

2.3.2 Maximum saturation loading

The maximum saturation loading, or q_{max}, is one of the three parameters needed to specify the isotherms in the Gaussian model. Loughlin and Abouelnasr [36] implemented the Rackett equation combined with crystallographic data for the zeolite in order to evaluate the saturation loading for subcritical n alkanes on 5A zeolites. The saturation density model was derived by starting with the first principle relation:

$$q_{max}\left(\frac{g}{100\ gZ}\right) = 100\,\frac{\rho_{sat}\varepsilon_Z}{\rho_Z} \qquad 2.34$$

In cases where there is a fraction of binder in the pellet, ω, the following relation is used to relate q^*_{max} based on adsorbent to q_{max} based on crystal.

$$q\,*_{max}\left(\frac{g}{100\ gZ}\right) = q_{max}\omega \qquad 2.35$$

The saturation density for subcritical liquids is calculated using the modified Racket equation:

$$V_{sat} = \frac{1}{\rho_{sat}} = \left(\frac{RT_C}{P_C MW}\right) Z_{RA}^{\{1+(1-T_r)^{0.2857}\}} \qquad 2.36$$

where Z_{ra} is a constant specified for the modified Rackett equation; values are listed in the paper by Spencer and Danner [37].

Combining equations 2.34 and 2.36 gives:

$$q_{max}\left(\frac{g}{100\ gZ}\right) = 100\,\frac{\varepsilon_Z}{\rho_Z}\left(\frac{P_C MW}{RT_C}\right) Z_{RA}^{-\{1+(1-T_r)^{0.2857}\}} \qquad 2.37$$

As for supercritical adsorption on alkanes it is important to note that the reduced critical temperature for the adsorbed phase, $T_{CAR,}$ is not taken as 1. This is because the critical region for the adsorbed phase starts earlier than in the case of vapor-liquid systems. According to Loughlin and Abouelnasr [36], the value of T_{CAR} is taken to be 0.975 for alkanes C_3 to C_{18}, whereas for methane and ethane the values of T_{CAR} are taken as 0.83 and 0.96 respectively. Beyond these subcritical temperatures the theoretical value of q_{max} suggested by Loughlin and Abouelnasr [36] was 8±1 g /100gZ.

2.3.3 Predicting adsorption data by the Gaussian model

Using the Gaussian model, Abouelnasr and Loughlin [38] developed predictive criteria for supercritical n alkane adsorption data on 5A zeolite. Adsorption data for nC_1 through nC_{12} was collected from 18 different studies. A total of 63 isotherms were used to test the Gaussian model. Again, three parameters are needed to specify the isotherm, q_{max}, P_{50}, and σ. Abouelnasr and Loughlin [38] followed specified criteria of choosing the participating isotherms in this study. Isotherms were compared with each other and screened to delete any inconsistent data that might have resulted due to capillary condensation effects. Isotherms were also deleted if they did not follow the majority pattern or if they crossed other isotherms. An example would be the data for nC_{10} and nC_{12} as shown in Figure 2.7. The darker lines in the figure are misplaced compared to the rest of the isotherms. Those isotherms belong to nC_{10} and nC_{12} and they are studied separately due to their inconsistency [38]. The isotherm region where $\theta \leq 0.01$ was truncated as the Gaussian model does not apply near Henry's Law region.

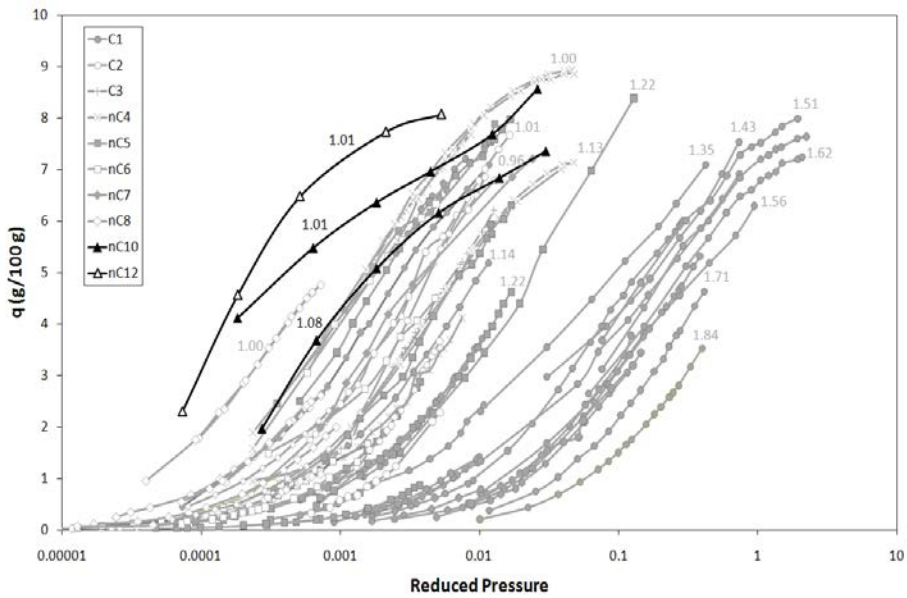

Figure 2.7: Isotherms nC_1 through nC_8 compared to isotherms nC_{10} and nC_{12} [38].

In order to find the value of P_{50} and σ a regression analysis is done. According to equation 2.26, a plot of *log P* vs. Φ^{-1} should yield a slope equal to σ and an intercept equal to $log\ P_{50}$. Equation 2.26 can be written in terms of reduced pressure as well with no change since the critical pressure will cancel from both sides of the equation. Figure 2.8 shows the linearized isotherms from which the parameters are derived for each isotherm. It was found that the average value of sigma is 0.96 with a standard deviation of 0.127 [38]. The regression value started at 0.976 with an average of 0.996 and a standard deviation of 0.005 [38]. This analysis strongly indicates that the model is a strong fit for the data.

Figure 2.9 overlays all isotherms (nC_1 through nC_{10}) on a single characteristic plot of θ vs. $(P_r / P_{50})^{1/\sigma}$. All data points fall perfectly on the S shaped curve, also indicating that the model shows a good representation of the data. In Figure 2.10 n-pentane data were laid over the Gaussian model; both were in a very good agreement.

The isosteres for 50% loading of nC_1 through nC_{10} were plotted in Figure 2.11. The slopes represent the heat of adsorption at 50% loading; summarized in Table 2.2.

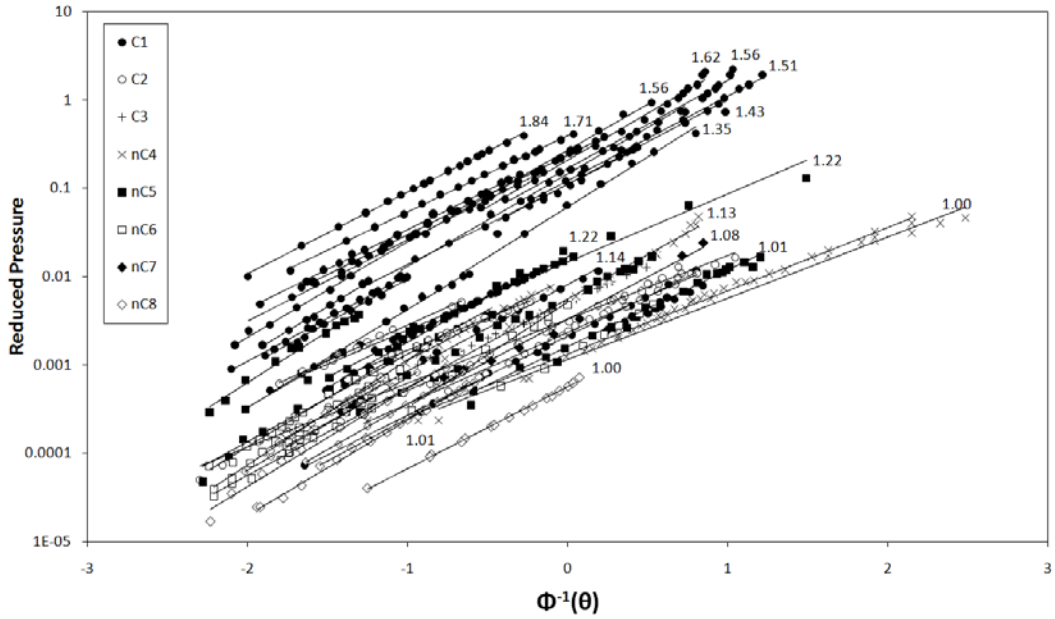

Figure 2.8: Linearized isotherms for nC_1 through nC_8 [38].

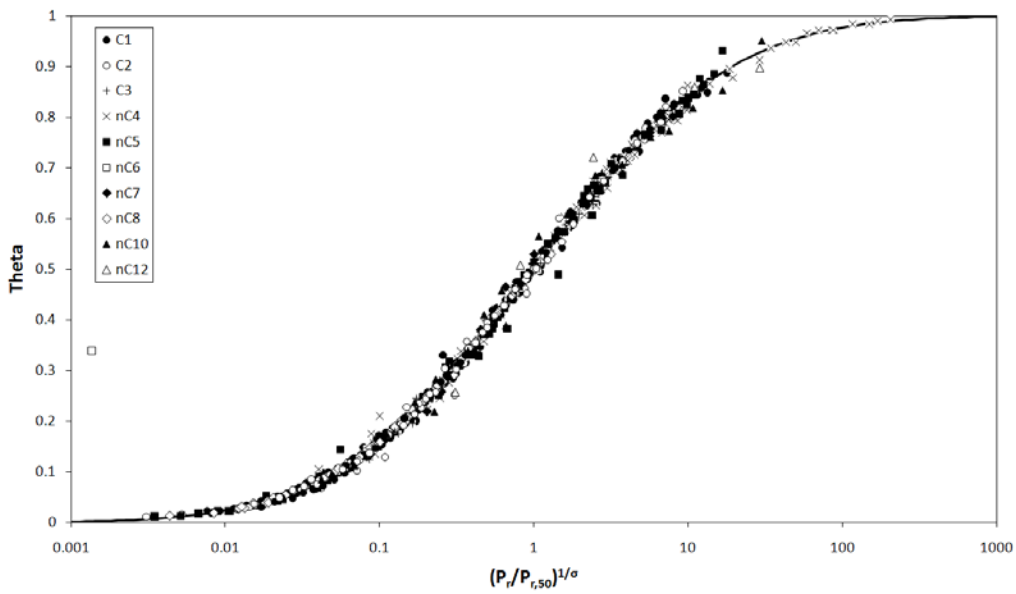

Figure 2.9: Normalized isotherms of nC_1 through nC_{10} [38].

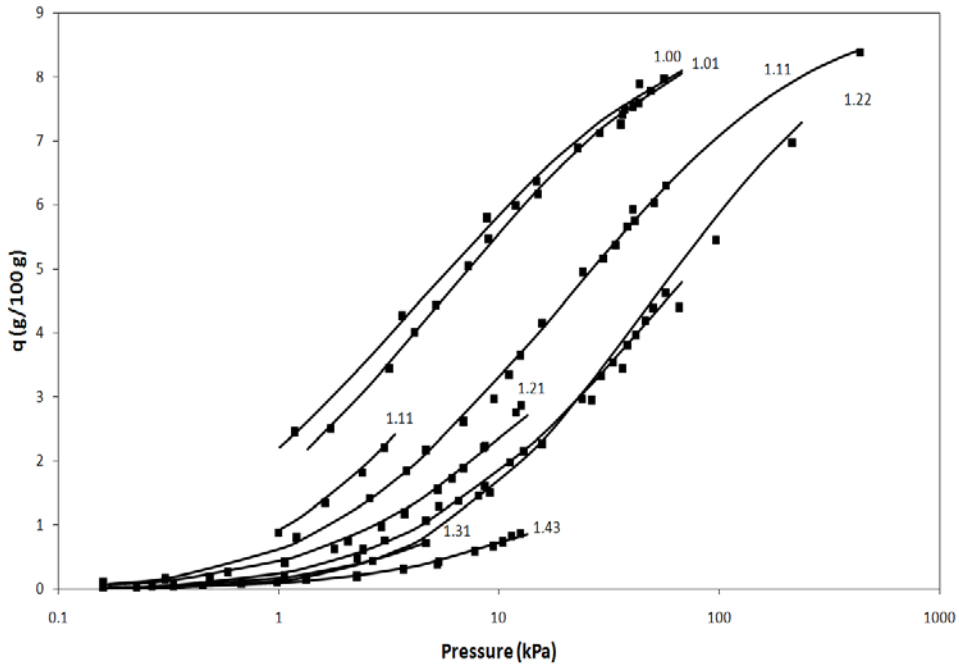

Figure 2.10: Isotherms of n-Pentane overlaid with Gaussian isotherm model [38].

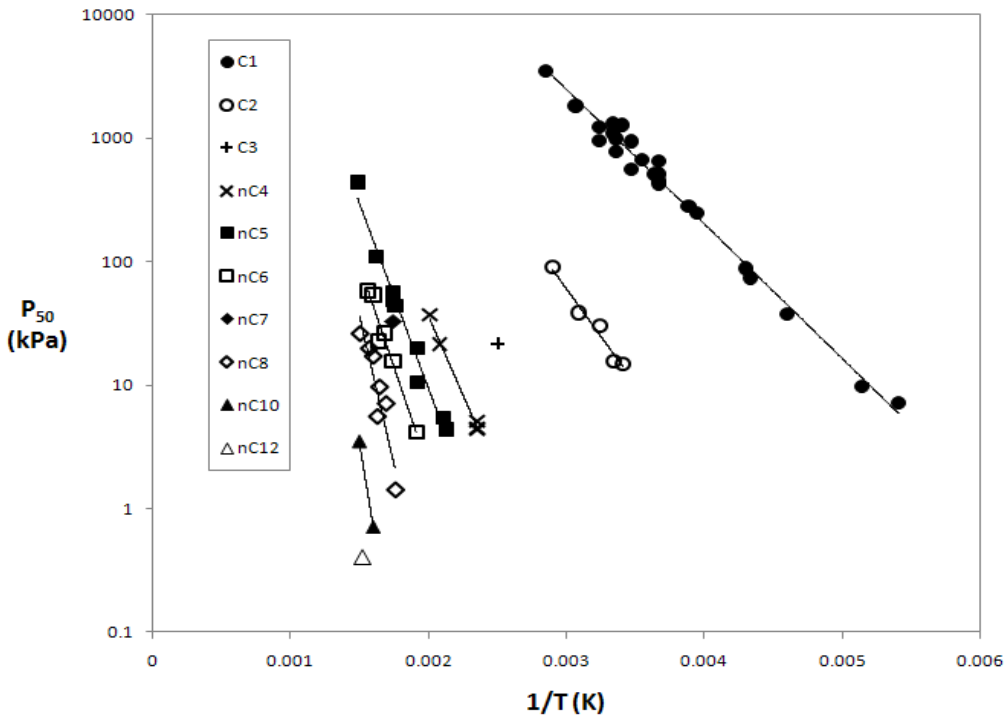

Figure 2.11: Isosteres for 50% loading for nC_1 through nC_{10} [38].

Table 2.2: Heats of adsorption at 50% loading

Carbon Number	$(-\Delta H_{50})$ kcal/mole
1	5.0
2	7.1
3	
4	11.9
5	13.7
6	15.1
7	
8	22.1
10	30.8

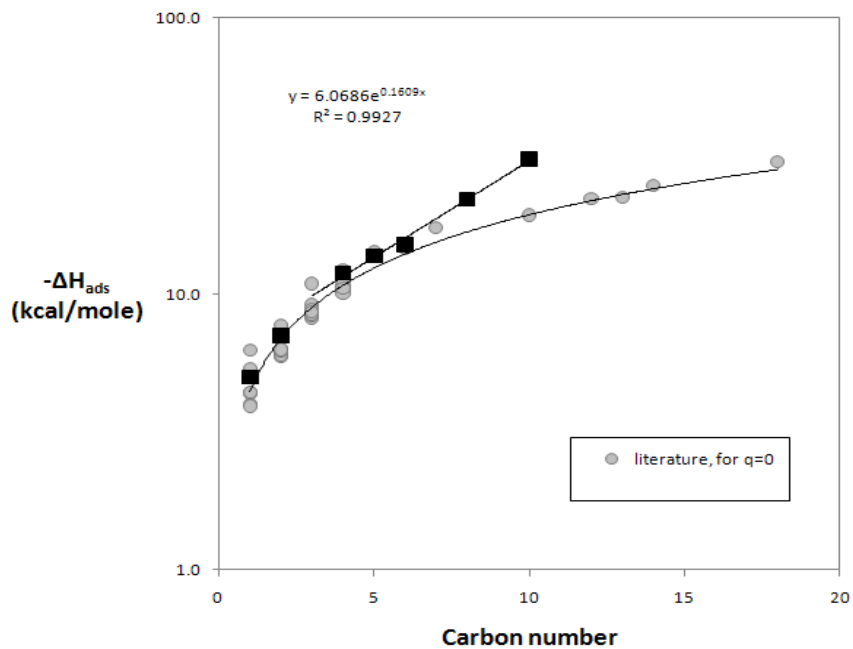

Figure 2.12: Heats of adsorption at 50% loading according to Table 2.2 (dark squares) [38].

The following equation for the heat of adsorption was derived from Figure 2.12 as the best fit equation.

$$(-\Delta H_{50})\, kcal/mol = \begin{cases} 5, & n = 1 \\ 7.1, & n = 2 \\ 6.07\exp(0.16n), & 3 \le n \le 10 \end{cases} \qquad 2.38$$

Similarly a best fit equation was derived for the pre-exponential factor for the isosteres, A:

$$A/P_c = \exp(0.0021n^3 + 0.15n^2 - 0.76n + 7.46) \qquad 2.39$$

where P_c is the critical pressure and n is the carbon number.

Equations 2.38 and 2.39 are used along with equations 2.40 and 2.41 in order to use the Gaussian model in the predictive mode [38]:

$$q = 9\ NORMSDIST\left(\frac{logP - logP_{50}}{\sigma}\right) \qquad 2.40$$

$$P_{r,50} = \frac{A}{P_c} e^{\Delta H_{50}/RT} \qquad 2.41$$

NORMSDIST is an EXCEL function as mentioned earlier. 9 in equation 2.40 is the value of q_{max} for the supercritical n alkane adsorption on 5A zeolite system.

Abouelnasr and Loughlin [38] chose n-pentane to predict its isotherm using the Gaussian model and compare it to the data available, as shown in Figure 2.13.

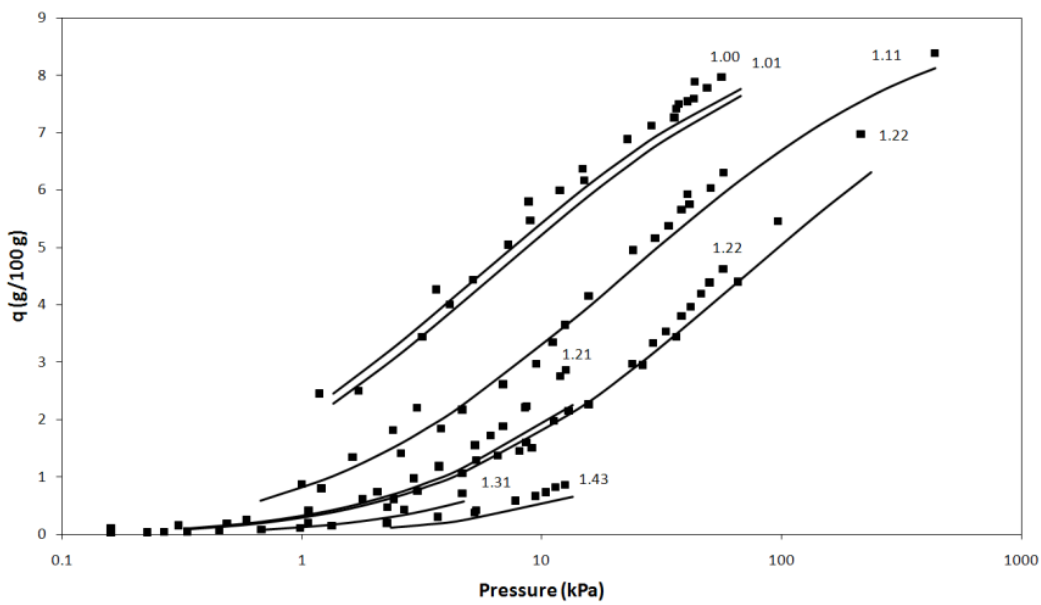

Figure 2.13: Predicted isotherms of n-pentane overlaid with adsorption data [38].

The Gaussian model is an excellent fit to the data proving its validity. Abouelnasr and Loughlin [38] also predicted isotherms for n-decane at temperatures that have not been measured before. Figure 2.14 shows the predicted isotherms for n-decane at T_r =1.01 and 1.08.

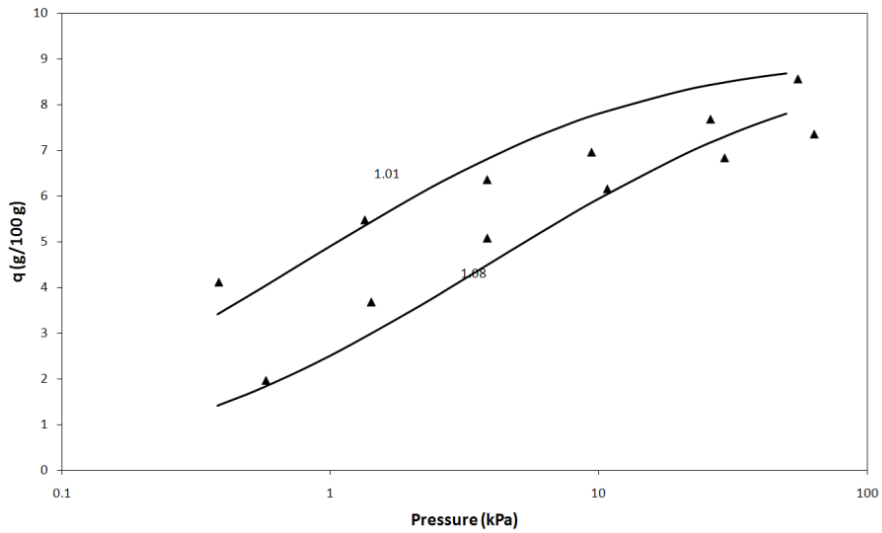

Figure 2.14: Isotherms for n-decane, overlaid with predicted Gaussian isotherm model [38].

2.4 Conclusion

The Gaussian model proved to be a good fit for the supercritical adsorption data of n alkanes from C_1 to nC_{12}. The model is specified by three parameters, q_{max}, P_{50} and σ. In the case of supercritical n alkane adsorption data the value of q_{max} was taken to be 9 g /100 g zeolite. $P_{50}$is the pressure at 50% of the maximum loading and was calculated for each isotherm. σ is the standard deviation for the entire isotherm and was found to be equal to 1 for all supercritical n alkane data. The data conformed to the linear Gaussian model isotherm equation proving its applicability for this type of isotherms.

The Gaussian adsorption isotherm can be used to predict supercritical isotherms for n alkane on 5A zeolite by using the pre defined model parameters, q_{max} and σ, and the correlated parameter for the isostere relation, P_{50}. Finally, the isotherm can predict the adsorption equilibrium data of n alkane /5A zeolite systems. In the next section of this study the Gaussian adsorption model will be evaluated for the following systems:

- Supercritical and subcritical alkanes /13X.
- Supercritical and subcritical alkenes /13X.
- Subcritical aromatics /13X.

CHAPTER 3: Sorption of alkanes on 13X

3.1 Introduction

Data for the adsorption of alkanes on 13X zeolites were gathered from thirteen different studies, listed in Table 3.1, done by different researchers between the years (1957-2010). The isotherms were digitized and systematically evaluated according to the following criteria:

a. In a plot of q vs. $log\ P_r$ all isotherms of a given substance should have the same shape.
b. In the same plot, isotherms should have the same pattern of increasing T_r from left to right as P_r increases.
c. In the same plot, isotherms of the same substance should never cross.

Isotherms that do not meet the criteria were either deleted or truncated to remove any inconsistency that might exist. Table 3.1 lists each study in column 1 and the corresponding alkane and isotherm temperatures in column 2. Isotherms were taken from both supercritical and subcritical regions. Column 3 specifies which isotherms or studies were deleted and the reason for the deletion. The method of adsorption measurement is also represented in column 4. Alkanes included in this study are: nC_1-nC_8, i-C_4, i-C_5, and neo-C_5.

Table 3.1: Data on the adsorption of alkanes on 13X.

Authors	Reduced Temperature	Reason Deleted	Method	% Crystal	Paper
Barrer (1956)	C_1: 0.472, 1.02, 1.43, 1.56 C_2: 0.637, 0.895, 0.976, 1.0, C_3: 0.833, 0.873 n-C_4: 0.701, 0.713, 0.724, 0.736, 0.748, 0.76, 0.771, 0.783, 0.795, 0.807 i-C_4: 0.731, 0.743, 0.755, 0.768, 0.78, 0.792, 0.804, 0.817, 0.829, 0.841 n-C_5: 0.635, 0.645,		Gravimetric & Volumetric	0.8	Ba439(56) [12]

	0.656, 0.667, 0.677, 0.688, 0.698, 0.709, 0.72, 0.73 i-C_5: 0.647, 0.658, 0.669, 0.68, 0.691, 0.702, 0.713, 0.723, 0.734, 0.745 neo-C_5: 0.687, 0.698, 0.71, 0.722, 0.733, 0.745, 0.756, 0.768, 0.779, 0.791 n-C_6: 0.587, 0.597, 0.606, 0.616, 0.626, 0.636, 0.646, 0.656, 0.666, 0.675 n-C_7: 0.552, 0.561, 0.57, 0.579, 0.589, 0.598, 0.607, 0.616, 0.626, 0.635 i-C_8: 0.548, 0.557, 0.566, 0.576, 0.585, 0.594, 0.603, 0.612, 0.622, 0.631 n-C_8: 0.55, 0.568, 0.586, 0.603				
Cavenate and Grande (2004)	C_1: 1.56, 1.62, 1.69	Deleted because they are crossing all other C_1 isotherms	Gravimetric	0.83	Ca1095(04) [39]
Da Silva (1999)	C_3:0.819, 0.873, 0.927, 1.01, 1.14, 1.28		Magnetic Suspension Microbalance	0.83	Si2051(99) [22]
Granato and Rodrigues (2007)	C_3:0.819, 0.873, 0.927, 1.01, 1.14, 1.28	All are deleted since the reference does not exist	Packed Bed Column	0.8	Gr7239(07) [40]
Hyun and Danner (1982)	C_2: 0.895, 0.977, 1.06, 1.22 iC_4: 0.731, 0.792, 0.915		Volumetric	0.8	Hy196(82) [17]
Lamia (2007)	C_3: 0.9, 0.954, 1.01, 1.06 iC_4: 0.817, 0.866, 0.915, 0.964		Magnetic Suspension Microbalance	0.83	La2539(07) [25]

Loughlin (1990)	C_1: 1.44, 1.57, 1.71, 1.84 C_3: 0.744, 0.811, 0.879, 0.946		Volumetric	0.8	lo1535(90) [18]
Lopes and Grande (2010)	C_1: 1.59, 1.62, 1.69	Deleted because percentage binder is not available	Magnetic Suspension Microbalance	N/A	lo184(10) [27]
Paul and Riki (1980)	C_1: 1.51, 1.56, 1.62		Packed Bed Column	0.8	Pa616(80) [16]
Ruthven (1976)	nC_7: 0.757, 0.809, 0.848, 0.903		Cahn Vacuum Microbalance	crystal	Ru882(76) [15]
Salem (1998)	C_1: 1.35, 1.43, 1.51, 1.62, 1.67		Gravimetric	0.8	Sa3376(98) [21]
Vermesse (1996)	C_1: 1.56		Volumetric	0.83	Ve4190(96) [41]
Zhdanov (1962)	nC_6: 0.587	The pelleted isotherms for n-C_6 are deleted since they are inconsistent in position.	McBain-Back balance	0.8, crystal	Zh445(62) [14]

3.2 Methane

Figure 3.1 shows methane isotherms taken from six different studies: Salem et al. [21], Barrer and Sutherland [12], Loughlin et al. [18], Paul et al. [16], Cavenati et al. [39] and Vermesse et al. [41]. A pelleted sample with 20% binder content was used in all studies. The isotherms start at a T_r of 0.47, on the left hand side of the graph, to a T_r of 1.84 on the right hand side. As seen in Figure 3.1 the isotherm at T_r =1.565, taken from Vermesse et al. [41], was measured at a pressure range that is different than the other studies. The isotherm could not be verified and therefore was omitted. In addition, Data from Cavenati et al. [39] show visible inconsistency with the rest of the data. Those isotherms appear to be crossing the rest of isotherms and hence were deleted. The Barrer and Sutherland [12] isotherm at T_r =0.472 exhibits capillary condensation as can be seen from the convex points at the higher pressures. In order to eliminate that, the convex points were deleted. Figure 3.2 shows all the isotherms after screening which are consistent and does not cross at any point.

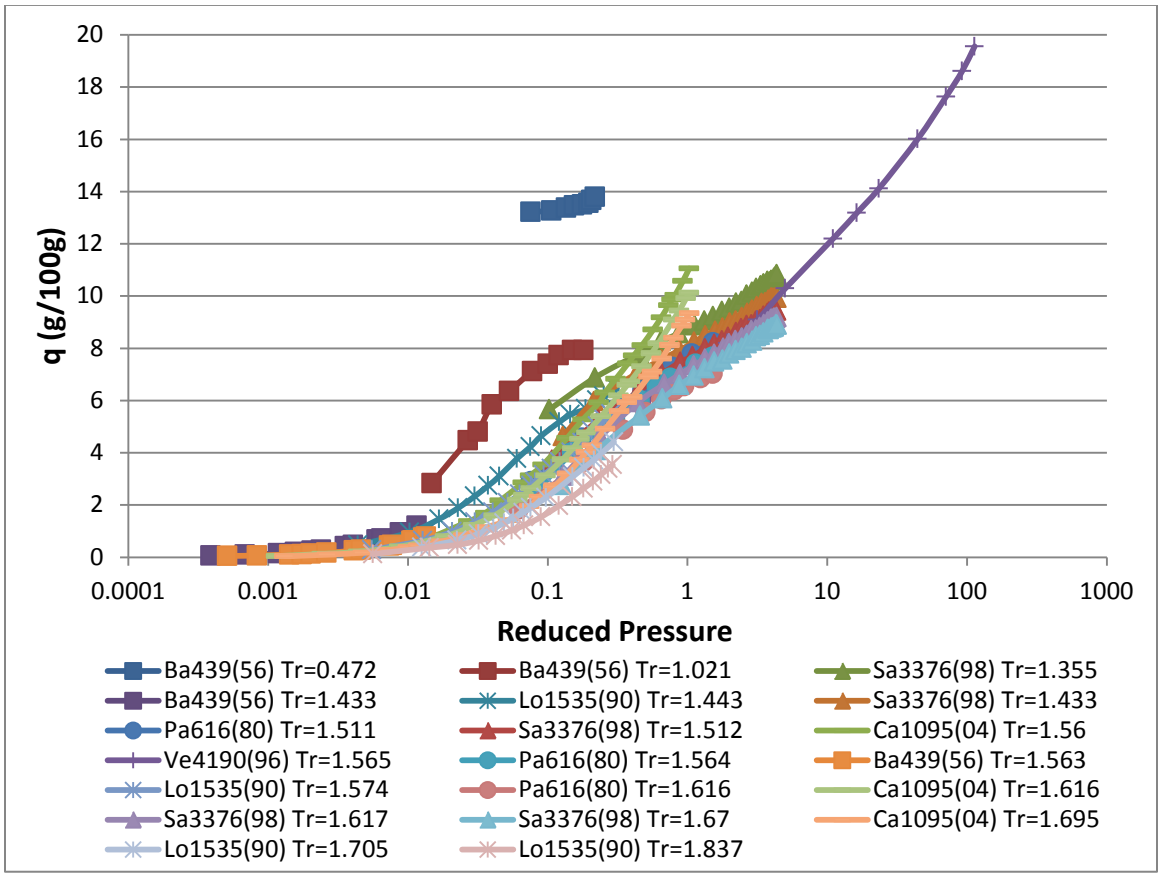

Figure 3.1: Isotherms for methane on 13X (before screening).

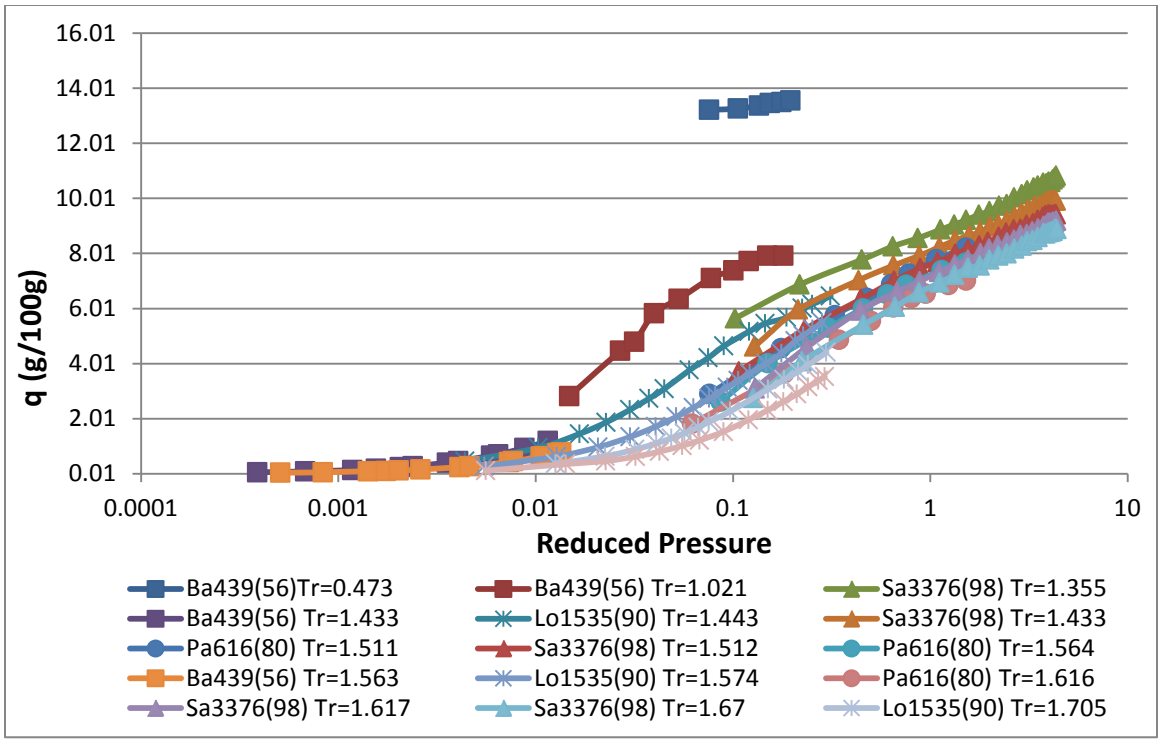

Figure 3.2: Isotherms for methane on 13X (after screening).

Data for methane were mainly in the supercritical region, $T_r > 0.83$, except for one isotherm at $T_r = 0.472$. The maximum saturation loading was taken equal to 12 g /100g Z. The linearized probability plot of reduced pressure P_r vs. $\Phi^{-1}(\theta)$ is shown in Fig. 3.3 for all the screened isotherms of methane ranging from a T_r of 0.472 to 1.873. The isotherms are perfectly linear and parallel with increasing T_r from right to left. The slopes of these isotherms, σ, are plotted as a function of reduced temperature in Figure 3.4. The values, as shown in the Figure, oscillate around 1 for all the isotherms from all the studies which indicates a good agreement with the model. Methane isosteres are constructed by plotting the y-intercept of the linearized isotherms, log P_{r50}, as a function of 1 /T_r, shown in Figure 3.5. All isotherms are included except the subcritical isotherm from Barrer and Sutherland [12] because it is the only subcritical temperature and, hence, it lies outside the range of the other isotherms. All lines show a good linear fit and they appear to be parallel with each other.

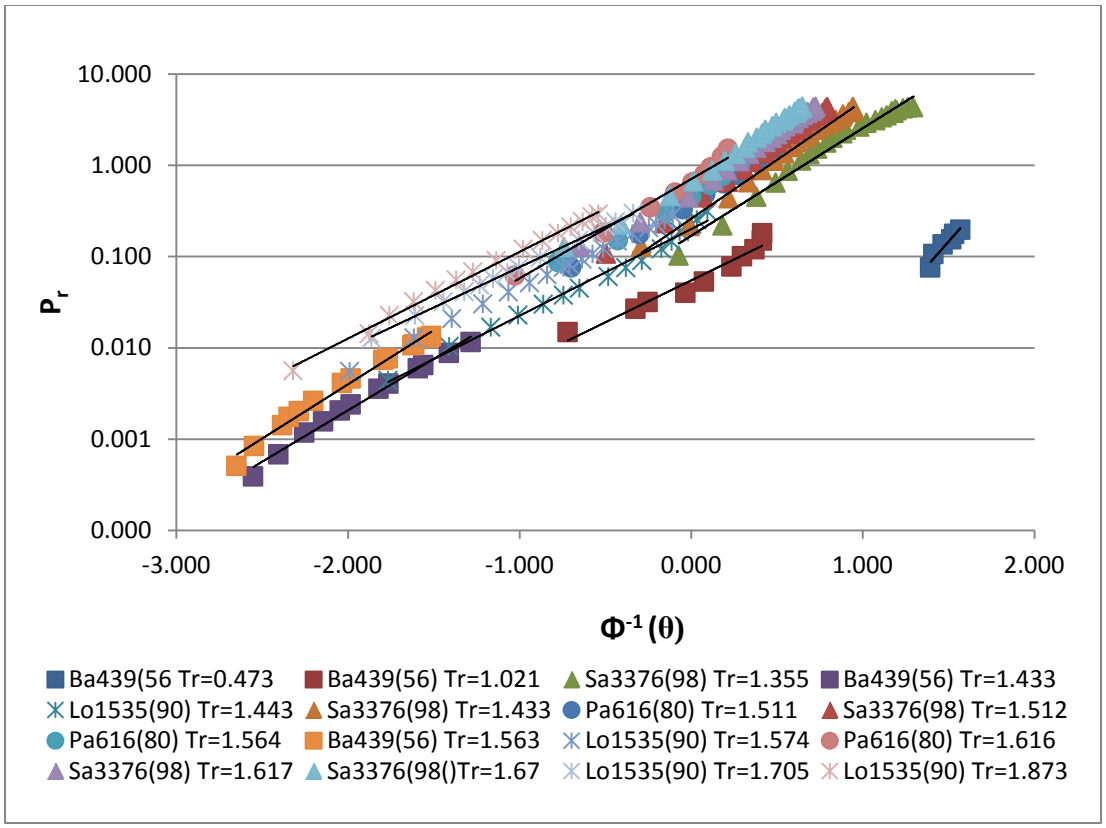

Figure 3.3: Linearized isotherms for methane on 13X.

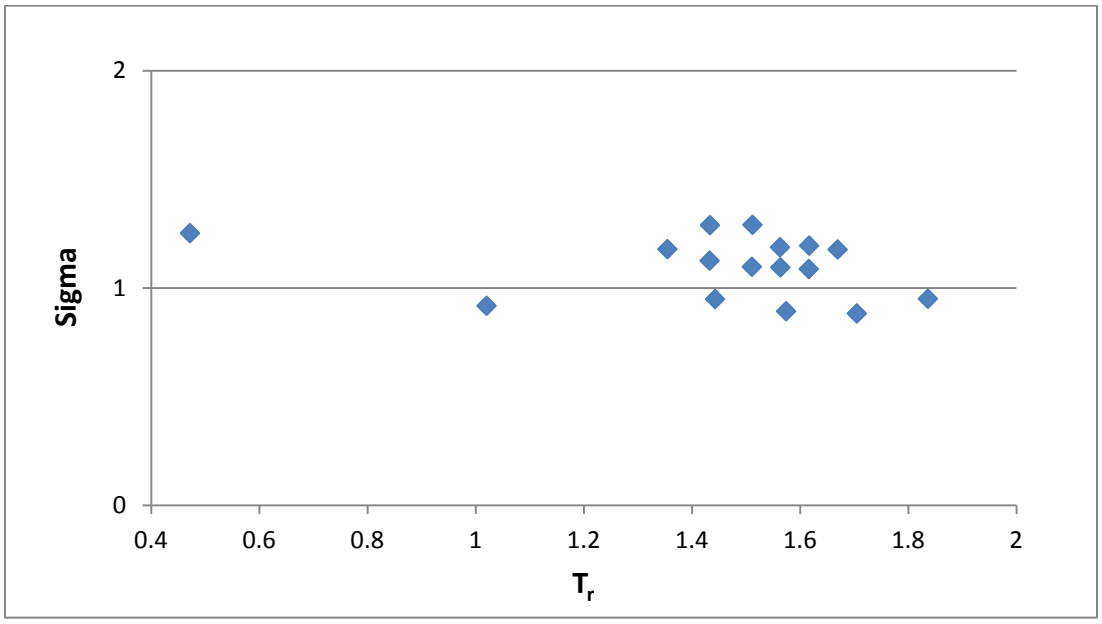

Figure 3.4: Sigma, the slope of the linearized isotherms, as a function of reduced temperature, for methane.

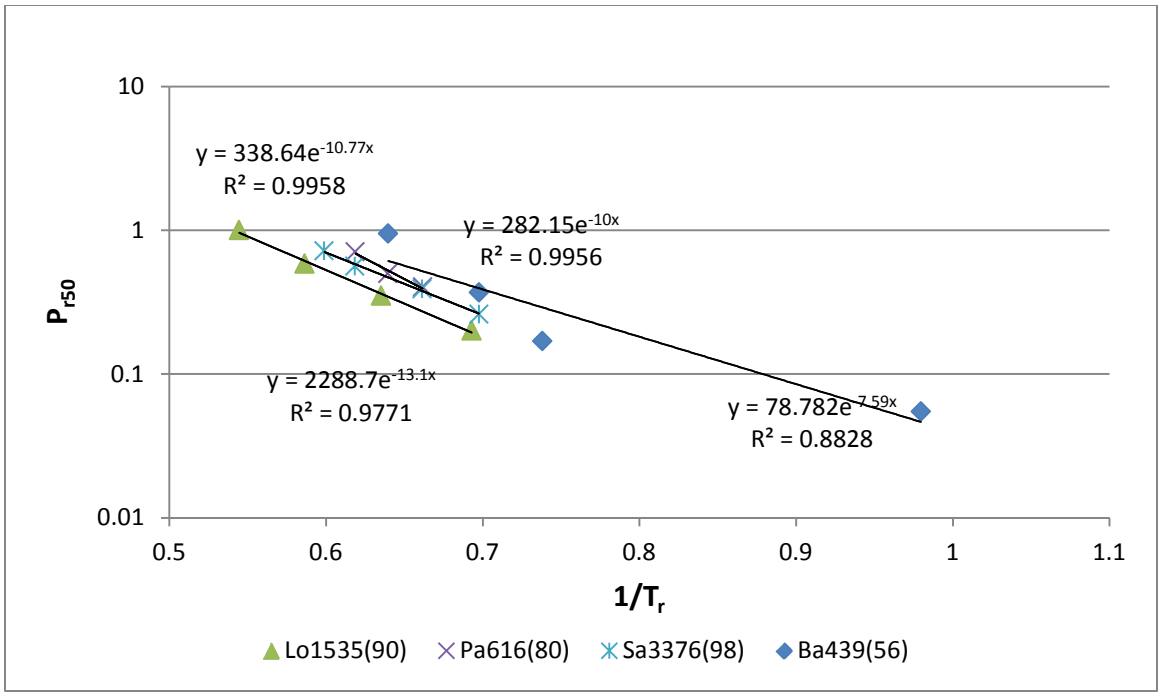

Figure 3.5: log Pr_{50} vs. $1/T_r$ for methane on 13X.

The slopes of the isosteres represent the heat of adsorption at 50% loading *(-ΔH_{50})*. In order to calculate the value of the slope of Figure 3.6 is used along with the following isostere relation:

$$P_{50} = ae^{-\Delta H_{50}/RT} \qquad 3.1$$

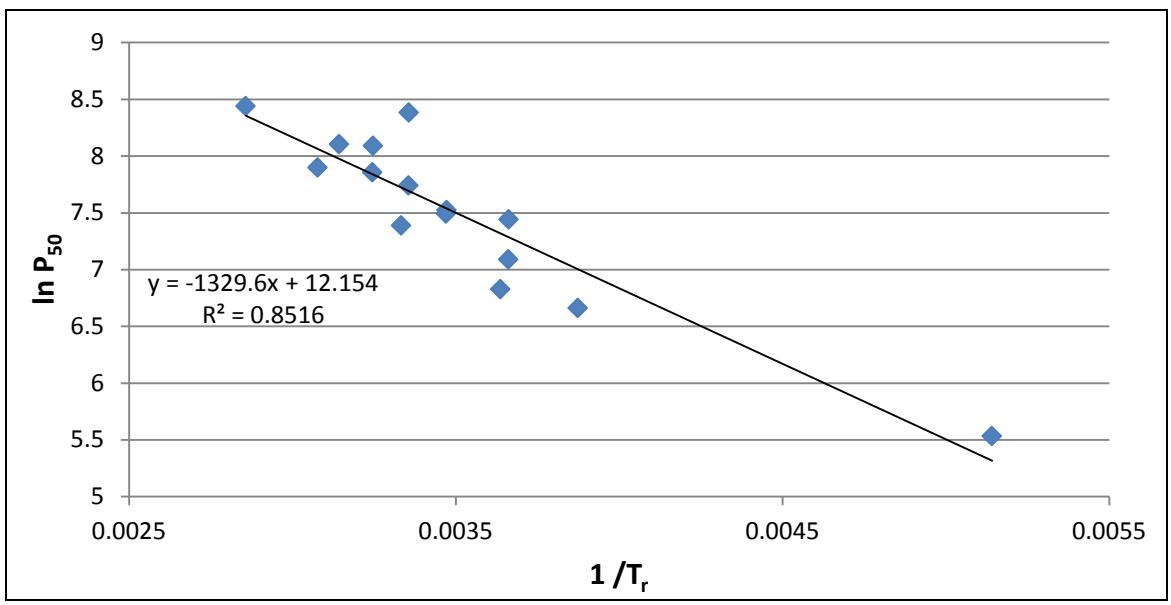

Figure 3.6: ln P_{50} vs. 1/T for methane on 13X.

$$\ln P_{50} = \frac{-\Delta H_{50}}{R} * \frac{1}{T} + \ln a \quad 3.2$$

$$slope = \frac{-\Delta H_{50}}{R} = -1329.6 \quad 3.3$$

$$R = 1.98 * 10^{-3}\ kcal/mole.K \quad 3.4$$

$$-(\Delta H_{50}) = 1329.6 * 1.98 * 10^{-3} = 2.63\ kcal/mol. \quad 3.5$$

$$Intercept = \ln a = 12.15 \quad 3.6$$

$$a = e^{12.15} = 1.89 * 10^{5} \quad 3.7$$

Table 3.2: Values of ($-\Delta H_{ads}$) for methane.

$-\Delta H_{50}$ (kcal /mol)	$-\Delta H_{0lit.}$ (kcal /mol)	a
2.63	5.12 [18]	1.89E+05

The value of the heat of adsorption at 50% loading of methane is compared to the value at 0% loading taken from the study of Loughlin et al. [18]. The value calculated by the Gaussian model is less than the one found in literature. This result is expected as the heat of adsorption is different at different loadings and it is expected to decrease at higher loadings for 13X.

3.3 Ethane

Data for ethane adsorption were collected from Hyun and Danner [17] and Barrer and Sutherland [12] for a T_r range of 0.637, on the right hand side of the plot, to 1.22 on the left, as shown in Figure 3.7. Both subcritical and supercritical isotherms were considered in the study. The data appear to be consistent with increasing T_r from right to left. One isotherm from Barrer and Sutherland [12] at T_r =1.0 comes before an isotherm from Hyun and Danner [17] at T_r =0.977. It is not known which one is out of place; therefore, both isotherms were retained.

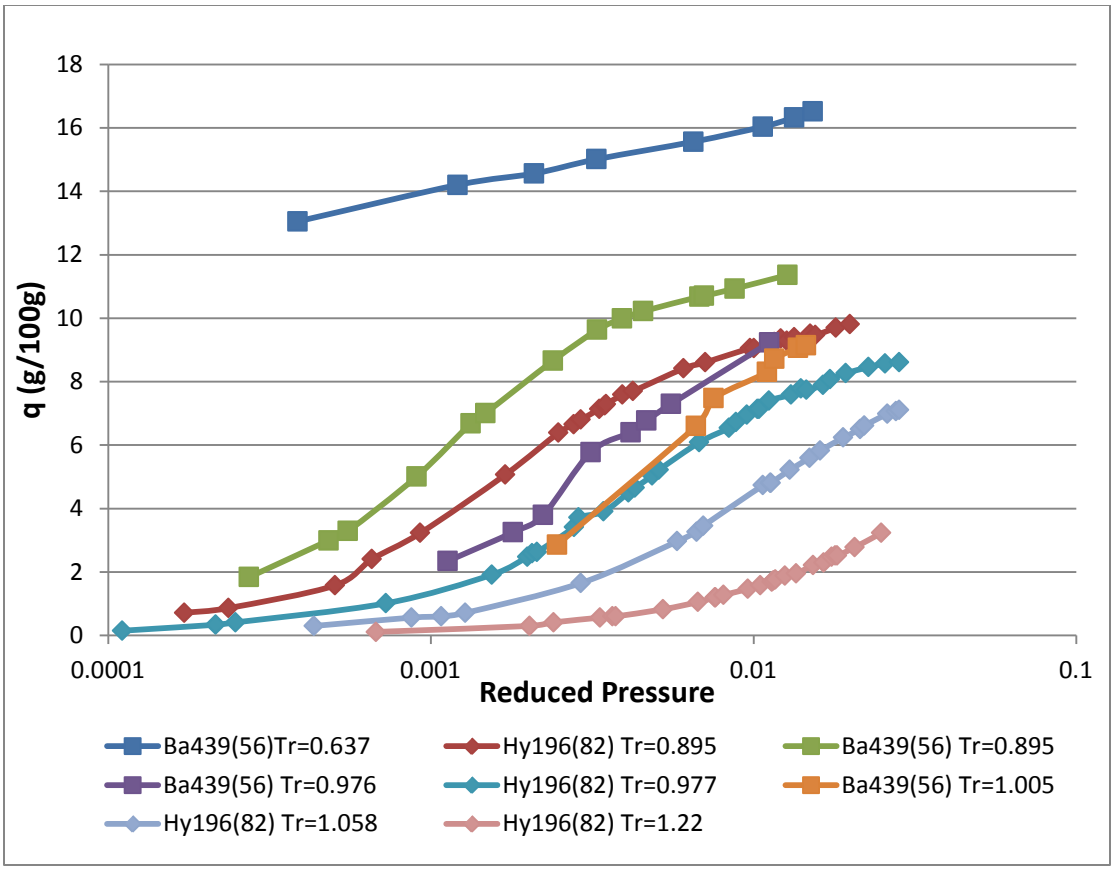

Figure 3.7: Isotherms for ethane on 13X.

The maximum saturation loading of ethane on 13X at supercritical temperatures is taken as 12 g /100g. Ethane linearized isotherms are shown in Figures 3.8 and 3.9 for subcritical and supercritical temperatures, respectively. The two subcritical isotherms at T_r =0.895 in Figure 3.8 are in agreement with each other where they show a good linear fit and end with a small curvature at the same place. The isotherm at T_r =0.637 is also linear and exhibit some curvature at the end but in an inward direction. As for the supercritical isotherms in Figure 3.9, the lines are remarkably straight and consistent with each other except for one isotherm at T_r =1 from Barrer and Sutherland [12] as it can be seen overlaying the isotherm at T_r =0.977. The slopes of the linearized isotherms, σ, are plotted as a function of reduced temperature for both supercritical and subcritical data in Figure 3.10. The values lie between 0.5 and 1 except at T_r =0.637 it goes up to 1.3.

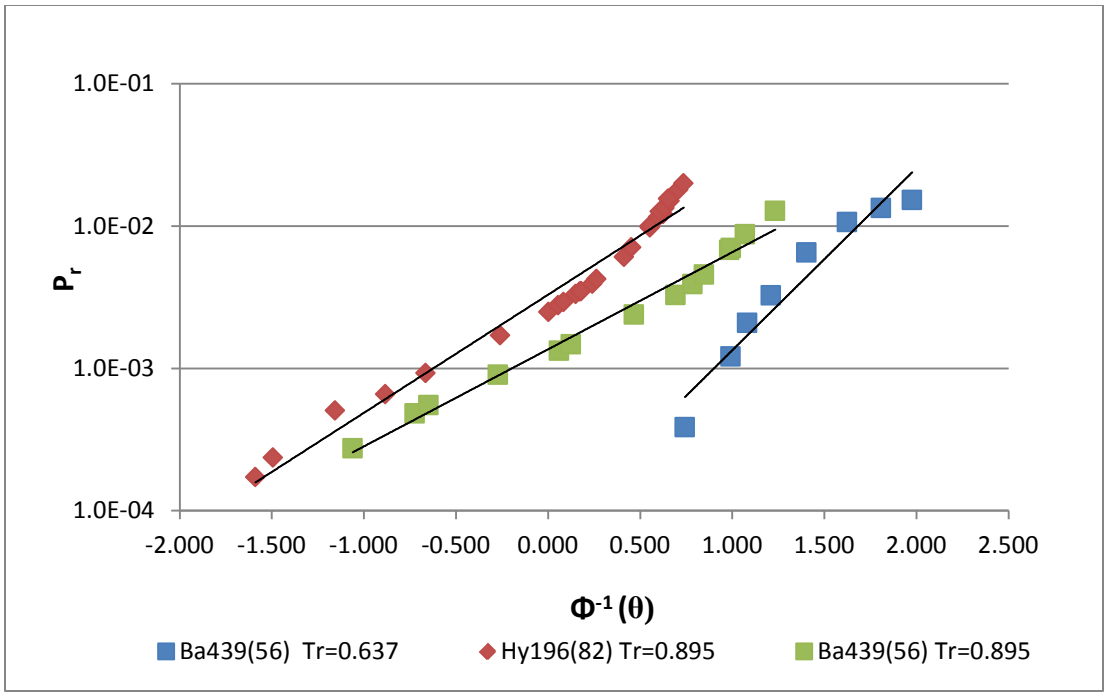

Figure 3.8: Linearized isotherms for ethane on 13X at subcritical temperatures.

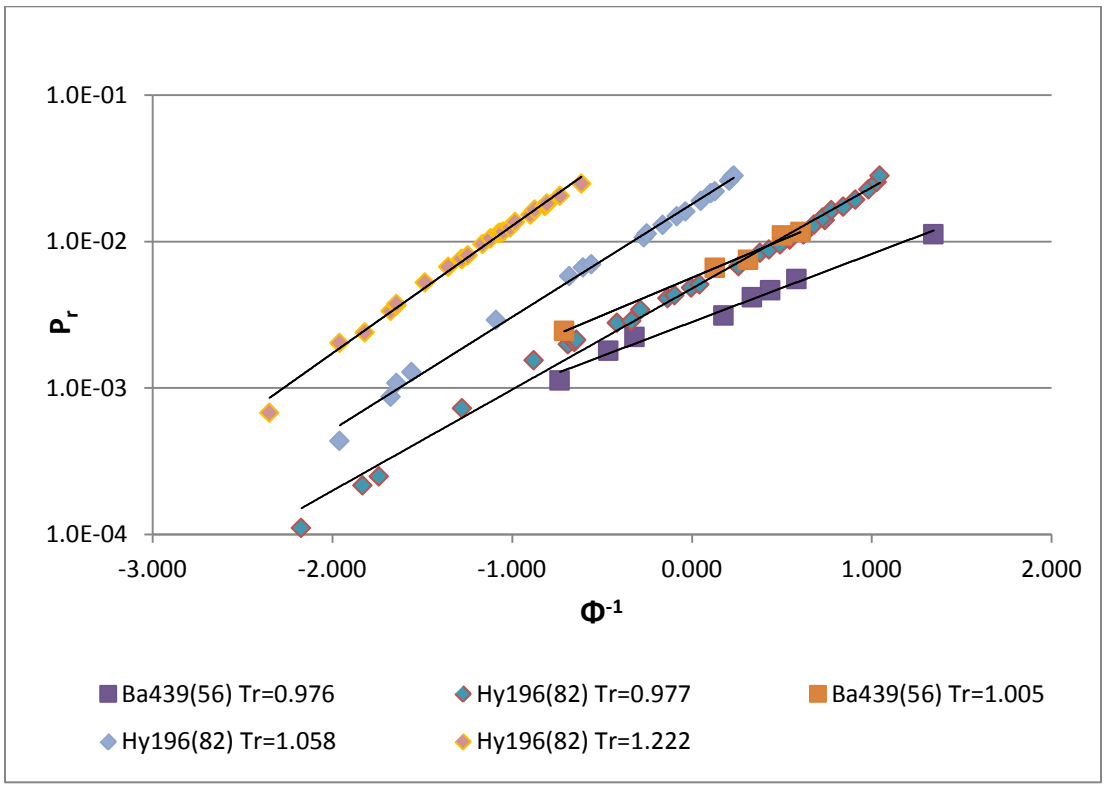

Figure 3.9: Linearized isotherms for ethane on 13X at supercritical temperatures.

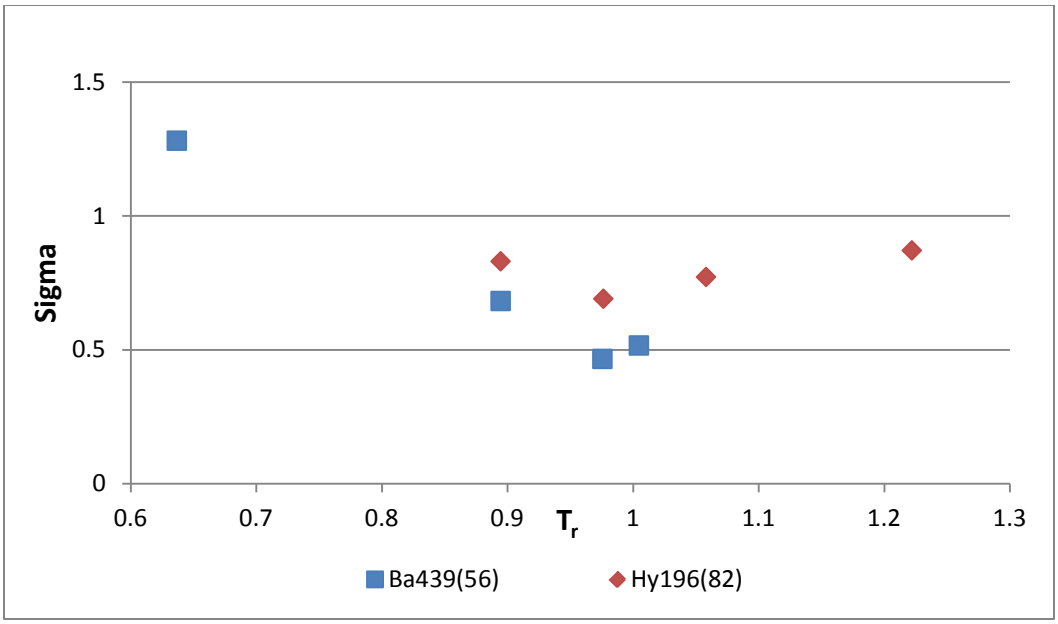

Figure 3.10: Sigma, the slope of the linearized isotherms, as a function of reduced temperature, for ethane on 13X.

Plotting the y-intercept of the linearized isotherms, *log* P_{r50}, as a function of $1/T_r$, shown in Figure 3.5, generates constant θ lines that are analogous to the constant loadings P_{r50} lines (isosteres). This is because data from the subcritical region are included and hence q_{max} is changing according to the Rackett equation leaving only the ratio q/q_{max} (or θ) at a constant value of 0.5.Isosteres on the other hand should be at a constant loading, q. Constant θ lines at 50% loading of ethane on 13X are shown in Figure 3.11. The lines are linear and consistent with each other.

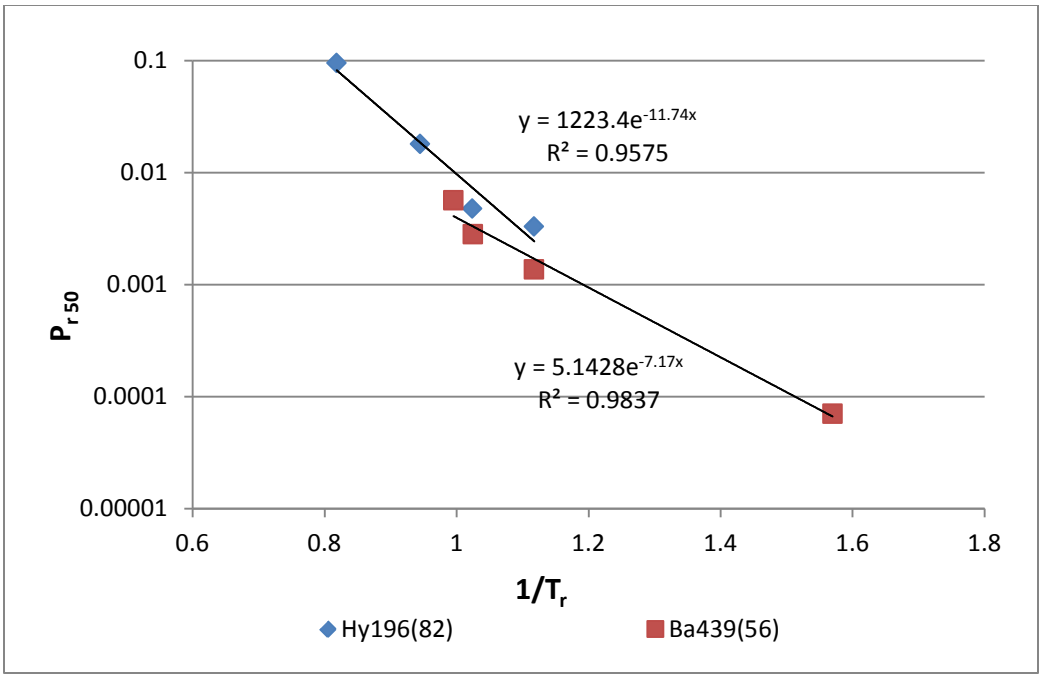

Figure 3.11: log P_{r50} vs. $1/T_r$ for ethane on 13X.

The slope of the constant theta lines in Figure 3.12 is used to calculate the heat of adsorption at 50% loading. The intercept is used to calculate the pre-exponential factor, a.

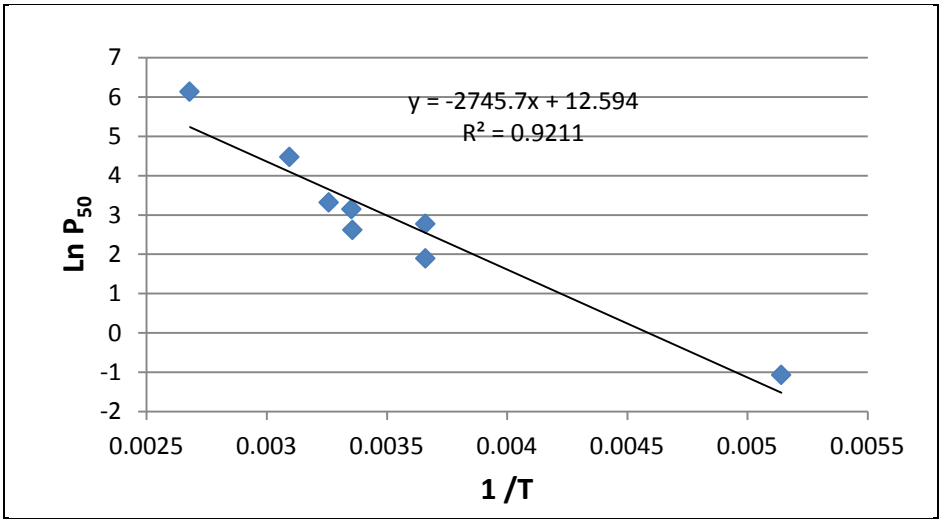

Figure 3.12: ln P_{50} vs. 1/T for ethane on 13X.

$$-(\Delta H_{50}) = 2745 * 1.98 * 10^{-3} = 5.4\ \ kcal/mol. \quad 3.8$$

$$a = e^{11.59} = 2.93 * 10^{5} \quad 3.9$$

Table 3.3: Values of ($-\Delta H_{ads}$) for ethane on 13X.

$-\Delta H_{50}$ (kcal /mol)	$-\Delta H_{0lit.}$ (kcal /mol)	a
5.43	5.97 [17]	2.93E+05

The value of the heat of adsorption at 50% loading of ethane is compared to the value at 0% loading taken from Hyun and Danner [17]. The value calculated by the Gaussian model is slightly less than the one found in literature.

3.4 **Propane**

Propane isotherms are shown in Figure 3.13. Data were collected from several studies: Lamia et al. [25], Loughlin et al. [18], Da Silva and Rodrigues [22], and Barrer and Sutherland [12]. Isotherms were both in subcritical and supercritical regions with a T_r range of (0.74-1.28) T_r. As shown in Figure 3.13, the isotherms exhibit the same behavior. The temperatures increase from right to the left gradually and consistently. Therefore, all isotherms from the mentioned studies are retained with no truncation or deletion.

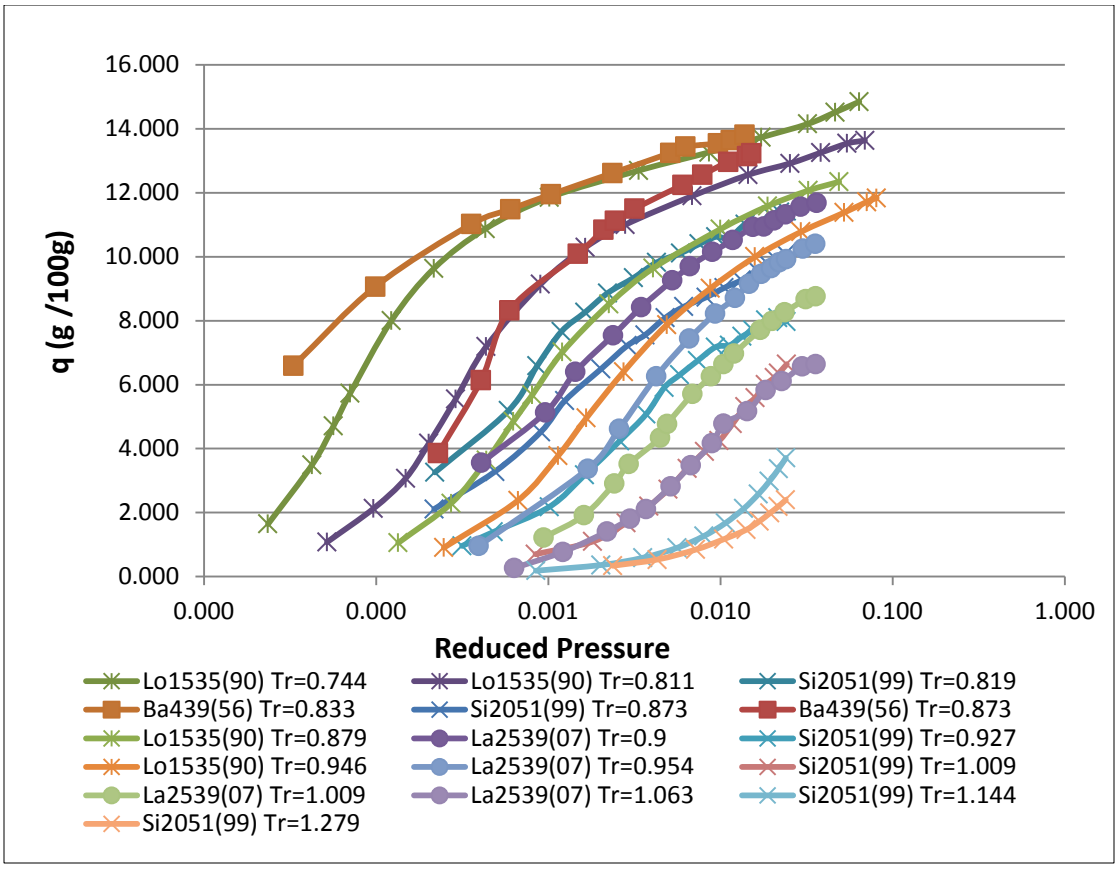

Figure 3.13: Isotherms of propane on 13X.

The maximum saturation loading of propane on 13X at supercritical temperatures is taken as 12 g /100g. Linearized isotherms of propane are shown in Figures 3.14 and 3.15 for subcritical and supercritical temperatures, respectively. The subcritical linearized isotherms, in Figure 3.8, range from T_r =0.744 to T_r =0.954 and include four different studies. Comparing them to each other, the temperature does not increase in a consistent manner. The shapes, on the other hand are similar for more than one study. For example, comparing the isotherms from Da Silva and Rodrigues [22] and Loughlin et al. [18], and some of the isotherms from Barrer and Sutherland [12], one can see that they are both concaved up in the same manner. As for the supercritical isotherms in Figure 3.15, the lines are remarkably straight and consistent with each other as T_r is increasing in the right direction, from left to right. The slopes of the linearized isotherms, σ, are plotted as a function of reduced temperature for both supercritical and subcritical data in Figure 3.16. The values are closer to 1 in the supercritical region while as we go towards lower subcritical temperature, the sigma goes up to 1.5 or slightly higher.

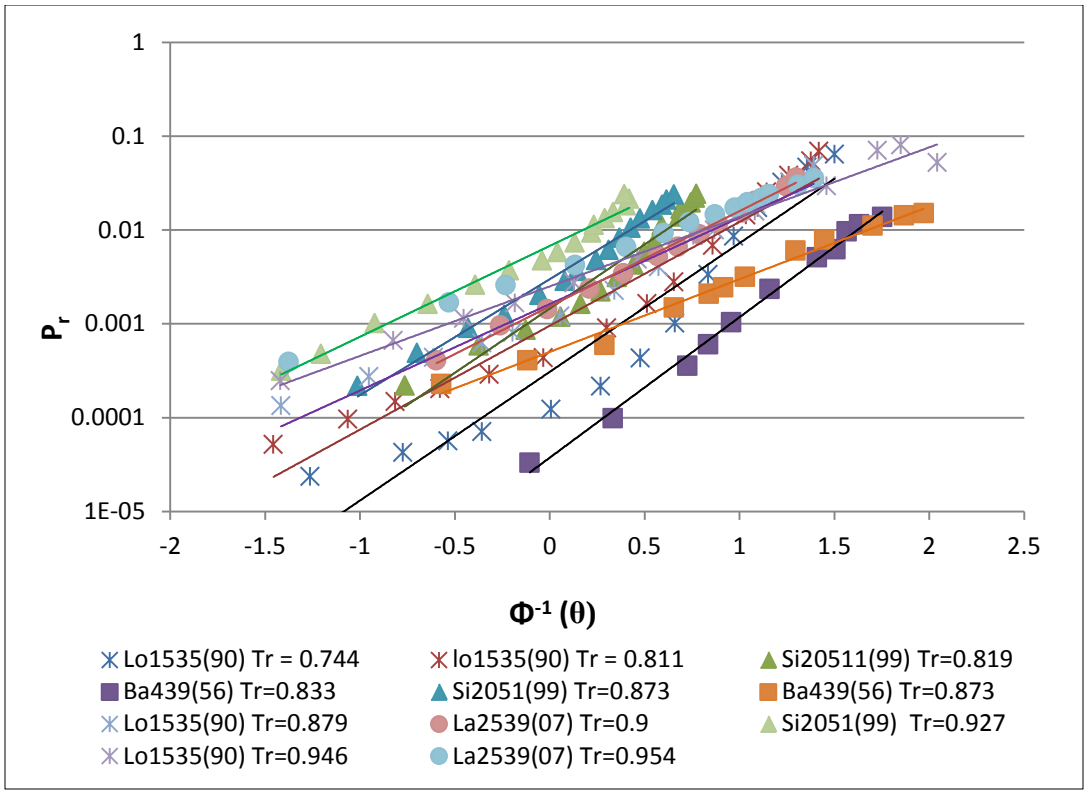

Figure 3.14: Linearized isotherms for propane on 13X at subcritical temperatures.

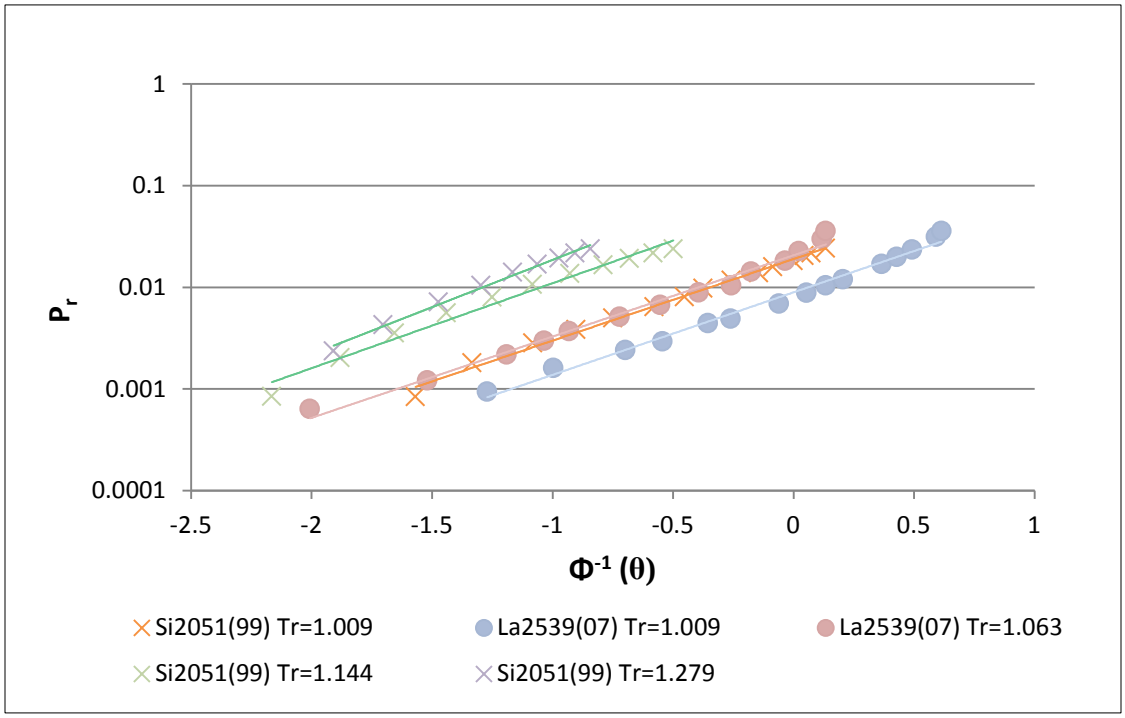

Figure 3.15: Linearized isotherms for propane on 13X at supercritical temperatures.

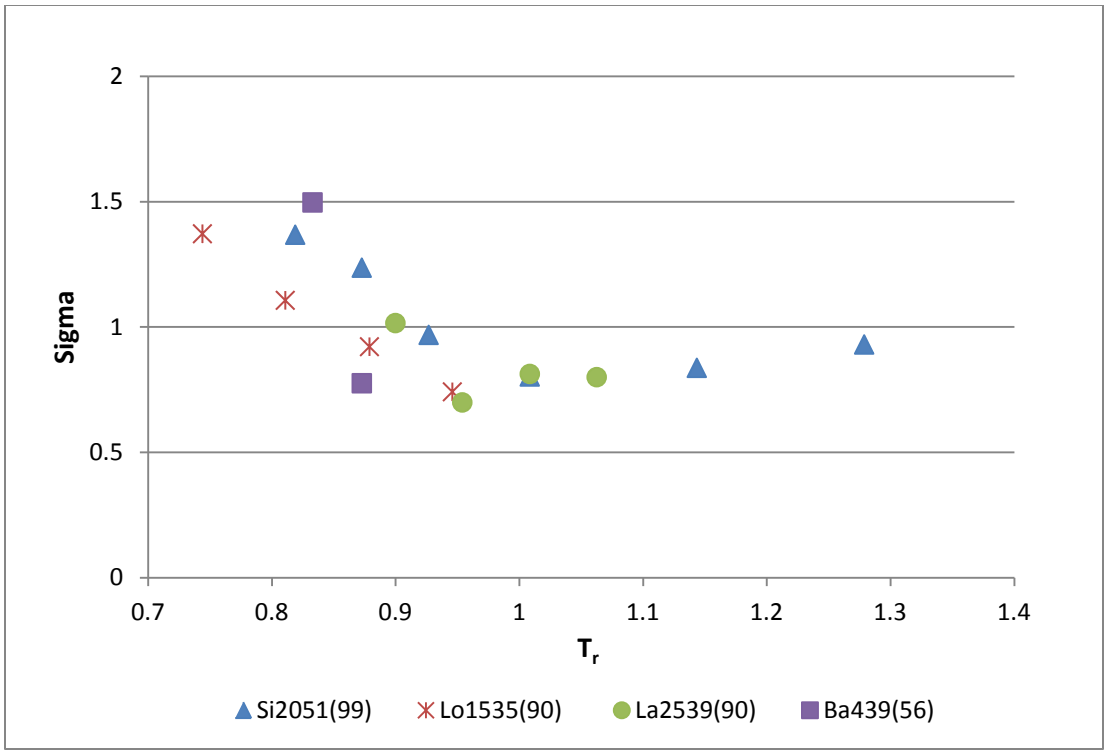

Figure 3.16: Sigma, the slope of the linearized isotherms, as a function of reduced temperature, for propane on 13X.

The constant θ lines at 50% loading of propane on 13X are shown in Figure 3.17. The lines are linear and consistent.

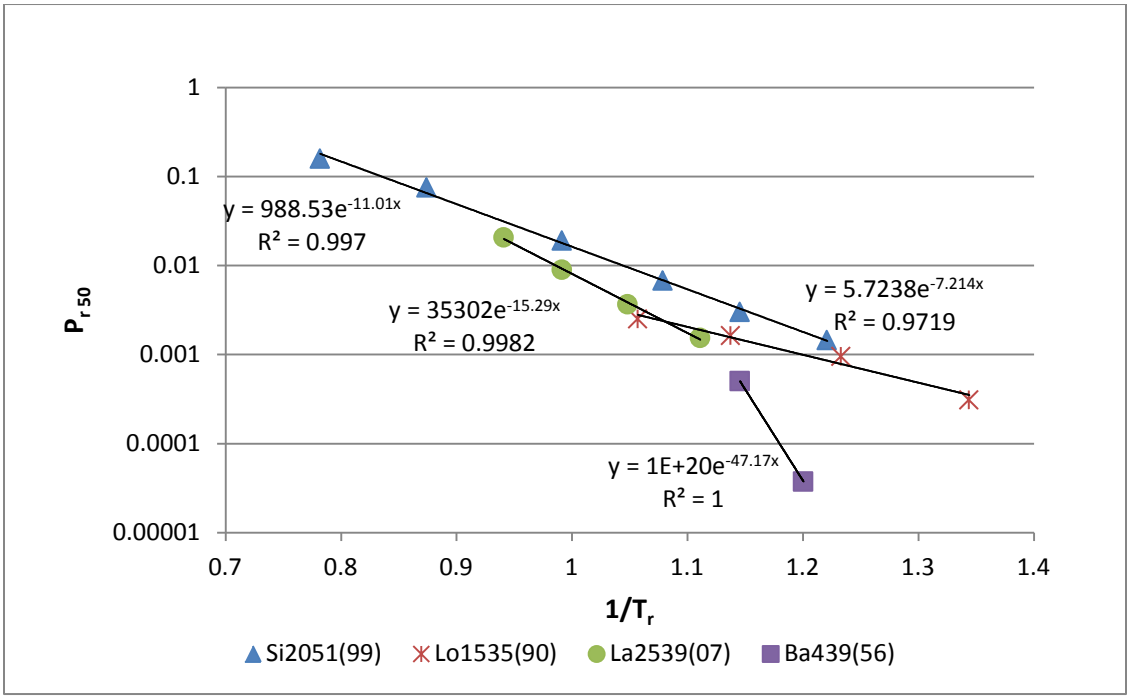

Figure 3.17: log P_{r50} vs. $1/T_r$ for propane on 13X.

The slope of the lines in Figure 3.18 is used to calculate the heat of adsorption at 50% loading of propane. The intercept is used to calculate the pre-exponential factor, a.

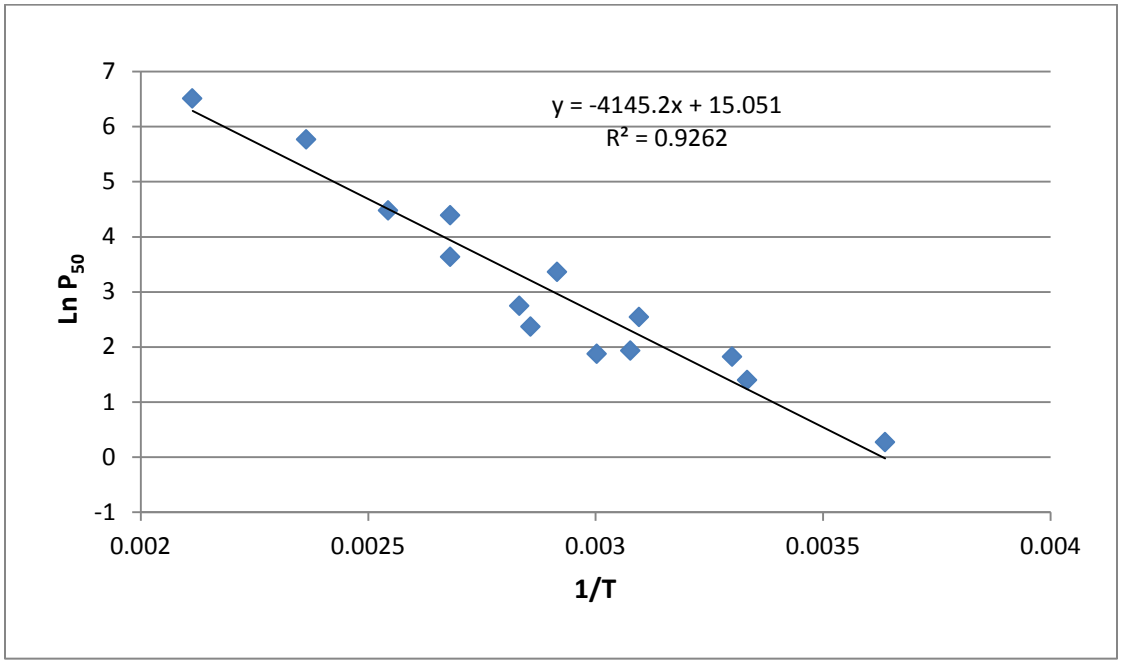

Figure 3.18: ln P_{50} vs. 1/T for propane on 13X.

$$-(\Delta H_{50}) = 4145 * 1.98 * 10^{-3} = 8.2 \ \ kcal/mol. \qquad 3.10$$

$$a = e^{15.05} = 3.43 * 10^{6} \qquad 3.11$$

Table 3.4: Values of ($-\Delta H_{ads}$) for propane on 13X.

$-\Delta H_{50}$ (kcal /mol)	$-\Delta H_{0lit.}$ (kcal /mol)	a
8.21	7.8 [18]	3.43E+06

The value of the heat of adsorption at 50% loading of propane is compared to the value at 0% loading taken from the study of Loughlin et al. [18]. The value calculated by the Gaussian model is slightly more than the one found in literature at 0% loading.

3.5 n-butane

Figure 3.19 represents the adsorption isotherms for n-butane found in a single study by Barrer and Sutherland [12]. T_r starts at 0.7 on the left hand side of the plot to a T_r of 0.81 on the right hand side of the plot; hence, all isotherms are in subcritical region. The isotherms were all consistent in shape and behavior as they were all extracted from a single study. With the lack of another judge on the consistency, the isotherms were all retained as they are.

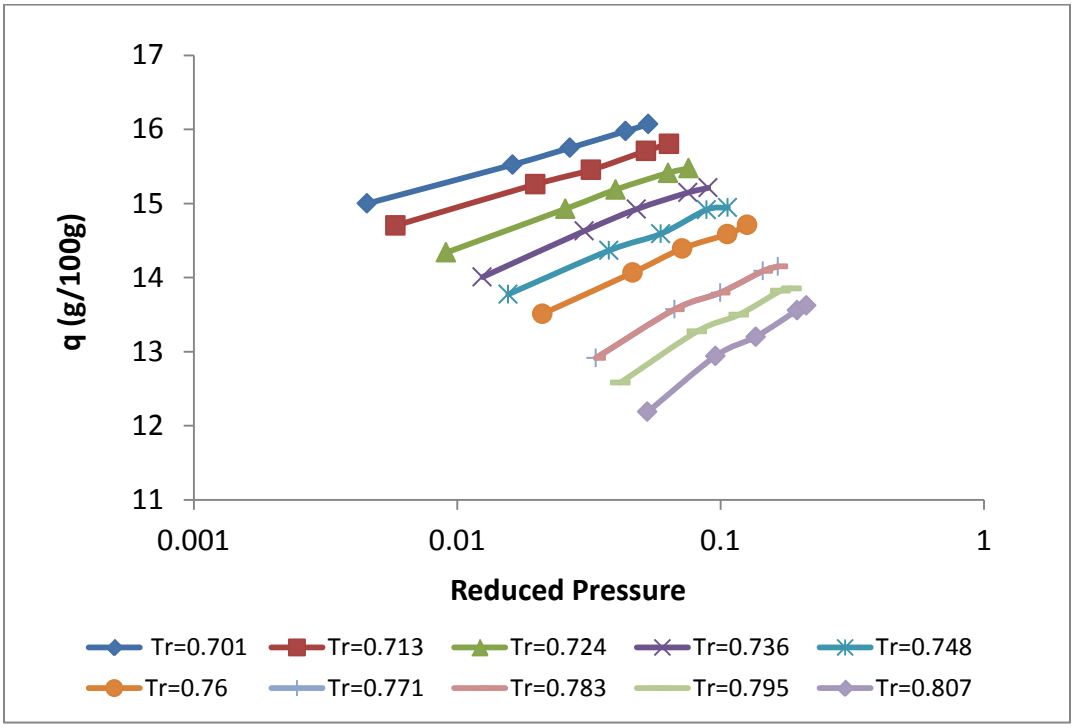

Figure 3.19: Isotherms for n-butane on 13X.

The linearized isotherms are shown on Figure 3.20 starting from a T_r of 0.7 from the left and decreasing gradually to 0.81 on the right. All lines are perfectly linear and parallel to each other. The slopes of the linearized isotherm are plotted against T_r, in Figure 3.21, where the values are of sigma decrease smoothly from 4 to 2 as T_r increases. Figure 3.22 shows the constant θ lines, analogous to the isosteres, of n-butane. With a regression value of 0.98, the data is a good linear ft.

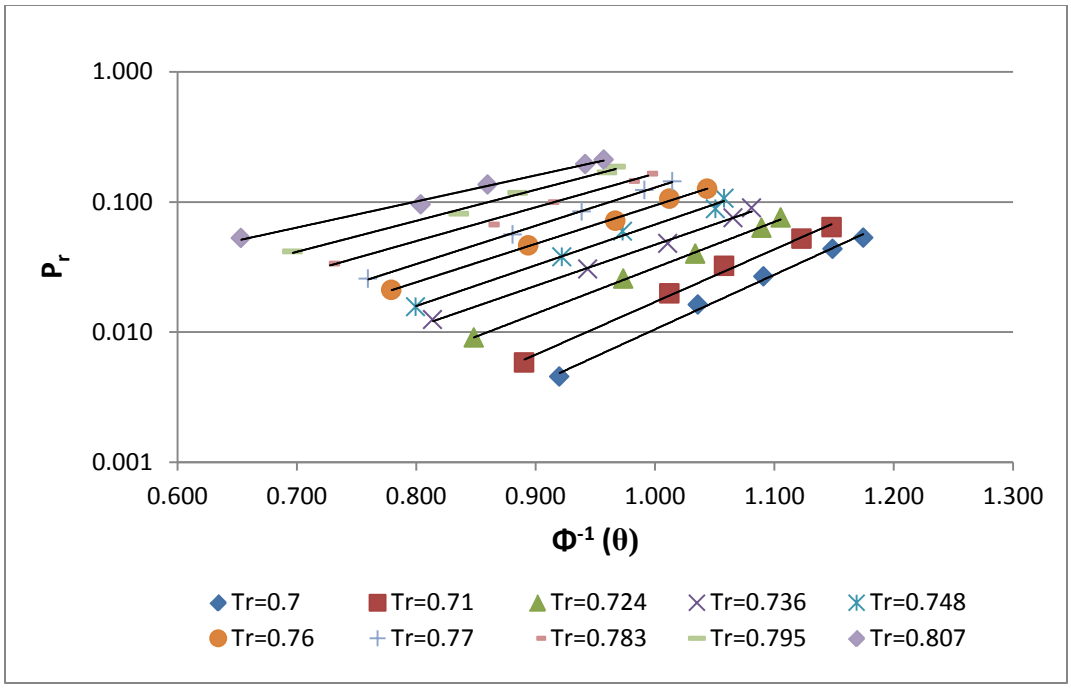

Figure 3.20: Linearized isotherms for n-butane on 13X.

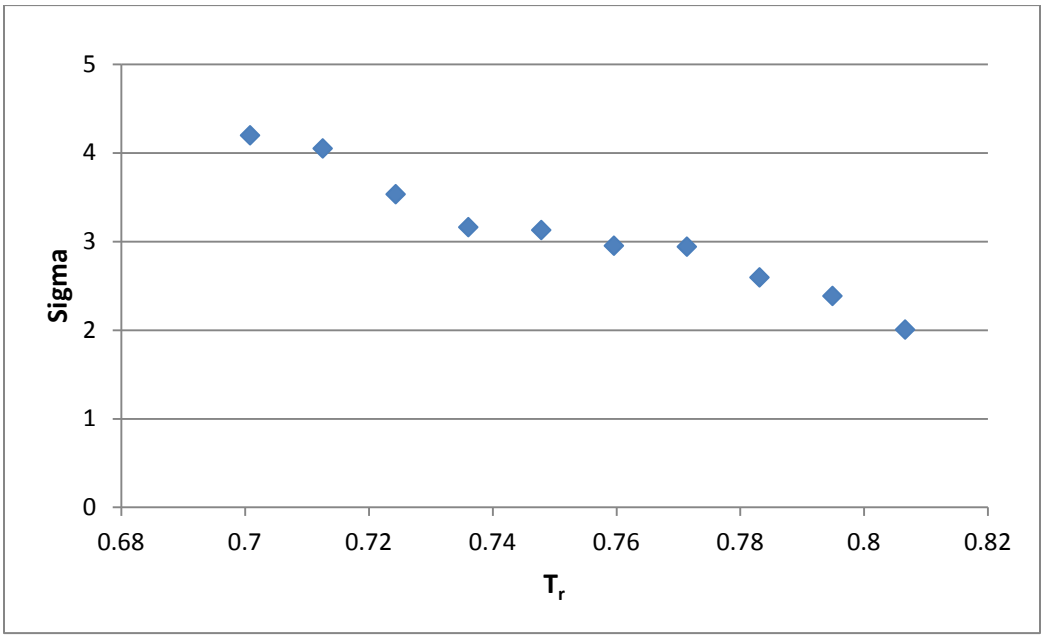

Figure 3.21; Sigma, the slope of the linearized isotherms, as a function of reduced temperature, for n-butane on 13X.

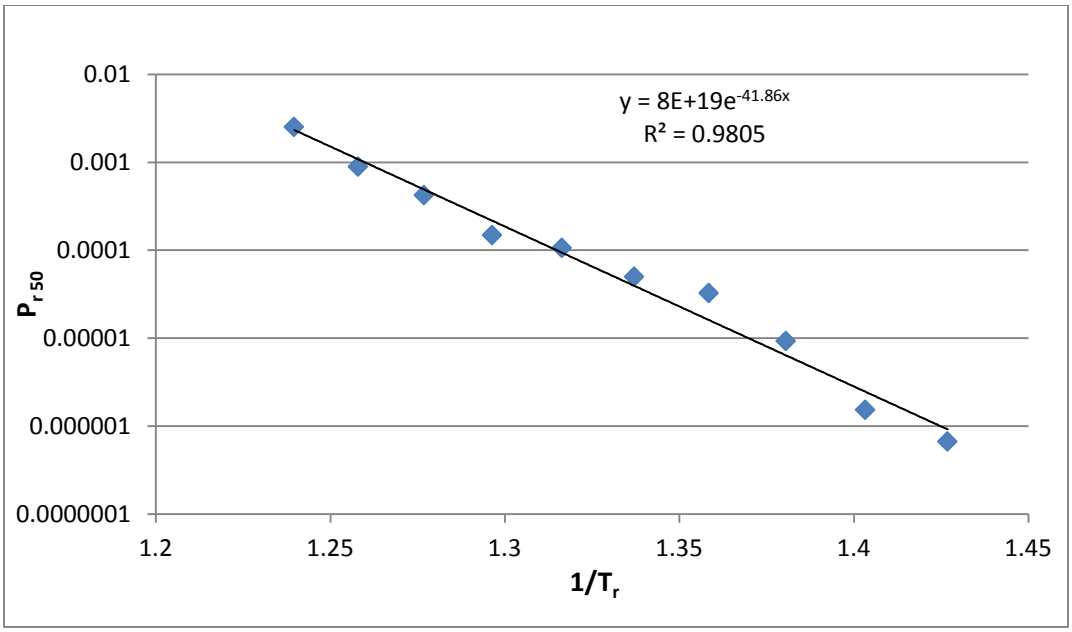

Figure 3.22: log P_{r50} vs. $1/T_r$ for n-butane on 13X.

The value of the heat of adsorption at 50% loading for n-butane is calculated from the slope of Figure 3.23.

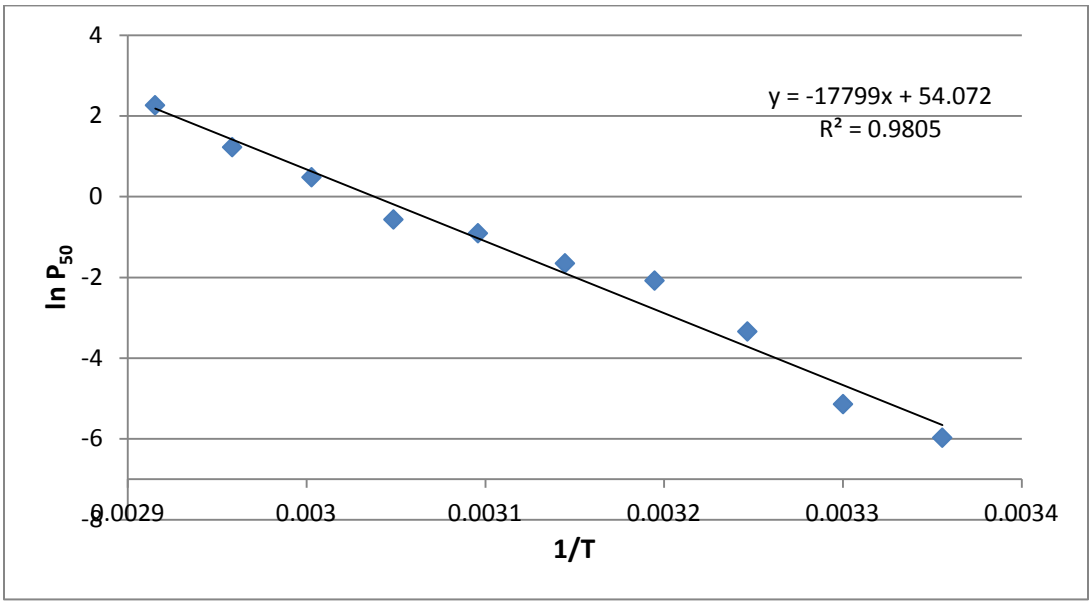

Figure 3.23: ln P_{50} vs. 1/T for n-butane on 13X.

$$-(\Delta H_{50}) = 17799 * 1.98 * 10^{-3} = 35.24 \ kcal/mol. \quad 3.12$$

$$a = e^{15.05} = 3.13 * 10^{23} \quad 3.13$$

Table 3.5 Values of ($-\Delta H_{ads}$) for n-butane on 13X.

$-\Delta H_{50}$ (kcal /mol)	$-\Delta H_{0lit.}$ (kcal /mol)	a
35.24	14.50 [12]	3.13E+28

The value of the heat of adsorption at 50% loading of n-butane is compared to the value at 0% loading taken from the study of Barrer et al. [12]. The value calculated by the Gaussian model is significantly higher than the one found in literature at 0% loading.

3.6 iso-butane

Figure 3.24 represents the isotherms for iso-butane including three different studies by Hyun and Danner [17], Lamia et al. [25] and Barrer and Sutherland [12], across a T_r range of 0.73 from the left to 0.82 to the right. Isotherms are consistent with each other with each other in shape and position where T_r increase gradually from left to right except for one isotherms from Hyun and Danner [17] at a T_r = 0.79 which comes between two isotherms from Lamia et al. [25]. at T_r = 0.82 and T_r =0.87. Nevertheless, the isotherm is retained because it is consistent with the other Barrer and Sutherland [12] isotherms.

Linearized isotherms for iso-butane on 13X are shown on Figure 3.25. The lines are straight and parallel for the data from Barrer and Sutherland [12]. The lines from the other studies are curved especially at high pressures. The slopes of the linearized probability lines, σ, plotted against reduced temperature are shown in Figure 3.26. The value of sigma in the study of Barrer and Sutherland [12] along with some isotherms from Hyun and Danner [17] are close to 2 while in the study of Lamia et al. [25] sigma decreases from 3 to 1 with increasing T_r. Sigma also decreases to 1 for Hyun and Danner [17] as T_r increases. The line analogous to the isostere in Figure 3.27 shows a good linear fit of the data, within each study. The lines are straight and both Barrer and Sutherland [25] and Lamia et al. [12] are parallel.

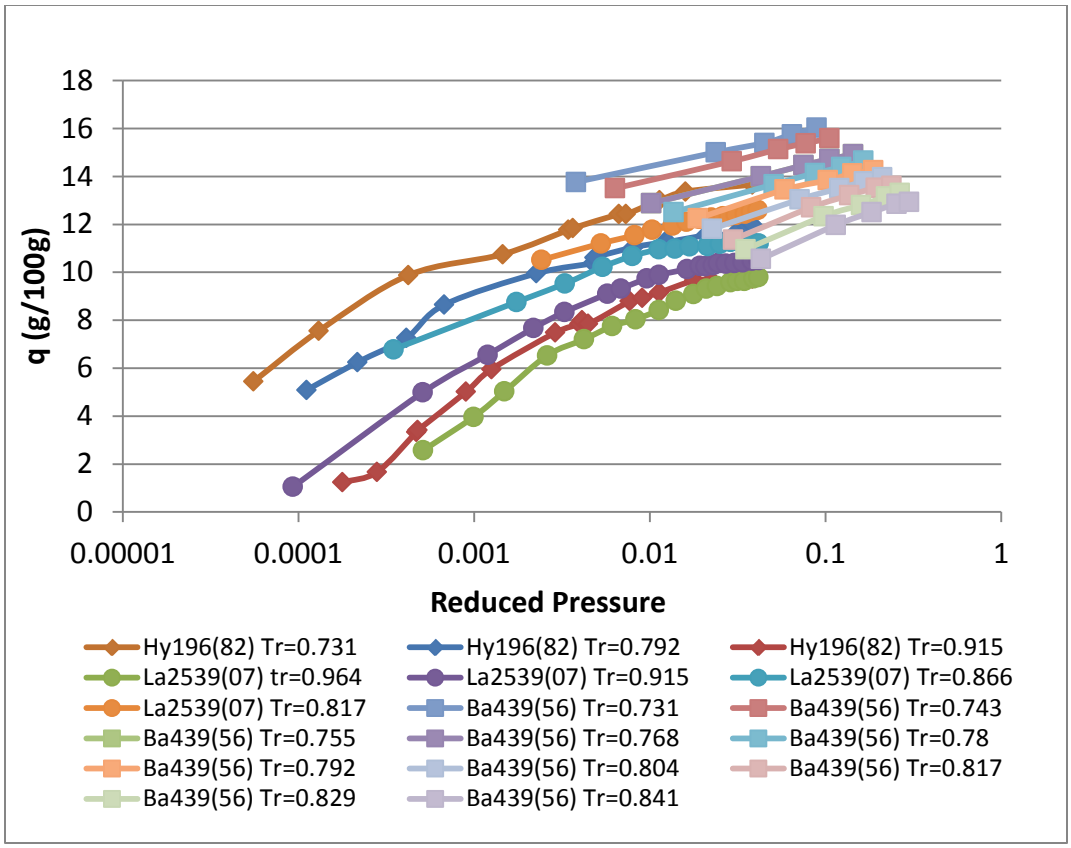

Figure 3.24: Isotherms for iso-butane on 13X.

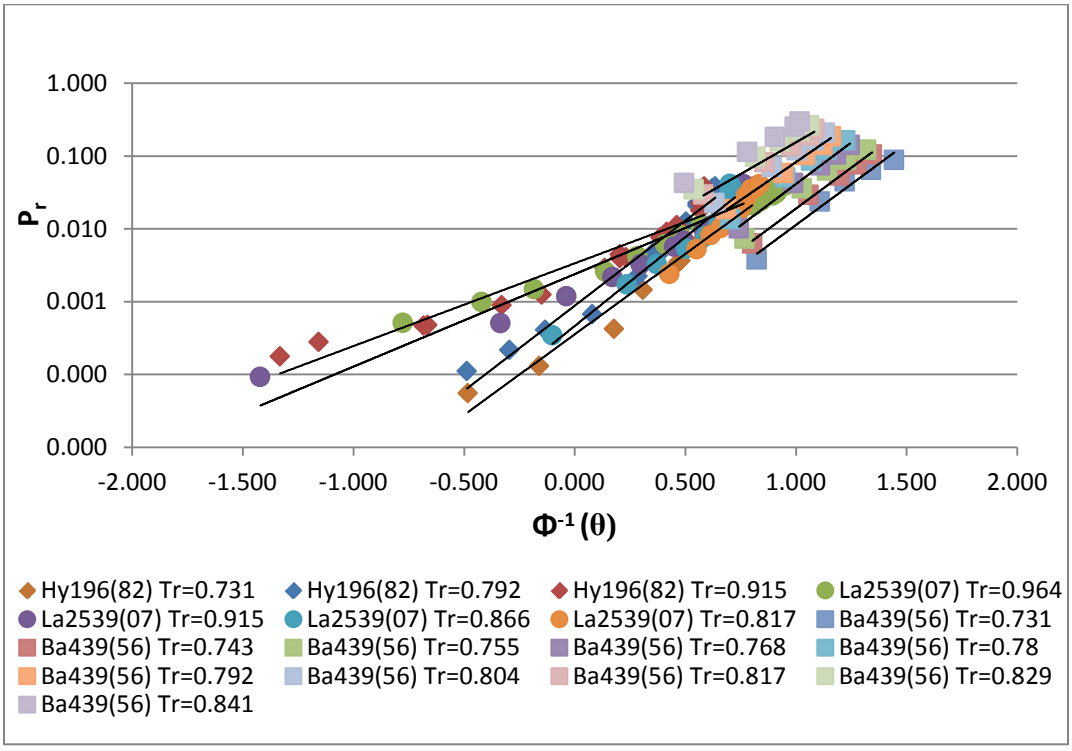

Figure 3.25: Linearized isotherms for iso-butane on 13X.

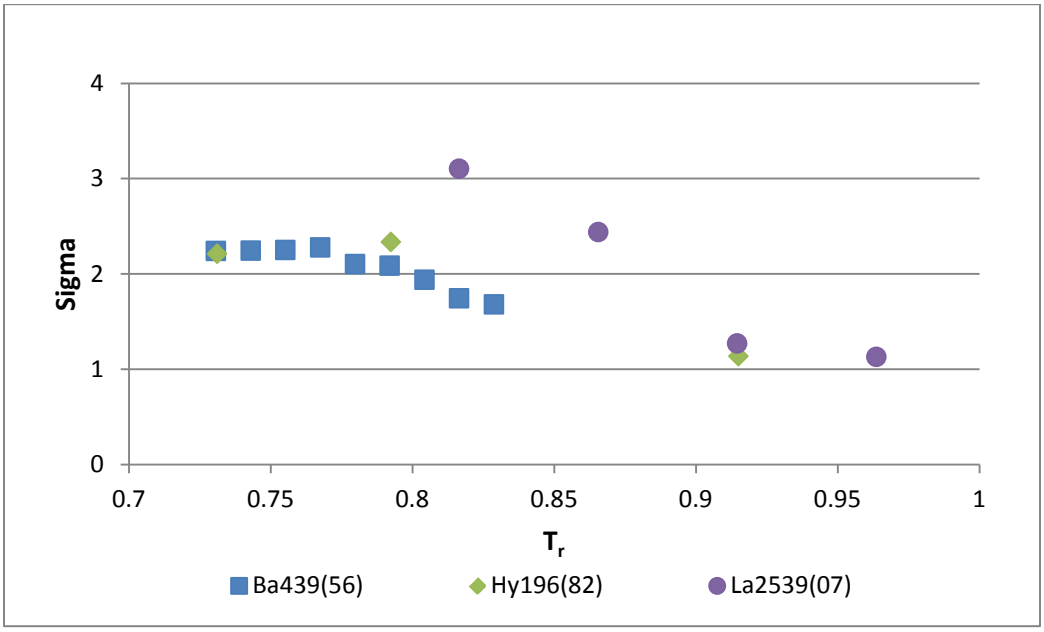

Figure 3.26: Sigma, the slope of the linearized isotherms, as a function of reduced temperature, for iso-butane on 13X.

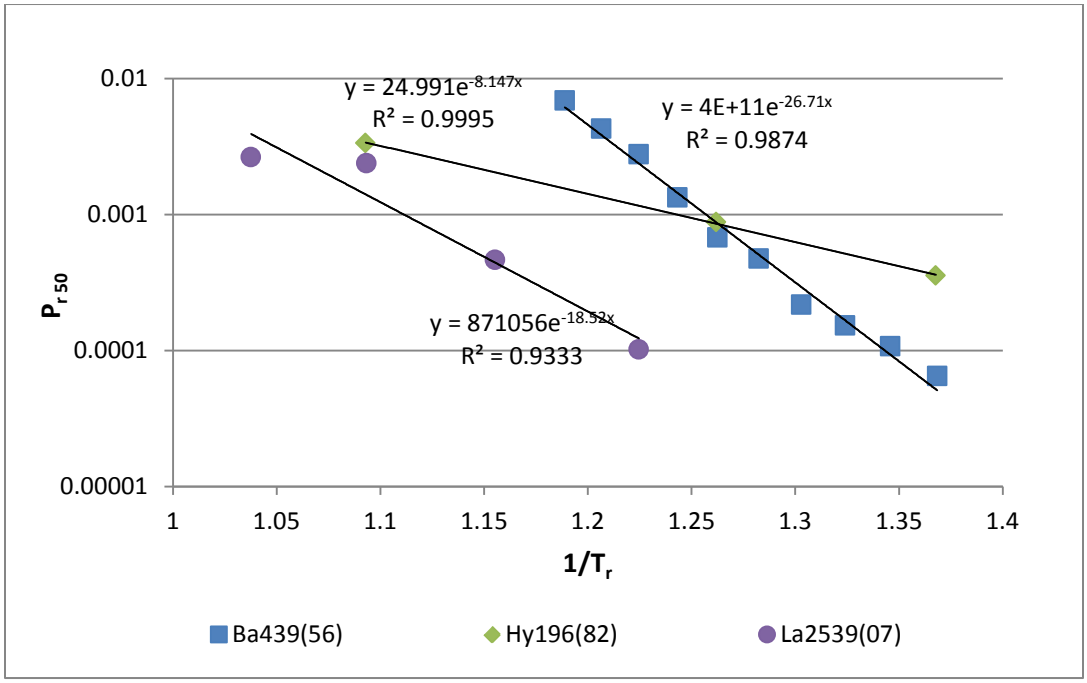

Figure 3.27: log P_{r50} vs. $1/T_r$ for iso-butane on 13X.

From Figure 3.28, the heat of adsorption a 50% loading of iso-butane is calculated using the average of the slopes of the constant θ lines from Lamia et al. [25] and Hyun and Danner [17] and compared to the value found in literature at 0% loading.

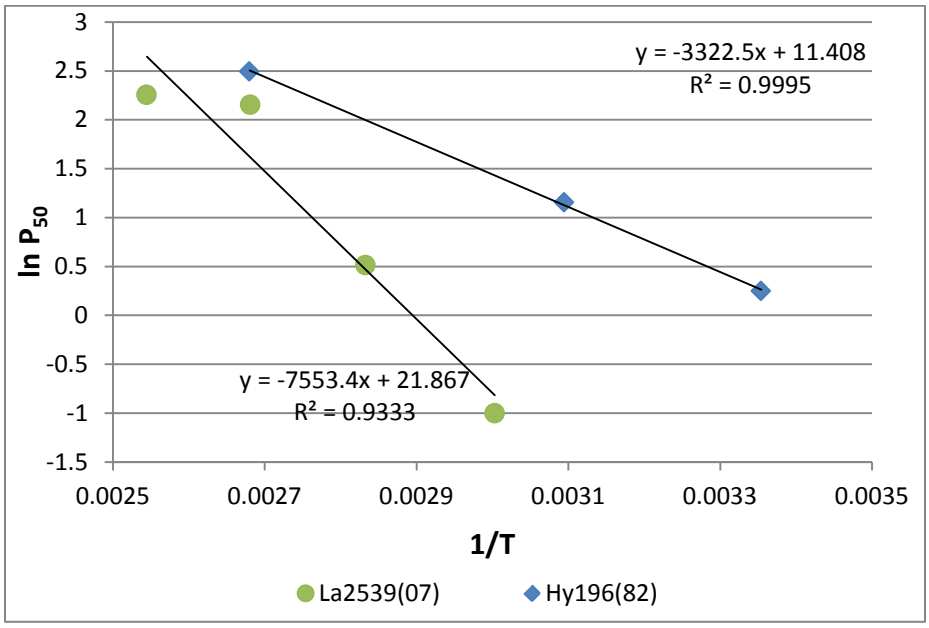

Figure 3.28: ln P_{50} vs. 1/T for iso-butane on 13X.

$$-(\Delta H_{50}) = [(7553 + 3322)/2] * 1.98 * 10^{-3} = 10.76 \ \ kcal/mol. \qquad 3.14$$

$$a = e^{21.9} = 3.24 * 10^{9} \qquad 3.15$$

Table 3.5: Values of ($-\Delta H_{ads}$) for iso-butane on 13X.

$-\Delta H_{50}$ (kcal /mol)	$-\Delta H_{0lit.}$ (kcal /mol)	a
10.76	9.4 [17], 9.9 [25]	3.24E+09

The value of the heat of adsorption at 50% loading of iso-butane is compared to the value at 0% loading. The value calculated by the Gaussian model is higher than the one found in literature at 0% loading.

3.7 n-pentane

Figure 3.29 represents the adsorption isotherms for n-pentane found in a single study by Barrer and Sutherland [12]. T_r starts at 0.635 on the left hand side of the plot and ends at a T_r of 0.73 on the right hand side of the plot. The isotherms were all consistent in shape and behavior as they were all extracted from a single study. With the lack of another judge on the consistency, the isotherms were all retained as they are. The study was based on an 80% crystal sample of 13X.

The linearized isotherms in the case of n-pentane on 13X are shown in Figure 3.30. The lines are remarkably straight and parallel with consistently increasing T_r from right to left. Looking at Figure 3.31, the sigma values start around 5 and decrease smoothly with increasing T_r to 3.5. The constant θ line analogous to the isostere in Figure 3.32 shows a good linear fit of the data with an R value of 0.928.

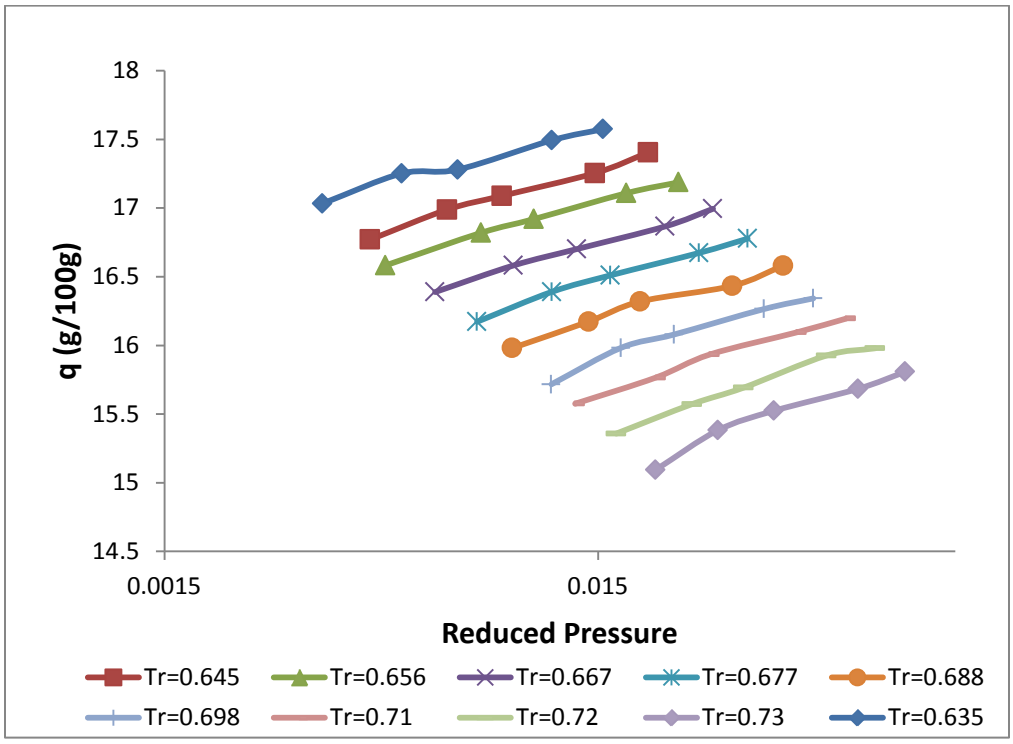

Figure 3.29: Isotherms for n-pentane on 13X.

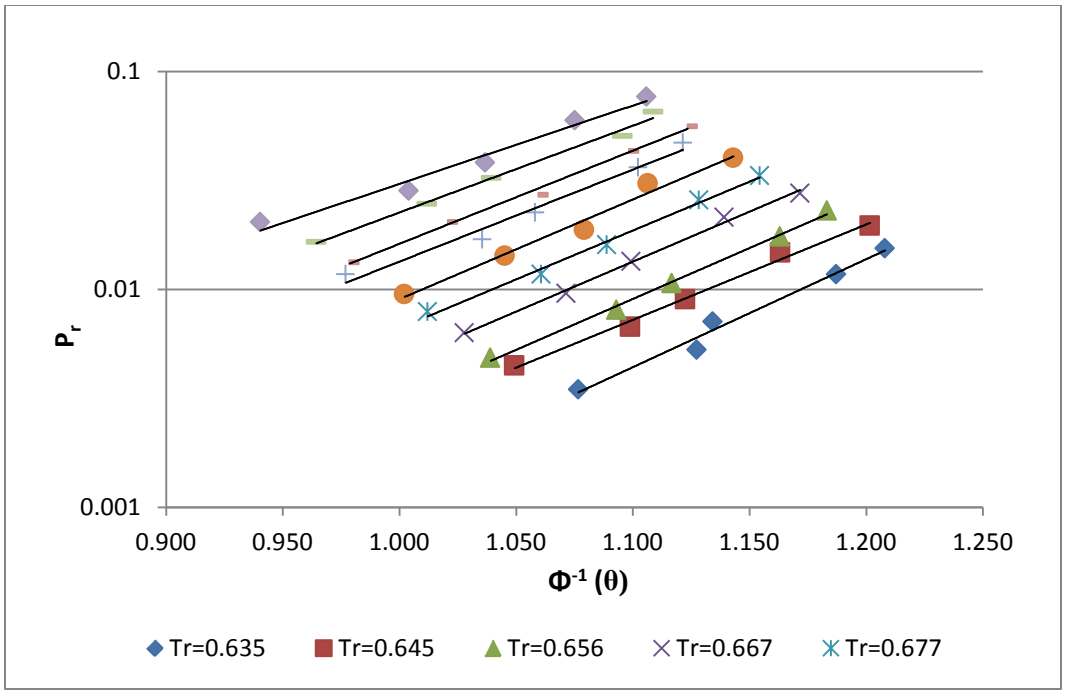

Figure 3.30: Linearized isotherms for n-pentane on 13X.

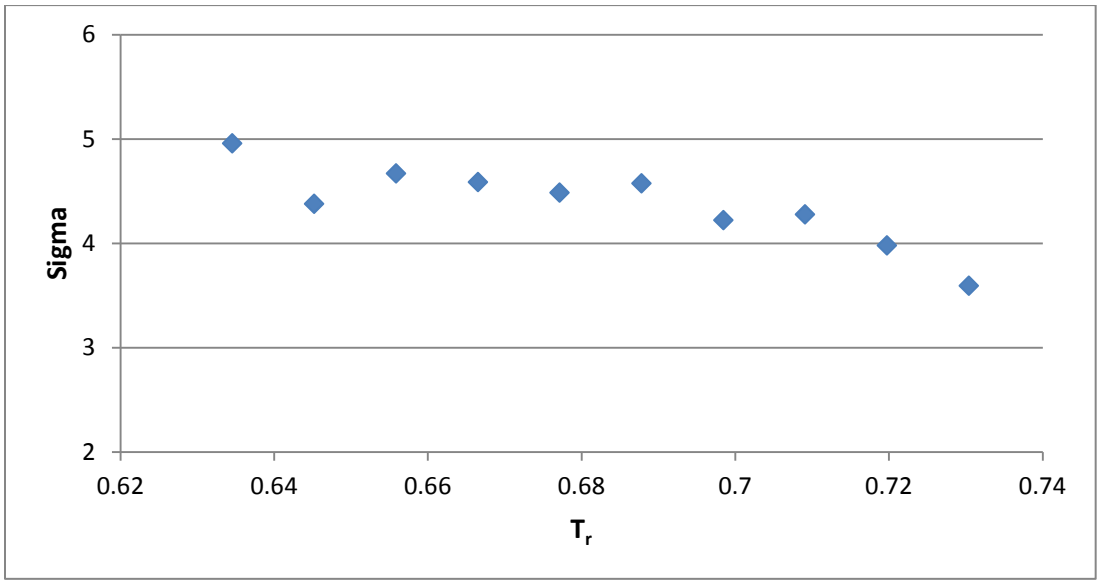

Figure 3.31: Sigma, the slope of the linearized isotherms, as a function of reduced temperature, for n-pentane on 13X.

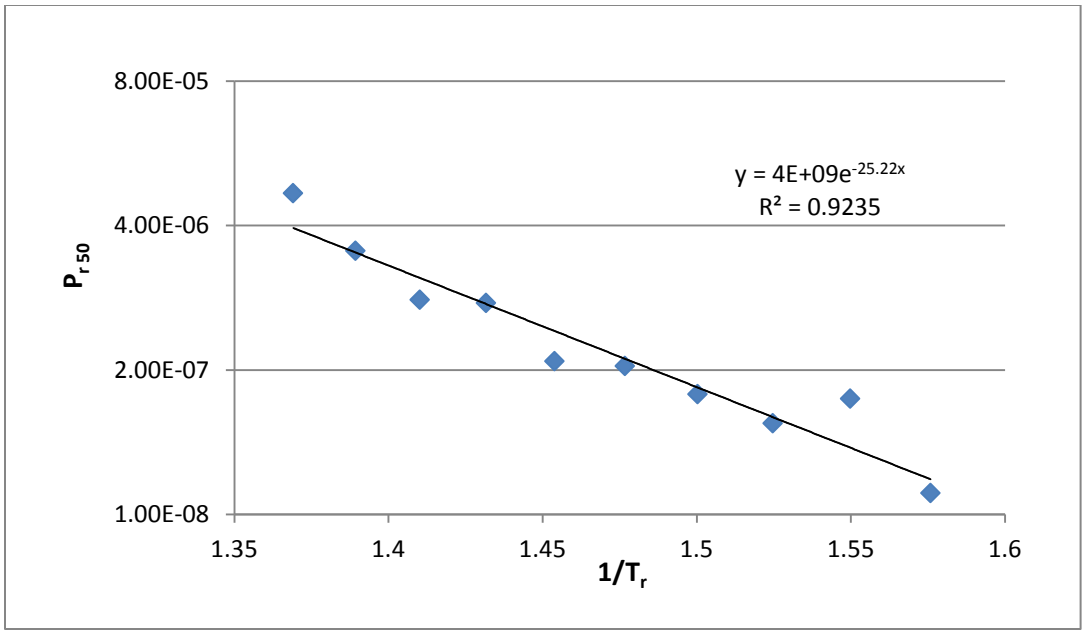

Figure 3.32: log P_{r50} vs. $1/T_r$ for n-pentane on 13X.

The heat of adsorption a 50% loading of n-pentane is calculated from Figure 3.33:

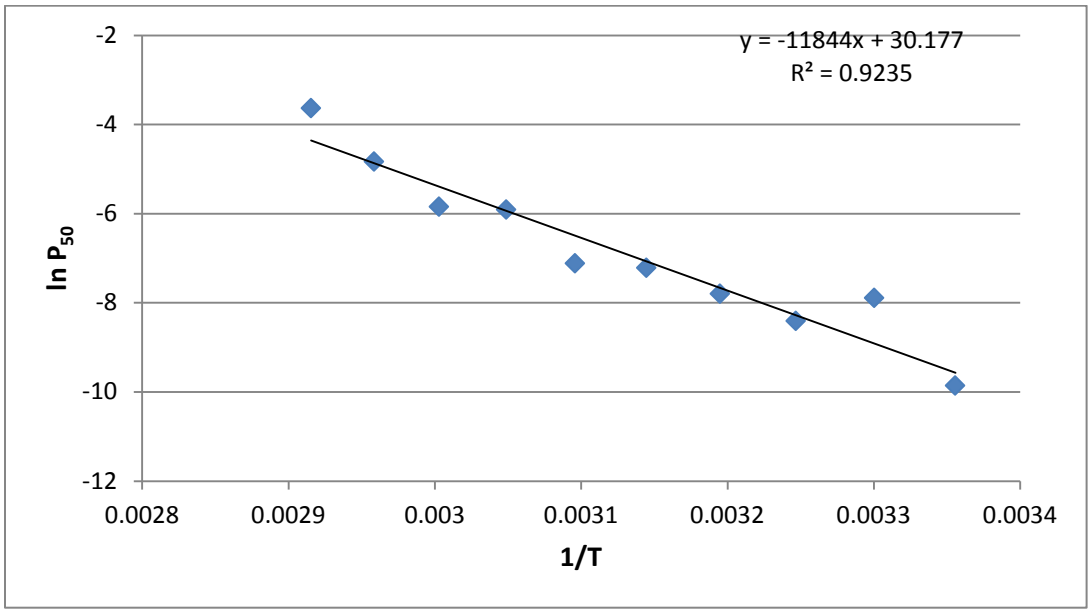

Figure 3.33: ln P_{50} vs. 1/T for n-pentane on 13X.

$$-(\Delta H_{50}) = 11844 * 1.98 * 10^{-3} = 23.45 \ \ kcal/mol. \quad 3.16$$

$$a = e^{30.1} = 1.18 * 10^{13} \quad 3.17$$

Table 3.6: Values of ($-\Delta H_{ads}$) for n-pentane on 13X.

$-\Delta H_{50}$ (kcal /mol)	$-\Delta H_{0lit.}$ (kcal /mol)	a
23.45	17.20 [12]	1.18E+13

The value of the heat of adsorption at 50% loading of n-pentane is compared to the value at 0% loading taken from the study of Barrer and Sutherland [12]. The value calculated by the Gaussian model is higher than the one found in literature at 0% loading.

3.8 iso-pentane

Figure 3.34 represents the adsorption isotherms for iso-pentane found in a single study by Barrer and Sutherland [12]. T_r starts at 0.647 on the left hand side of the plot and ends at a T_r of 0.745 on the right hand side of the plot. The isotherms were all consistent in shape and behavior as they were all extracted from a single study. With the lack of another judge on the consistency, the isotherms were all retained as they are. The study was based on an 80% crystal sample of 13X.

The linearized isotherms of iso-pentane on 13X are shown in Figure 3.35. The lines are remarkably straight and parallel with consistently increasing T_r from right to left. Looking at Figure 3.36, the sigma values start around 8 and decrease with increasing T_r to a value of 3. The constant θ line, in Figure 3.37, analogous to the isostere shows an excellent linear fit of the data with an R value of 0.978.

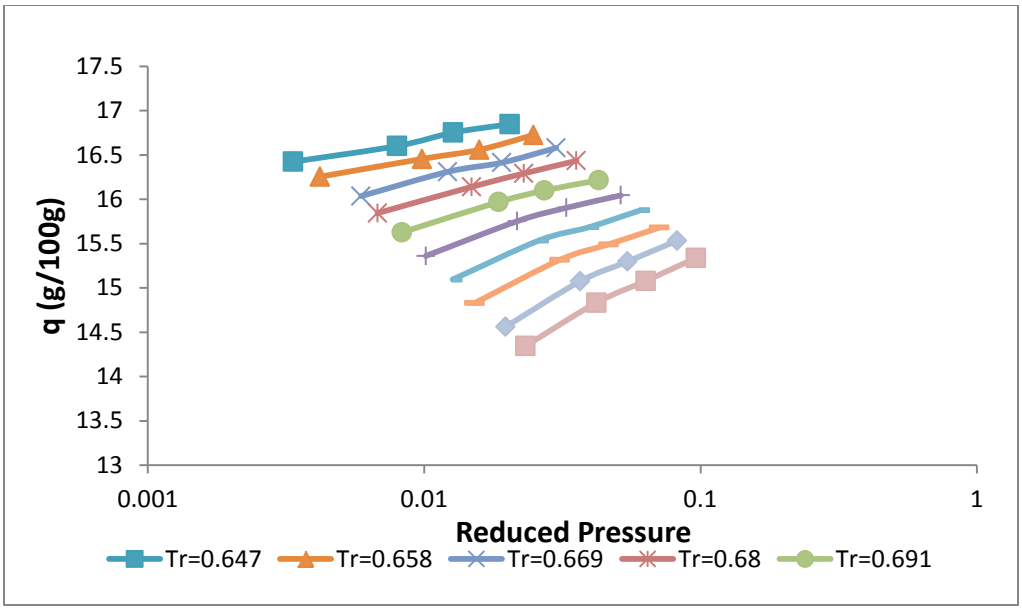

Figure 3.34: Isotherms for iso-pentane on 13X.

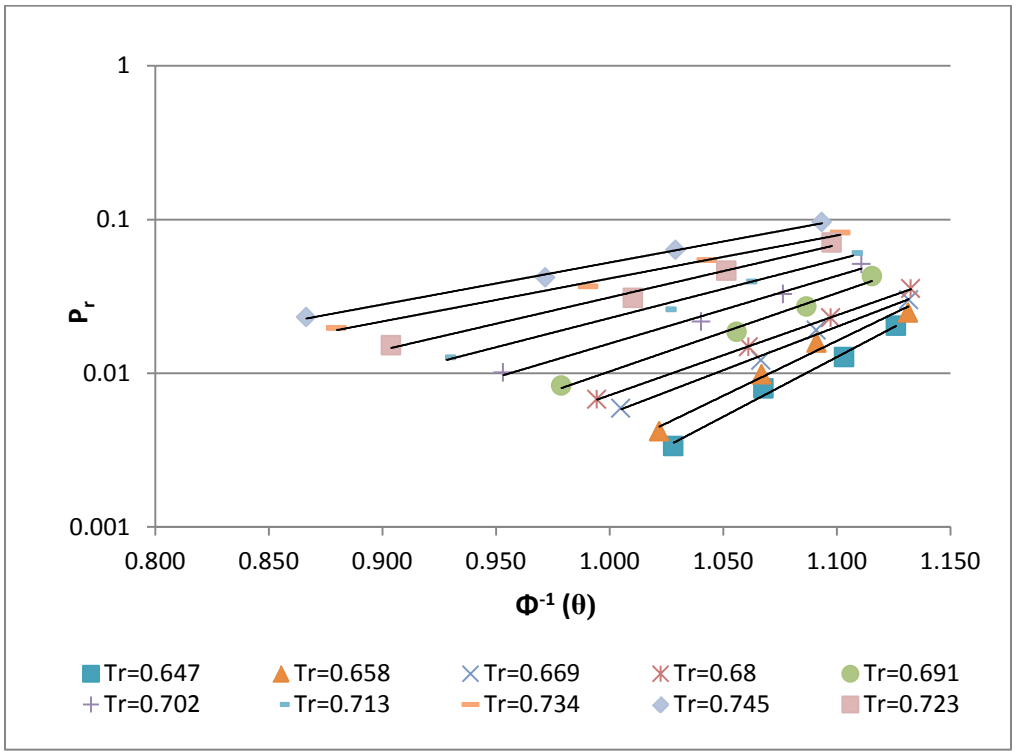

Figure 3.35: Linearized isotherms for iso-pentane on 13X.

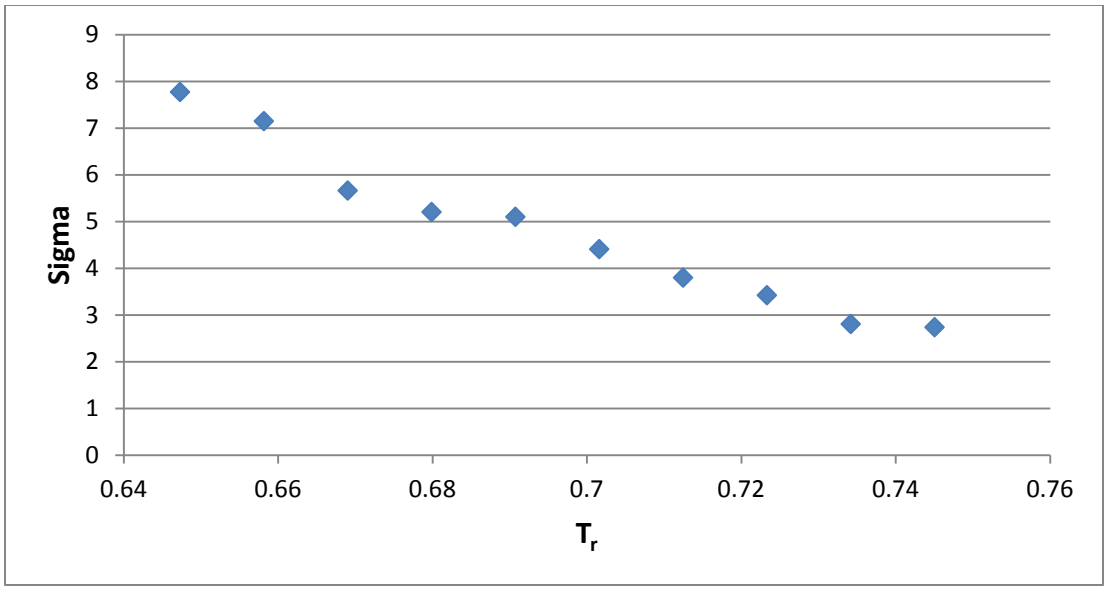

Figure 3.36: Sigma, the slope of the linearized isotherms, as a function of reduced temperature, for iso-Pentane.

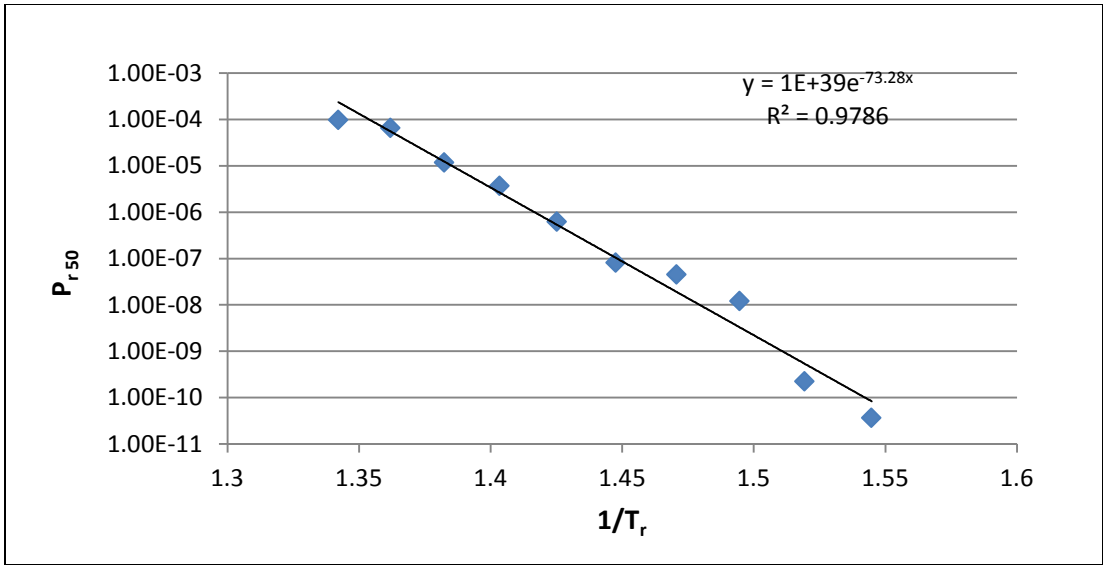

Figure 3.37: log P_{r50} vs. $1/T_r$ for iso-pentane on 13X.

The heat of adsorption a 50% loading of iso-pentane is calculated from Figure 3.38:

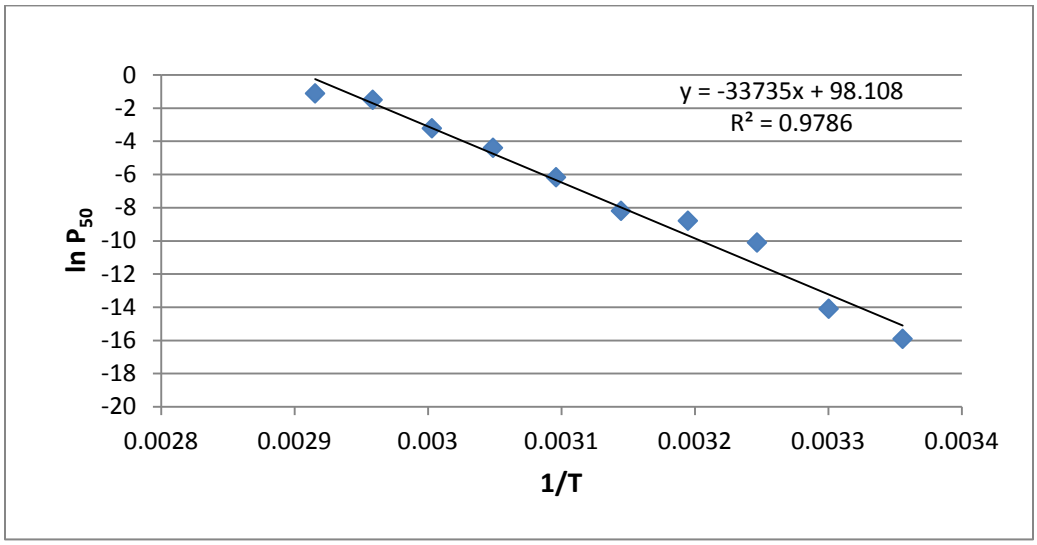

Figure 3.38: ln P_{50} vs. 1/T for iso-pentane on 13X.

$$-(\Delta H_{50}) = 33735 * 1.98 * 10^{-3} = 66.80 \ \ kcal/mol. \qquad 3.18$$

$$a = e^{98.1} = 4.02 * 10^{42} \qquad 3.19$$

Table 3.7: Values of ($-\Delta H_{ads}$) for iso-pentane on 13X.

$-\Delta H_{50}$ (kcal /mol)	$-\Delta H_{0lit.}$ (kcal /mol)	a
66.80	17.20 [12]	4.02E+42

The value of the heat of adsorption at 50% loading of iso-pentane is compared to the value at 0% loading taken from the study of Barrer and Sutherland [12]. The value calculated by the Gaussian model is much higher than the one found in literature at 0% loading.

3.9 neo-pentane

Figure 3.39 represents the adsorption isotherms for neo-pentane found in a single study by Barrer and Sutherland [12]. T_r starts at 0.687 on the left hand side of the plot and ends at a T_r of 0.791 on the right hand side of the plot. The isotherms were all consistent in shape and behavior as they were all extracted from a single study. With the lack of another judge on the consistency, the isotherms were all retained as they are. The study was based on an 80% crystal sample of 13X.

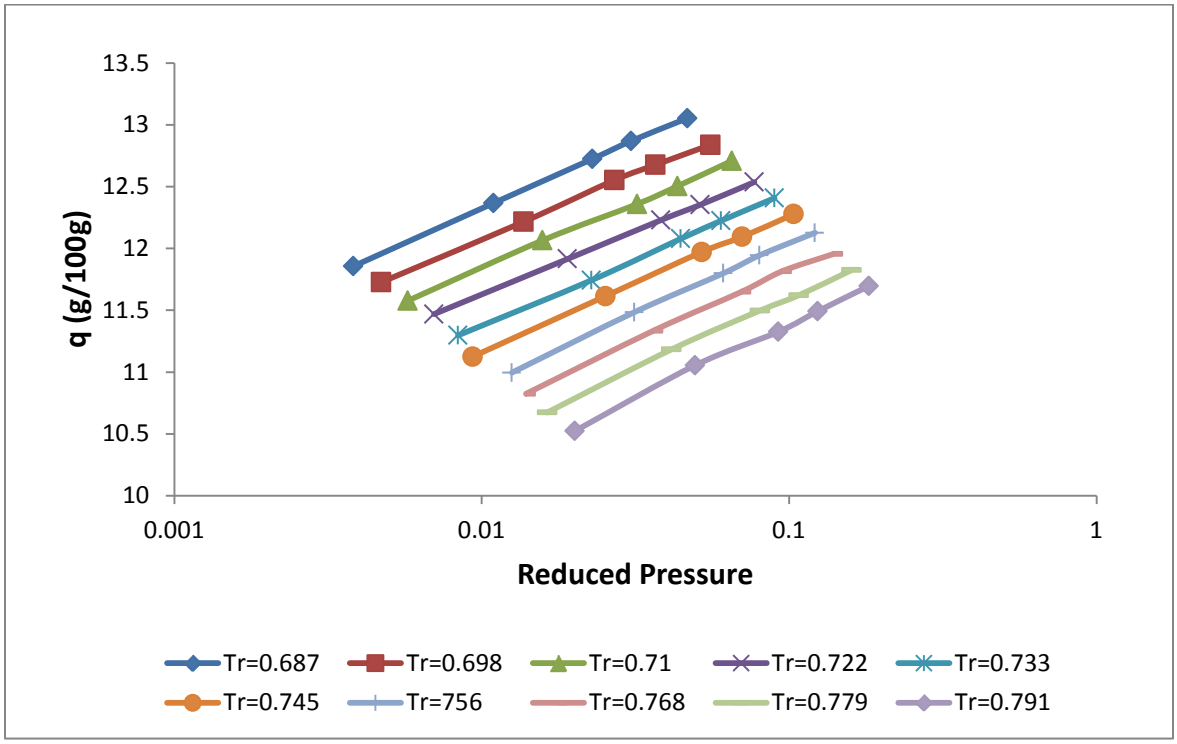

Figure 3.39: Isotherms for neo-pentane on 13X.

The linearized isotherms of neo-pentane on 13X are shown in Figure 3.40. The lines are remarkably straight and parallel with consistently increasing T_r from right to left. Looking at Figure 3.41, the sigma values oscillate around 6 until T_r =0.74, where it decrease to a value of 5. The constant θ line in Figure 3.42 shows an excellent linear fit of the data with an R value of 0.97.

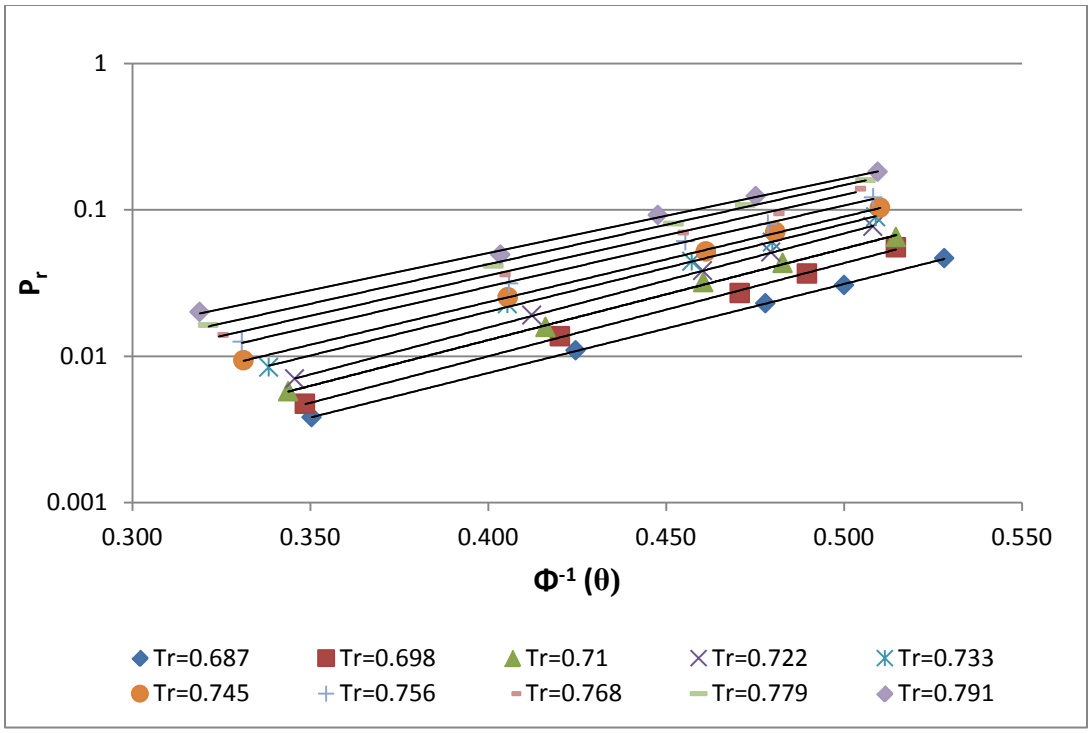

Figure 3.40: Linearized isotherms for neo-pentane on 13X.

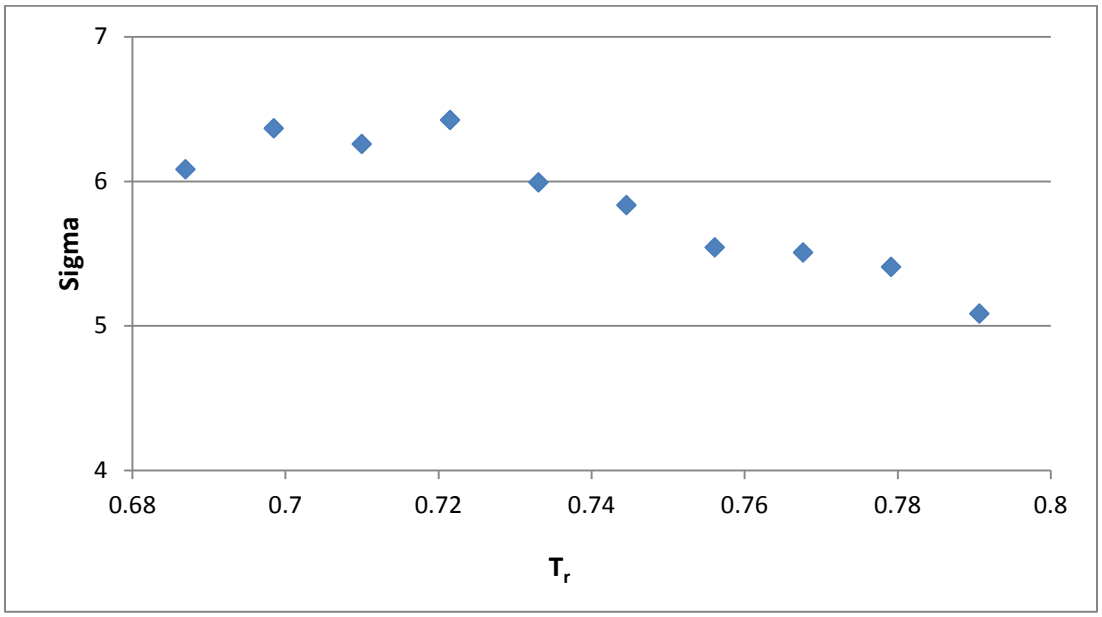

Figure 3.41: Sigma, the slope of the linearized isotherms, as a function of reduced temperature, for neo-pentane on 13X.

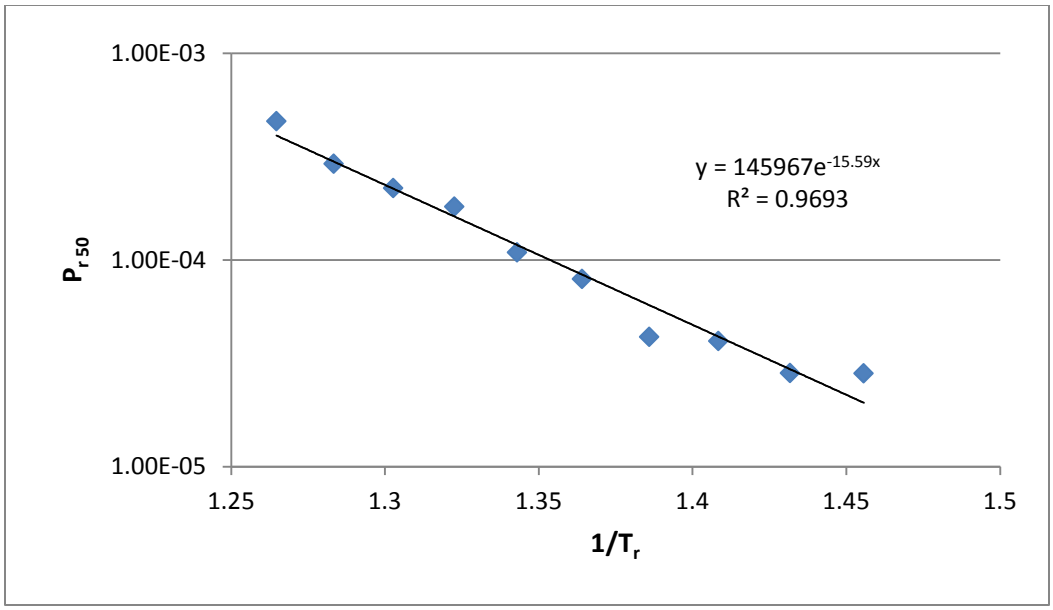

Figure 3.42: log P_{r50} vs. $1/T_r$ for neo-pentane on 13X.

The heat of adsorption a 50% loading of neo-pentane is calculated from Figure 3.43:

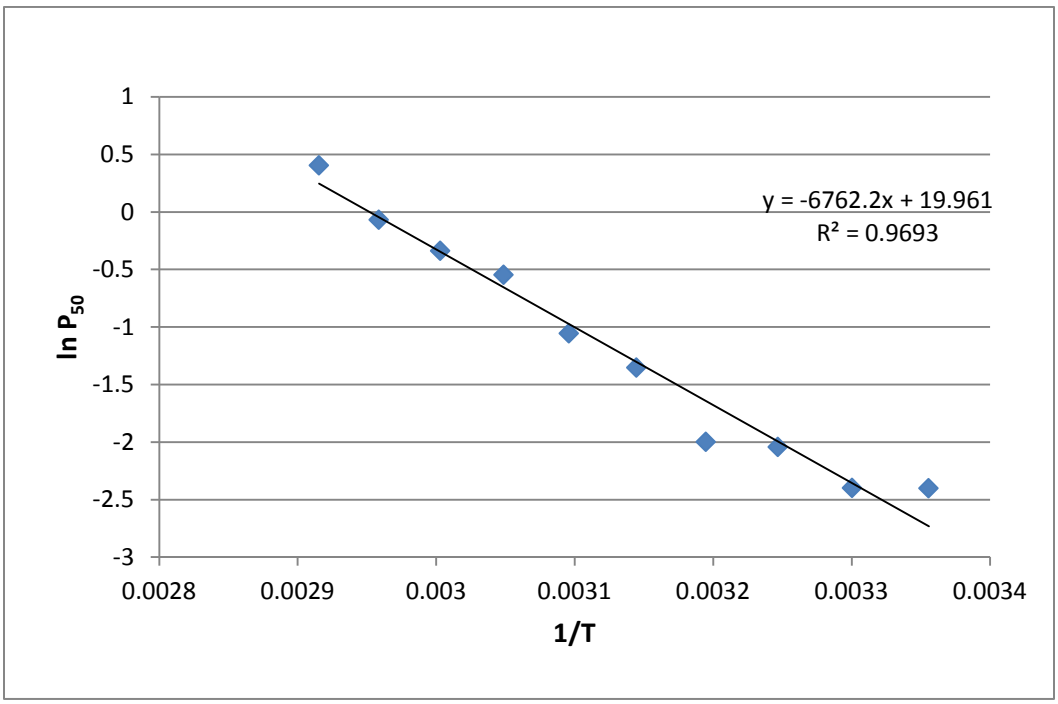

Figure 3.43: ln P_{50} vs. 1/T for neo-pentane on 13X.

$$-(\Delta H_{50}) = 6762 * 1.98 * 10^{-3} = 13.40 \ \ kcal/mol. \qquad 3.20$$

$$a = e^{19.96} = 4.66 * 10^{8} \qquad 3.21$$

Table 3.8: Values of ($-\Delta H_{ads}$) for neo-pentane on 13X.

$-\Delta H_{50}$ (kcal /mol)	$-\Delta H_{0lit.}$ (kcal /mol)	a
13.40	13.3 [12]	4.66E+08

The value of the heat of adsorption at 50% loading of neo-pentane is compared to the value at 0% loading taken from the study of Barrer and Sutherland [12]. The value calculated by the Gaussian model is equal one found in literature at 0% loading.

3.10 **n-Hexane**

Figure 3.44 shows the isotherms for n-hexane from two different studies by Barrer and Sutherland [12] and Zhdanov et al. [14] spanning a T_r range of 0.587 from the left to 0.675 on the right. Two isotherms from Zhdanov et al. [14] at T_r = 0.587 are included. The top study refers to a crystal sample while the bottom one refers to a pelleted sample of type Linde 13X with 20% binder content.

The pelleted isotherm from Zhdanov et al. [14] appears to cross the isotherm from Barrer and Sutherland [12] at T_r = 0.646 and is inconsistent in position. Moreover, unlike the crystal Zhdanov et al. isotherm, it exhibits capillary condensation due to the presence of the binder in a pelleted sample. Hence the pelleted sample from the Zhdanov study was deleted. All other isotherms were retained, as shown in Figure 3.45.

The linearized probability plot for n-hexane is shown in Figure 3.46 for all the screened isotherms of n-hexane ranging from a T_r of 0.597 to 0.675. The isotherms are remarkably linear and parallel except for the isotherm from Zhdanov et al. [14] where it is crossing the isotherm at T_r = 0.597. The slopes, σ, oscillate around for Barrer and Sutherland [12] isotherms as T_r increases while it is equal to 13 for Zhdanov et al. [14] isotherms, Figure 3.47. The constant θ lines of 50% loading are shown in Figure 3.48. Data from Barrer and Sutherland [12] show a good linear fit, although the line seems to shift upwards after T_r = 0.6. This may be due to the fact that at T_r< 0.6, the temperature are very low. Only one point is available from Zhdanov et al. [14]; therefore it cannot be regressed.

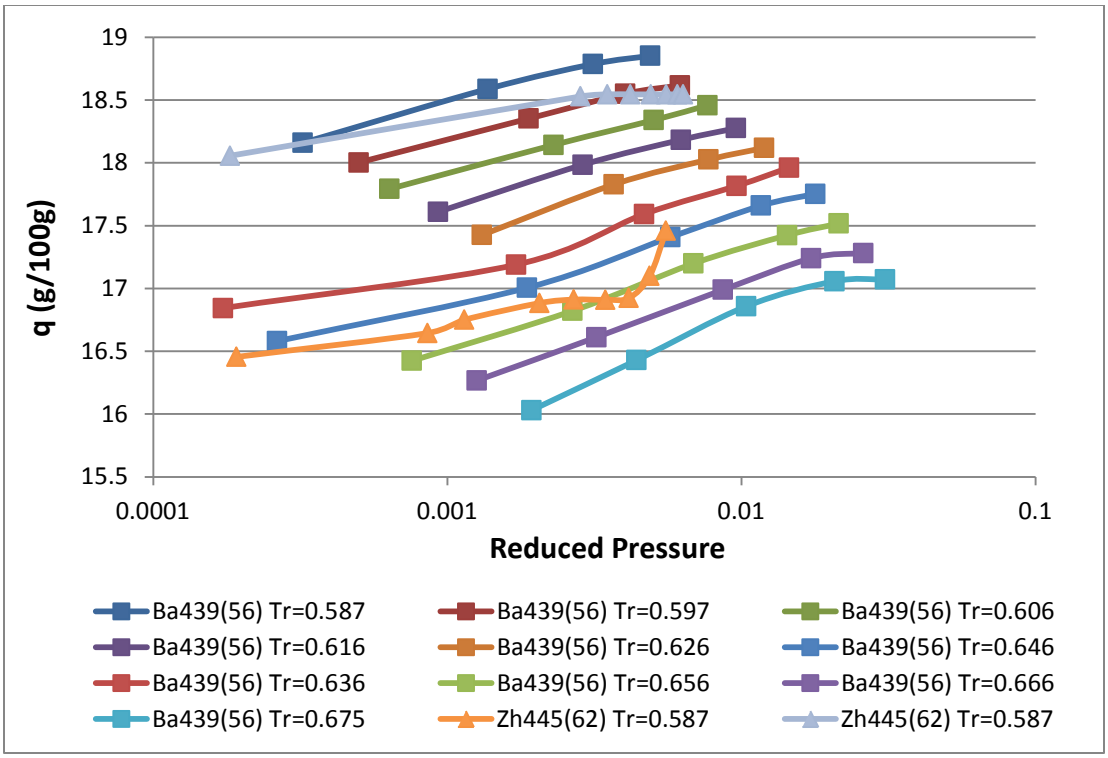

Figure 3.44: Isotherms for n-hexane on 13X (before screening).

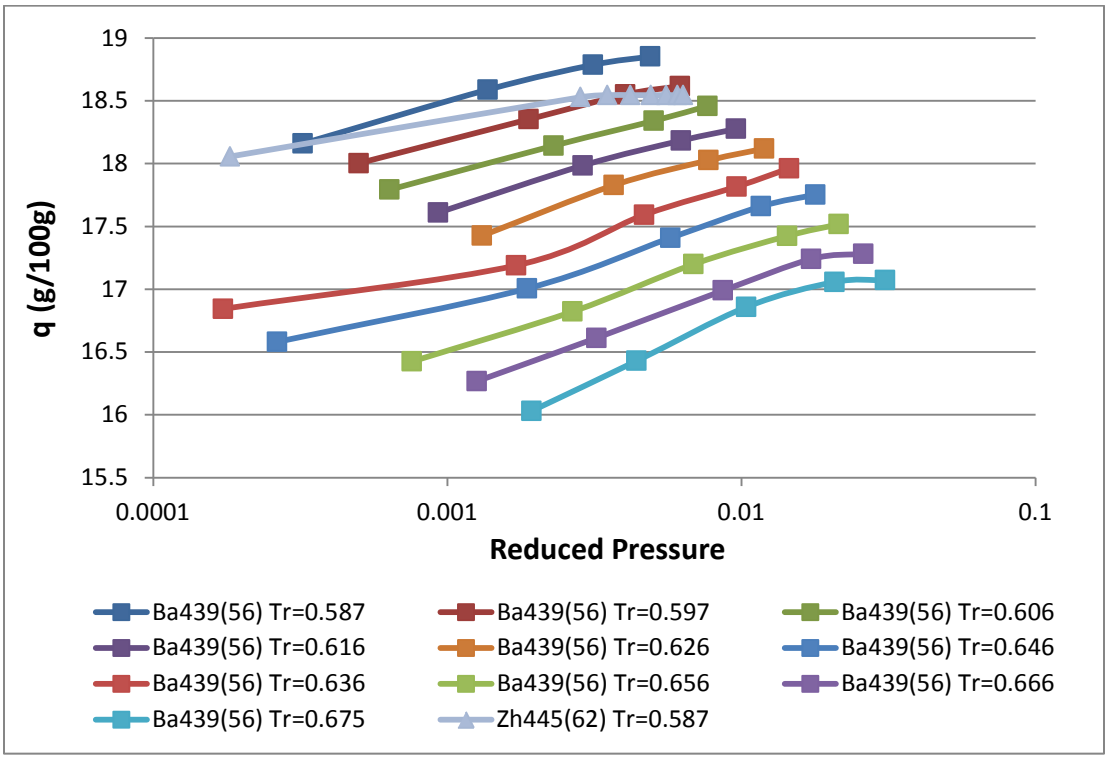

Figure 3.45: Isotherms for n-hexane on 13X (after screening).

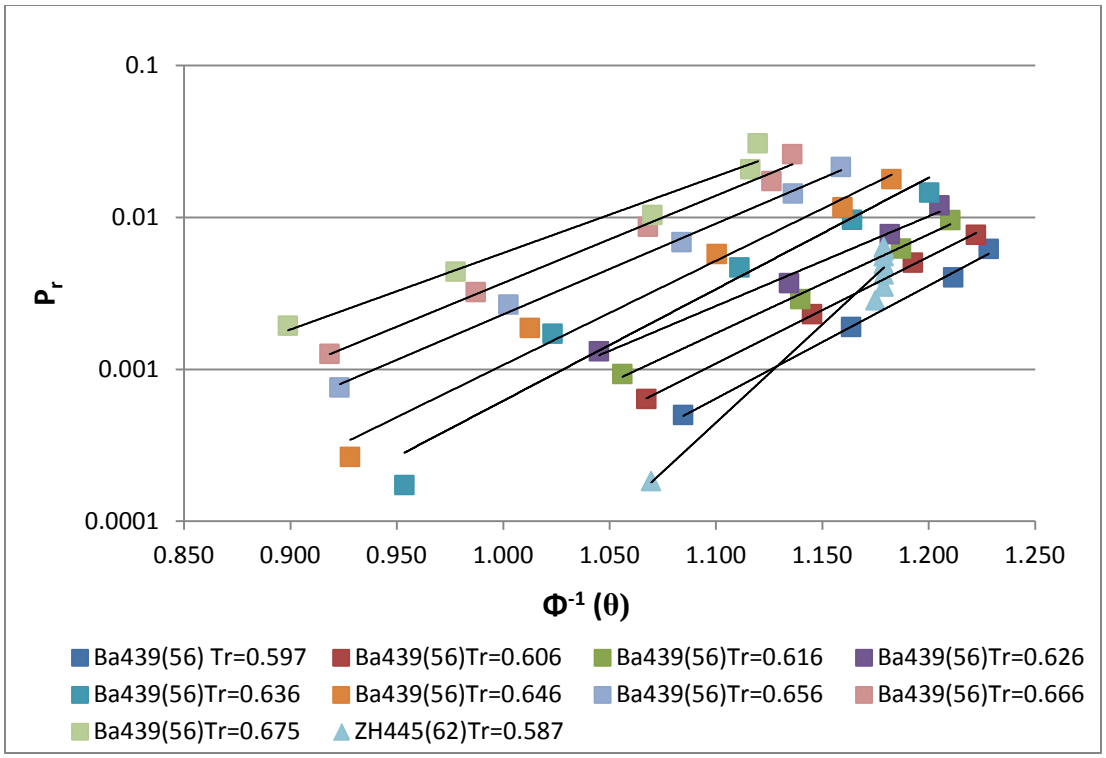

Figure 3.46: Linearized isotherms of n-hexane on 13X.

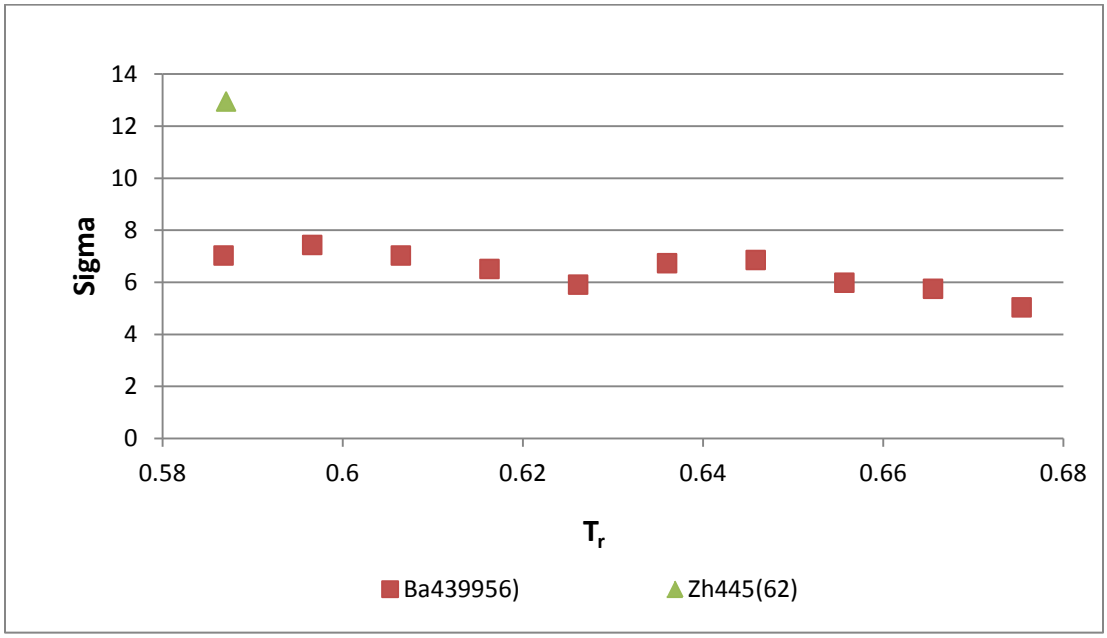

Figure 3.47: Sigma, the slope of the linearized isotherms, as a function of reduced temperature, for n-hexane on 13X.

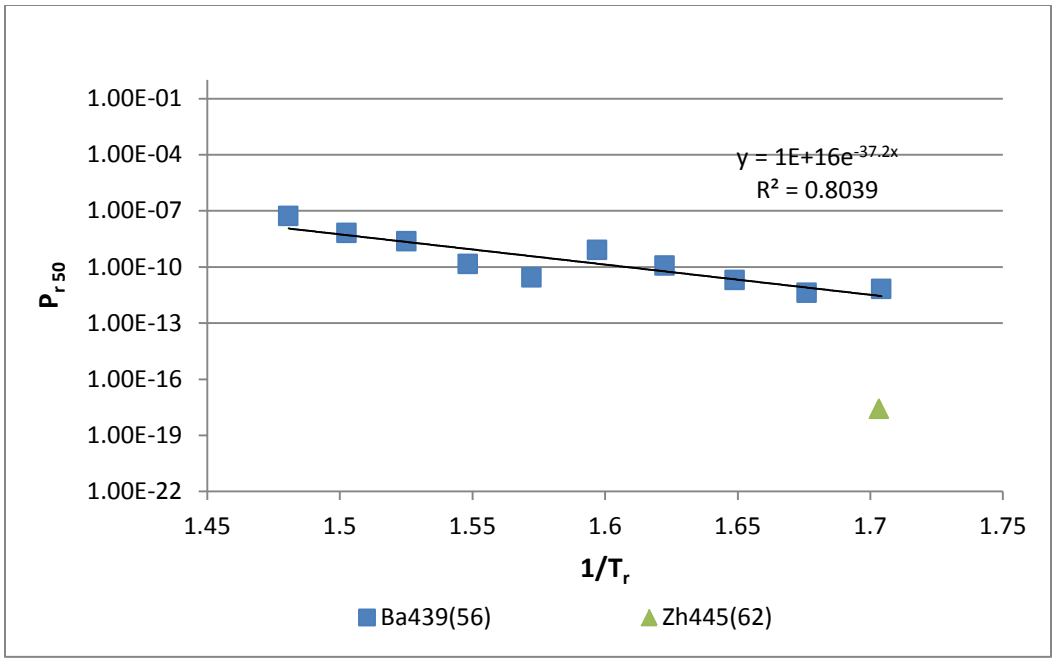

Figure 3.48: log P_{r50} vs. $1/T_r$ for n-hexane on 13X.

The heat of adsorption a 50% loading of hexane is calculated from Figure 3.49:

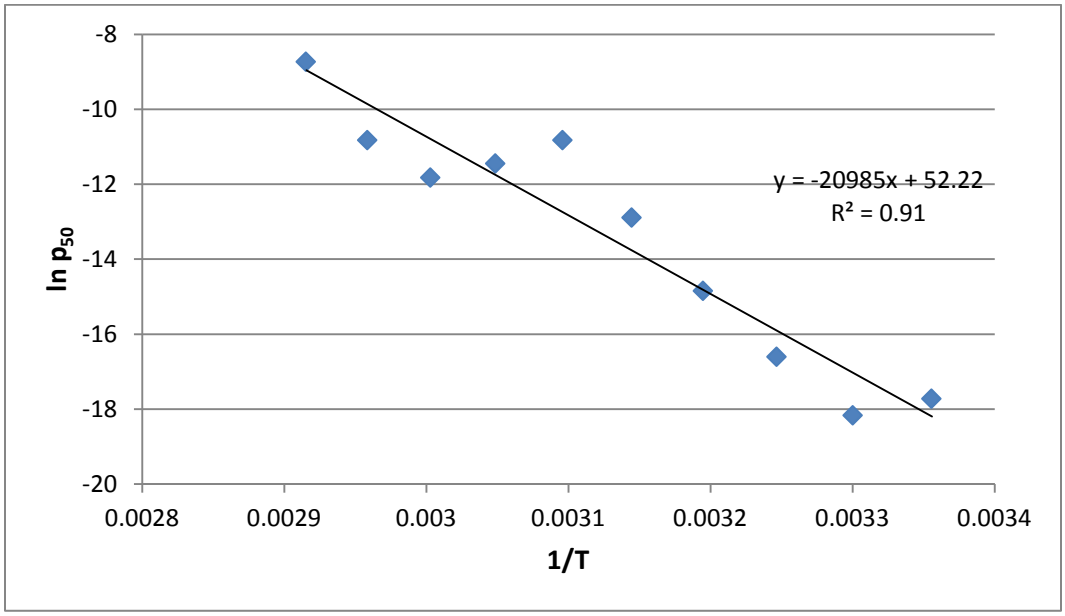

Figure 3.49: ln P_{50} vs. 1/T for n-hexane on 13X.

$$-(\Delta H_{50}) = 20985 * 1.98 * 10^{-3} = 41.55 \ \ kcal/mol. \quad 3.22$$

$$a = e^{52.2} = 4.68 * 10^{22} \quad 3.23$$

Table 3.9: Values of ($-\Delta H_{ads}$) for n-hexane on 13X.

$-\Delta H_{50}$ (kcal /mol)	$-\Delta H_{0lit.}$ (kcal /mol)	a
41.55	20.7 [12]	4.68E+22

The value of the heat of adsorption at 50% loading of n-hexane is compared to the value at 0% loading taken from the study of Barrer and Sutherland [12]. The value calculated by the Gaussian model is double the value found in literature at 0% loading.

3.11 n-Heptane

Figure 3.50 represents the isotherms for n-heptane including two studies by Barrer and Sutherland [12] and Ruthven and Doetsch [15] across a T_r range of 0.55 from the left to 0.90 to the right. Barrer et al. [12] uses a pelleted sample of Linde 13X with 20% binder content while Ruthven and Doetsch [15], on the other hand, use a crystal 13X sample. Isotherms seem to be consistent with each other with no signs of capillary condensation. Hence, all isotherms were retained from the chosen studies. Data, as shown in Figure 5.7, are separated to upper and lower regions. The upper region, consisting of isotherms from Barrer and Sutherland [12] at a T_r range of 0.5 to 0.6, is closer to the saturation region. The lower region, consisting of the isotherms from Ruthven and Doetsch [15], has a lower concentration data with a T_r range of 0.76 to 0.90.

Linearized isotherms for n-heptane on 13X are shown on Figure 3.51. The lines are straight, parallel and range from a reduced temperature of 0.9 from the left to 0.55 to the right. The slopes of the linearized probability lines, σ, plotted against reduced temperature are shown in Figure 3.52. The value of sigma from the data of Ruthven and Doetsch [15], the low saturation region, is equal to 1 while in Barrer and Sutherland [12], the high saturation region, the values of sigma increase from 4 to 6. However, these results are slightly inconsistent with earlier results in that σ increases as the T_r increases. In all earlier studies of alkanes, σ increases as T_r decreases. At this time, it is not known whether this is an artifact or a true reflection of what is occurring.

Constant θ lines for n-heptane appear to separate into two regions in Figure 3.53; in the lower region the slope is positive for the isotherms of Barrer and Sutherland [12] indicating the heat of sorption is positive which is physically impossible whereas the isotherms from Ruthven and Doetsch [15] in the upper region slope downward. This change in behavior might be due to a change in phase from adsorbed liquid to a solid that might occur at such low subcritical temperatures.

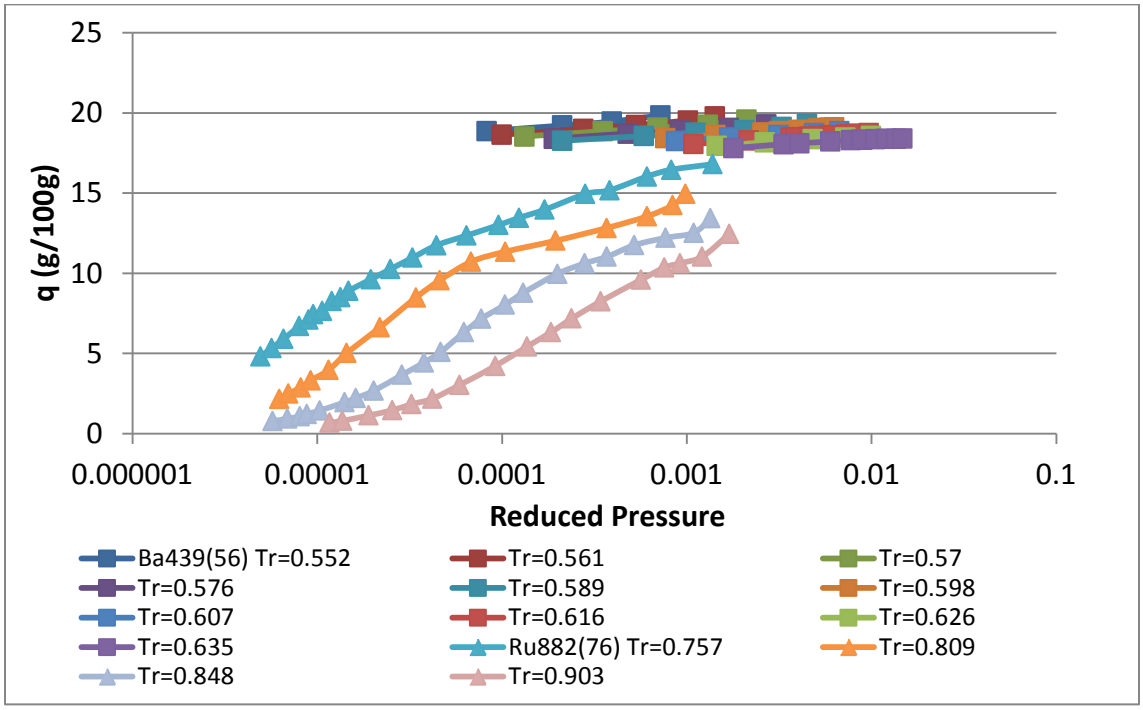

Figure 3.50: Isotherms for n-heptane on 13X.

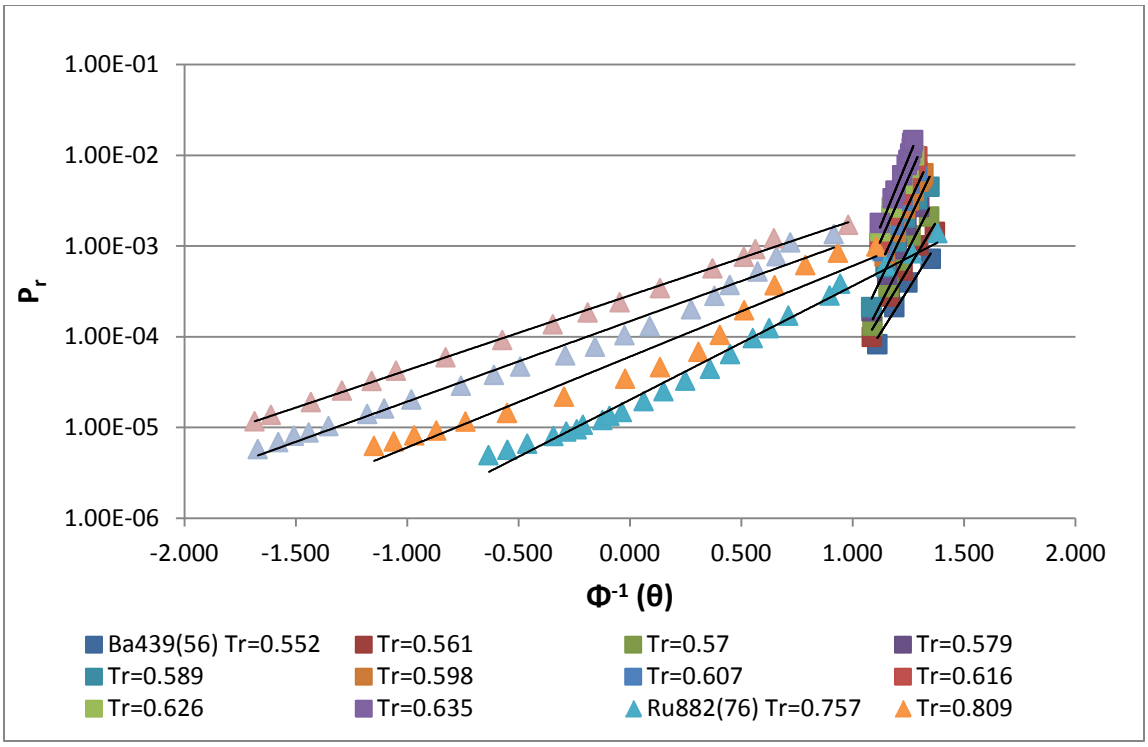

Figure 3.51: Linearized isotherms for n-heptane on 13X.

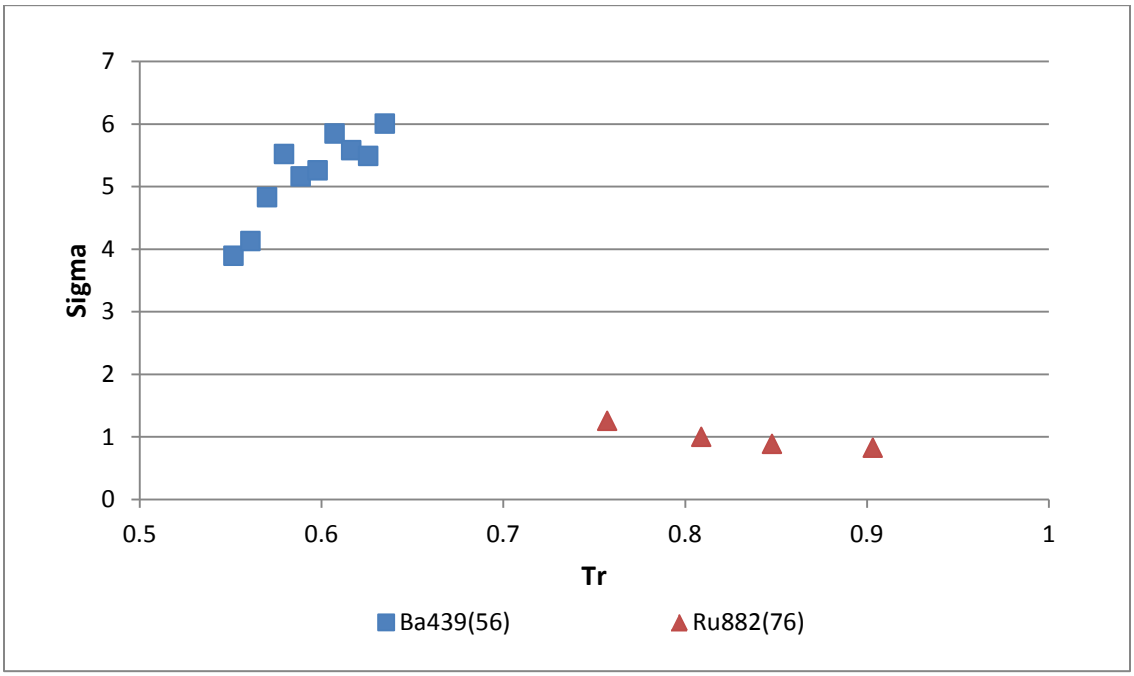

Figure 3.52: Sigma, the slope of the linearized isotherms, as a function of reduced temperature, for n-heptane on 13X.

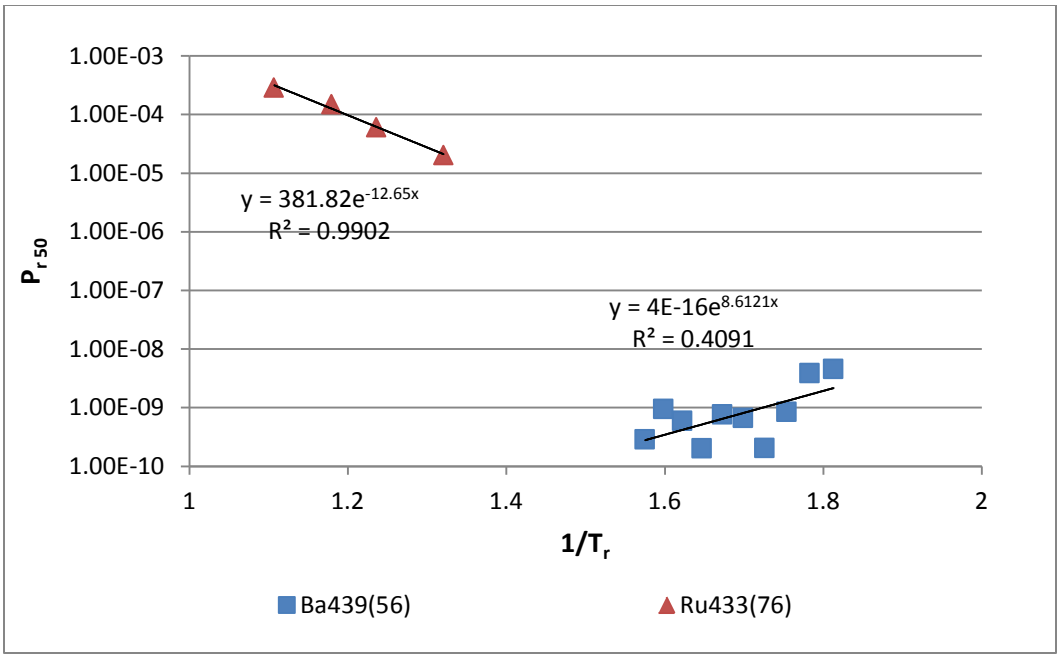

Figure 3.53: log P_{r50} vs. $1/T_r$ for n-heptane on 13X.

The heat of adsorption a 50% loading of n-heptane is calculated from the data of Ruthven and Doetsch [15] in Figure 3.54:

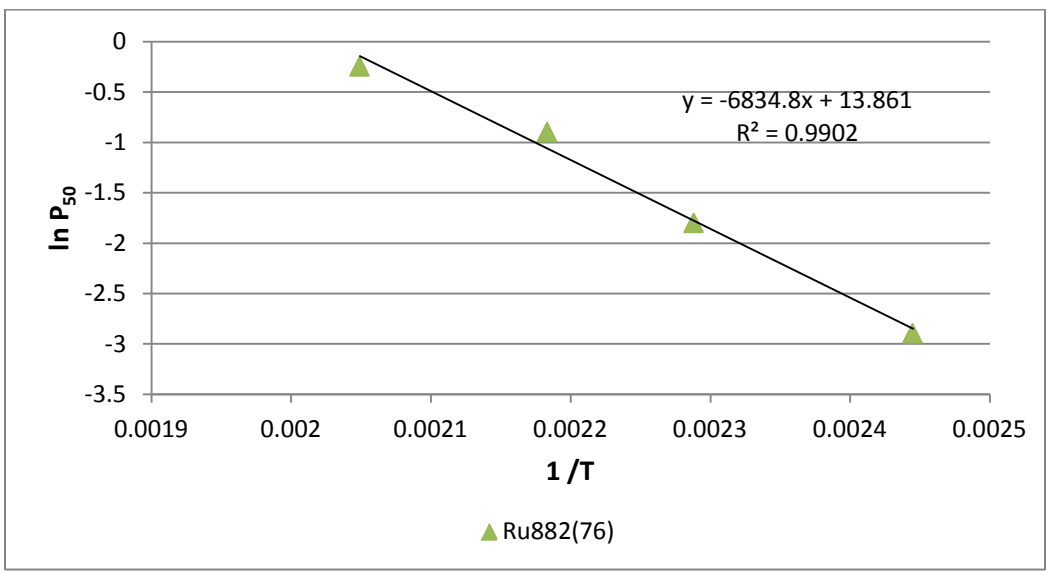

Figure 3.54: ln P_{50} vs. 1/T for n-heptane on 13X.

$$-(\Delta H_{50}) = 6834 * 1.98 * 10^{-3} = 13.53 \ \ kcal/mol. \qquad 3.24$$

$$a = e^{13.86} = 1.04 * 10^{6} \qquad 3.25$$

Table 3.10: Values of ($-\Delta H_{ads}$) for n-heptane on 13X.

$-\Delta H_{50}$ (kcal /mol)	$-\Delta H_{0lit.}$ (kcal /mol)	a
13.53	15.2 [15]	1.04E+06

The value of the heat of adsorption at 50% loading of n-heptane is compared to the value at 0% loading taken from the study of Ruthven and Doetsch [15]. The value calculated by the Gaussian model is less than the value found in literature at 0% loading.

3.12 n-Octane

Figure 3.55 represents the adsorption isotherms for n-octane found in a single study by Barrer and Sutherland [12]. T_r starts at 0.55 on the left hand side of the plot and ends at a T_r of 0.60 on the right hand side of the plot. The isotherms were all consistent in shape and behavior as they were all extracted from a single study. With the lack of another judge on the consistency, the isotherms were all retained as they are. The study was based on an 80% crystal sample of 13X.

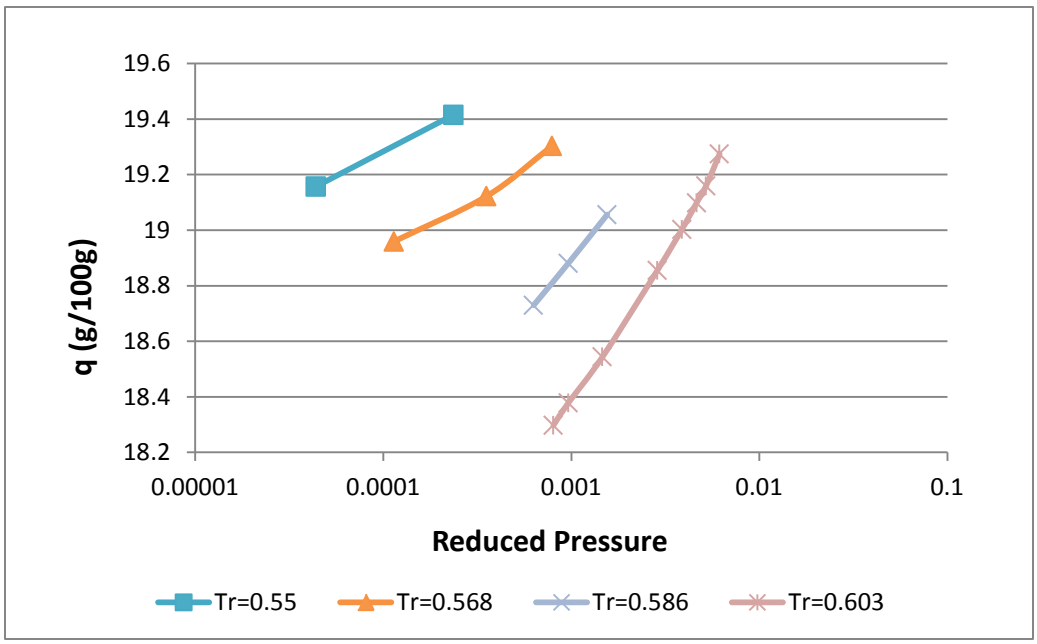

Figure 3.55: Isotherms for n-octane on 13X.

The linearized isotherms of n-octane on 13X are shown in Figure 3.56. The lines are straight with consistently increasing T_r from right to left. As shown in Figure 3.57, the sigma values decrease from 12 to 4 with increasing T_r. The constant θ in Figure 3.58 shows a good linear fit of the data with an R value of 0.95.

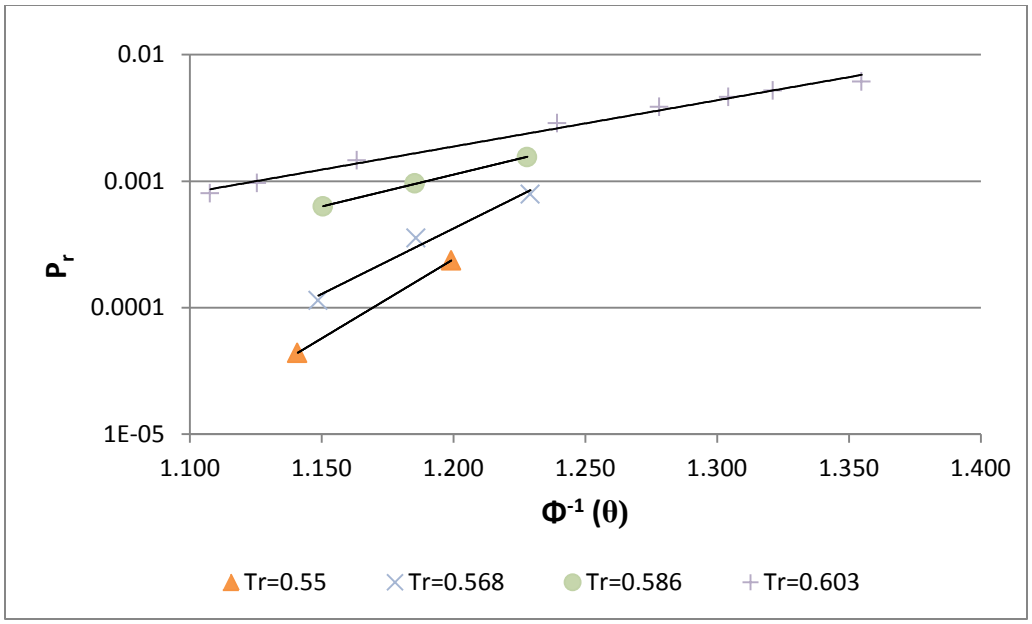

Figure 3.56: Linearized isotherms for n-octane on 13X.

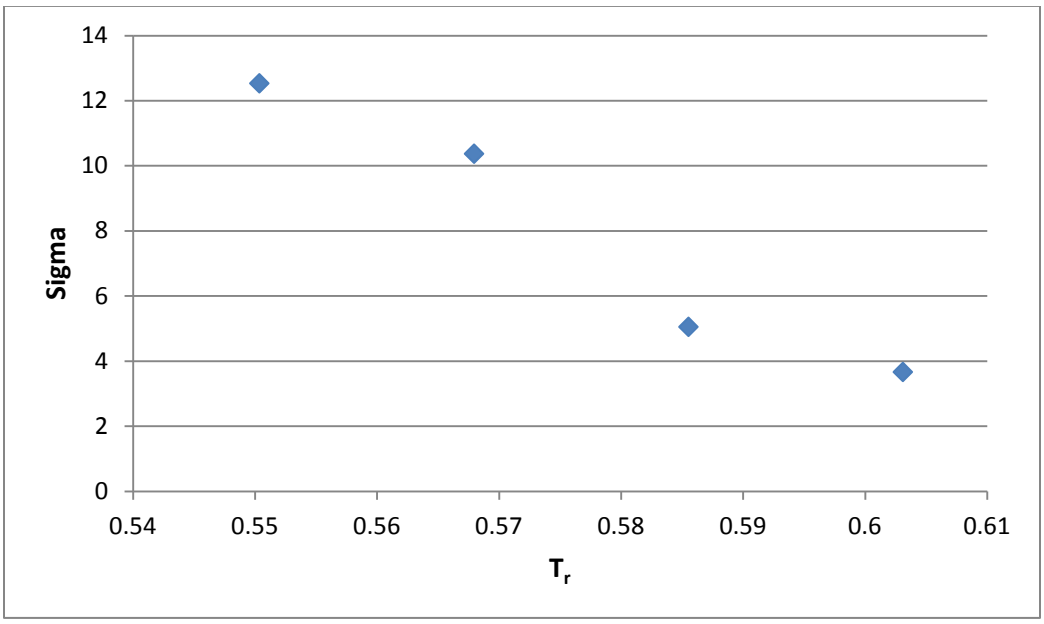

Figure 3.57: Sigma, the slope of the linearized isotherms, as a function of reduced temperature, for n-octane on 13X.

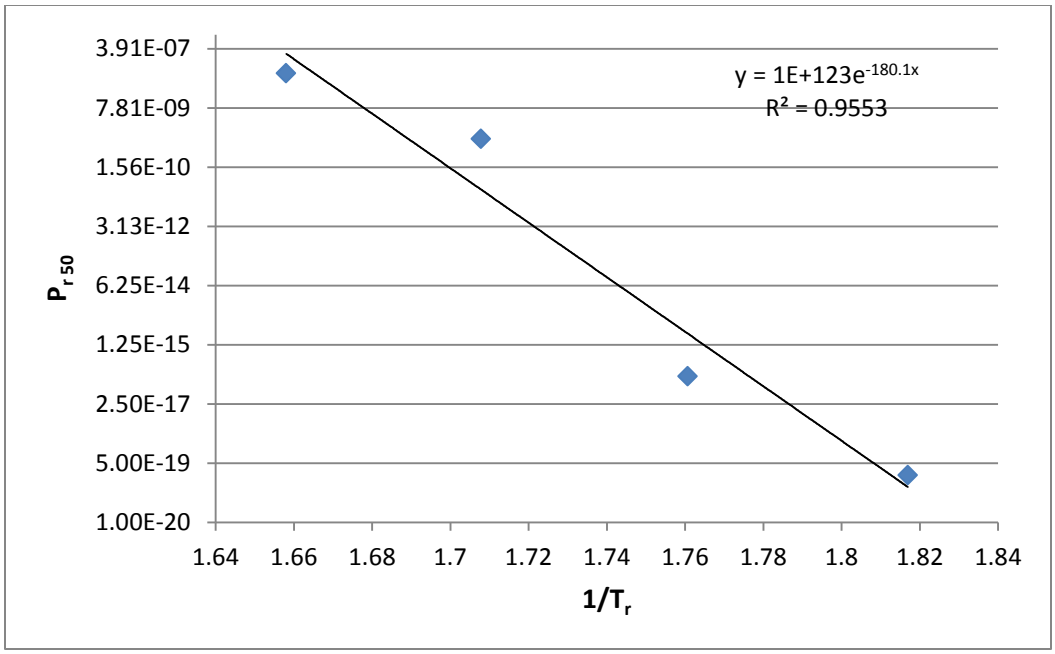

Figure 3.58: log P_{r50} vs. $1/T_r$ for n-octane on 13X.

The heat of adsorption a 50% loading of n-octane is calculated from the slope in Figure 3.59:

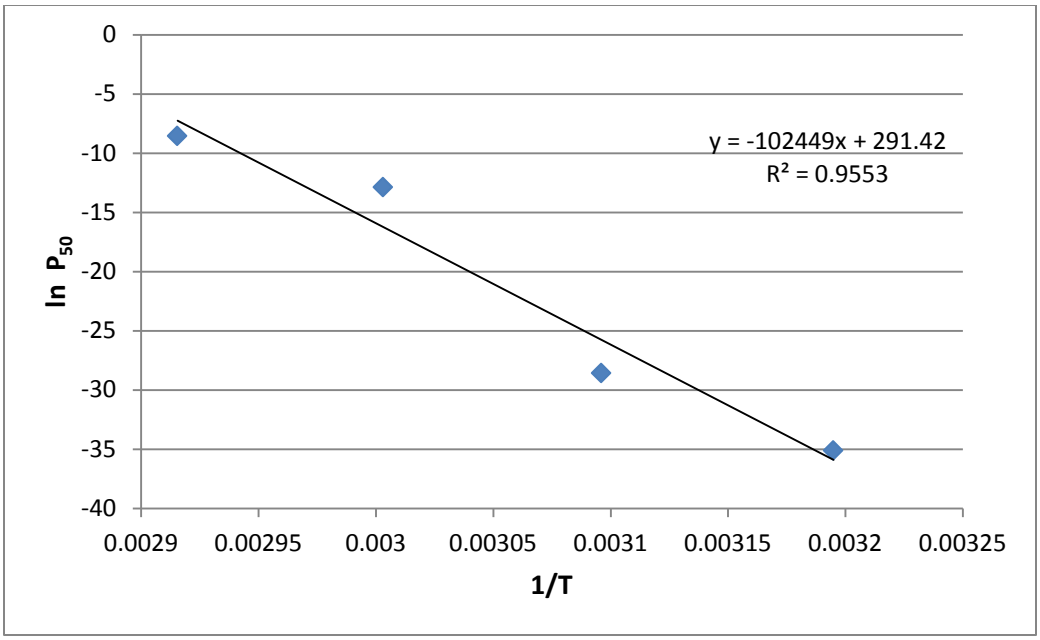

Figure 3.59: ln P_{50} vs. $1/T_{for}$ n-octane on 13X.

$$-(\Delta H_{50}) = 10244 * 1.98 * 10^{-3} = 20.28\ \ kcal/mol. \quad 3.26$$

$$a = e^{291.4} \quad 3.27$$

Table 3.11: Values of ($-\Delta H_{ads}$) for n-octane on 13X.

$-\Delta H_{50}$ (kcal /mol)	$-\Delta H_{0lit.}$ (kcal /mol)	a
20.28	21 [12]	$e^{291.4}$

The value of the heat of adsorption at 50% loading of n-octane is compared to the value at 0% loading taken from the study of Barrer and Sutherland [12]. The value calculated by the Gaussian model is slightly less than the value found in literature at 0% loading.

3.13 **iso-octane**

Figure 3.55 represents the adsorption isotherms for iso-octane found in a single study by Barrer and Sutherland [12]. T_r starts at 0.55 on the left hand side of the plot and ends at a T_r of 0.63 on the right hand side of the plot. The isotherms were all consistent in shape and behavior as they were all extracted from a single study where they are based on an 80% crystal sample of 13X.

Isotherms at Tr =0.55, 0.566, 0.557 and 0.576 exhibit capillary condensation, therefore, some of the data were omitted at the high pressure region. Figures 3.60 and 3.61 show the isotherms before and after alteration, respectively.

The linearized isotherms of iso-octane on 13X are shown in Figure 3.62. The lines are straight and parallel with T_r increasing consistently from right to left. As shown in Figure 3.63, the sigma values start at a value of 10 and then decrease with increasing T_r to a value of 8 and finally to 5. Only at one isotherm, T_r =0.566, sigma increases to a value of 12.5 and then decreases again. The constant θ line in Figure 3.58 shows a good linear fit of the data with an R value of 0.85 except two isotherms, at T_r =0.566 and T_r =0.57, which are inconsistent with the trend of the other isotherms.

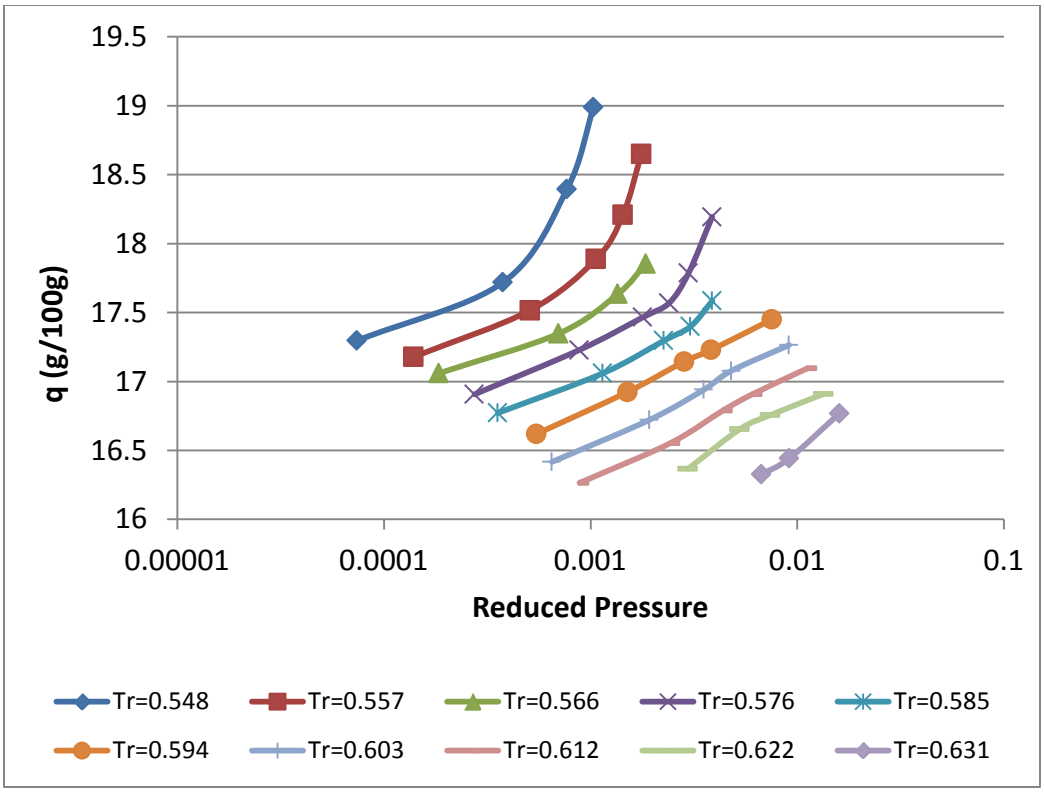

Figure 3.60: Isotherms for iso-octane on 13X (before modification).

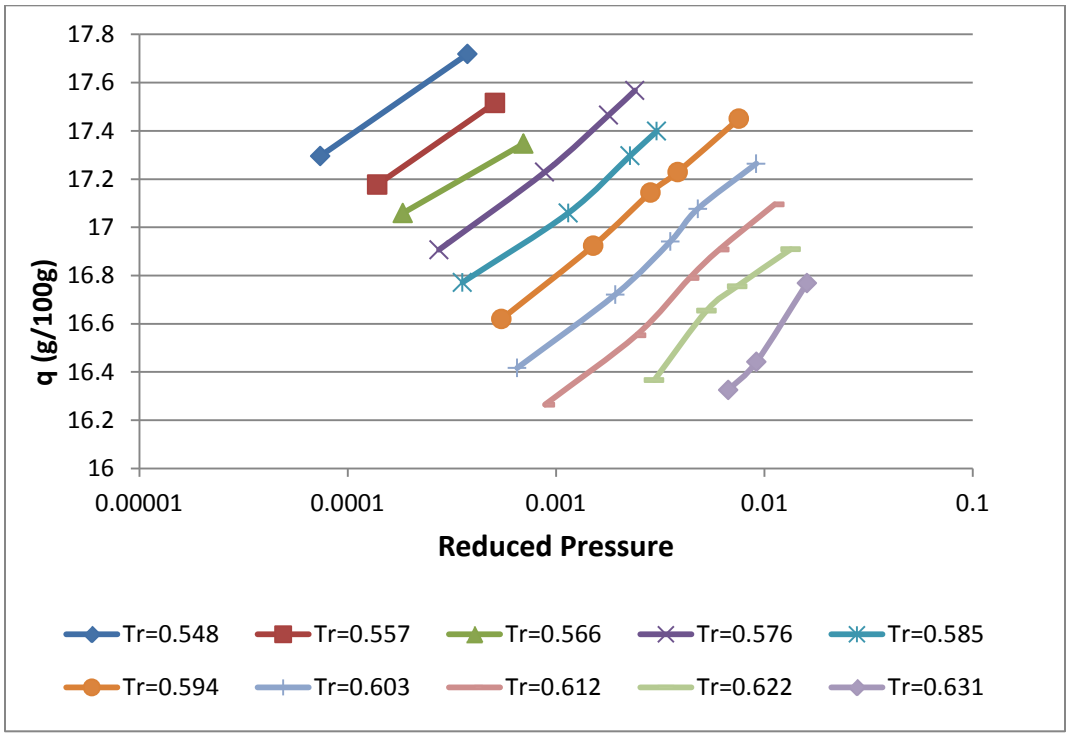

Figure 3.61: Isotherms for iso-octane on 13X (after modification).

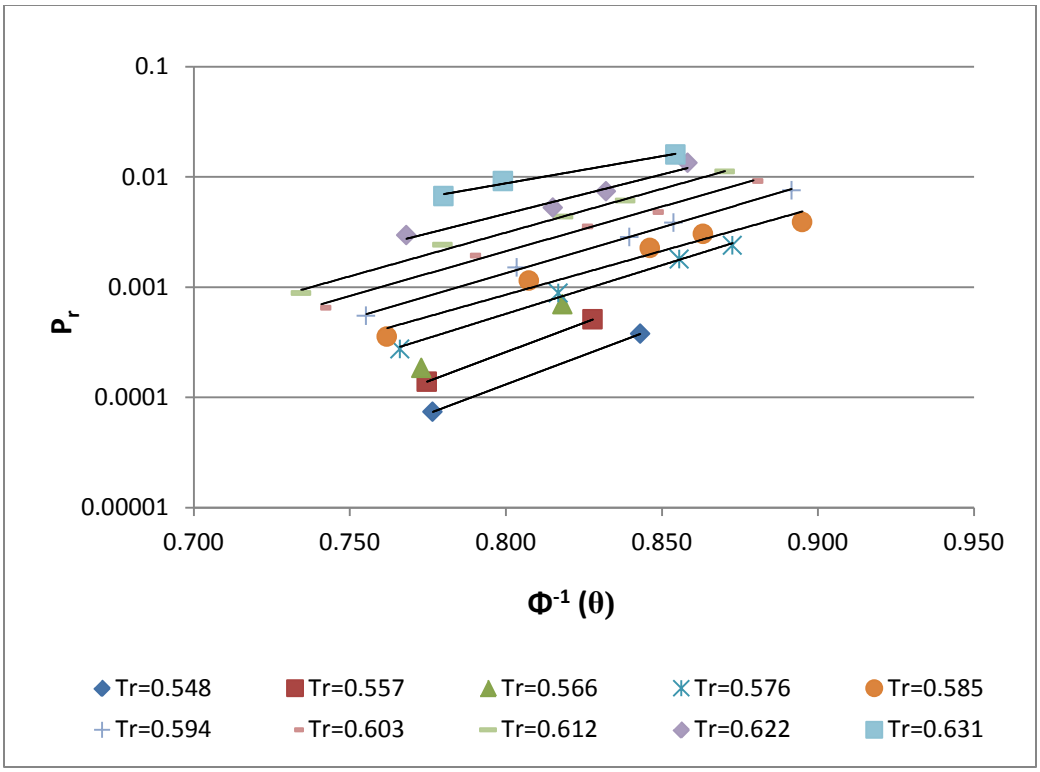

Figure 3.62: Linearized isotherms for iso-octane on 13X.

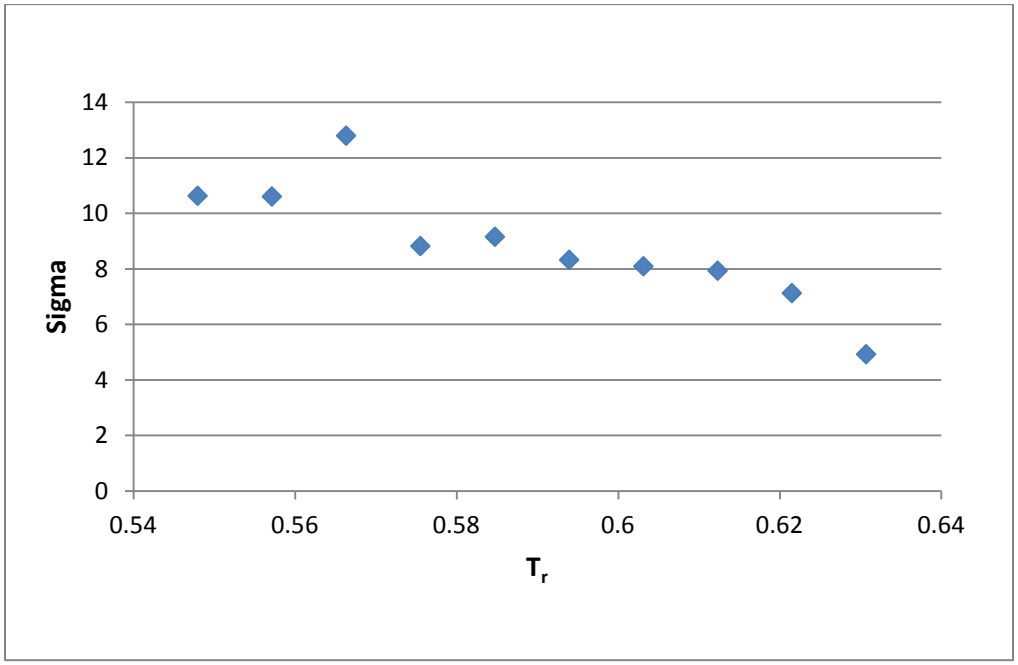

Figure 3.63: Sigma, the slope of the linearized isotherms, as a function of reduced temperature, for iso-Octane on 13X.

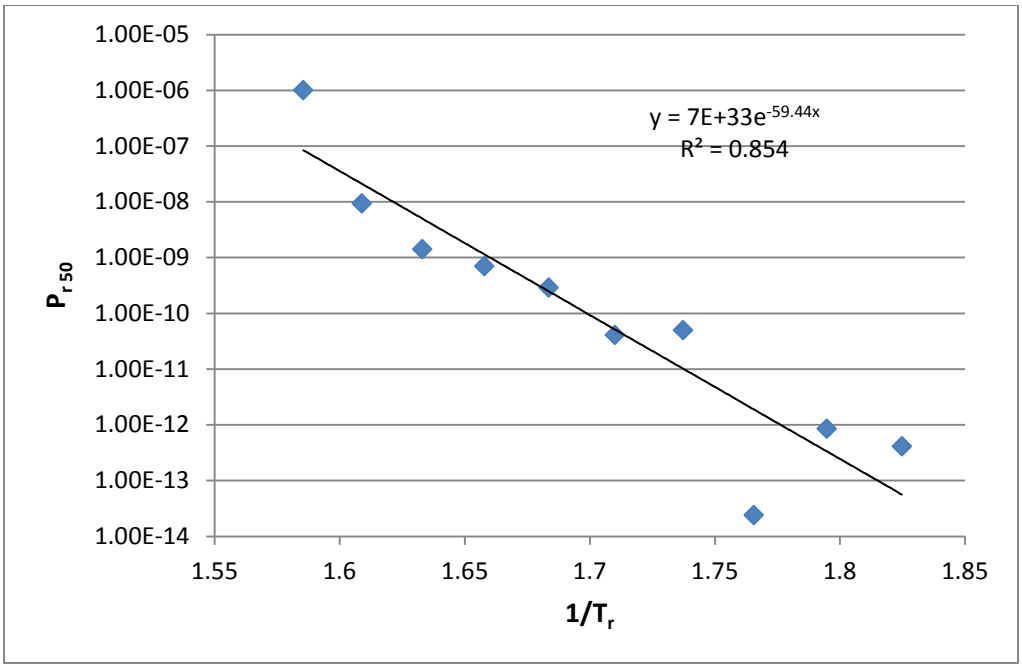

Figure 3.64: log P_{r50} vs. $1/T_r$ for iso-octane on 13X.

The heat of adsorption a 50% loading of iso-octane is calculated from the slope in Figure 3.65:

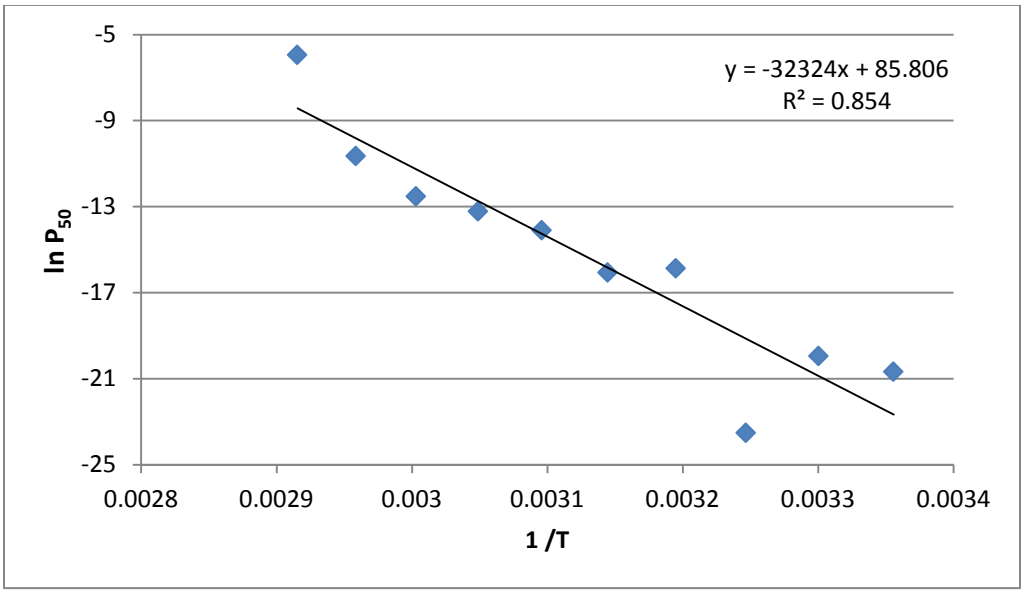

Figure 3.65: $\ln P_{50}$ vs. $1/T_{for}$ iso-octane on 13X.

$$-(\Delta H_{50}) = 32324 * 1.98 * 10^{-3} = 64.00 \ \ kcal/mol. \quad 3.28$$

$$a = e^{85.8} \quad 3.29$$

Table 3.12: Values of ($-\Delta H_{ads}$) for iso-octane on 13X.

$-\Delta H_{50}$ (kcal /mol)	$-\Delta H_{0lit.}$ (kcal /mol)	a
64.00	21.3 [12]	$e^{85.8}$

The value of the heat of adsorption at 50% loading of iso-octane is compared to the value at 0% loading taken from the study of Barrer and Sutherland [12]. The value calculated by the Gaussian model is much higher than the value found in literature at 0% loading.

3.14 Discussion and Conclusion

The value of q_{max} for supercritical adsorption data of alkanes on 13X was taken as 12 g /100g Z. This value was deduced from the results of a previous study done by Abouelnasr and Loughlin [36], on the saturation loading of n alkanes on 5A zeolite, by taking the cavity size ratio of 13X zeolite to 5A zeolite and multiplying it by 9, q_{max} for 5A zeolite. As for the subcritical data, q_{max} was calculated using the crystallographic data and the modified Rackett equation which resulted in a different loading at θ=50% for each isotherm. Therefore, the value of $log\ P_{r50}$is at constant loading only when the isotherms are in the supercritical region, otherwise, the value is said to be at a constant θ.

Consistency of P_{r50} values is affected by the need of extrapolation in some cases where the linearized isotherms do not extend to $\Phi^{-1}(\theta)$ =0. This is apparent in the case of n-butane in Figure 3.20. All linear isotherms were extrapolated to $\Phi^{-1}(\theta)$ =0 in order to get the value of $log\ P_{r50}$. The uncertainty in these values affects the ΔH_{50}values calculated from the plot of $ln\ P_{50}$ vs. $1/T$. Iso-butane linear isotherms from Barrer and Sutherland [12] data, in Figure 3.25, were also extrapolated which reflected on the value of ΔH_{50} giving it a higher value than the one resulting from the other two studies which were not extrapolated. Figures 3.30, 3.35 and 3.39 also show how all the linear isotherms of n, iso- and neo-pentanes, respectively, were extrapolated to a value of zero in order to calculate $log\ P_{r50}$ which also reflected on the value of ΔH_{50} for both n pentane and iso-pentane. The isotherms of neo-pentane were closer to zero and hence the extrapolation is more accurate.

The same situation is encountered in the n-hexane isotherms for $log\ P_{r50}$ values and ΔH_{50} values. For n-heptane, only Barrer and Sutherland [12] data had to be extrapolated. Moreover, $log\ P_{r50}$ values shows an anomaly when plotted against $1/T$, as they increased with increasing $1/T$. the data points were; therefore, excluded from the ΔH_{50}calculations.n-octane linear isotherms in Figure 3.56 were the furthest from zero among all other alkanes. $log\ P_{r50}$ values contain a huge uncertainty especially that the extrapolation was carried on a two or three point lines for most of the isotherms. Iso-octane linear isotherms in Figure 3.62 were closer to zero than for n octane but extrapolation was also done for lines with two to three points only for three of its isotherms.

When looking at P_r vs. $\Phi^{-1}(\theta)$ plots, it is seen that the data conforms to the linear fit for all species. Some of the isotherms, nevertheless, exhibit some concavity or convexity at some part of the line. Methane linear isotherms in Figure 3.3 show an excellent linear fit with straight lines except for two isotherms from Barrer and Sutherland [12] at T_r = 0.473 and T_r = 1.02 and one isotherm from Salem et al. [21] at T_r = 1.35. The three isotherms exhibit a curvature that might be due to an artifact of the data in the study itself or due to the measurement procedure followed. Ethane linear isotherms are separated as subcritical and supercritical in Figures 3.8 and 3.9, respectively. The two subcritical isotherms at T_r = 0.895 in Figure 3.8 show a good linear fit at the beginning but are curved only at the end of the line. The Barrer and Sutherland [12] isotherm at T_r =0.637 is convex and does not look like the other two subcritical linear isotherms. The source of this curvature is unknown at this point and might be linked to the source of the data itself. Moreover, errors in digitizing the data from the isotherm plots in the study may contribute to the irregularity of these fits. The supercritical isotherms in Figure 3.9 are good linear fits with no curvatures. Figure 3.14 shows the subcritical linearized isotherms for propane. The isotherms from Loughlin et al. [18] are concaved up at the beginning and then concaved down at the end. The three isotherms from this study have the same shape and are not linear. The isotherms from Da Silva and Rodrigues [22] show a good linear fit at the beginning but are curved up at the end, all at the same position. The other isotherms in the Figure are good linear fits of the data. Again, as in ethane, supercritical linearized isotherms shown in Figure 3.15 are remarkably linear compared

to the subcritical ones. n-butane linearized isotherms in Figure 3.20 are all remarkably linear. Figure 3.25 shows the linearized isotherms for iso-butane where all the Barrer and Sutherland [12] isotherms are good linear fits. Isotherms from the studies of Hyun and Danner [17] and Lamia et al. [25]at T_r = 0.915 start linear and end with a curvature while the rest show a good linear fit. All the pentanes linearized isotherms in Figures 3.30, 3.35 and 3.39 are remarkably linear. n-Hexane linearized isotherms in Figure 3.46 are all remarkably linear except for the isotherm at T_r =0.587 where one point at the lowest P_r is inconsistent with the others. This irregular point might be an artifact of the data or due to an inaccuracy in reading the isotherm plots from the study paper. n-Heptane linearized isotherms in Figure 3.51 are good linear fits with no irregularities. Similarly, n-octane and iso-octane linearized isotherms are all remarkably linear. From this discussion it is concluded that the data mostly conform to the linear model especially at supercritical temperatures ($T_r > 0.85$). Minor inconsistencies are encountered at subcritical data but the reason for that is not confirmed at this point especially that some isotherms had the same inconsistent shape although they were from different studies.

The sigma fit for each alkane discussed in this chapter seems to be directly related to the isotherm temperature. The supercritical isotherms for methane have sigma values that are all around 1, as in Figure 3.4. Ethane isotherms are all at a T_r range of (0.89-1.2) except for one isotherms at T_r =0.637 from Barrer and Sutherland [12]. Sigma values have a range of (0.5-0.8). The value of sigma at T_r =0.637 is not considered accurate since, as mentioned before, the linearized isotherm was not linear but had a convex shape. Therefore, the slope of the trend line doesn't represent the true value of sigma for this isotherm. Propane sigma values also have a range of (0.7-0.9) at T_r (0.9-1.28). Sigma increases as T_r goes below 0.85 to a value of 1.7, as in Figure 3.16. n-butane starts at a sigma value of 4 at T_r =0.7 and decreases to 2 at T_r = 0.8, as shown in Figure 3.21. The n-butane sigma value does not reach 1 since T_r does not go above 0.85. The same temperature/ sigma relation is observed in iso-butane, as shown in Figure 3.26. Isotherms of $T_r > 0.85$ have a sigma value around 1 which increases to 2 and 3 for lower T_r values ($T_r < 0.85$). Higher sigma values (4 to 5) are encountered in n-pentane that has isotherms with $T_r < 0.73$, Figure 3.31. Figure 3.36 shows the sigma fit for iso-pentane. The isotherms are in the T_r range of (0.65-0.72) and, as expected, sigma starts at 8 and

decreases gradually with increasing T_r until 3, which is still higher than the sigma values encountered at $T_r > 0.85$ for other alkanes. Neo-pentane isotherms have a slightly higher T_r range (0.69-0.8) than iso-pentane. Therefore, its sigma values start at a lower value of 6 and decrease gradually to 5 with increasing T_r, see Figure 3.41. Similar to the pentanes is the n-hexane sigma fit in Figure 3.47. The sigma value at T_r =0.587 from Zhdanov et al. [14] is not considered as the true sigma value for the isotherm. As mentioned before the linearized isotherm from this study is driven by a single inconsistent point that gives it a false slope as seen in Figure 3.46. All the other isotherms have a sigma value between 6 and 7 at a T_r range of (0.58-0.68). The relatively high sigma value with such low T_r values is again visible in this case.

n-Heptane isotherms fall in two T_r regions, one at T_r (0.55-0.63) and the other at T_r (0.76-0.9). Figure 3.52 shows how each range falls under a different sigma level. As expected, the low subcritical temperatures have the higher sigma values (4 to 6) while the higher temperatures have a sigma value around 1. Both n-octane and iso-octane in Figures 3.57 and 3.63 have similar sigma fits. Both have similar high sigma values at similar low T_r values ($T_r < 0.65$).

The calculated values of σ were plotted as a function of reduced temperature for all the isotherms of the alkanes discussed in this chapter (Figure 3.66). The data were in both subcritical and supercritical regions, (0.6-2) T_r. Studying Figure 3.66, it is realized that the data change below $T_r = 0.85$. Sigma values for ($T_r > 0.85$) range from 0.5 to 1 while above that sigma starts at 2 and goes up to 13. This change in behavior at $T_r = 0.85$ suggests that the critical reduced temperature of the adsorbed phase is lower than the VLE critical reduced temperature which is equal to 1.

The value of sigma also increases with the carbon number as shown in Figure 3.66. Methane, ethane, propane and the butanes start from the right of the graph at a sigma value of 1 which increases as we go left with the pentanes, hexane, heptane and the octanes until a value of 13. A similar trend is seen in the sigma fit for alkanes on 5A zeolite. The values of sigma in the case of 5A zeolite doesn't not go as high as in the case of 13X because only supercritical temperatures ($T_r > 0.975$) are considered for 13X. Nevertheless, the similarity between both trends validates the Gaussian model.

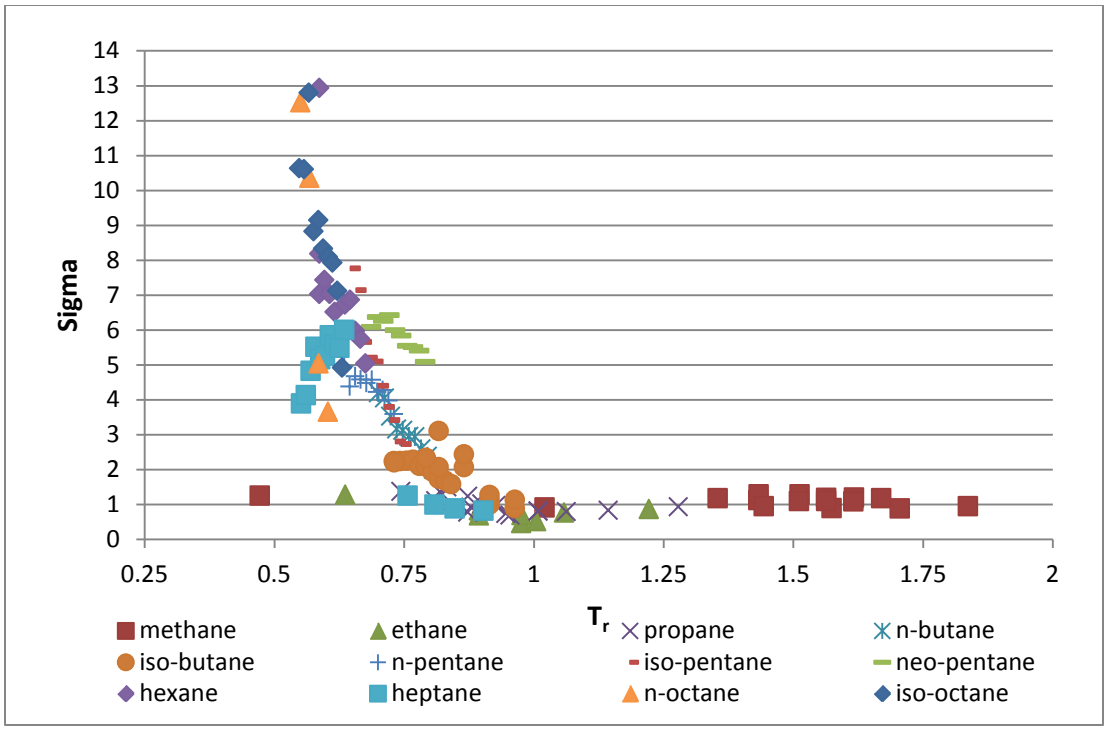

Figure 3.66: Sigma, the slope of the linearized isotherms, as a function of reduced temperature, for all chosen alkanes marked according to species .

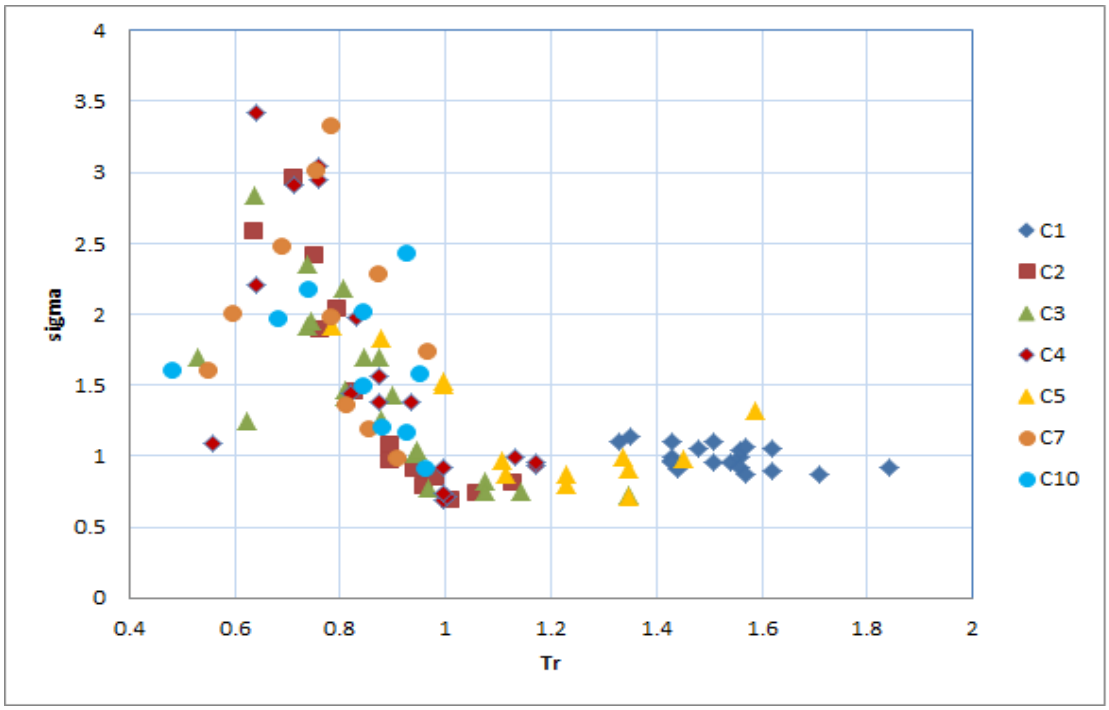

Figure 3.67: Sigma, the slope of the linearized isotherms, as a function of reduced temperature, for alkanes on 5A zeolite.

The plots analogous to the isosteres for 50% loading for all the chosen alkanes in this section are represented in Figure 3.68. All of the lines are straight and follow a consistent pattern starting with the lowest carbon number on the upper left of the graph and moving down gradually to the right with the higher carbon numbers. The magnitude of the slopes of these isosteres *(-ΔH 50 /R)* increase from left to right as the molecular weight of the aromatic compounds increases.

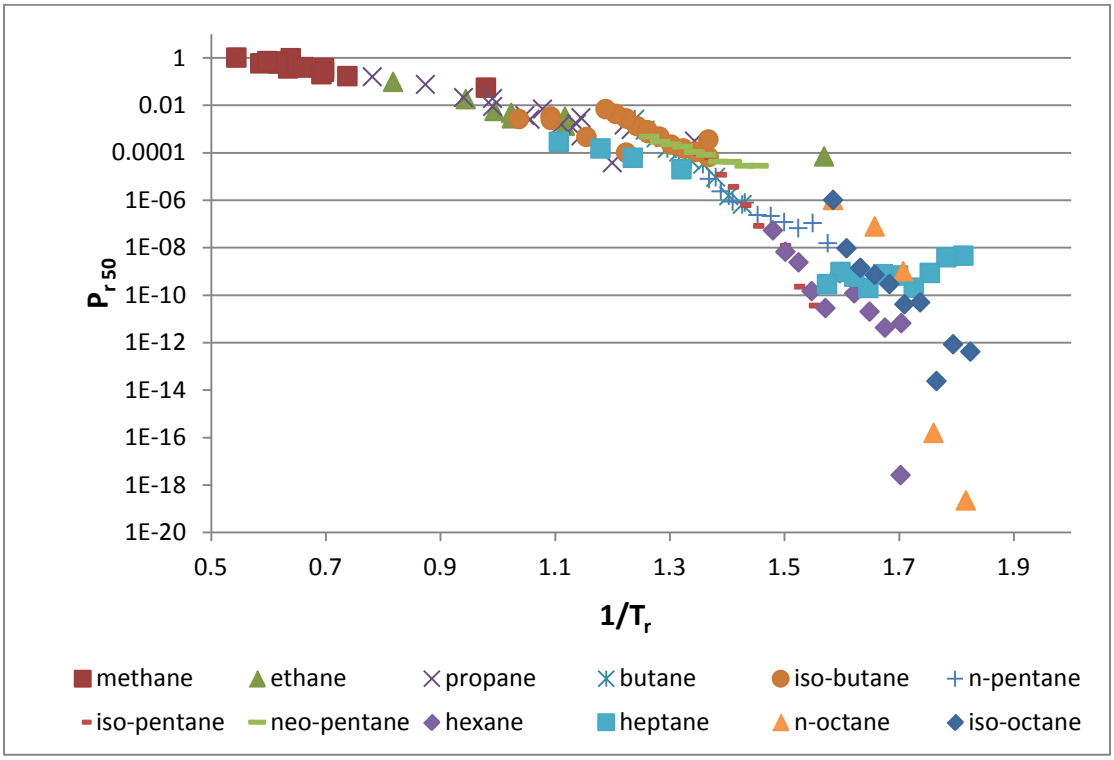

Figure 3.68: Isosteres of 50% loading for all the chosen alkanes.

Tables 3.13 and 3.14 summarize the *(-ΔH$_{ads}$)* values at both 50% and 0% loadings. Two sets of results were found and, hence, were tabulated in separate Tables. Table 3.13 contains values of the heat of adsorption that are either slightly lower or very close to the heat of adsorption at 0% loading taken from literature. Those species, except for neo-pentane and n-octane, have isotherms with T_r>0.85 and hence a sigma value that is close to 1.It is important to note that in the calculation of *(-ΔH 50)* for iso-butane the data from Barrer and Sutherland [12] were excluded so that the extrapolation effect of the P_{r50} values will not affect the results. Data from this study were also excluded in *(-ΔH 50)* calculations for n-heptane because, as mentioned earlier they showed an anomaly at low

T_r values. Table 3.14 contains values that are remarkably higher than literature values. Those species have isotherms with $T_r < 0.8$ and sigma values higher than 2. These results suggest that for low subcritical temperatures, the model does not give a reasonable predictions of *(-ΔH 50)*. Also, there appear to be a strong relation between the sigma value and the *(-ΔH 50)* values. It is not know why both n-octane and neo-pentane behave differently although their sigma values and T_r range fall in the category of Table 3.14.It is important to note that the extrapolation of log P_{r50} values for n-octane was not accurate as mentioned before. Therefore, *(-ΔH 50)* values may contain a lot of uncertainty and the fact that it is found close to literature value may be a coincidence. Also, the neo-pentane isotherms do not include $T_r < 0.68$ and might; therefore, agree more with this category.

Table 3.13: Values of ($-\Delta H_{ads}$) for the chosen alkanes.

	$-\Delta H_{50}$ (kcal /mol)	$-\Delta H_{0lit.}$ (kcal /mol)	a (Gaussian)
Methane	2.63	5.12 [18]	1.89E+05
Ethane	5.43	5.97 [17]	2.93E+05
Propane	8.21	7.80 [18]	3.43E+06
iso-butane	10.76	9.40 [17]	1.97E+15
neo-pentane	13.40	13.30 [12]	4.66E+08
Heptane	13.53	15.20 [15]	1.04E+06
n-octane	20.28	21.00 [12]	$e^{291.4}$

Table 3.14: Values of ($-\Delta H_{ads}$) for the chosen alkanes.

	$-\Delta H_{50}$ (kcal /mol)	$-\Delta H_{0lit.}$ (kcal /mol)	a (Gaussian)
n-butane	35.24	14.50 [12]	3.13E+28
n-pentane	23.45	17.20 [12]	1.18E+13
iso-pentane	66.80	17.20 [12]	4.02E+42
Hexane	41.55	20.70 [12]	4.68E+22
iso-octane	64.00	21.30 [12]	$e^{85.8}$

CHAPTER 4: Sorption of alkenes on 13X

4.1 Introduction

Search of the literature for adsorption data of alkenes on 13X resulted in the literature references listed in Table 4.1. Isotherms were in the subcritical and supercritical regions with a T_r range of (0.8-1.3) T_r. The data are collected from 5 different studies between the years (1976- 2008), as listed in column 1 of Table 4.1. Column 2 of the same Table lists the reduced temperatures of the isotherms chosen from the corresponding study. The adsorption measurement methods as well as the percent crystal are itemized in columns 3 and 4 respectively. The isotherm data were systematically standardized and evaluated according to the same criteria followed previously for n-alkanes. Table 4.1 also shows which isotherms were not included in the study and the reason for that deletion. A total of three alkenes are included in these studies which are: ethylene, propylene, and 1-butene.

Table 4.1: Data on the adsorption of alkenes on 13X.

Authors	Reduced Temperature	Reason Deleted	Method	% Crystal	Paper
Da Silva and Rodrigues (1999)	Propylene: 0.83, 0.885, 0.94, 1.02, 1.16, 1.3		Magnetic Suspension Microbalance	0.83	Si2051(99) [22]
Granato et al. (2007)	Propylene: 0.83, 0.885, 0.94, 1.02, 1.16, 1.3	All are deleted since the reference does not exist	Packed Bed Column	0.8	Gr7239(07) [40]
Hyun and Danner (1982)	Ethylene: 1.06, 1.14, 1.32		Volumetric	0.8	Hy196(82) [17]
Lamia et al. (2007)	Propylene: 0.913, 0.967, 1.02, 1.08		Magnetic Suspension Microbalance	0.83	La2539(07) [25]
Lamia et al. (2008)	1-butene: 0.794, 0.841, 0.889, 0.937		Gravimetric	0.83	La1124(08) [26]

4.2 Ethylene

Figure 5.12 represents the adsorption isotherms for ethylene found in a single study by Hyun and Danner [17]. T_r starts at 1.06 on the left hand side of the plot to a T_r of 1.32 on the right hand side of the plot. The isotherms were all consistent in shape and behavior as they were all extracted from a single study. With the lack of another judge on the consistency, the isotherms were all retained as they are. The study was based on a pelleted sample of 13X with 80% crystal.

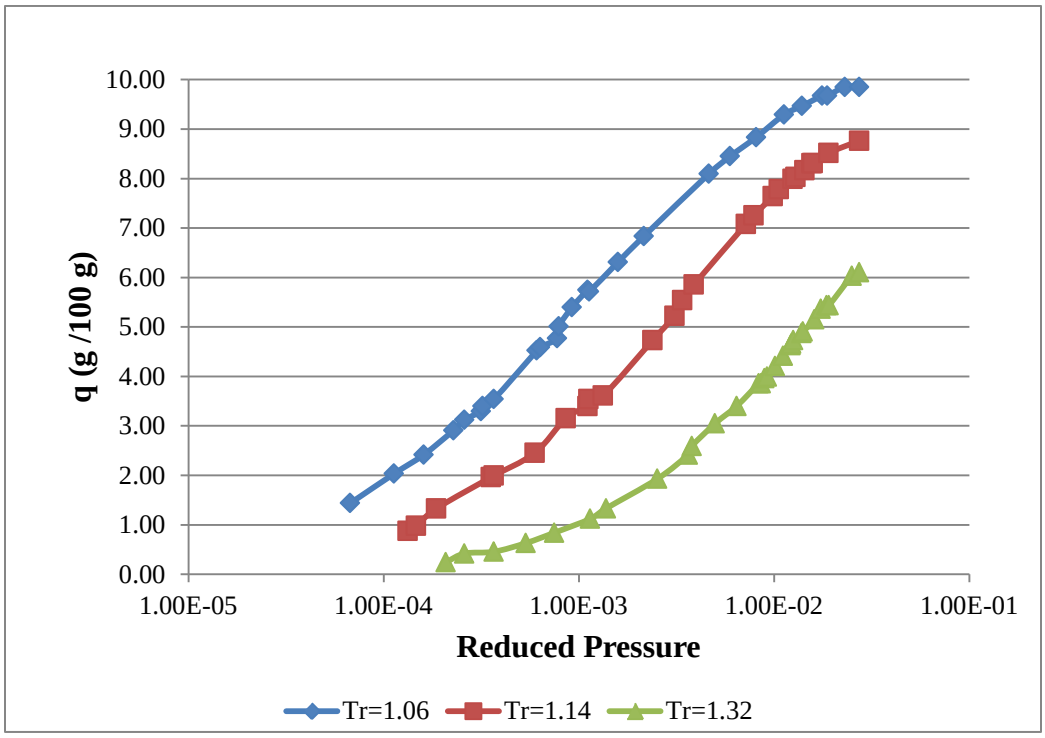

Figure 4.1: Isotherms for ethylene on 13X.

Data for ethylene are in the supercritical region, $T_r > 1$. The maximum saturation loading was taken equal to 12 g /100g Z. The linearized probability plot of reduced pressure P_r vs. $\Phi^{-1}(\theta)$ is shown in Figure 4.2 ranging from a T_r of 1.06 to 1.32. The isotherms are perfectly linear and parallel with increasing T_r from right to left. The slopes of these isotherms, σ, are plotted as a function of reduced temperature in Figure 4.3. The values, as shown in the Figure, are around 1 for all the isotherms.

The isosteres at constant loading are constructed by plotting the y-intercept of the linearized isotherms, *log* P_{r50}, as a function of 1 /T_r, shown in Figure 4.4. The line is perfectly linear with an R value of 1.

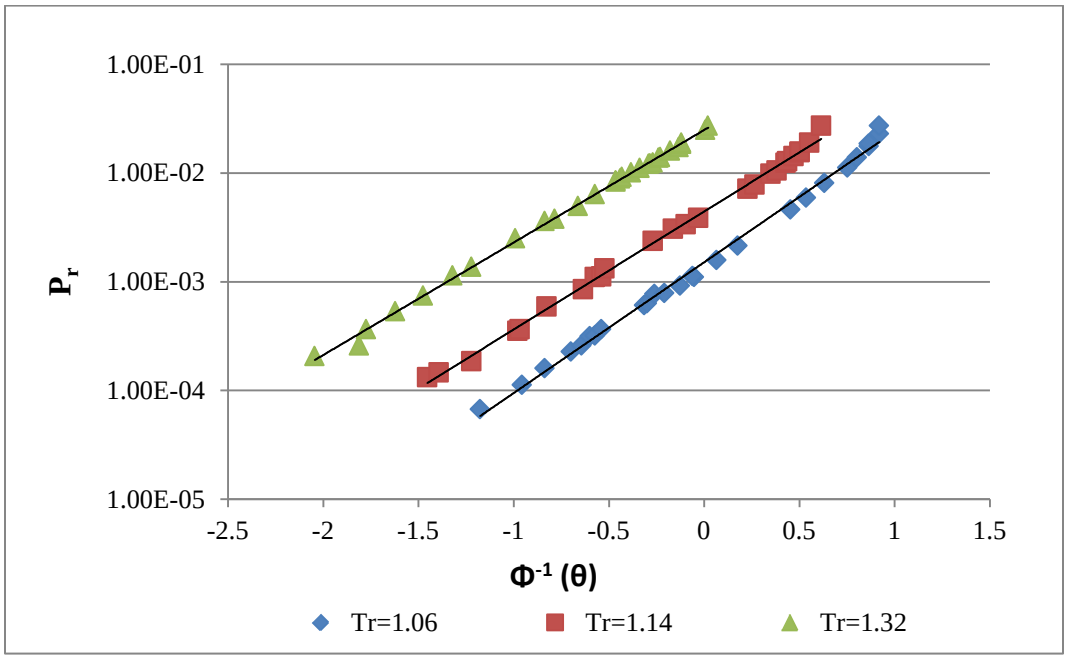

Figure 4.2: Linearized isotherms for ethylene on 13X.

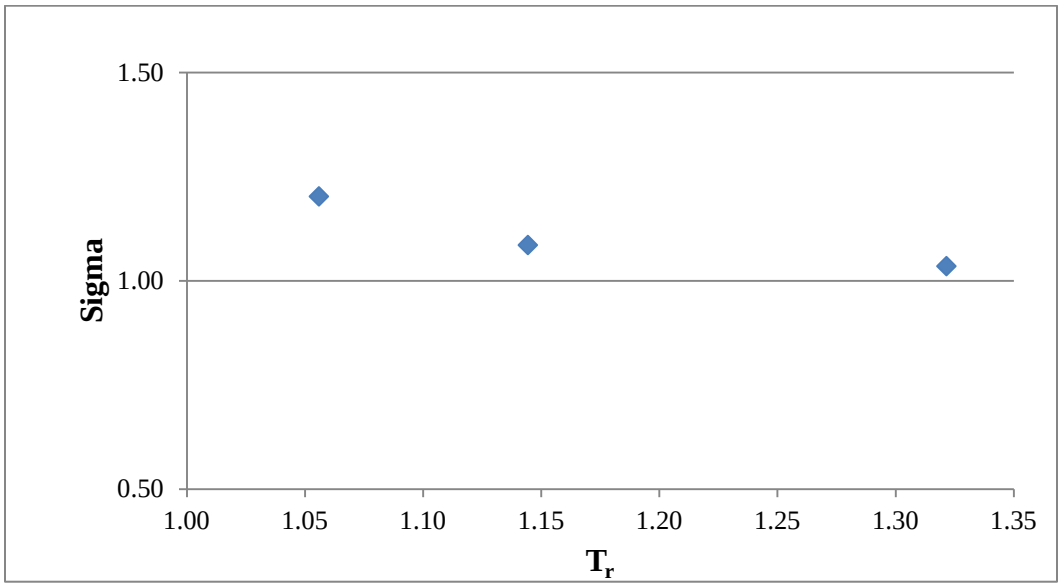

Figure 4.3: Sigma, the slope of the linearized isotherms, as a function of reduced temperature, for ethylene on 13X.

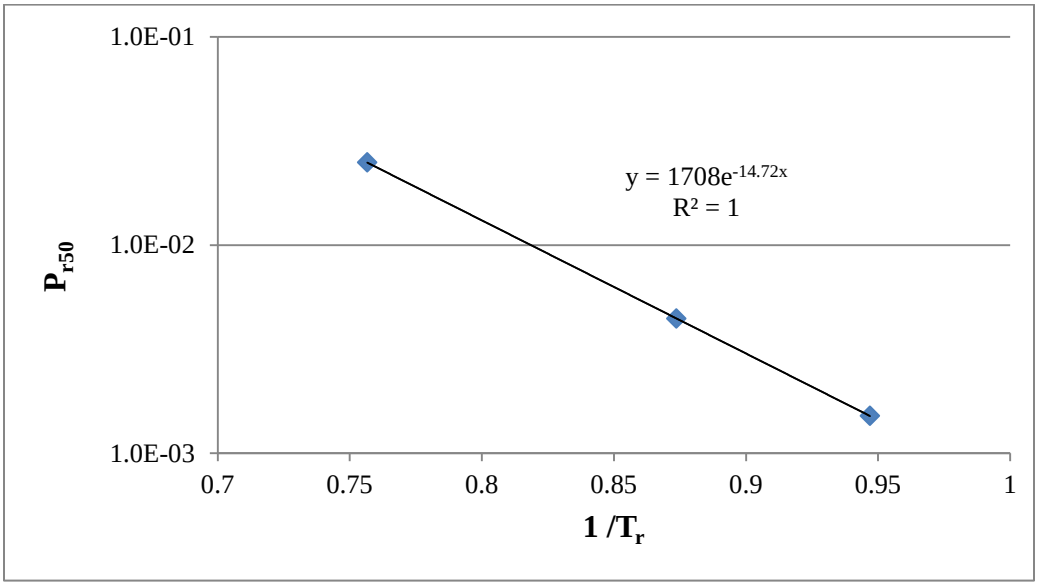

Figure 4.4: log P_{r50} vs. $1/T_r$ for ethylene on 13X.

The value of the heat of adsorption at 50% loading for ethylene is calculated from the slope of Figure 4.5 and compared to the value found in literature at 0% loading; Table 4.2.

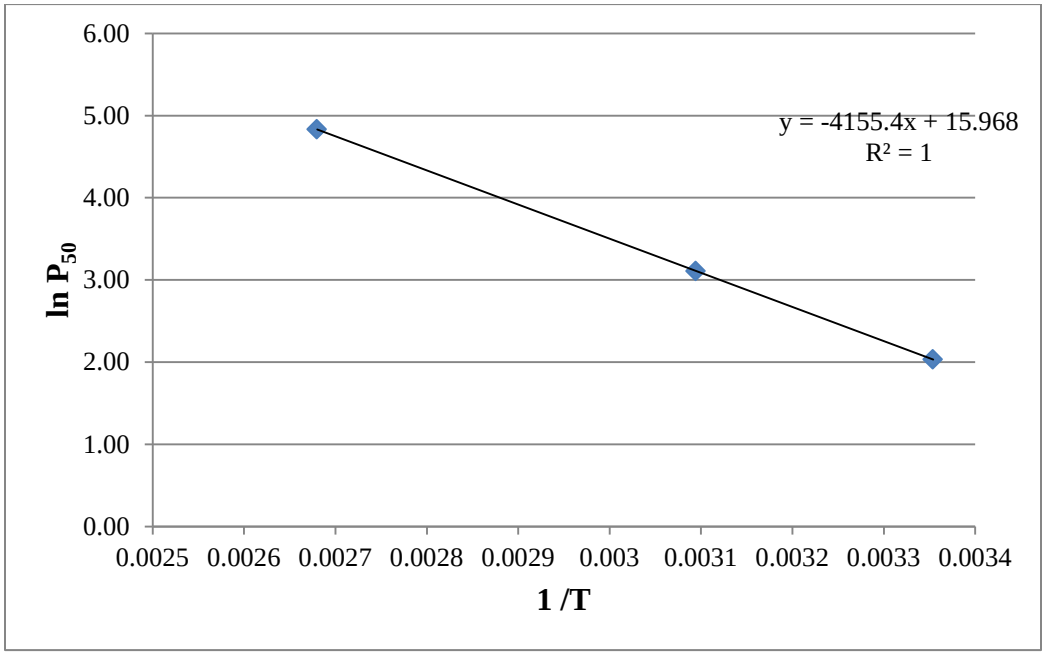

Figure 4.5: ln P_{50} vs. 1/T for ethylene on 13X.

$$-(\Delta H_{50}) = 4155 * 1.98 * 10^{-3} = 8.22\ kcal/mol. \quad 4.1$$

$$a = e^{15.96} = 8.5 * 10^{6} \quad 4.2$$

Table 4.2: Values of ($-\Delta H_{ads}$) for ethylene.

$-\Delta H_{50}$ (kcal /mol)	$-\Delta H_{0lit.}$ (kcal /mol)	a
8.54	9.10 [17]	1.50E+07

The value of ($-\Delta H_{50}$) for ethylene is slightly less than the value of ($-\Delta H_{0lit.}$).

4.3 Propylene

Figure 4.6 shows propylene isotherms taken from three different studies: Granato et al. [40], Lamia et al. [25], and Da Silva and Rodrigues [22]. Isotherms from Granato et al. [40] were all deleted because there was no reference for them in literature. Figure 4.7shows the rest of the isotherms after removing Granato et al. [40] data. All other isotherms from Lamia et al. [25] and Da Silva and Rodrigues [22] are consistent in shape and position except for one isotherm from Lamia et al. [25] at T_r= 0.91 which comes between T_r= 0.89 and T_r = 0.83 from Da Silva and Rodrigues [22]. Nevertheless, the isotherm was not deleted because of its proximity to the other isotherm at T_r = 0.89. A pelleted 13X zeolite sample with 17% binder content was used.

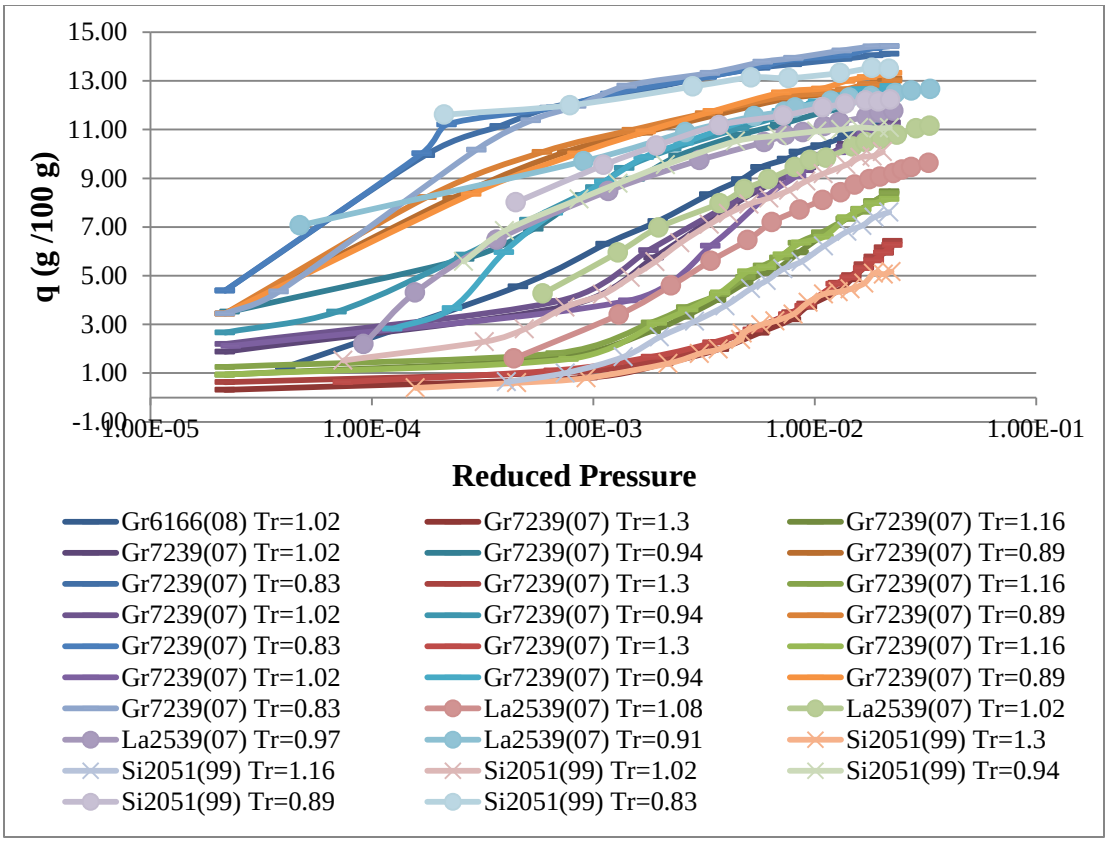

Figure 4.6: Isotherms for propylene on 13X (before screening).

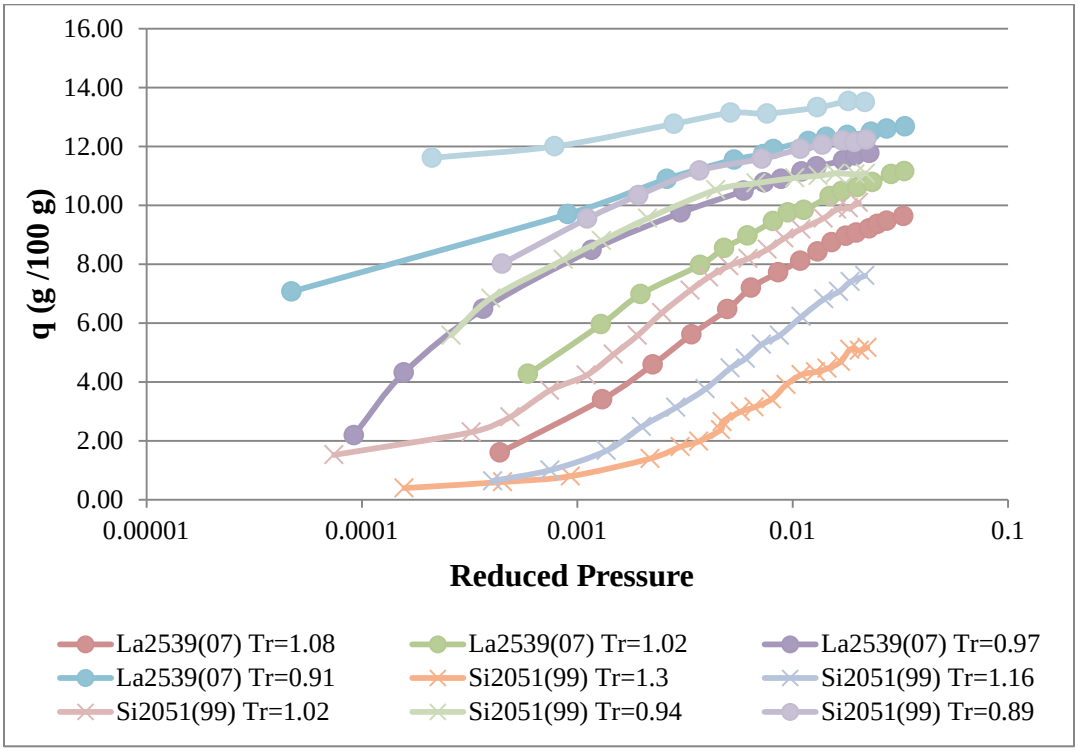

Figure 4.7: Isotherms for propylene on 13X (after screening).

Data for propylene are in both subcritical and supercritical regions with a range of (0.83-1.08) T_r. The maximum saturation loading is taken as 12 g /100g Z. Propylene linearized isotherms are shown in Figures 4.8 and 4.9 for subcritical and supercritical temperatures, respectively. The four subcritical isotherms in Figure 3.8 are crossing each other. The isotherms at T_r = 0.83 and T_r = 0.91 are linear while the others show some curvature. As for the supercritical isotherms in Figure 4.9, the lines from both studies are remarkably straight, parallel and consistent with each other with T_r gradually decreasing from left to right. The slopes of the linearized isotherms, σ, are plotted as a function of reduced temperature for both supercritical and subcritical data in Figure 4.10. Sigma starts at two in the subcritical region and decreases with increasing temperature to a value of 1 at the supercritical region. One isotherm at T_r = 0.83 has a higher sigma value of 4.3. The constant θ lines at 50% loading of ethane on 13X are shown in Figure 4.11. The lines from both studies are linear and consistent with each other with an R value of 0.98 for the Lamia et al. [25] isotherms and 0.85 for the Da Silva and Rodrigues [22] isotherms. The lower R value of Da Silva and Rodrigues [22] isotherms is due to one point at T_r = 0.83 that is slightly off the linear trend.

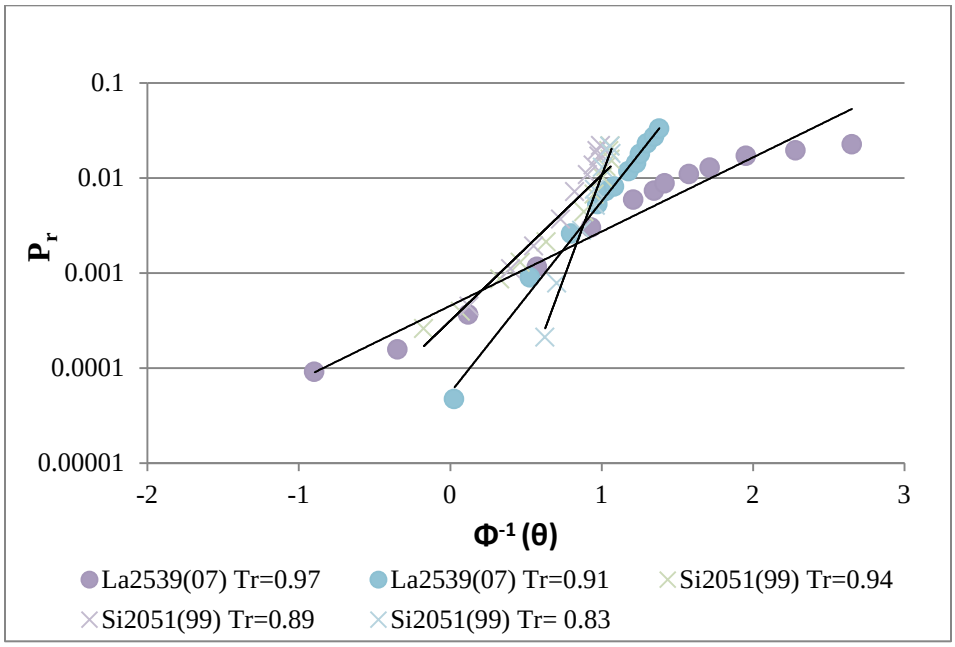

Figure 4.8: Linearized isotherms for propylene on 13X (subcritical region).

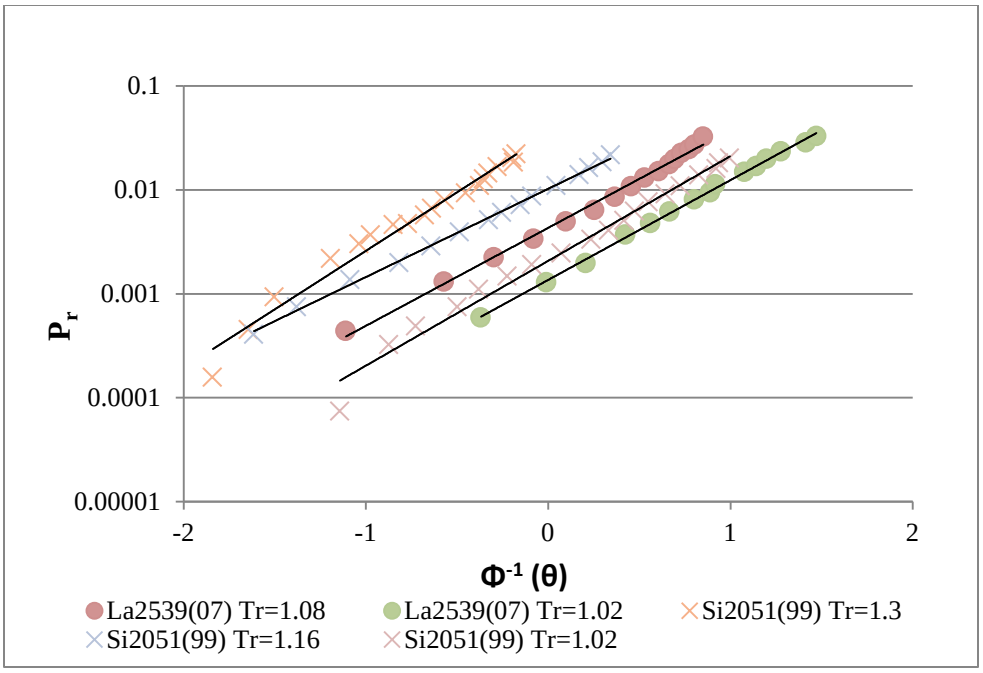

Figure 4.9: Linearized isotherms for propylene on 13X (supercritical region).

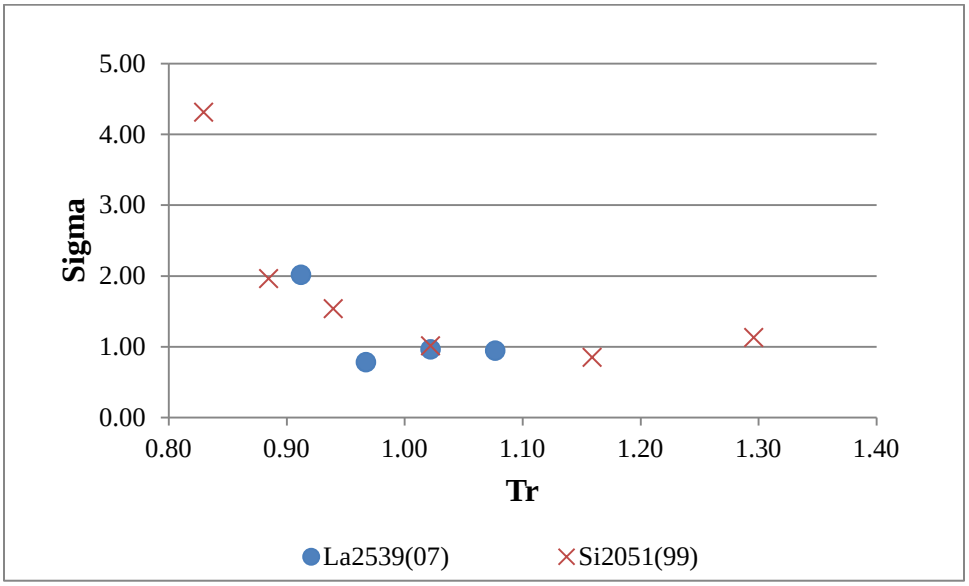

Figure 4.10: Sigma, the slope of the linearized isotherms, as a function of reduced temperature, for propylene on 13X.

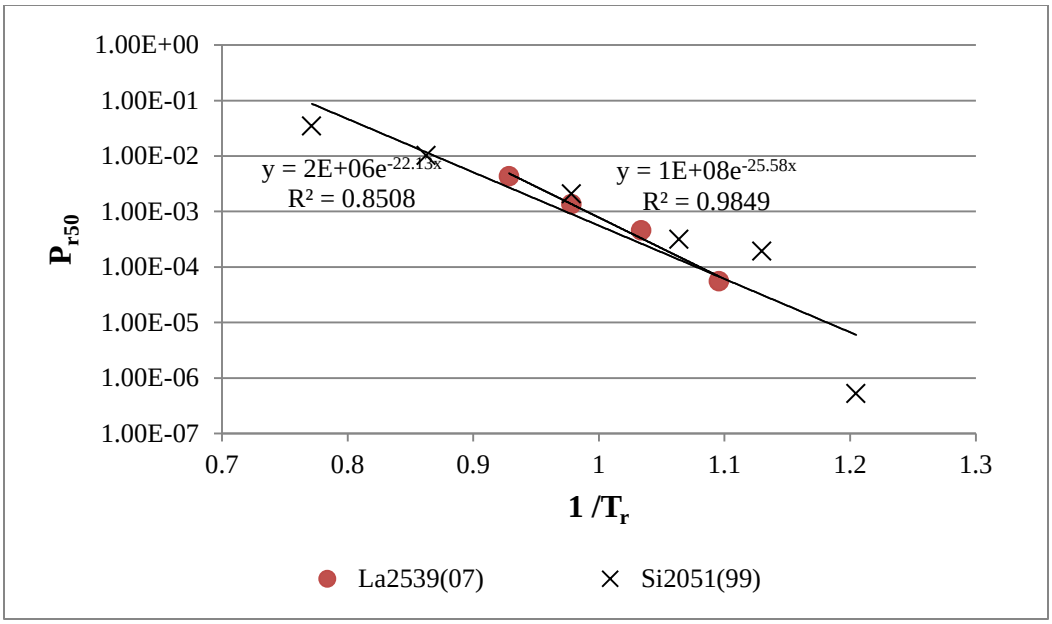

Figure 4.11: log P_{r50} vs. $1/T_r$ for propylene on 13X.

The value of the heat of adsorption at 50% loading for propylene is calculated from the slope of Figure 4.12 and compared to the value found in literature at 0% loading. The isotherm at T_r =0.83 was excluded because it was inconsistent with the other values as mentioned in Figure 4.11.

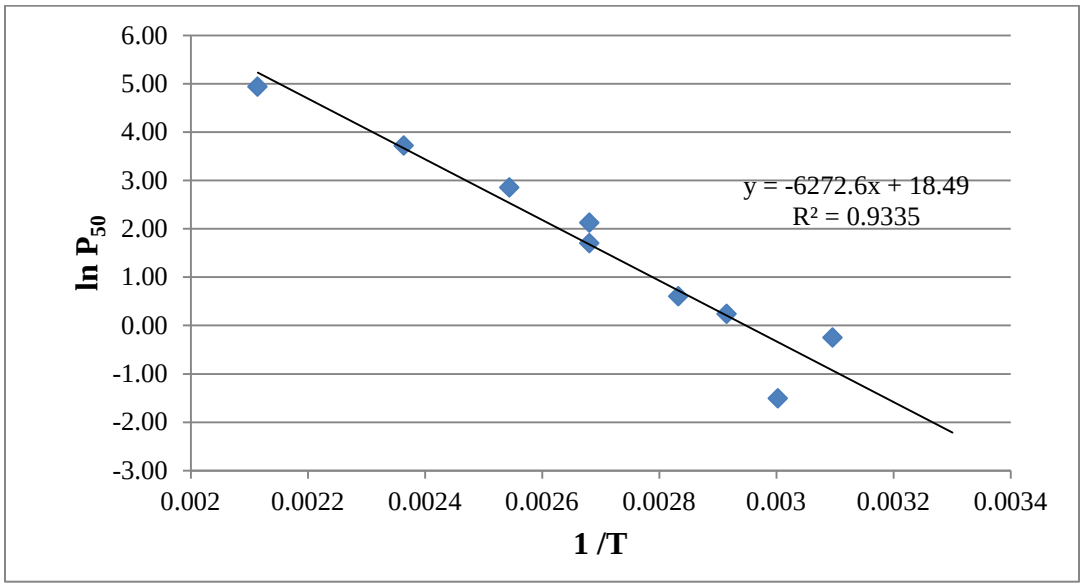

Figure 4.12: ln P_{50} vs. 1/T for propylene on 13X.

$$-(\Delta H_{50}) = 5490 * 1.98 * 10^{-3} = 10.87\ kcal/mol. \quad 4.3$$

$$a = e^{16.62} = 1.65 * 10^{7} \quad 4.4$$

Table 4.3: Values of ($-\Delta H_{ads}$) for propylene.

$-\Delta H_{50}$ (kcal /mol)	$-\Delta H_{0lit.}$ (kcal /mol)	a
10.87	10.13 [25]	1.65E+07

The value of the heat of adsorption at 50% loading of propylene is compared to the value at 0% loading taken from the study of Lamia et al. [25]. The value calculated by the Gaussian model is approximately equal to the one found in literature.

4.4 1- butene

Figure 3.19 represents the adsorption isotherms for 1-butene found in a single study by Lamia et al. [26]. T_r starts at 0.79 on the left hand side of the plot to a T_r of 0.94 on the right hand side of the plot; hence, all isotherms are in subcritical region. The isotherms were all consistent in shape and behavior as they were all extracted from a single study. With the lack of another judge on the consistency, the isotherms were all retained as they are. A pelleted sample of 13X zeolite with 80% crystal is used.

The linearized isotherms are shown on Figure 4.14.All lines are linear but they cross each other. The slopes of the linearized isotherm are plotted against T_r, in Figure 4.15, where the values of sigma increase from 2.7 to 4, at T_r =0.84, and then decrease back to 1.7. Figure 4.16 shows the constant θ lines of 1-butene. With a regression value of 0.47, the data is a poor linear fit mainly because of the isotherm at T_r= 0.84 show inconsistency with other data.

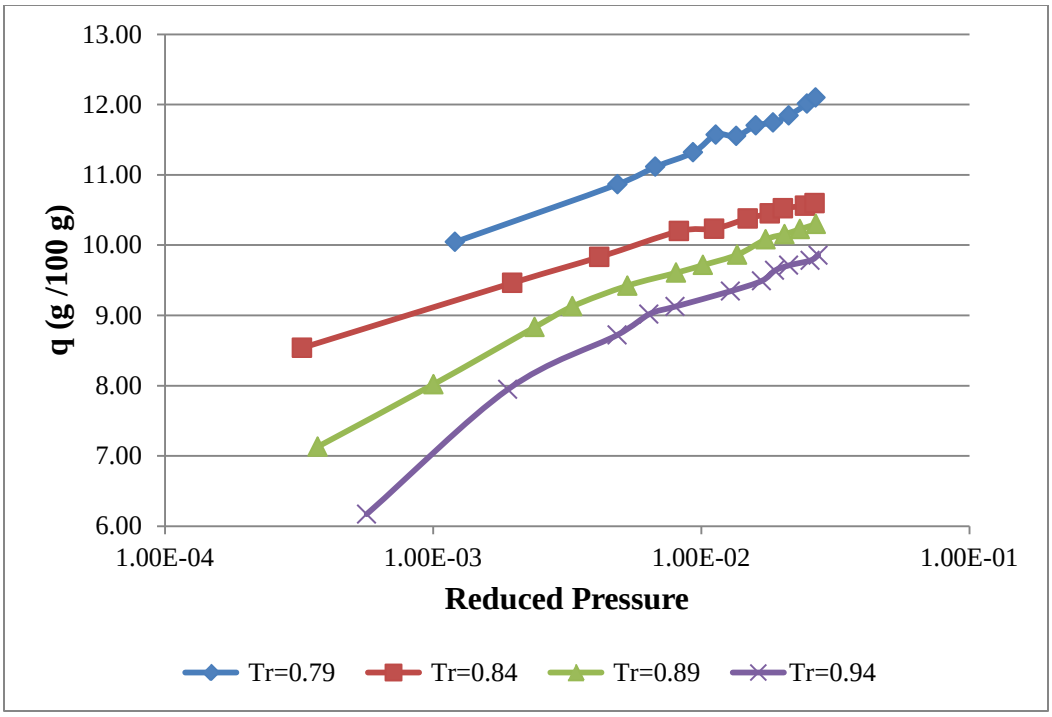

Figure 4.13: Isotherms for 1-butene on 13X.

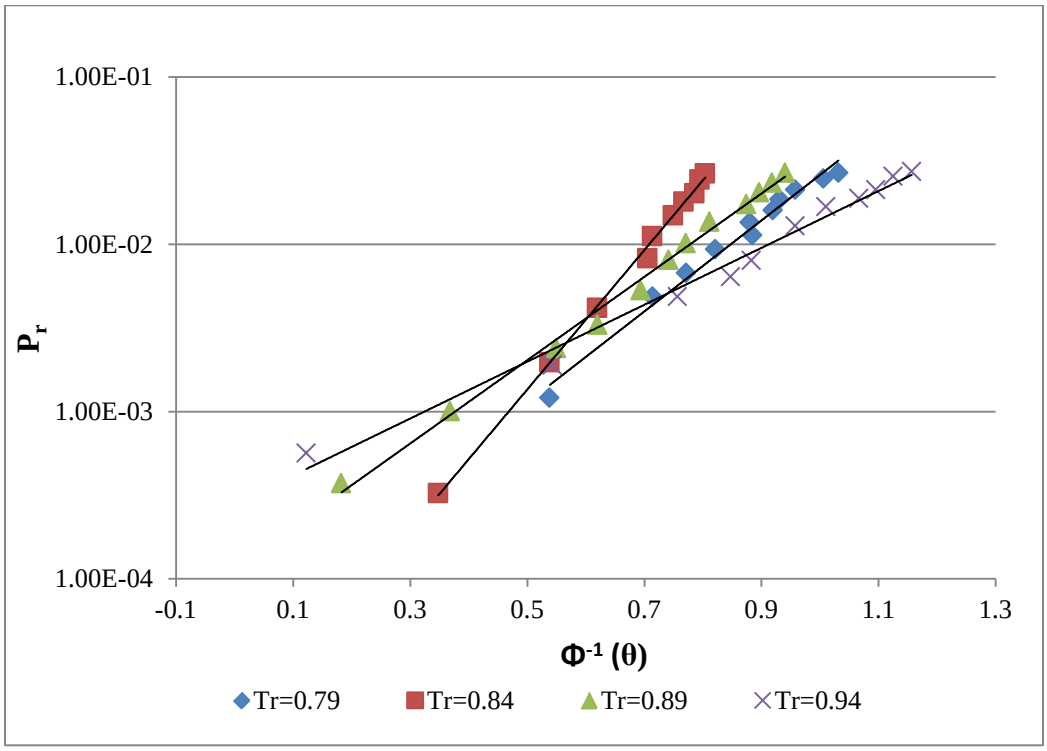

Figure 4.14: Linearized isotherms for 1-butene on 13X.

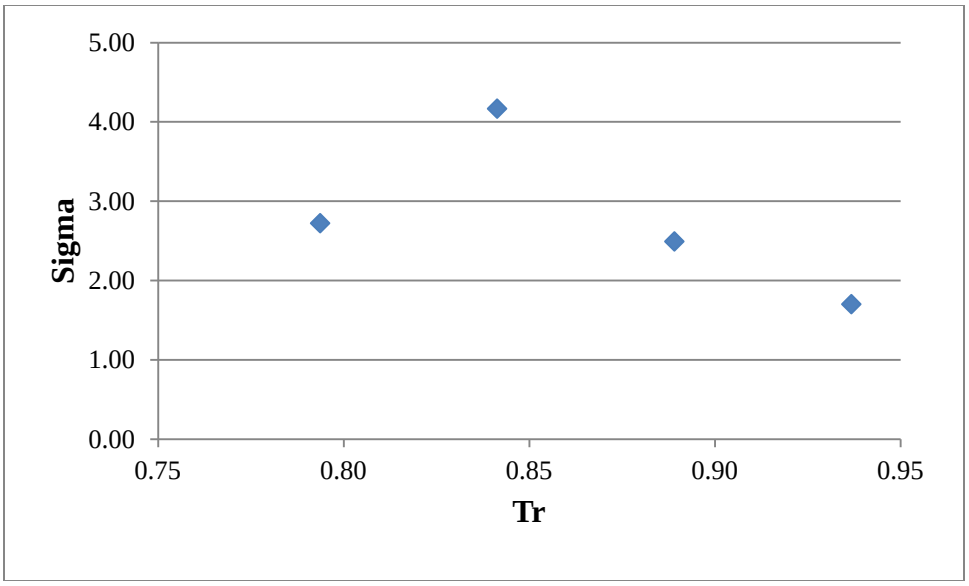

Figure 4.15: Sigma, the slope of the linearized isotherms, as a function of reduced temperature, for 1-butene on 13X.

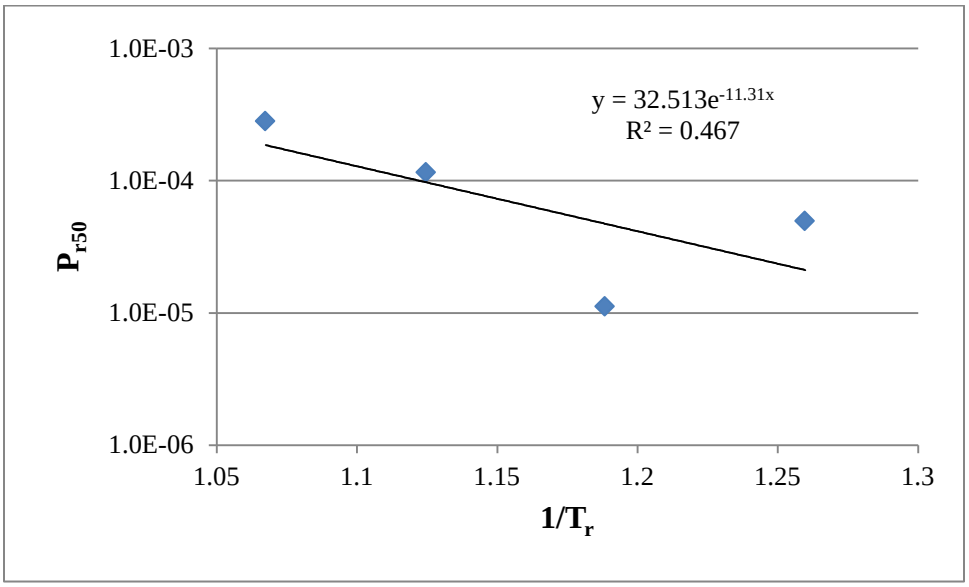

Figure 4.16: log P_{r50} vs. $1/T_r$ for1-butene on 13X.

The value of the heat of adsorption at 50% loading for 1-butene is calculated from the slope of Figure 4.17 and compared to the value found in literature at 0% loading.

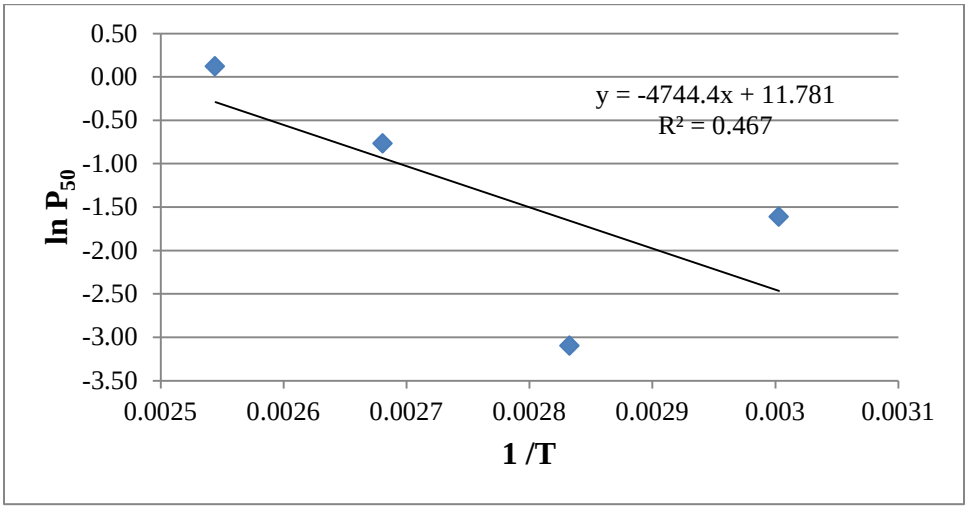

Figure 4.17: ln P_{50} vs. 1/Tfor1-butene on 13X.

$$-(\Delta H_{50}) = 4744 * 1.98 * 10^{-3} = 9.40\ kcal/mol. \quad 4.5$$

$$a = e^{11.78} = 1.30 * 10^{5} \quad 4.6$$

Table 4.4: Values of ($-\Delta H_{ads}$) for 1-butene.

$-\Delta H_{50}$ (kcal /mol)	$-\Delta H_{0lit.}$ (kcal /mol)	a
9.40	13.00 [26]	1.30E+05

The value of the heat of adsorption at 50% loading of 1-butene is compared to the value at 0% loading taken from the study of Lamia et al. [26]. The value calculated by the Gaussian model is less than the one found in literature.

4.5 Discussion and Conclusion

The value of q_{max} for supercritical adsorption data of alkenes on 13X was taken as 12 g /100g Z for the same reason discussed for alkanes. As for the subcritical data, q_{max} was calculated using the crystallographic zeolitic data and the modified Rackett equation which resulted in a different loading at θ=50% for each isotherm. Therefore, the value of $log\ P_{r50}$ is at constant loading only when the isotherms are in the supercritical region, otherwise, the value is said to be at a constant θ.

Ethylene linearized isotherms in Figure 4.2 were not extrapolated giving consistent $log\ P_{r50}$ values. The lines show a good linear fit of the data. The isotherm at T_r = 1.06 exhibits a slight curvature. Propylene subcritical linearized isotherms, in Figure 4.8, did not require extrapolation to get $log\ P_{r50}$ except at one isotherm at T_r = 0.83. The isotherms are remarkably linear except at T_r = 0.97 where the upper half of the isotherm is concaved down. The isotherms also cross each other at several points. The supercritical isotherms, in Figure 4.9, show a better linear fit than the subcritical ones and are parallel with no need for extrapolation except at T_r = 1.3. One point at the end of the isotherms at T_r = 1.3 and T_r = 1.02, which are from the same study, falls out of the linear line. This might be as a result of an artifact of the data. Linearized isotherms for 1-butene, shown in Figure 4.14, are good linear fits with no curvature. The $log\ P_{r50}$ values were extrapolated to zero but the extrapolation is accurate given the linearity and sufficient amount of points for the regression. As in the case of propylene, the isotherms cross each other but at more than one point.

Ethylene has sigma values that are all around 1 for the T_r range of (1.06-1.32). Propylene has a sigma value of 1 for all T_r > 0.97 as shown in Figure 4.10. Sigma increases to 2 at T_r = 0.9 and reaches a value of 4.3 at T_r = 0.83. This relatively high value of sigma is inconsistent with the other data and might be due to an artifact of the data.1-butene also exhibits higher sigma values than usual for such temperature ranges (T_r > 0.8), as shown in Figure 4.15. Note that both the subcritical linearized isotherms of propylene and ethylene cross each other and exhibit the same behavior. As a matter of fact only isotherms from Lamia et al. [25] cross each other for both species which suggests that the uncertainty exists in the data itself.

The calculated values of σ were plotted as a function of reduced temperature for all the isotherms of the alkenes discussed in this chapter (Figure 4.18). The data were in subcritical and supercritical regions in the range(0.8-1.35) T_r. Sigma values are approximately equal to 1 except for 1-butene and some of the propylene data where it reaches a value of 4.3 at low subcritical temperatures. As explained earlier the unexpectedly high sigma value may be due to an artifact of the data.

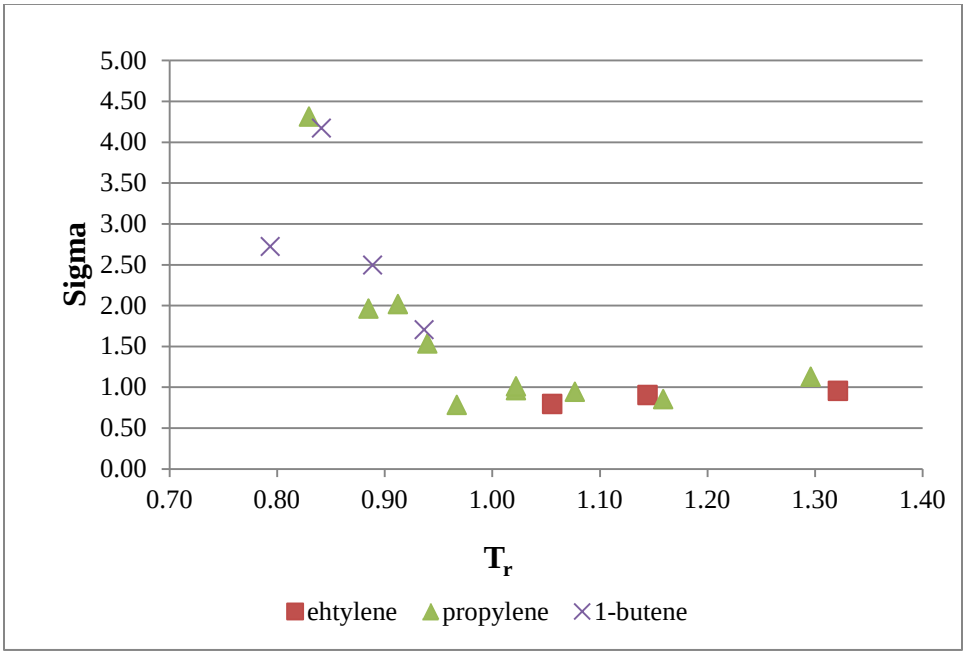

Figure 4.18: Sigma, the slope of the linearized isotherms, as a function of reduced temperature, for all chosen alkenes marked according to species.

The constant θ lines analogous to the isosteres at 50% loading for all the chosen alkenes in this section are represented in Figure 4.24. All of the lines are straight and follow a consistent pattern starting with the lowest carbon number on the upper left of the graph and moving down gradually to the right towards higher carbon numbers. The magnitude of the slopes of these isosteres $(-\Delta H_{50}/R)$ is approximately equal.

Table 4.5 summarizes the ΔH_{ads} values at both 50 % and 0 % loadings. The heat of adsorption calculated by the Gaussian model was slightly lower than the heat of adsorption at 0% loading taken from literature in the case of 1-butene while the values were approximately equal in case of ethylene and propylene. The anomaly of the sigma

values in the case of 1-butene explains the low value of *(-ΔH 50)*. Propylene also had high sigma values but only in the subcritical region. The supercritical sigma value of 1 may have balanced the effect of the high sigma in the subcritical data, hence, resulting in a reasonable *(-ΔH 50)* value.

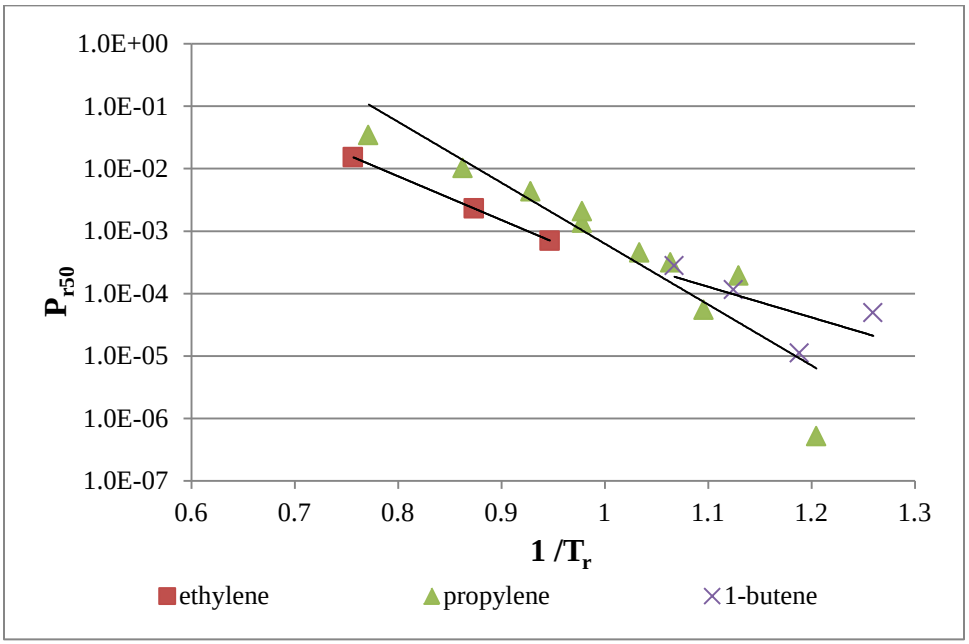

Figure 4.19: log P_{r50} vs. $1/T_r$ for all the chosen alkenes.

Table 4.5: Values of ($-\Delta H_{ads}$) for the chosen alkenes.

	$-\Delta H_{50}$ (kcal /mol)	$-\Delta H_{0lit.}$ (kcal /mol)	a
Ethylene	9.02	9.10 [17]	1.50E+07
Propylene	10.87	10.13 [25]	1.65E+07
1-butene	9.40	13.00 [26]	1.30E+05

CHAPTER 5: Sorption of aromatics or cyclic hydrocarbons on 13X

5.1 Introduction

Search of the literature for adsorption data of aromatics on 13X resulted in the literature references listed in Table 5.1. All of the chosen isotherms were in the subcritical region, $T_r < 1$ in the case of aromatics. The data is collected from 7 different studies between the years 1957 and 2006, listed in column 1 of Table 5.1. Column 2 of the same Table lists the reduced temperatures of the isotherms chosen from the corresponding study. The adsorption measurement methods as well as the percent crystal are itemized in columns 3 and 4 respectively. The isotherm data were systematically standardized and evaluated according to the same criteria followed previously for n-alkanes and alkenes. Table 5.1 also shows which isotherms were not included in the study and the reason for their deletion. The six aromatic compounds included in this study are: benzene, toluene, 1, 3, 5-triethylbenzene, 1, 2, 3, 5-tetramethylbenzene, naphthalene, mesitylene and one cyclic compound cyclohexane. Table 5.2 lists some of the physical properties of these materials.

Table 5.1: Data on the adsorption of aromatics and cyclohexane on 13X.

Author	Reduced Temperature	Reason Deleted	Method	% Crystal	Paper
Barrer et al. (1957)	benzene: 0.53, 0.539, 0.557, 0.575, 0.592, 0.61 toluene: 0.529, 0.546, 0.563, 0.58, 0.597		Gravimetric & Volumetric	crystal	Ba1111(57) [13]
Ruthven and Kaul (1993)	mesitylene:0.632, 0.695, 0.868, 0.899, 0.943 naphthalene: 0.632, 0.699, 0.732, 0.766, 0.806, 0.832 1,2,3,5-		Gravimetric by Cahn Vacuum Microbalance	Crystal	Do2047(93) [20]

	tetramethylbenzene: 0.806, 0.853, 0.898, 0.937 1,3,5-triethylbenzene: 0.849, 0.891, 0.928, 0.964 1,3-dimethylnaphthalene: 0.75				
Pinto et al. (2005)	toluene: 0.504		Gravimetric	0.8	Pi253(05) [24]
Ruthven and Tezel (1990)	benzene: 0.717		Gravimetric	Crystal	Ru581(90) [19]
Ruthven and Doetsch (1976)	benzene: 0.778, 0.815, 0.868, 0.913 toluene: 0.774, 0.825, 0.867 cyclohexane: 0.812, 0.867, 0.909, 0.968		Cahn Vacuum Microbalance	crystal	Ru882(76) [15]
Zhdanov et al. (1962)	benzene: 0.53	The pelleted isotherms are deleted since they are inconsistent in position.	McBain-Back balance	0.8, crystal	Zh445(62) [14]

Table 5.2: Physical properties of the chosen aromatics and cyclic compound [42].

	Formula	Formula weight	Specific gravity	Melting point (°C)	T_{rM}	Boiling point (°C)
Benzene	C_6H_6	78.11	0.88	5.50	0.49	80.10
Toluene	$C_6H_5.CH_3$	92.13	0.87	-95.00	0.30	110.80
Mesitylene	$C_6H_3(CH_3)_3$	120.19	0.86	-45.00	0.36	164.80
Naphthalene	$C_{10}H_8$	128.16	1.14	80.20	0.47	217.90
1,2,3,5-tetramethylbenzene	$C_6H_2(CH_3)_4$	134.12	0.89	-24.00	0.37	198.00
1,3,5-triethylbenzene	$C_6H_3(C_2H_5)_3$	162.27	0.86	-66.00	0.30	215.00
Cyclohexane	C_6H_{12}	84.16	0.78	6.50	0.55	80.74

5.2 Benzene

Figure 5.1 shows the isotherms for benzene including four different studies by Barrer et al. [13], Zhdanov et al. [14], Ruthven and Doetsch [15], and Ruthven and Tezel [19], spanning a T_r range of 0.53 from the left to 0.87 on the right. The two isotherms from Zhdanov et al. [14] at T_r = 0.53 are included. The top study refers to a crystal sample while the bottom one refers to a pelleted sample of type Linde 13X. The pelleted isotherm appears to cross the Ruthven isotherm and is inconsistent with the other Zhdanov et al. [14] isotherm. Moreover, unlike the crystal sample isotherm, it exhibits capillary condensation due to the presence of the binder in a pelleted sample. Hence, the pelleted sample from Zhdanov et al. [14]was deleted. The data, as shown in Figure 5.2, appears to exist in two separate regions. The upper region, consisting of isotherms from Barrer et al. [13] and Zhdanov et al. [14], is closer to the saturation region at a T_r range of 0.53 to 0.61. The lower region, consisting of the isotherms from Ruthven and Doetsch [15], and Ruthven and Tezel [19], has a lower concentration data with a T_r range of 0.72 to 0.91.

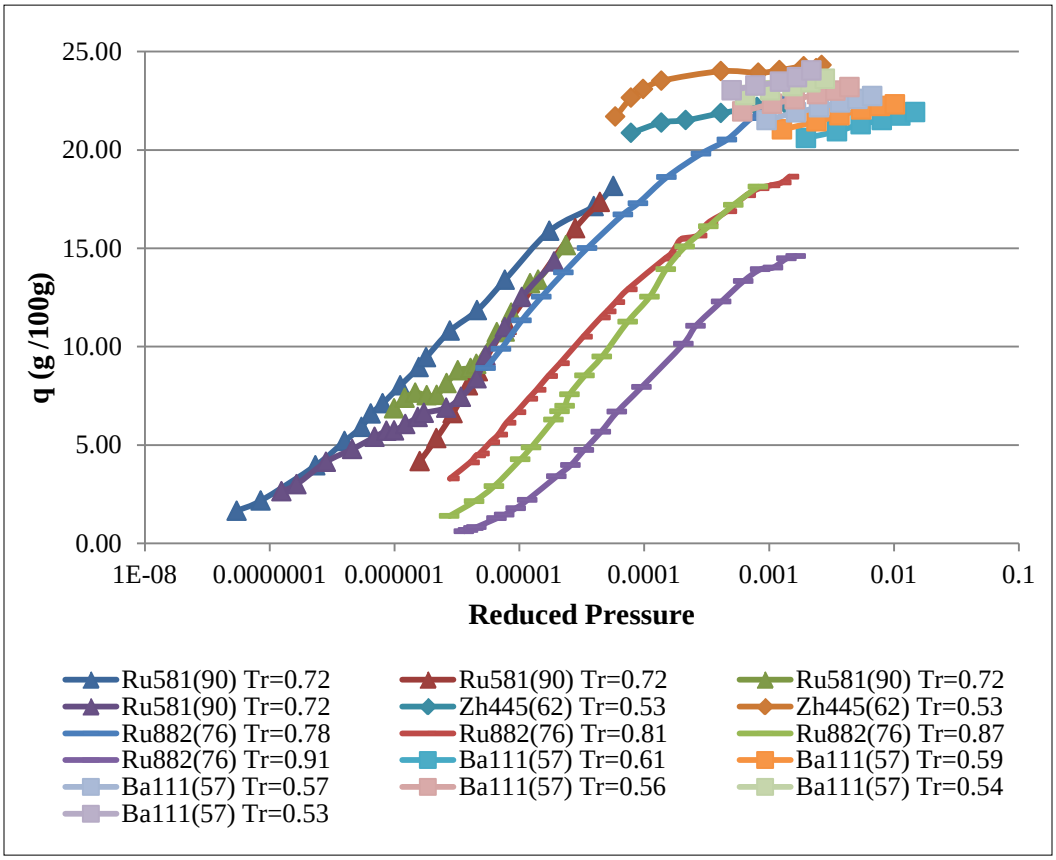

Figure 5.1: Isotherms for benzene on 13X.

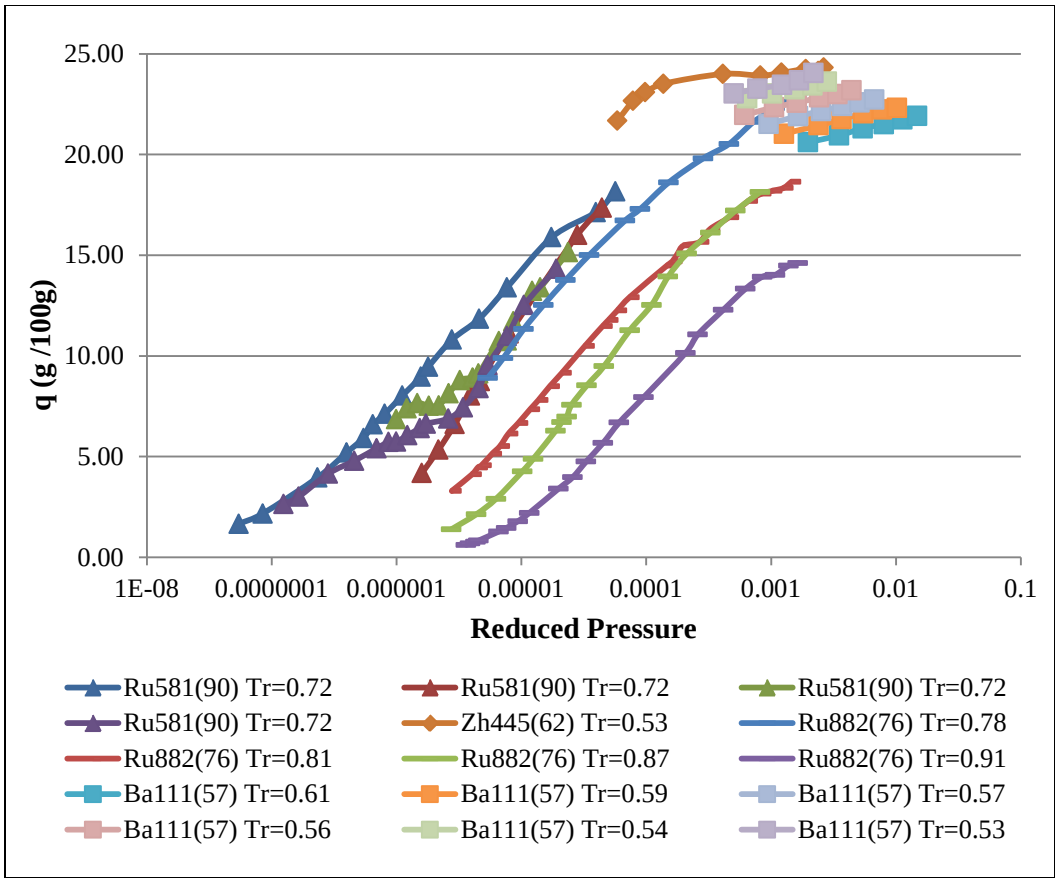

Figure 5.2: Isotherms for benzene after deleting Zhdanov pelleted isotherm on13X.

The linearized probability plot of reduced pressure P_r vs. $\Phi^{-1}(\theta)$ is shown in Figure 5.3 for all the screened isotherms of benzene ranging from a T_r of 0.53 to 0.91. The isotherms are remarkably linear and the slopes, σ, are close to 1 for both Ruthven and Doetsch [15] and Ruthven and Tezel [19] in the lower region of the Figure while it is close to 5 for the data from [13] and Zhdanov et al. [14] in the upper region of the Figure. Zhdanov et al. [14] data has two regions one that is near saturation along with Barrer et al. [13] isotherms and the other region is at lower loadings along with isotherm data from Ruthven and Doetsch [15] and Ruthven and Tezel [19]. Figure 5.4 shows the σ vs. T_r plot where there appear to be two sets of data, one at a value of 5 for [13] and Zhdanov et al. [14]data, and the other around the value of 1 for Ruthven and Doetsch [15] and Ruthven and Tezel [19] data. The constant θ lines at 50% loading are shown in Figure 5.5 as log P_{r50} vs. 1/ Tr. The lines are straight and follow a consistent pattern.

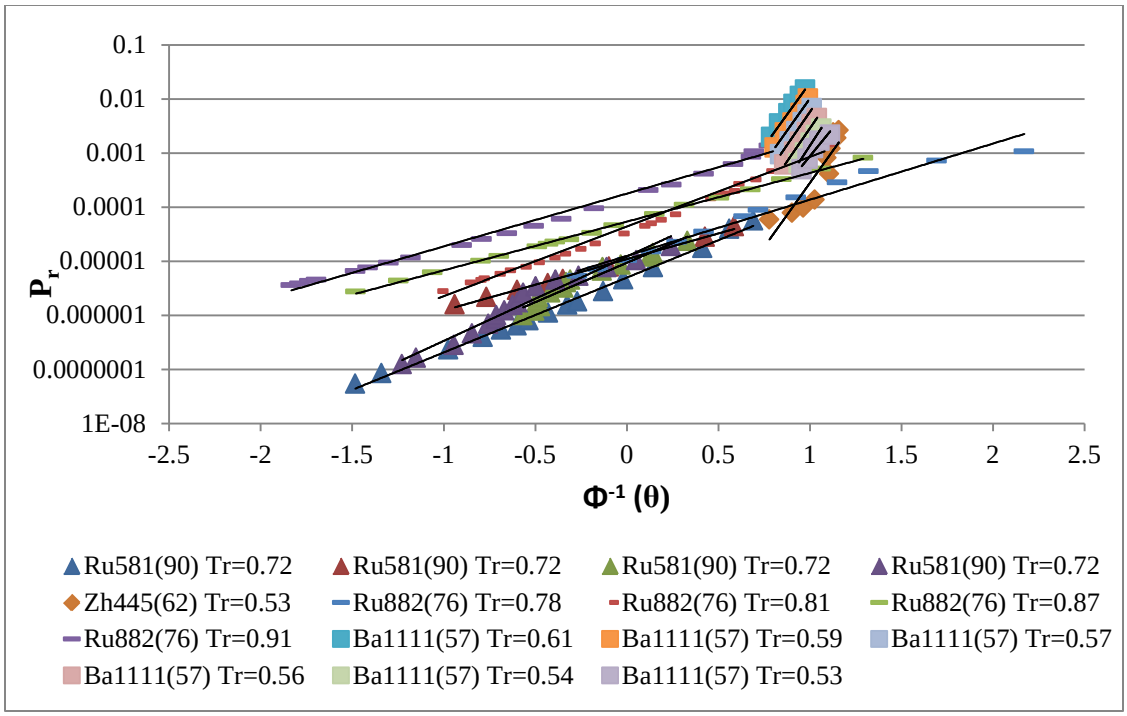

Figure 5.3: Linearized isotherms for benzene on 13X.

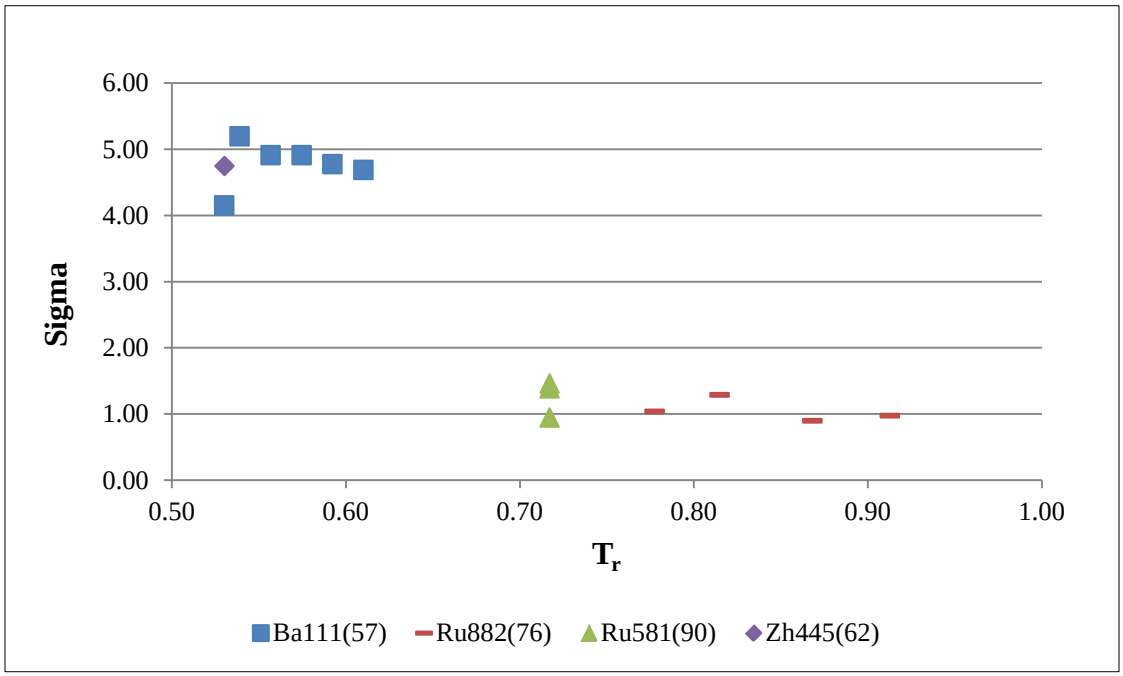

Figure 5.4: Sigma, the slope of the linearized isotherms, as a function of reduced temperature, for benzene on 13X.

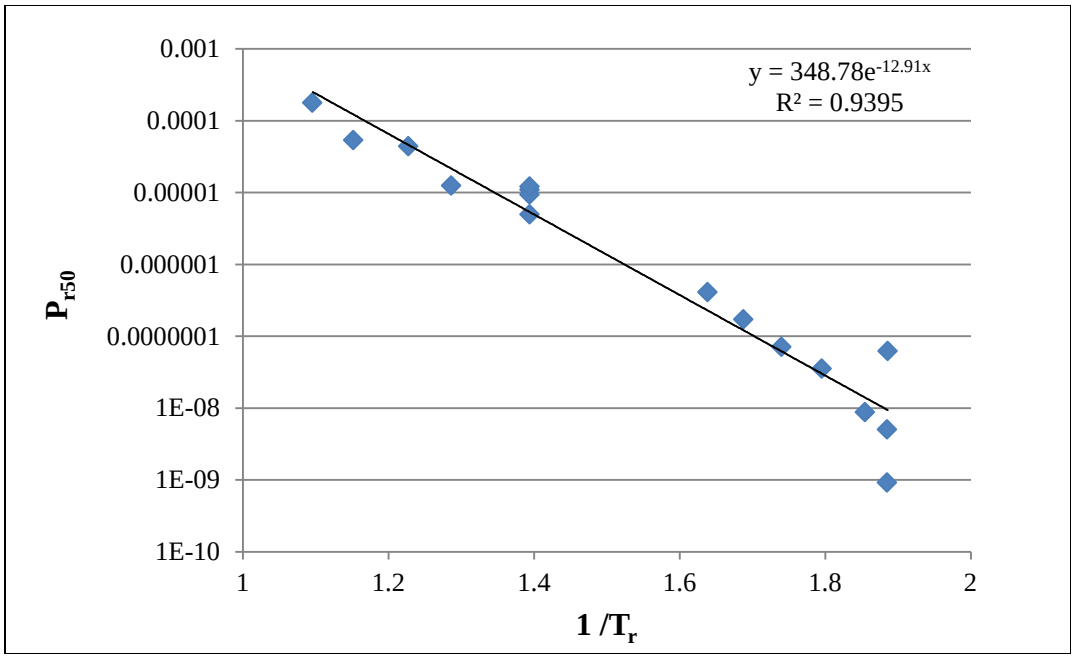

Figure 5.5: log P_{r50} vs. $1/T_r$ for benzene on 13X.

Figure 5.6 is also an isostere plot but with ln P_{50} vs. 1/T. The slope of this line, $(-\Delta H_{50})/R$, is used to calculate the heat of adsorption at 50% loading and compare it to values extracted from literature, as shown below:

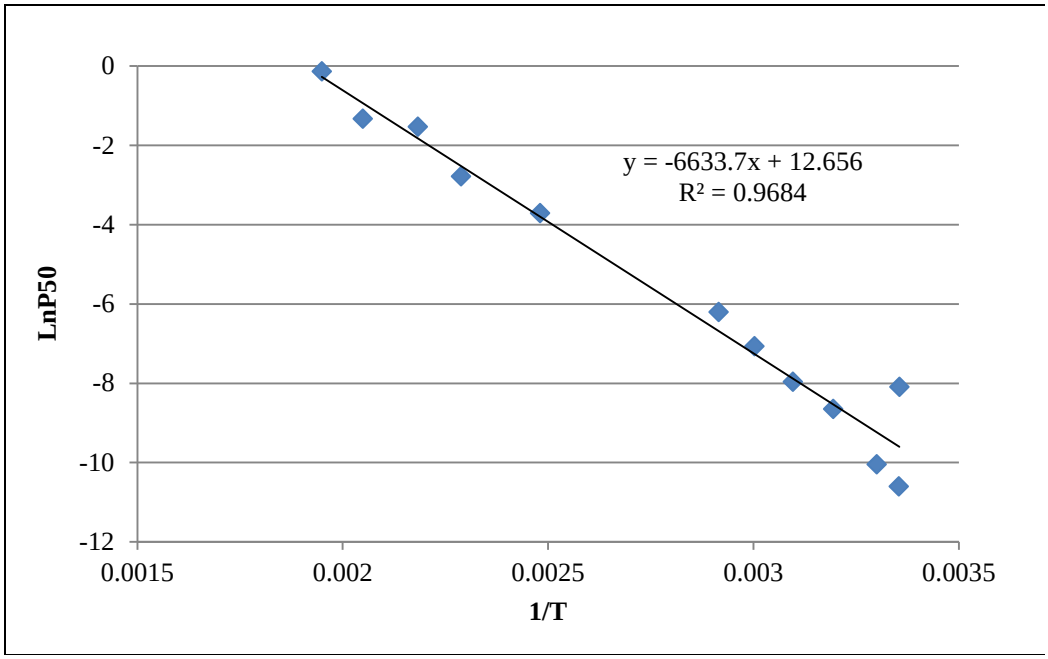

Figure 5.6: ln P_{50} vs. 1/T for benzene on 13X.

$$-(\Delta H_{50}) = 6633.7 * 1.98 * 10^{-3} = 13.13\ kcal/mol. \quad 5.1$$

$$a = e^{12.65} = 3.14 * 10^{5} \quad 5.2$$

Table 5.3: Values of ($-\Delta H_{ads}$) for benzene.

$-\Delta H_{50}$ (kcal /mol)	$-\Delta H_{0lit.}$ (kcal /mol)	a
13.13	18.5 [15]	3.14E+05

The value of ($-\Delta H_{0lit}$) taken from Ruthven and Doetsch [15] is higher than the one found by the Gaussian model. As the heat of adsorption calculated by the Gaussian model is taken at 50% of the saturation loading while in literature it is reported at 0% loading, this difference may be expected.

5.3 Toluene

Figure5.7 represents the isotherms for toluene including three different studies by Barrer et al. [13], Ruthven and Doetsch [15], and Pinto et al. [24] across a T_r range of 0.53 from the left to 0.87 to the right. Both Barrer et al. [13] and Pinto et al. [24] use a pelleted sample of Linde 13X with 20% binder content. Ruthven and Doetsch [15], on the other hand, use a crystal 13X sample. Isotherms seem to be consistent with each other with no signs of capillary condensation. Hence, all isotherms were retained from the chosen studies. Data, as shown in Figure 5.7, are separated to upper and lower regions. The upper region, consisting of isotherms from Barrer et al. [13] and Pinto et al. [24], is closer to the saturation region at a T_r range of 0.5 to 0.6. The lower region, consisting of the isotherms from Ruthven and Doetsch [15], has a lower concentration data with a T_r range of 0.77 to 0.87.

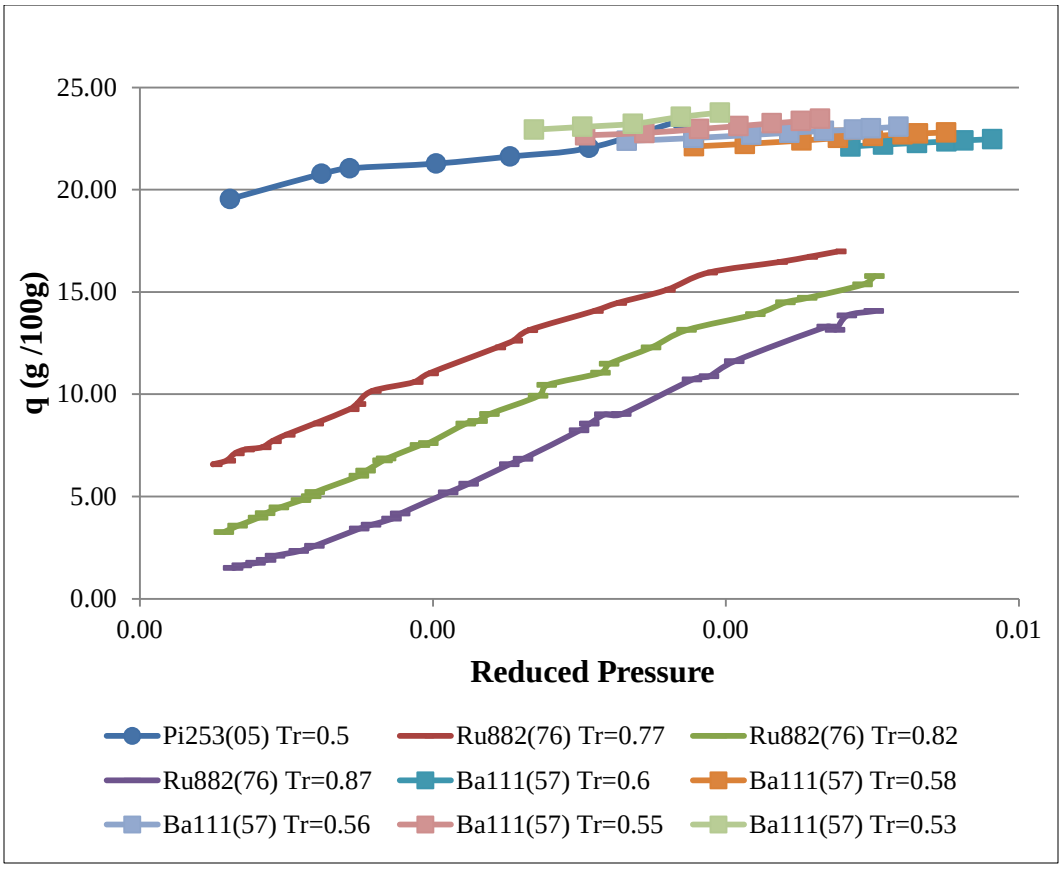

Figure 5.7: Isotherms for toluene on 13X.

Linearized isotherms for toluene on 13X are shown on Figure 5.8. The lines are almost straight and parallel and they range from a reduced temperature of 0.87 from the left to 0.53 to the right. The slopes of the linearized probability lines, σ, plotted against reduced temperature are shown in Figure 5.9. The value of sigma in the study of Ruthven and Doetsch [15] goes from 1 to 1.6 in the low saturation region while in the study of Barrer et al. [13] the range is from 4 to 7 in the saturation region. However, these results are slightly inconsistent with earlier results in that σ increases as the T_r increases. In all earlier studies for alkanes, alkenes and benzene σ increases as T_r decreases. At this time, it is not known whether this is an artifact or a true reflection of what is occurring. Constant θ lines for toluene appear to separate into two regions in Figure 5.10; in the lower region the slope is positive for the isotherms of Barrer et al. [13] indicating the heat of sorption is positive which is physically impossible whereas the isotherms from Ruthven and Doetsch [15] in the upper region slope downward. This change in behavior

might be due to a change in phase from adsorbed liquid to a solid that might occur at such low subcritical temperatures.

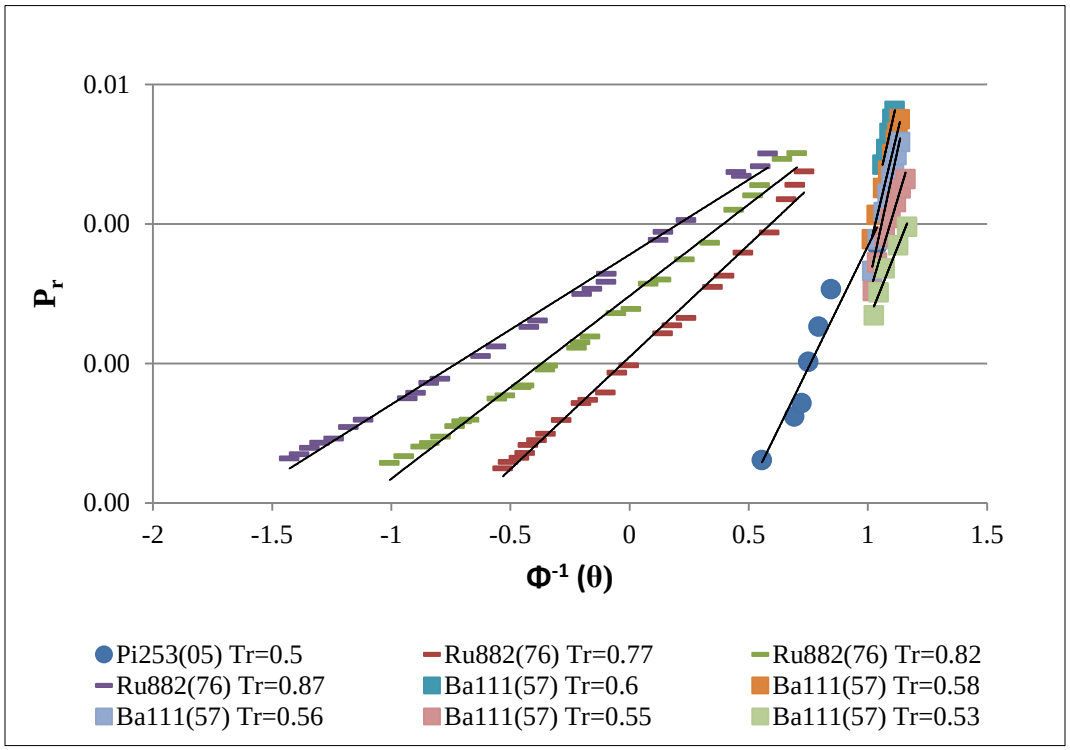

Figure 5.8: Linearized isotherms for toluene on 13X.

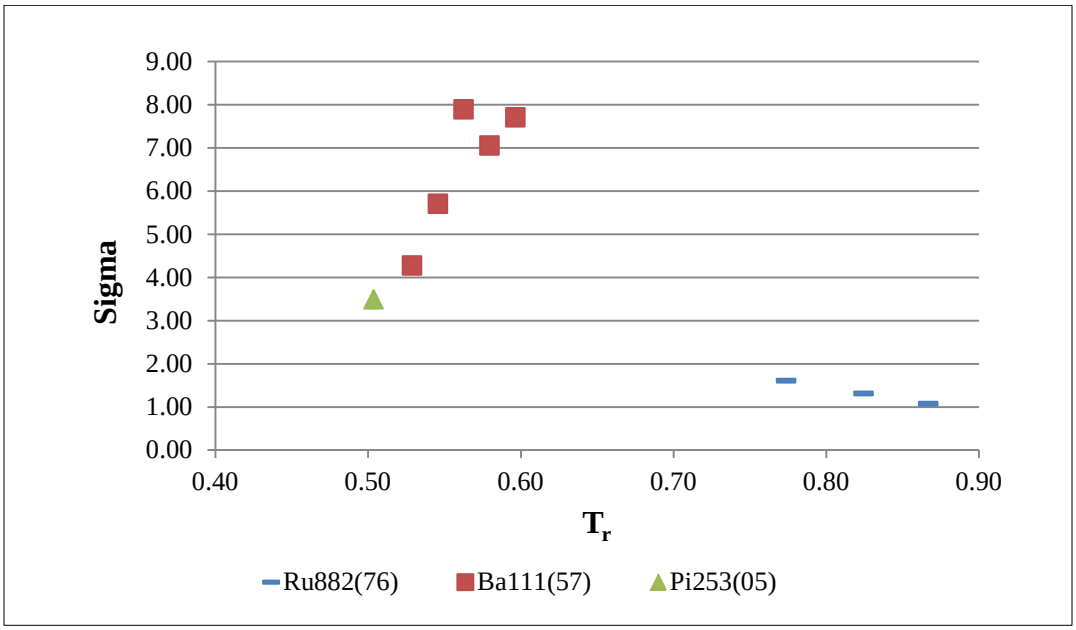

Figure 5.9: Sigma, the slope of the linearized isotherms, as a function of reduced temperature, for toluene on 13X.

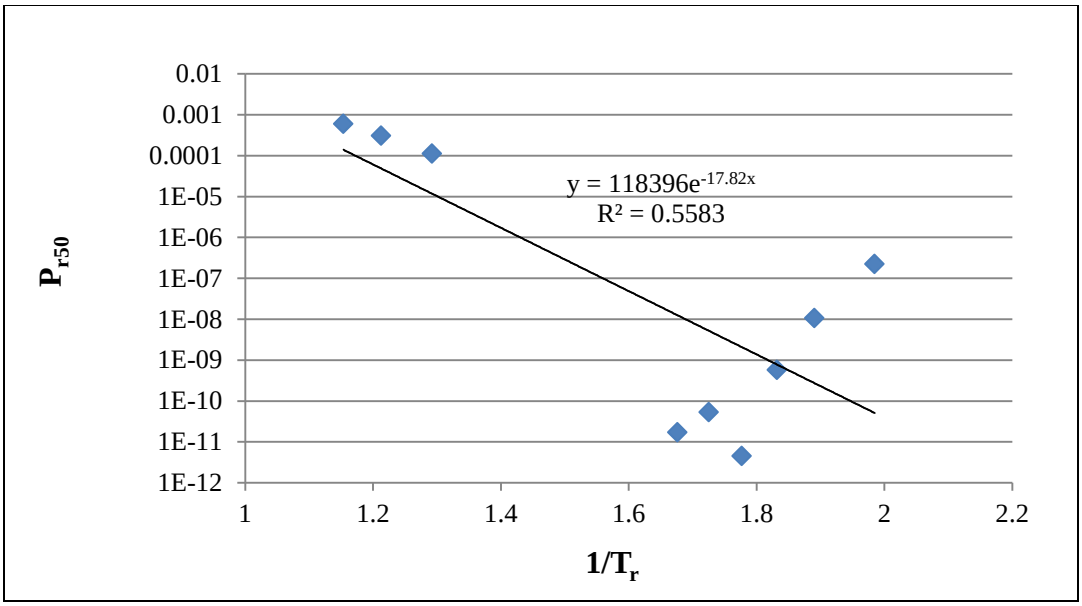

Figure 5.10: log P_{r50} vs. $1/T_r$ for toluene on 13X.

The slope of the isosteres in Figure 5.11 is used to calculate the heat of adsorption at 50% loading only the isotherms of T_r>0.65 were considered in this calculation as the one below this region shows an anomaly. The values were compared to those from literature at 0% loading.

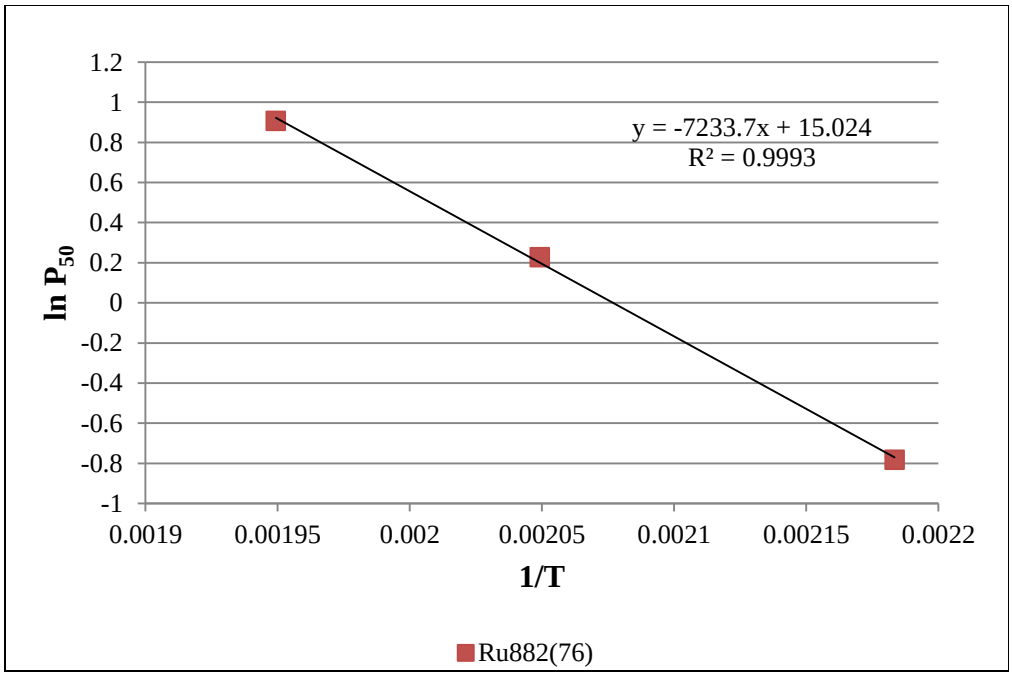

Figure 5.11: ln P_{50} vs. 1/T for toluene on 13X.

$$(\Delta H_{50}) = 7233.7 * 1.98 * 10^{-3} = 14.3\ kcal/mol. \quad 5.3$$

$$a = e^{15.02} = 3.20 * 10^{6} \quad 5.4$$

Table 5.4: Values of ($-\Delta H_{ads}$) for toluene.

$-\Delta H_{50}$ (kcal /mol)	$-\Delta H_{0lit.}$ (Kcal /mol)	a
14.3	21 [15]	3.2E+06

Again, as in benzene, the value of ($-\Delta H_{50}$) for toluene is less than ($-\Delta H_{0lit.}$).

5.4 Mesitylene

Figure 5.12 represents the adsorption isotherms for mesitylene found in a single study by Ruthven and Kaul [20]. T_r starts at 0.632 on the left hand side of the plot to a T_r of 0.943 on the right hand side of the plot. The isotherms were all consistent in shape and behavior as they were all extracted from a single study. With the lack of another judge on the consistency, the isotherms were all retained as they are. The study was based on a crystal sample of 13X with no percent binder.

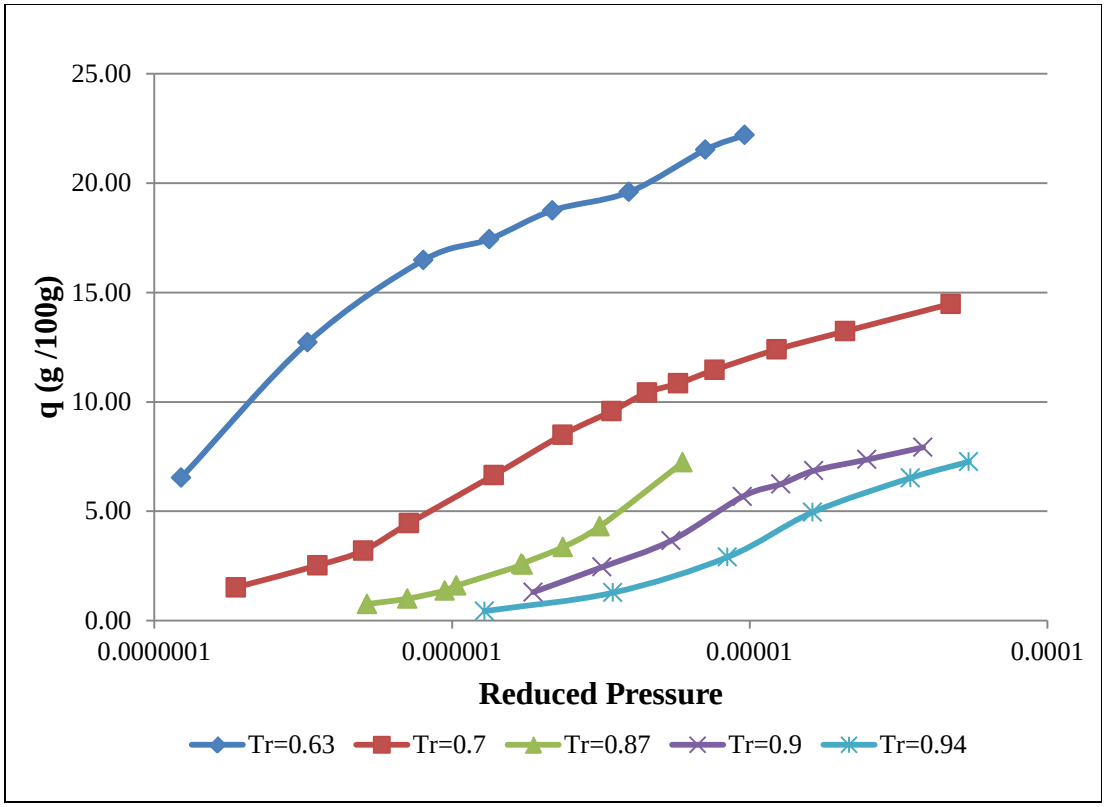

Figure 5.12: Isotherms for mesitylene on 13X.

The linearized isotherms are shown on Figure 5.13 starting from a T_r of 0.94 from the left to 0.63 on the right. Except for the isotherm at T_r = 0.63, the lines show a similar pattern where they start linear and end with a small upward curvature at around Φ^{-1} =-0.13, approximately. The slopes of the linearized isotherm are plotted against T_r, in Figure 5.14, where the values are all close to 1 across the T_r range of the study. Figure 5.15 shows the constant θ lines of mesitylene with a regression value of 0.81.

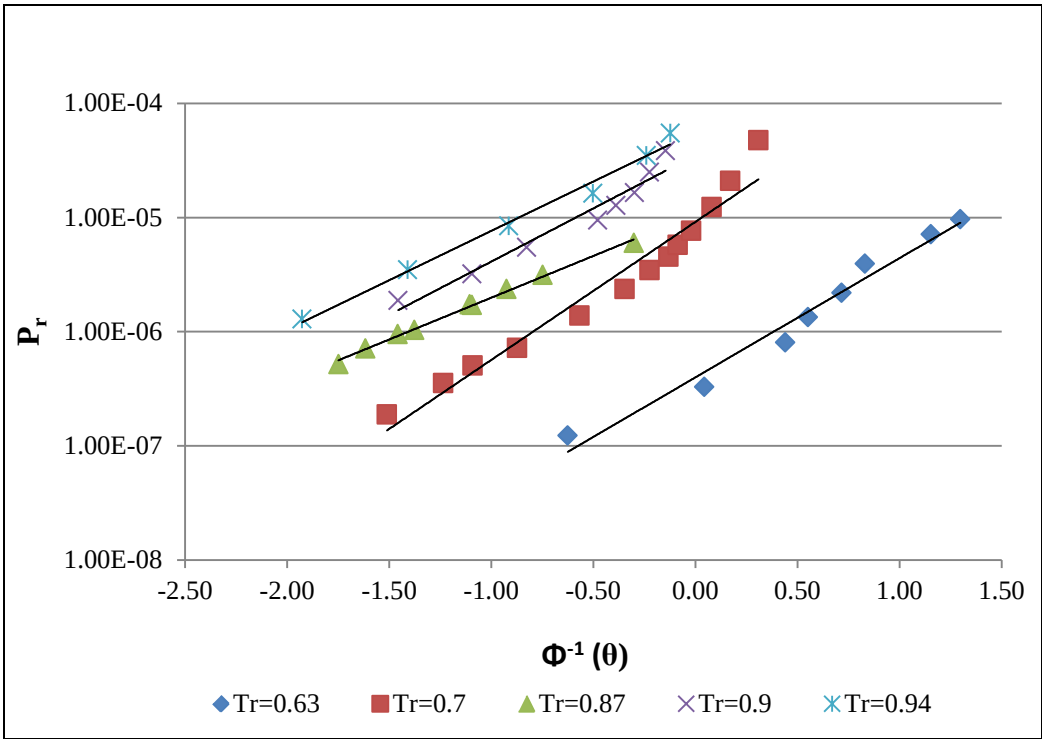

Figure 5.13: Linearized isotherms for mesitylene on 13X.

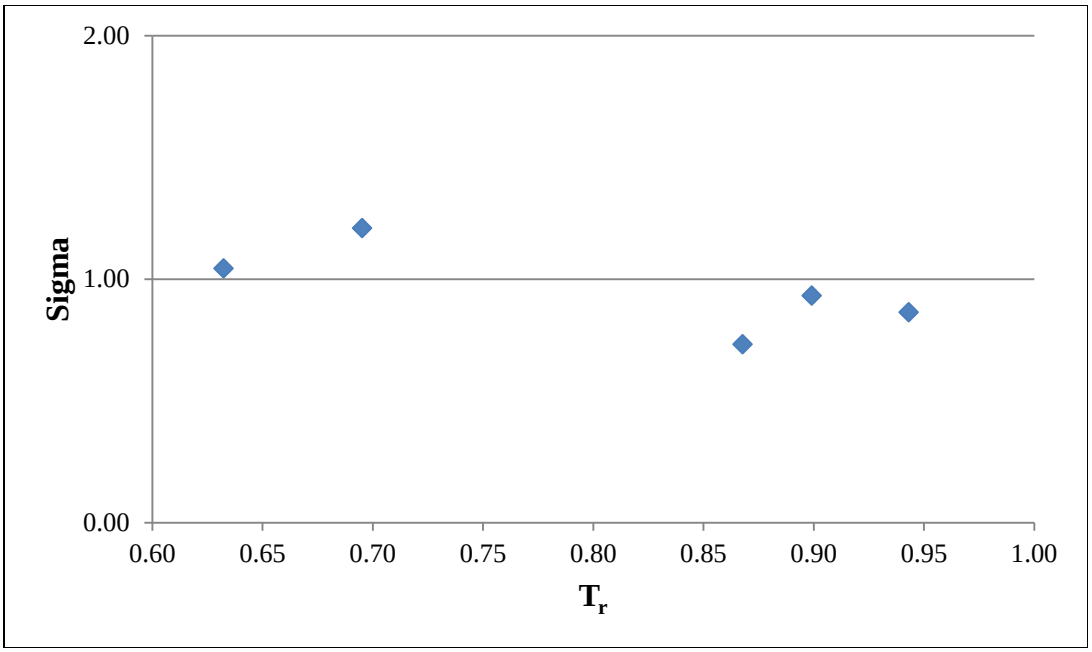

Figure 5.14: Sigma, the slope of the linearized isotherms, as a function of reduced temperature, for mesitylene on 13X.

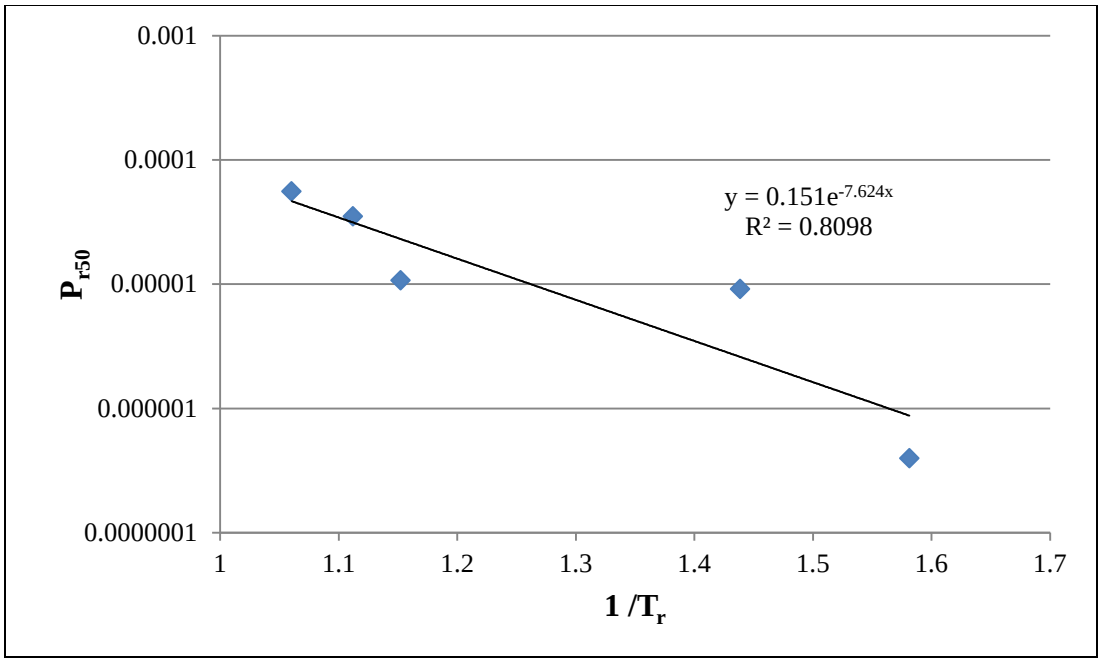

Figure 5.15: log P_{r50} vs. $1/T_r$ for mesitylene on 13X.

The value of the heat of adsorption at 50% loading for mesitylene is calculated from the slope of Figure 5.16.

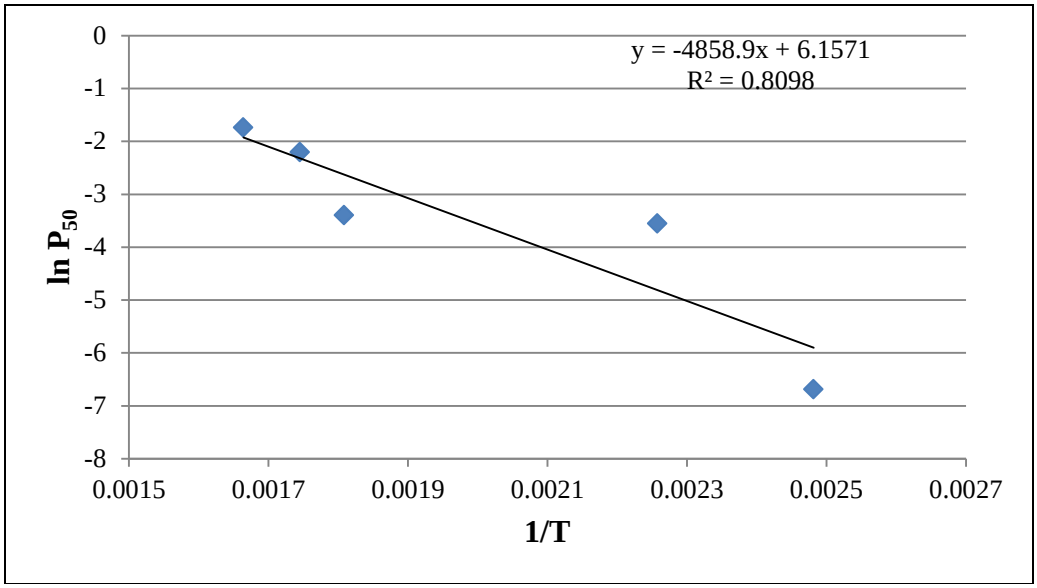

Figure 5.16: ln P_{50} vs. 1/T for mesitylene on 13X.

$$(\Delta H_{50}) = 4858.9 * 1.98 * 10^{-3} = 9.60\ kcal/mol. \quad 5.5$$

$$a = e^{15.02} = 468.7 \quad 5.6$$

Table 5.5: Values of ($-\Delta H_{ads}$) for mesitylene.

$-\Delta H_{50}$ (kcal /mol)	$-\Delta H_{0lit.}$ (kcal /mol)	a
9.6	23.3 [20]	468.7

The value of ($-\Delta H_{50}$) for mesitylene is less than half the value of ($-\Delta H_{lit.}$).

5.5 Naphthalene

Figure 5.17 represents the adsorption isotherms for naphthalene found in a single study by Ruthven and Kaul [20]. T_r starts at 0.632 on the left hand side of the plot to a T_r of 0.83 on the right hand side of the plot. The isotherms were all consistent in shape and behavior as they were all extracted from a single study. With the lack of another judge on the consistency, the isotherms were all retained as they are. The study was based on a crystal sample of 13X with no binder content.

The linearized isotherms in the case of naphthalene on 13X are shown in Figure 5.18. The lines are remarkably straight and parallel except for the right most isotherm at T_r =0.63. Looking at Figure 5.19 the sigmas clearly have a value of 1 for all isotherms except for that same isotherm at T_r =0.63 This may be due to phase change to a solid in the adsorbed matrix. The constant θ lines at 50% loading in Figure 5.20 shows a good linear fit of the data.

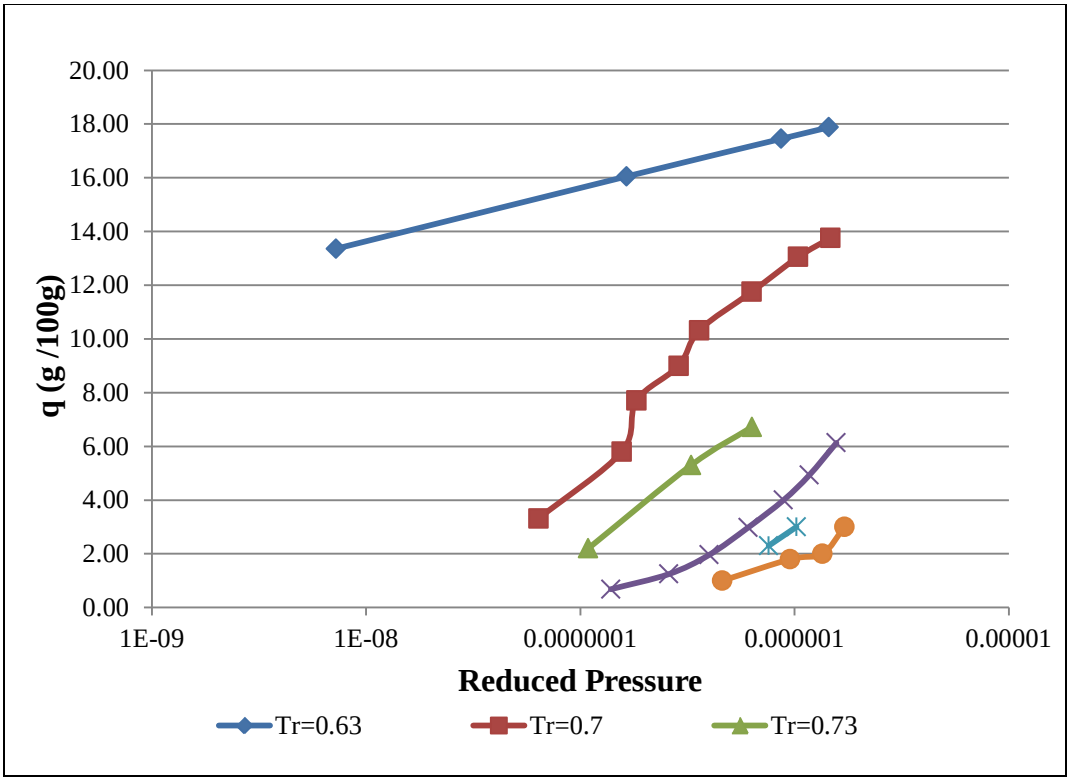

Figure 5.17: Isotherms for naphthalene on 13X.

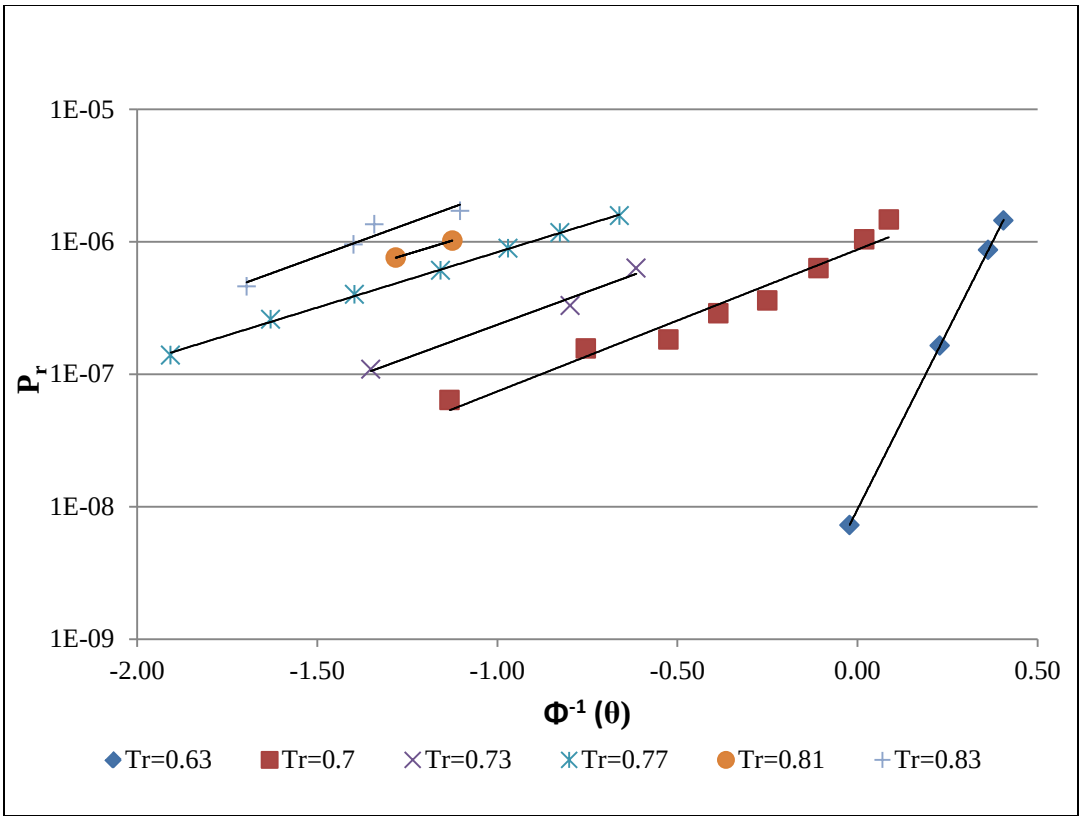

Figure 5.18: Linearized isotherms for naphthalene on 13X.

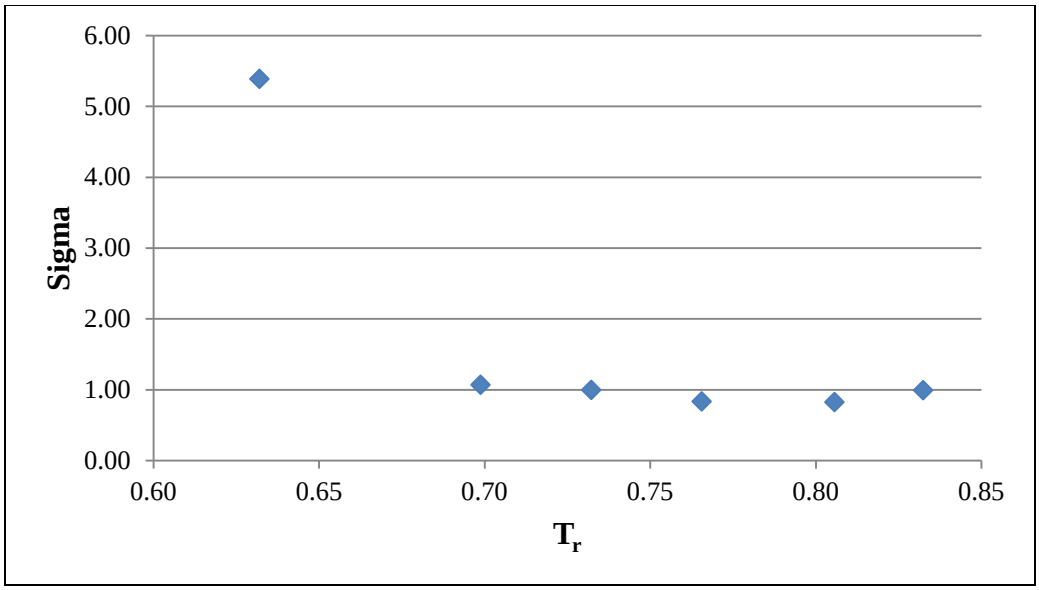

Figure 5.19: Sigma, the slope of the linearized isotherms, as a function of reduced temperature, for naphthalene on 13X.

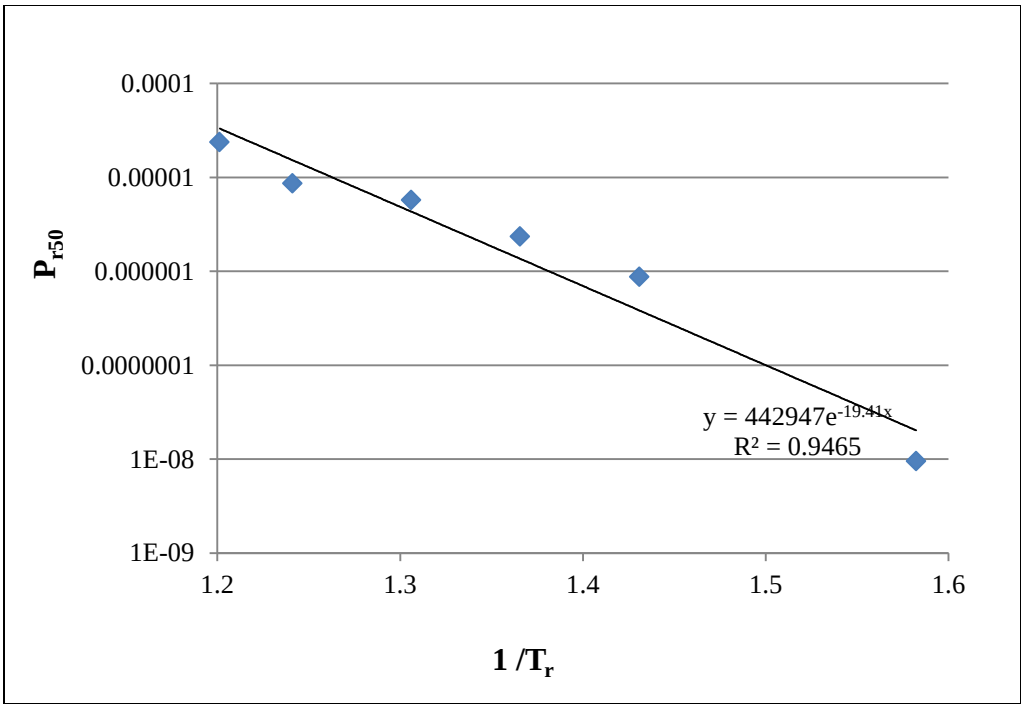

Figure 5.20: log P_{r50} vs. $1/T_r$ for naphthalene on 13X.

From Figure 5.21, the heat of adsorption a 50% loading of naphthalene is calculated and compared to the value found in literature at 0% loading.

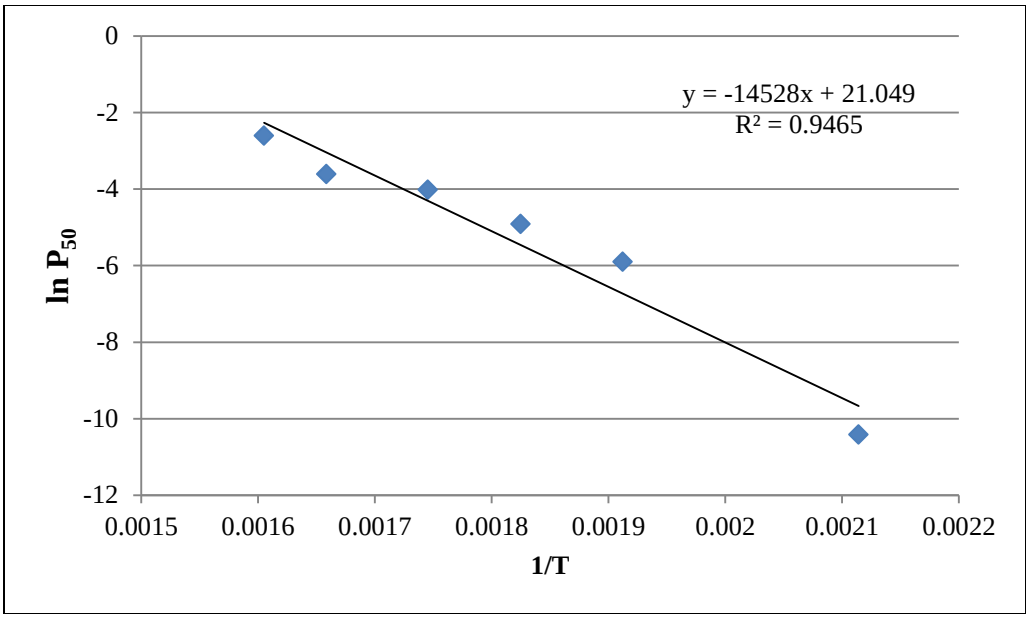

Figure 5.21: ln P_{50} vs. 1/T for naphthalene on 13X.

$$-(\Delta H_{50}) = 14528 * 1.98 * 10^{-3} = 28.8\ kcal/mol. \quad 5.7$$

$$a = e^{21.0} = 1.32 * 10^{9} \quad 5.8$$

Table 5.6: Values of ($-\Delta H_{ads}$) for naphthalene.

$-\Delta H_{50}$ (kcal /mol)	$-\Delta H_{0lit.}$ (kcal /mol)	a
28.8	25.5 [20]	1.32E+09

The value of ($-\Delta H_{50}$) for naphthalene is unexpectedly greater than ($-\Delta H_{0lit}$) found by Ruthven and Kaul [20] at 0% loading.

5.6 1,2,3,5 Tetramethylbenzene

Figure 5.22 represents the adsorption isotherms for 1,2,3,5-tetramethylbenzene found in a single study by Ruthven and Kaul [20]. T_r starts at 0.81 on the left hand side of the plot to a T_r of 0.94 on the right hand side of the plot. The isotherms were all consistent in shape and behavior as they were all extracted from a single study. With the lack of another judge on the consistency, the isotherms were all retained as they are with no cancellation or point deletion. The study was based on a crystal sample of 13X with no percent binder. Two crystal size fractions were used at a T_r of 0.81 and at a T_r of 0.85.

The linearized isotherms in the case of 1,2,3,5-tetramethylbenzene on 13X are shown in Figure 5.23. The lines are almost straight and parallel except at high P_r values where a small curvature is realized. As shown in Figure 5.24, the sigma clearly has a value close to 1 for all isotherms except for the isotherm at $T_r = 0.81$ at both crystal sizes, one of which has a value of 1.72 and the other is 2.17. The constant θ in Figure 5.25 shows a good linear fit of the data.

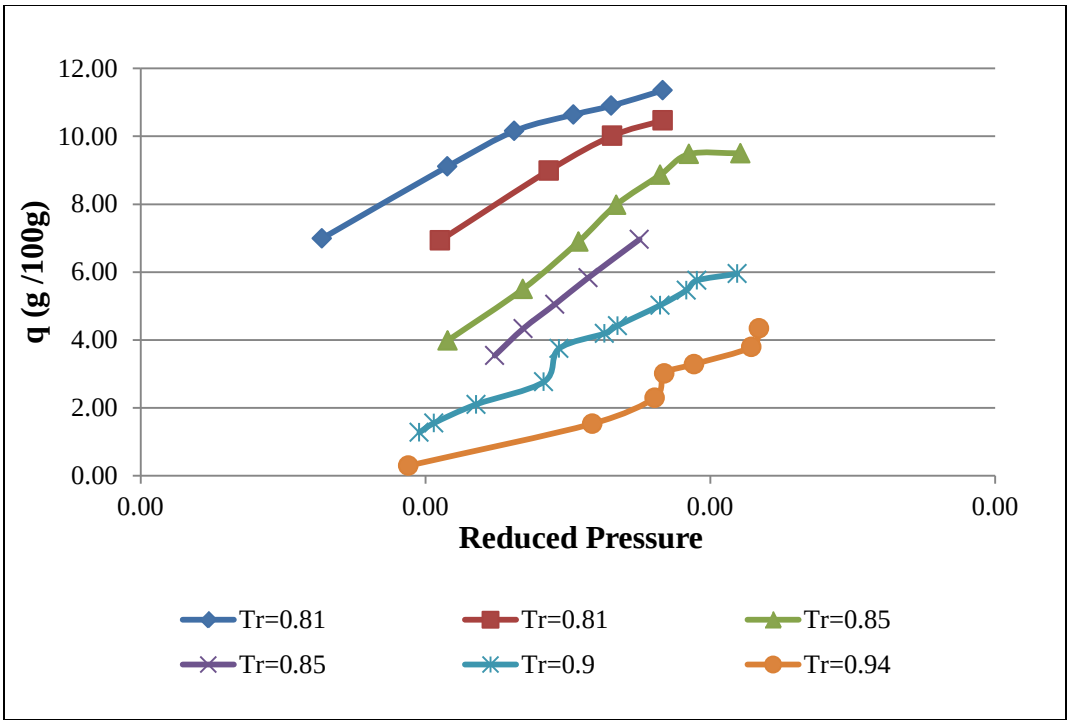

Figure 5.22: Isotherms for 1,2,3,5-tetramethylbenzene on 13X.

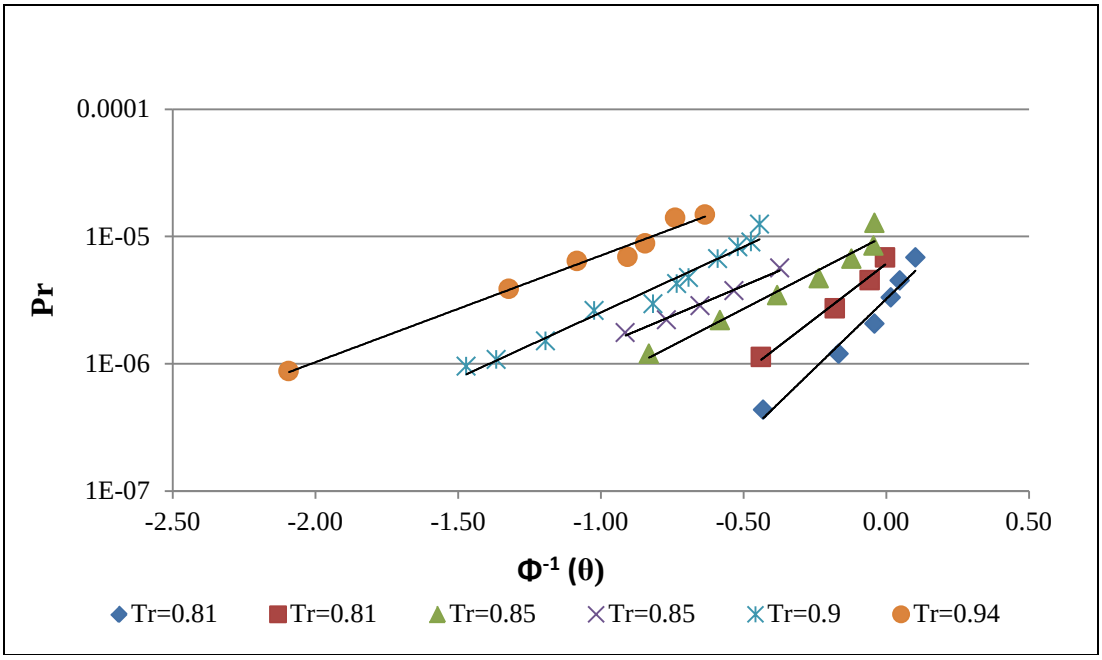

Figure 5.23: Linearized isotherms for 1,2,3,5- tetramethylbenzene on 13X.

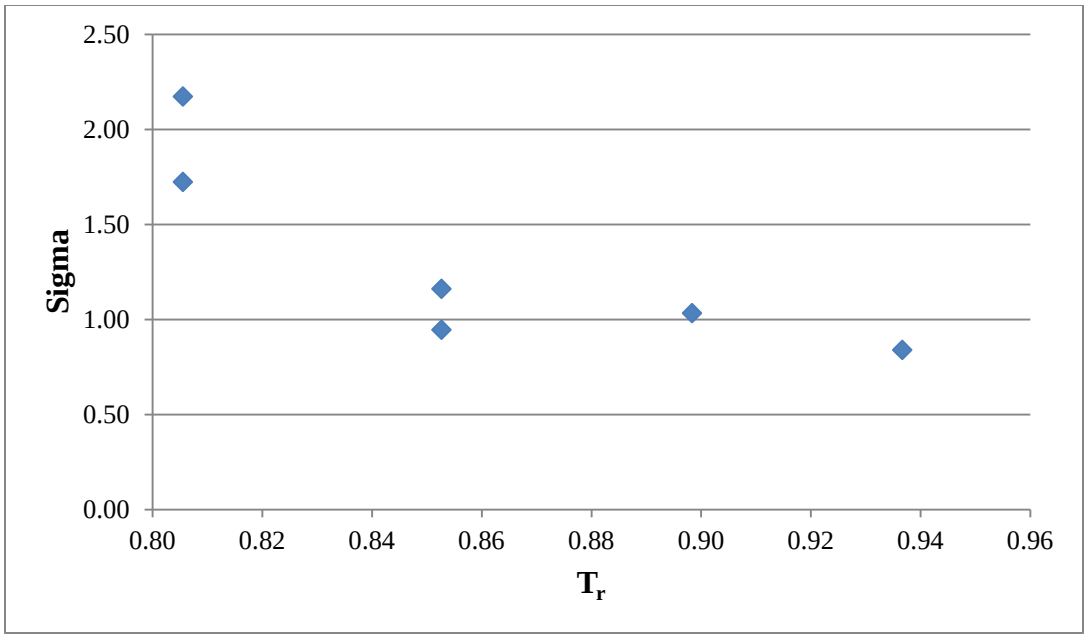

Figure 5.24: Sigma, the slope of the linearized isotherms, as a function of reduced temperature, for 1,2,3,5- tetramethylbenzene on 13X.

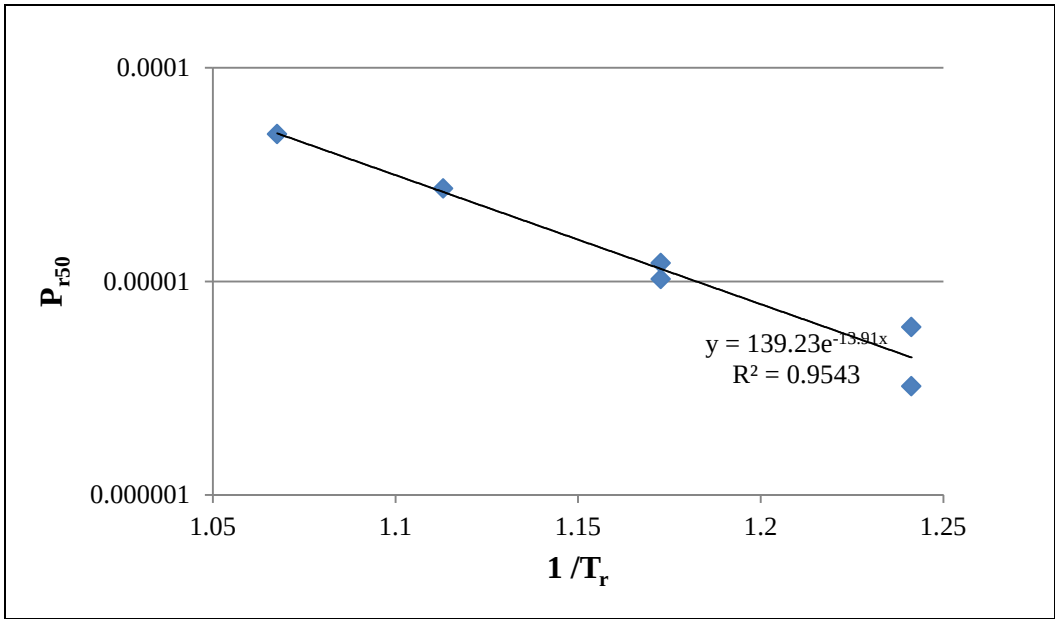

Figure 5.25: log P_{r50} vs. $1/T_r$ for1,2,3,5- tetramethylbenzene on 13X.

The heat of adsorption at 50% loading of 1,2,3,5-tetramethylbenzene is calculated using the slope of Figure 5.26.

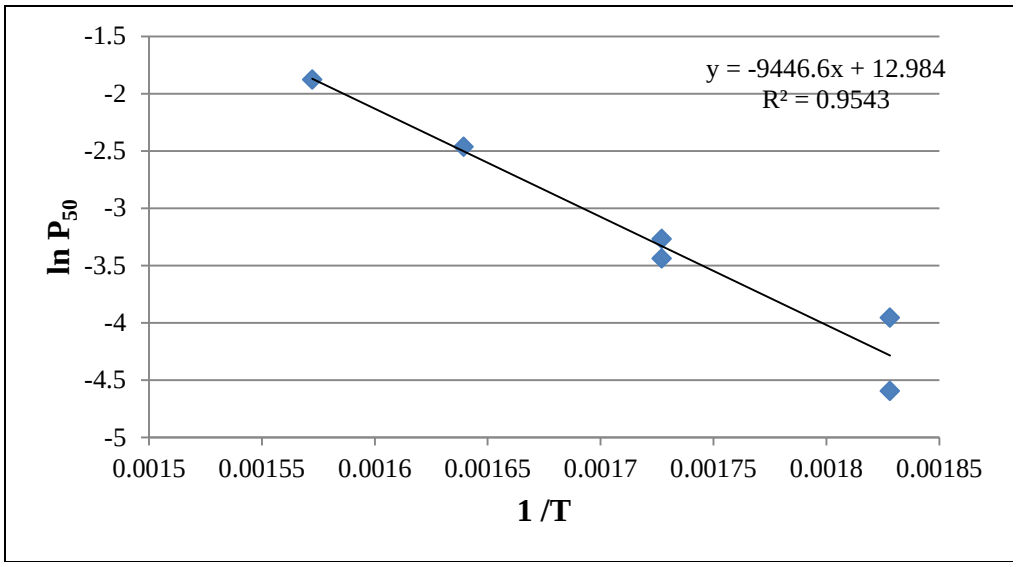

Figure 5.26: ln P_{50} vs. 1/T $_{for}$1, 2, 3, 5- tetramethylbenzene on 13X.

$$-(\Delta H_{50}) = 9446.6 * 1.98 * 10^{-3} = 18.70\ kcal/mol. \quad 5.9$$

$$a = e^{21.0} = 4.35 * 10^{5} \quad 5.10$$

Table 5.7: Values of ($-\Delta H_{ads}$) for 1, 2, 3, 5- tetramethylbenzene.

$-\Delta H_{50}$ (kcal /mol)	$-\Delta H_{0lit.}$ (kcal /mol)	a
18.7	27 [20]	4.35E+05

The value of ($-\Delta H_{50}$) is less than ($-\Delta H_{0lit.}$) as in the case of the previous aromatics.

5.7 1, 3, 5-Triethylbenzene

Figure 5.27 represents the adsorption isotherms for 1,3,5-triethylbenzene found in a single study by Ruthven and Kaul [20]. T_r starts at 0.85 on the left hand side of the plot to a Tr of 0.96 on the right hand side of the plot. The isotherms were all consistent in shape and behavior as they were all extracted from a single study. With the lack of another judge on the consistency, the isotherms were all retained as they are with no cancellation or point deletion. The study was based on a crystal sample of 13X with no percent binder.

The linearized isotherms for 1,3,5 triethylbenzene on 13X are shown in Figure 5.28. The first two isotherms at T_r = 0.96 and 0.89 are almost straight and parallel while the other two exhibit some curvature. As shown in Figure 5.29, the sigmas' range is 0.86 to 1.31 which is close to 1. The constant θ line in Figure 5.30 shows an excellent linear fit of data.

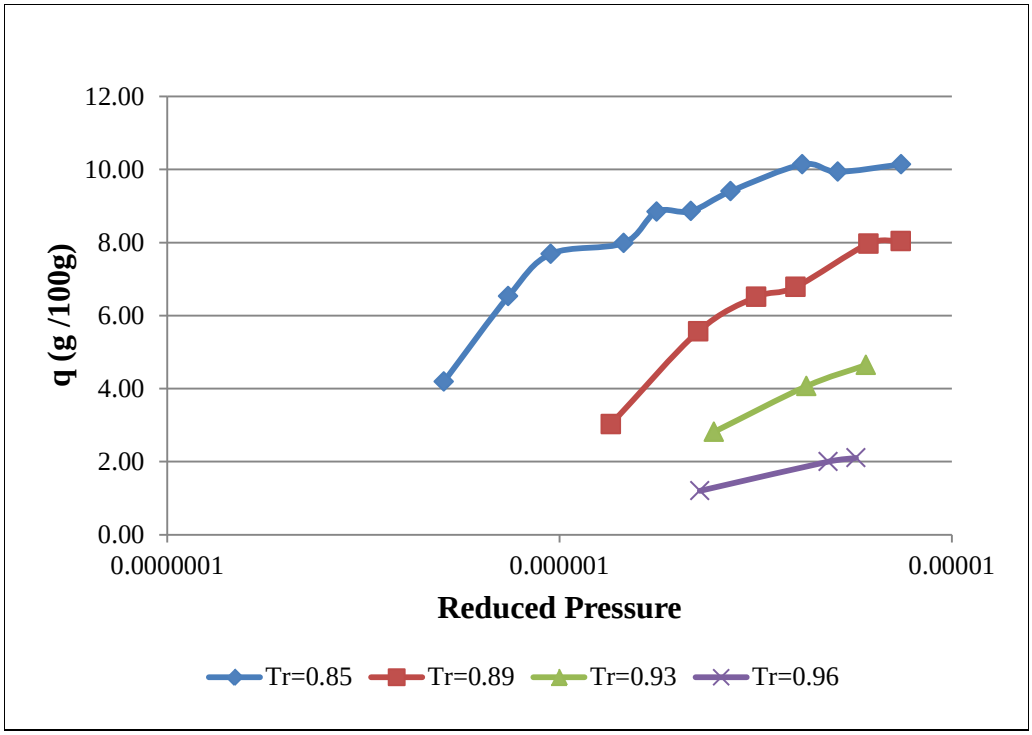

Figure 5.27: Isotherms for 1,3,5-triethylbenzene on 13X.

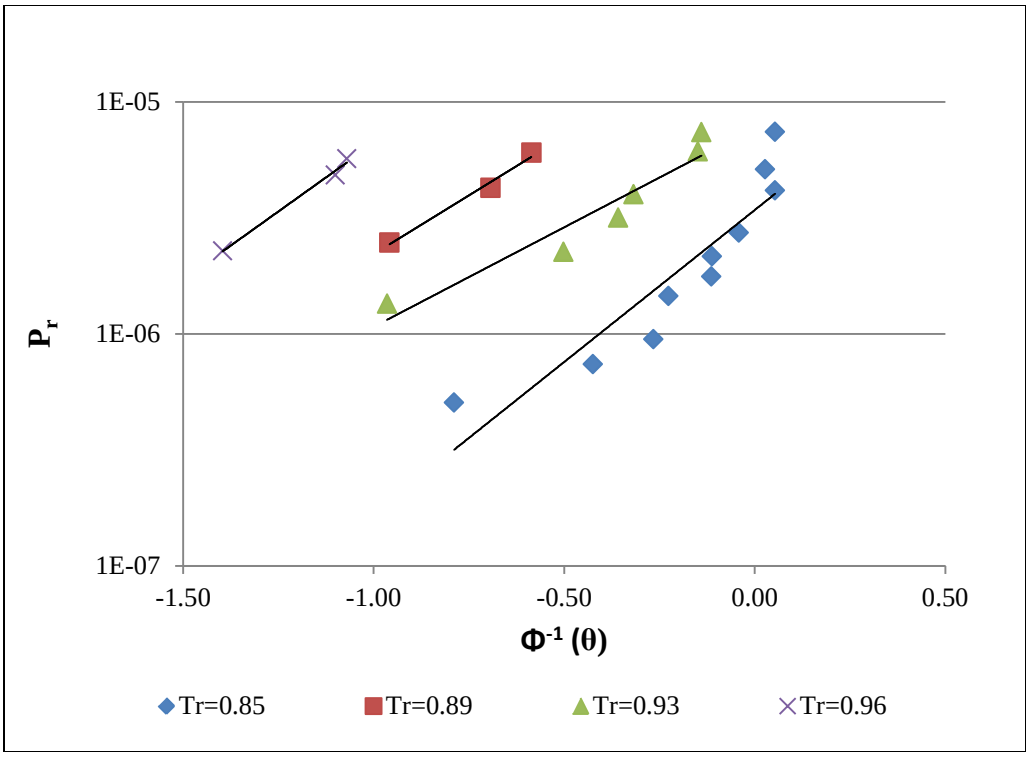

Figure 5.28: Linearized isotherms for 1,3,5-triethylbenzene on 13X.

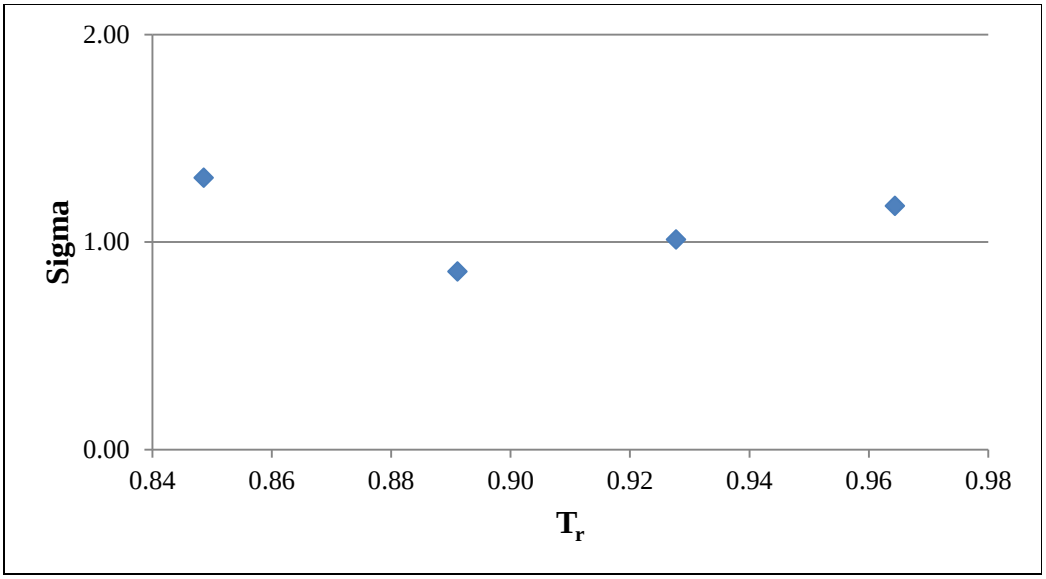

Figure 5.29: Sigma, the slope of the linearized isotherms, as a function of reduced temperature, for 1,3,5 triethylbenzene on 13X.

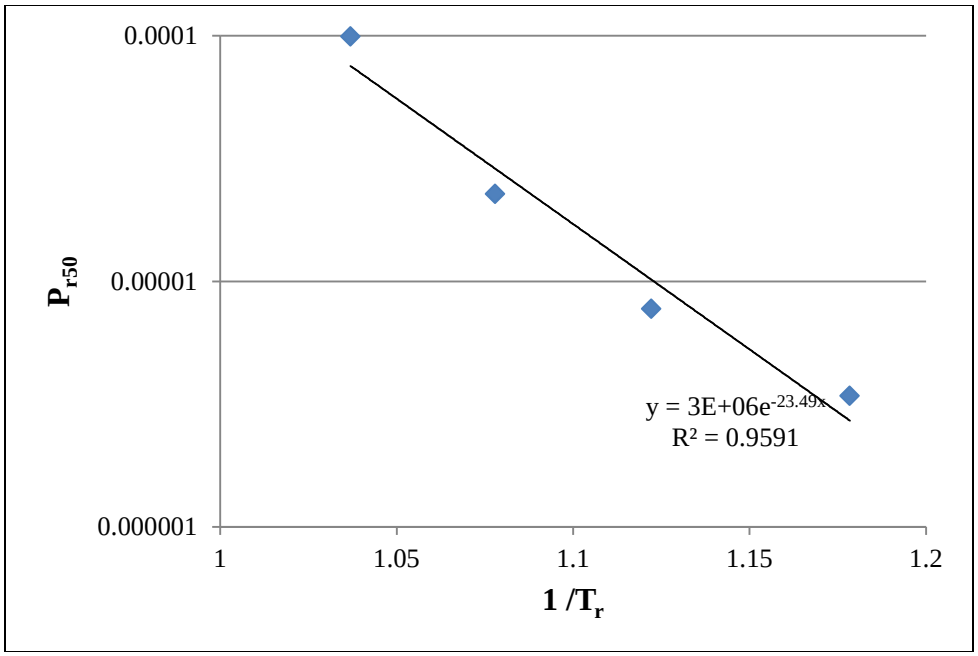

Figure 5.30: log P_{r50} vs. $1/T_r$ for1,3,5 triethylbenzene on 13X.

The heat of adsorption at 50% loading for 1,3,5-triethylbenzene is calculated from the slope of figure 5.31.

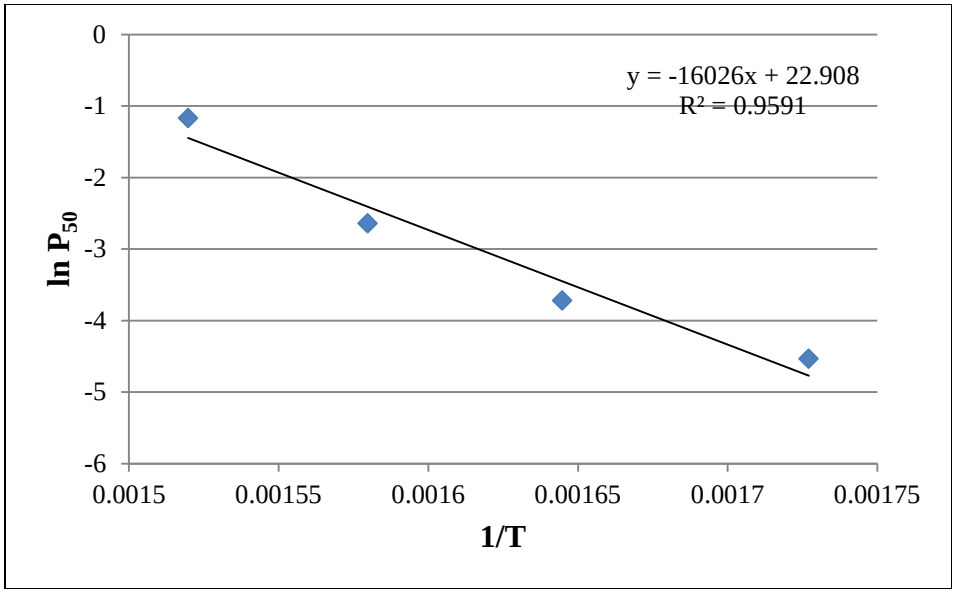

Figure 5.31: ln P_{50} vs. 1/Tfor1,3,5 triethylbenzene on 13X.

$$P_{50} = ae^{-\Delta H_{50}/RT}$$

$$-(\Delta H_{50}) = 16026 * 1.98 * 10^{-3} = 31.7\ kcal/mol. \quad 5.11$$

$$a = e^{21.0} = 8.82 * 10^{9} \quad 5.12$$

Table 5.8: Values of ($-\Delta H_{ads}$) for 1,3,5-triethybenzene.

$-\Delta H_{50}$ (kcal /mol)	$-\Delta H_{0lit.}$ (kcal /mol)	a
31.7	31 [20]	8.82E+09

The values of the heat of adsorption at 50% loading and 0% loading for 1,3,5-triethybenzene are very close to each other with the 1,3,5-triethylbenzene having the higher value. The result is unlike the previously discussed aromatics where the heat of the adsorption at 0% loading was significantly higher than at 50% loading.

5.8 Cyclohexane

Figure 5.32 represents the adsorption isotherms for cyclohexane found in a single study by Ruthven and Doetsch [15]. T_r starts at 0.81 on the left hand side of the plot to a T_r of 0.97 on the right hand side of the plot. The isotherms were all consistent in shape and behavior as they were all extracted from a single study. With the lack of another judge on the consistency, the isotherms were all retained as they are. The study was based on a 13X pure crystal sample.

Data for cyclohexane are all in the subcritical region. The linearized probability plot is shown in Figure5.33 ranging from a T_r of 0.81 to 0.97. The isotherms are perfectly linear and parallel with increasing T_r from right to left. The slopes of these isotherms, σ, are plotted as a function of reduced temperature in Figure 5.34. The values, as shown in the Figure, decrease from 0.75 to 0.6. Figure 5.35 represents the constant θ line at 50% loading of 1-hexene. The line is remarkably linear with an R value of 0.97.

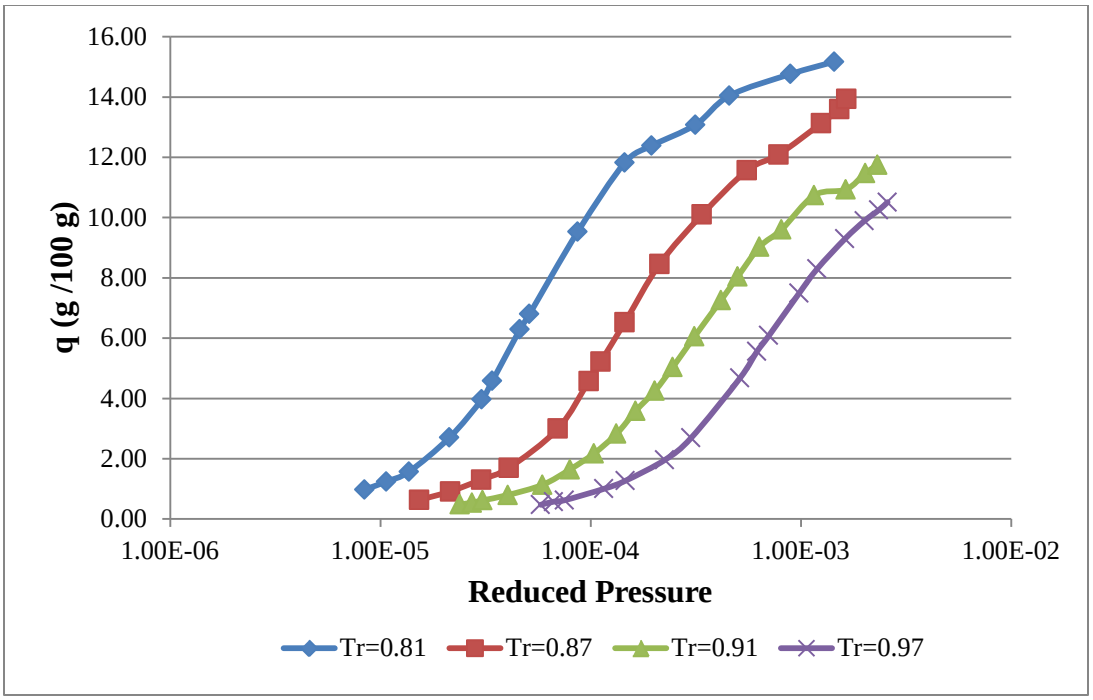

Figure 5.32: Isotherms for cyclohexane on 13X.

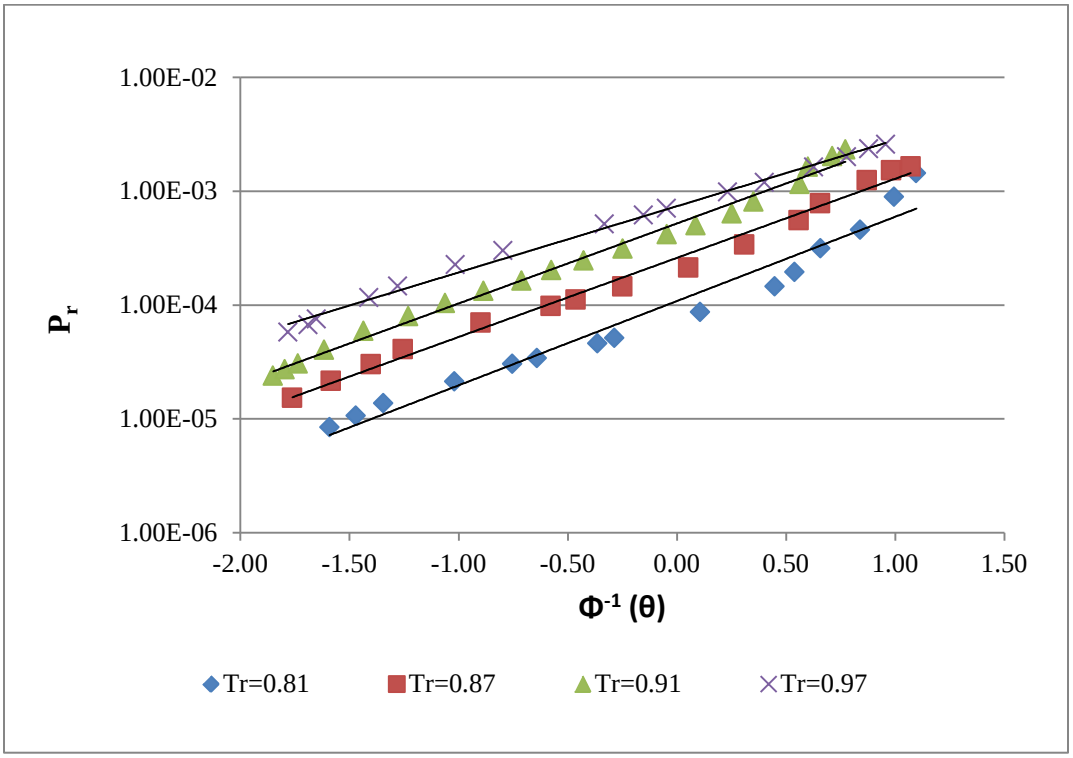

Figure 5.33: Linearized isotherms for cyclohexane on 13X.

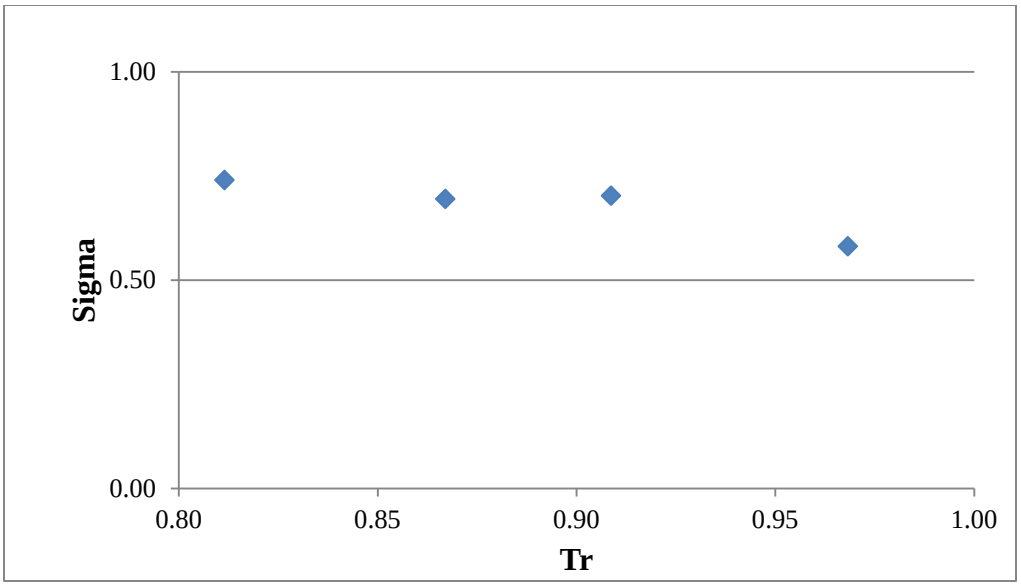

Figure 5.34: Sigma, the slope of the linearized isotherms, as a function of reduced temperature, for cyclohexane on 13X.

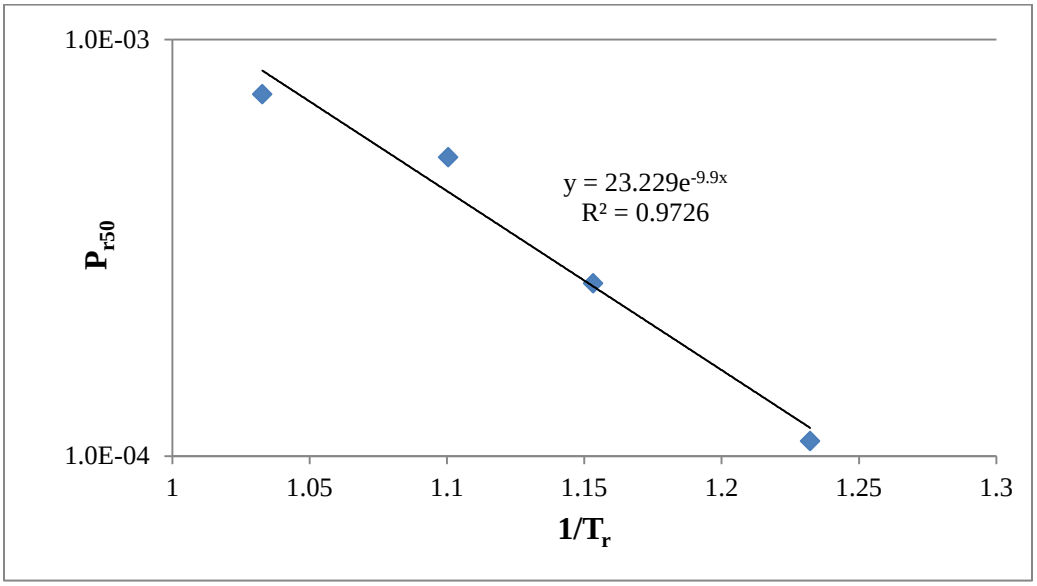

Figure 5.35: log P_{r50} vs. $1/T_r$ for cyclohexane on 13X.

The value of the heat of adsorption at 50% loading for cyclohexane is calculated from the slope of Figure 5.36 and compared to the value found in literature at 0% loading.

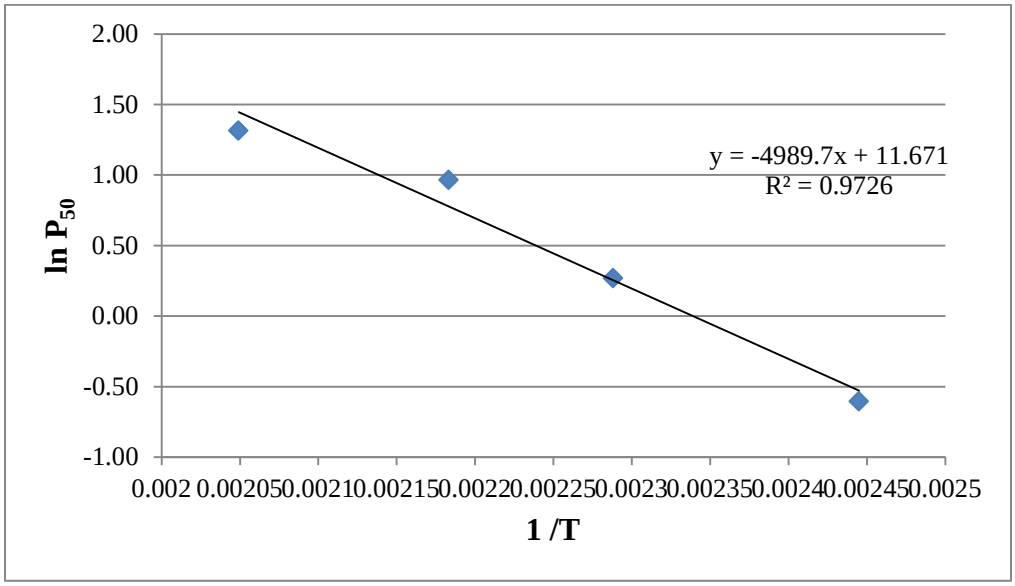

Figure 5.36: ln P_{50} vs. 1/T for cyclohexane on 13X.

$$-(\Delta H_{50}) = 4989 * 1.98 * 10^{-3} = 9.88\ kcal/mol. \quad 5.13$$

$$a = e^{11.67} = 1.17 * 10^{5} \quad 5.14$$

Table 5.9: Values of ($-\Delta H_{ads}$) for cyclohexane.

$-\Delta H_{50}$ (kcal /mol)	$-\Delta H_{0lit.}$ (kcal /mol)	a
9.88	13.40 [15]	1.17E+05

5.9 Discussion and Conclusion

The value of q_{max} for adsorption data of aromatics on 13Xwas calculated using zeolite crystallographic data and the modified Rackett equation and the Rackett equation. Different loadings at θ=50% resulted for each isotherm. Therefore, the value of $log\ P_{r50}$ is found at a constant θ.

Consistency of P_{r50} values is also affected by the need of extrapolation in some cases where the linearized isotherms do not extend to $\Phi^{-1}(\theta)$ =0. Benzene linearized isotherms in Figure 5.3 were extrapolated for Barrer et al. [13] isotherms only. Nevertheless, the values of $log\ P_{r50}$ were consistent with the other non-extrapolated values as shown in the constant θ lines in Figure 5.5. The lines are remarkably linear and show a good fit of the model. Toluene exhibits the same behavior that was encountered for heptane. Barrer et al. [13] isotherms are at low subcritical temperatures (T_r<0.6) and as shown in Figure 5.8, extrapolation was needed to get $log\ P_{r50}$ values. Figure 5.10 shows the similarity between n-heptane and toluene where the constant θ line shows the same anomaly for the low T_r values. This suggests that at such low temperatures a different trend is taking place either due to a gap in the model or due to an artifact of the data itself. The isotherms are also remarkably linear with no curvature. Mesitylene isotherms at T_r = 0.87, 0.9 and 0.94 were also extrapolated in Figure 5.13. The linearized isotherms exhibit some curvature, except at T_r = 0.87, which is reflected on the extrapolated $log\ P_{r50}$ values and ΔH_{50} values. The curvature starts at the end of T_r = 0.7, 0.9 and 0.94 but is concaved up and down for the whole isotherm at T_r = 0.63. The concavity of this isotherm might be due to an error in digitizing the isotherm data for the study or due to an artifact of the data itself. The effect of extrapolation can be seen in Figure 5.15 where the data seems to be inconsistent and scattered. Two of naphthalene $log\ P_{r50}$ values, at T_r = 0.73 and 0.84, contain a huge uncertainty especially that the extrapolation was carried on a two or three point lines that were far from zero, as in Figure 5.18. The linearity of the isotherms that contain less than three points cannot be judged but the other isotherms show a good linear fit with some minor concavity at T_r =0.7.

Three out of six isotherms were extrapolated in case of 1,2,3,5- tetramethylbenzene but the lines are linear and contained sufficient points to get good extrapolation results.

According to 1,3,5-triethylbenzene, extrapolation contained a huge uncertainty also due to insufficient data points and nonlinearity of some of the isotherms, at T_r = 0.85 and 0.93, as shown in Figure 5.28. Figure 5.33 shows the linearized isotherms for cyclohexane where no extrapolation was required for the data. The linearized isotherms are remarkably linear except at T_r = 0.81 where it exhibits some minor curvature that might result from an error in the data. Since the aromatics contained subcritical data only, the performance of the linearized isotherms could not be compared to supercritical ones, nevertheless, the behavior at subcritical temperature are similar to those of alkanes at the same temperatures.

As in the case of alkanes, sigma fits for the aromatic are related to the temperature of each isotherm. Benzene isotherms fall in two T_r regions, one at T_r (0.57-0.61) and the other at T_r (0.72-0.91). Figure 5.4 shows how each range falls under a different sigma level. As expected, the low subcritical temperatures have the higher sigma values (4 to 5) while the higher temperatures have a sigma value around 1. Toluene is very similar to benzene where there are two temperature ranges with the high sigma (3 to 6) at the lower T_r range and a sigma approximately equal to 1 at the higher T_r range, as in Figure 5.9. Mesitylene has sigma values that are all around 1 even though one isotherms is at T_r = 0.63. This is because the slope of the linearized isotherm at T_r = 0.63, shown in Figure 5.13, does not accurately represent the value of sigma due to its non-linearity. Naphthalene, in Figure 5.19, has one isotherm at T_r = 0.63 for which the sigma value is equal to 5 while the rest of the isotherms above T_r = 0.7 have a sigma value of 1. As shown in Figure 5.24, 1,2,3,5-tetramethylbenzene has sigma values of 1 for all of its isotherms at a T_r range of (0.85-0.94) and around 2 for one isotherm at a T_r = 0.81. Figure 5.29 shows the sigma fit for 1,3,5-triethylbenzene where all isotherms at the T_r range of (0.85-0.98) has a sigma value of 1, approximately. Sigma values for cyclohexane, shown in Figure 5.34, lie in the range of 0.58 to 0.75 were the isotherms have a T_r range of (0.81-0.97).

The calculated values of σ were plotted as a function of reduced temperature for all the isotherms of the aromatics discussed in this chapter (Figure 5.37). The data were all in the subcritical region concentrated in the higher T_r region (0.7-0.96) T_r. Most of the sigma values from all studies oscillate around one.

Benzene and toluene isotherms from the Barrer et al. [13] study, brown and blue squares in Figure 5.38, have sigma values close to 5. Around five, also, are the σ for benzene from Zhdanov et al. [14] and 1,3,5-triethybenzene from Ruthven and Kaul [20]. These relatively high sigma values are exhibited at isotherms of $T_r < 0.7$. Figure 3.67 shows how sigma values shifts up below $T_r = 0.7$. Sigma values for ($T_r > 0.7$) range from 0.75 to 1.Below $T_r = 0.7$ sigma starts at 2 and goes up to 8. This change in behavior at $T_r = 0.7$ suggests that the critical reduced temperature of the adsorbed phase is lower than the VLE critical reduced temperature which is equal to 1.

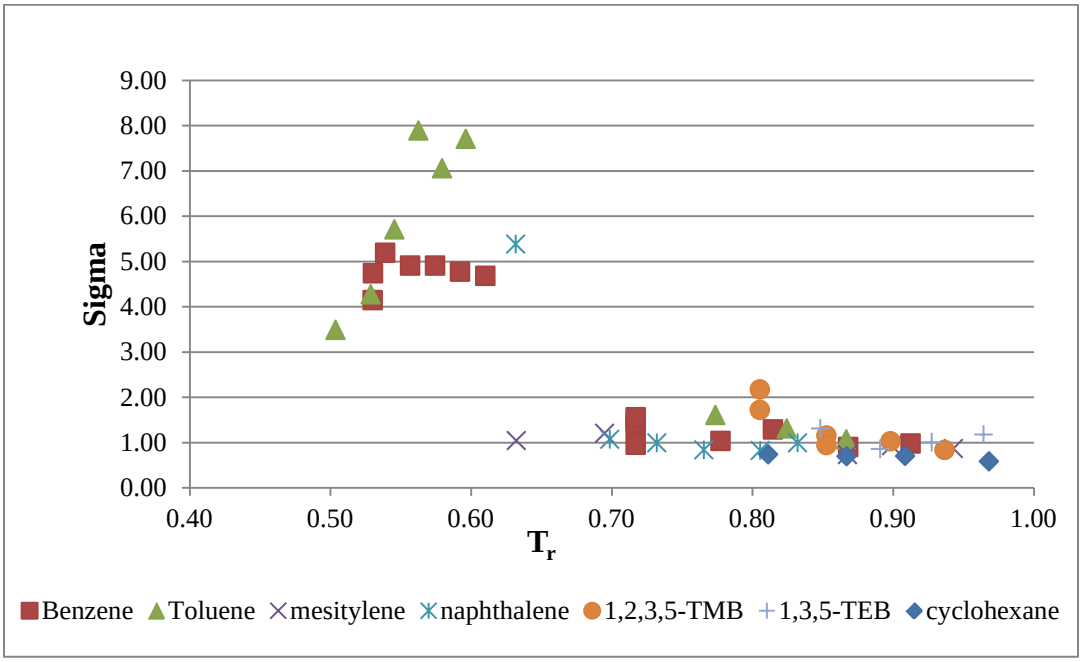

Figure 5.37: Sigma, the slope of the linearized isotherms, as a function of reduced temperature, for the chosen aromatics and cyclic compound marked according to species.

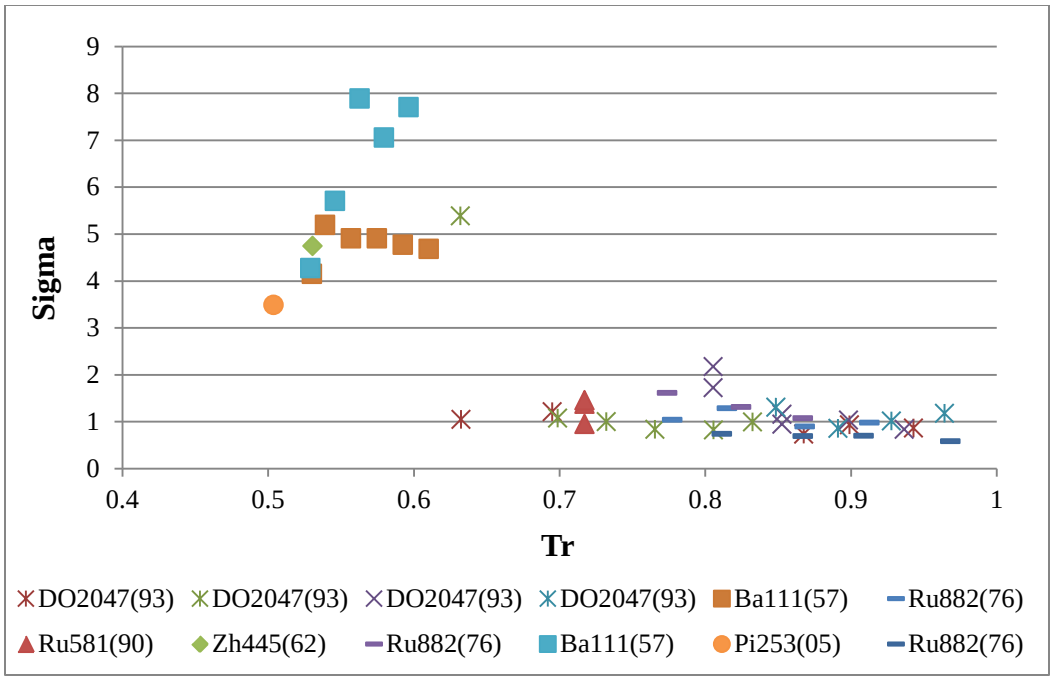

Figure 5.38: Sigma, the slope of the linearized isotherms, as a function of reduced temperature, for all chosen aromatics and cyclic compund marked according to the study.

The constant θ lines at 50% loading for all the chosen aromatics in this section are represented in Figure 5.39. All of the lines are straight and follow the same pattern except for part of the toluene isostere where it shows an anomaly. The magnitude of the slopes of these isosteres $(-\Delta H_{50}/R)$ increase from right to left as the molecular weight of the aromatic compounds increases. This is true except for mesitylene and 1,2,3,5-TMB where the values of $(-\Delta H_{50})$ are less than expected.

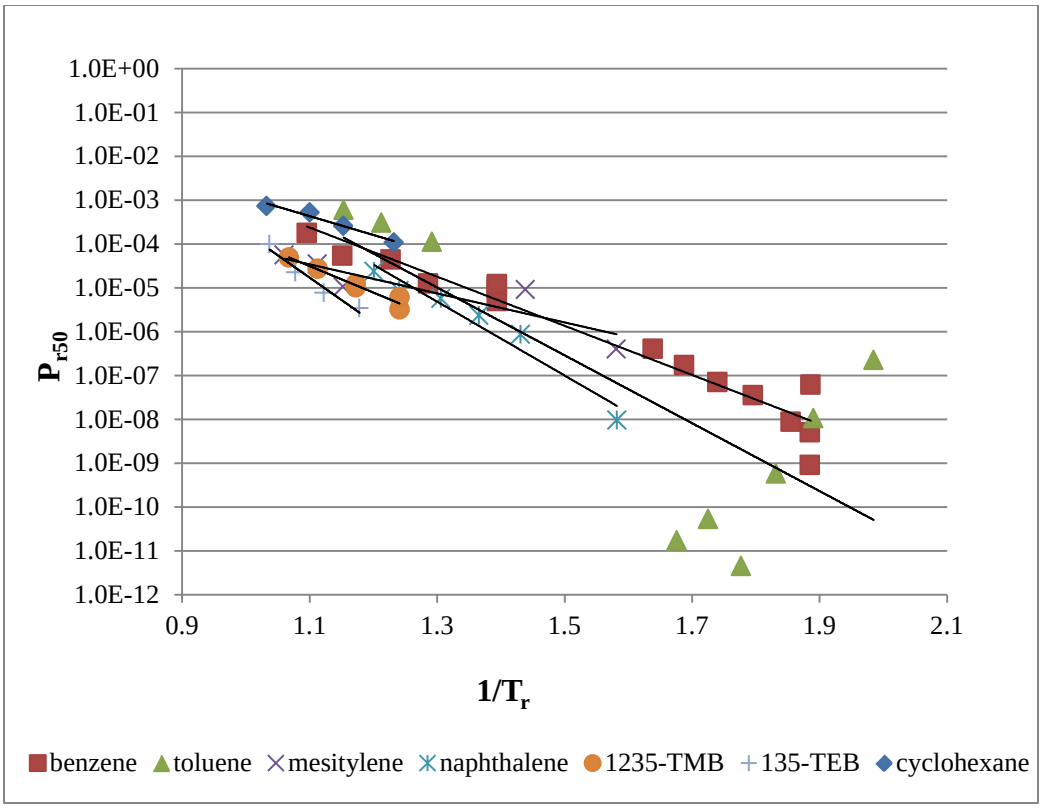

Figure 5.39: log P_{r50} vs. $1/T_r$ for all the chosen aromatics and cyclic compound.

Table 5.10 summarizes the ($-\Delta H_{ads}$) values at both 50% and 0% loadings. It can be established that the heat of adsorption at 50% loading is less than the heat of adsorption at 0% loading which indicates that the heat of adsorption decreases when the loading increases. Naphthalene is the only compound that has ($-\Delta H_{50}$) value that is higher than literature value. Going back to Figure 5.20, there is one point in the constant θ line that is affecting the slope. This point is for the isotherm at T_r =0.63 which has a sigma value of 5. As was discussed in alkanes, the value of sigma and ($-\Delta H_{50}$) value are related and the results for isotherms that do not have a sigma value of 1 seem to be different. Excluding this isotherm from the regression in Figure 5.20 will result in a ($-\Delta H_{50}$) value of 20 kcal /mol as compared to 28.8 kcal /mol. Naphthalene will, as a result, follow the trend of the other aromatics and have a value at 50% loading that is less than at 0% loading. The value of ($-\Delta H_{50}$) for 1,3,5-triethylbenzene in Table 5.10 might not reflect an accurate value. As discussed earlier the log P_{r50} values were extrapolated from the linearized isotherms that were also nonlinear for some isotherms, refer to Figure 5.28. This explains why the value would be slightly higher rather than less than the literature value.

Mesitylene has a slightly low *($-\Delta H_{50}$)* value compared to the one found in literature. Excluding the isotherm at T_r =0.63 from the regressed line in Figure 5.15 will result in a value of 22 kcal /mol which is remarkably better than the previous value of 9 kcal/mol. Doing the same for benzene (excluding isotherms with T_r< 0.7) raises the value of *($-\Delta H_{50}$)* to 16.1 kcal/mol. The low *($-\Delta H_{50}$)* value of 1,2,3,5-tetramethylbenzene can be justified by the fact that only four points are available in the regression as shown in Figure 5.26.

Table 5.10: Values of ($-\Delta H_{ads}$) for the chosen aromatics and cyclic compound.

	$-\Delta H_{50}$ (kcal /mol)	$-\Delta H_{0lit.}$ (kcal /mol)	a
benzene	13.13	18.5 [20]	3.14E+05
toluene	14.30	21.0 [20]	3.20E+06
mesitylene	9.60	23.3 [20]	4.70E+02
Naphthalene	28.8	25.5 [20]	1.32E+09
1,2,3,5-tetramethylbenzene	18.70	27.0 [20]	4.35E+05
1,3,5-triethylbenzene	31.70	31.0 [20]	8.82E+09
cyclohexane	9.88	13.40 [15]	1.17E+05

CHAPTER 6: Conclusion

Subcritical and supercritical adsorption data of chosen alkanes, alkenes and aromatics on 13X zeolite have been satisfactory modeled using the Gaussian adsorption isotherms. The parameters of the model are q_{max}, P_{50} and σ. q_{max} is the maximum saturation loading calculated zeolite crystallographic data and the Rackett equation for subcritical data and taken as a constant pre-defined value of 12 g/100g Z for supercritical data. P_{50} is the value of pressure at 50% of the maximum loading, q_{max}. σ is the standard deviation for the entire isotherm and was found to be:

- Alkanes: in the range of (0.5 to 1) for $T_r > 0.85$ and in the range (2 to 13) for $Tr < 0.85$.
- Alkenes: approximately 1 for a T_r range of (0.8-0.95).
- Aromatics: in the range of (0.75 to 1) for $T_r > 0.7$ and in the range (2 to 8) for $Tr < 0.75$.

The sigma values were combined for each group of hydrocarbons in a single plot against the reduced temperature and were found to follow a consistent pattern.

The adsorption data conformed to the linear relationship of the Gaussian adsorption isotherm model for the supercritical regions, in particular. Pr_{50} lines, analogous to isosteres, were plotted at a constant θ of 50 % and were found to be linear and consistent with slopes indicating the value of $(-\Delta H_{50})/R$. Some inconsistency resulted in the values of $logPr_{50}$ due to need for extrapolations of the linearized isotherm. P_{r50} lines were combined for each hydrocarbon group showing a consistent pattern and an increasing slope from lower to higher weight hydrocarbons. All $(-\Delta H_{50})$ values are summarized in Table 6.1.

Heats of adsorption at a constant θ of 50 % were calculated and found to be consistent with literature values for isotherms with a sigma value of 1. Isotherms with higher sigma values did not predict a good value of $(-\Delta H_{50})$. The fact that the heat of adsorption at 50 % loading is found to be less than at 0 % loading for most species indicates that the assumption that there is no interaction between molecules adsorbed on adjacent sites is not a valid one.

The results indicate that the heat of adsorption decreases at higher loadings. Both methane and ethane have values of the heat of adsorption that are around or below 5 kcal/mole indicating that both species are physisorbed not chemisorbed. Moreover, neglecting the effect of the square root in the isostere relation contributes to the inconsistency of $(-\Delta H_{50})$ results that are encountered in reduced temperatures below 0.6.

Table 6.1 also shows the highest sigma values encountered in isotherms of $T_r < 0.6$ for each species. This value increases with increasing carbon number for both alkanes and alkenes. The highest sigma is for n-octane and iso-octane and the lowest is for methane and ethane. It follows that as the carbon number increases, values of sigma for isotherms with $T_r < 0.6$ increase remarkably from a value of 1 in methane to a value of 13 in iso-octane. Similarly, the value of the highest sigma for isotherms with $T_r < 0.6$ for ethylene is equal to 1 which is lower than that of propylene and 1-butene which is equal to 4. Group contribution is of important significance in this analysis. As the number of CH_2 groups increases, isotherms with low subcritical temperatures have higher sigma values and hence the heat of adsorption at 50% loading becomes larger.

Figure 6.1 shows how all isotherms can be overlaid onto a single line, by normalizing the lines, according to equation 6.1.

$$log\left(\frac{P}{P_{50}}\right)^{1/\sigma} = \Phi^{-1}(\theta) \qquad 6.1$$

Values of P_{50} and σ are fitted to each isotherm separately. Data is also plotted on a characteristic curve by plotting θ vs. the normalized pressure term, $(P/P_{50})^{1/\sigma}$, giving it the familiar S-shaped curve of both the cumulative distribution. Both Figures indicate the data are very well described by the model, hence proving its validity.

In conclusion, the model fits the supercritical data remarkably for all species in the alkanes and aromatics. Nevertheless, the results clearly suggest that there is a gap in the model when it comes to subcritical regions especially for reduced temperatures below 0.7. The change in behavior for the data at around $T_r = 0.7$, particularly for aromatics, is of great significance especially that the acentric factor is calculated at that temperature. Adding such factor to the model at subcritical temperatures may result in a better fit for the data in this region. Moreover, the possibility of a phase change at such low subcritical temperatures might account for the deviations of the data.

Even though the freezing point of the selected hydrocarbons are below the isotherm temperatures considered in this study, it is possible that there is solid phase formed at temperatures as low as Tr = 0.5 because of the fact it is an adsorbed phase. Therefore it is recommended that more research is done around the subcritical region on the data itself as well as the model.

Table 6.1: Values of ($-\Delta H_{ads}$) and σ.

	$-\Delta H_{50}$ (kcal /mol)	$-\Delta H_{0lit.}$ (kcal /mol)	σ for T_r<0.6
methane	2.63	5.12 [18]	1.25
ethane	5.43	5.97 [17]	1.20
propane	8.21	7.80 [18]	1.80
iso-butane	10.76	9.40 [17]	3.00
neo-pentane	13.40	13.30 [12]	6.40
heptane	13.53	15.20 [15]	6.00
n-octane	20.28	21.00 [12]	12.00
n-butane	35.24	14.50 [12]	4.00
n-pentane	23.45	17.20 [12]	5.00
iso-pentane	66.80	17.20 [12]	7.70
hexane	41.55	20.70 [12]	6.00
iso-octane	64.00	21.30 [12]	13.00
ethylene	9.02	9.10 [17]	1.00
propylene	10.87	10.13 [25]	4.00
1-butene	9.40	13.00 [26]	4.1
benzene	13.13	18.5 [20]	5.00
toluene	14.30	21.0 [20]	8.00
mesitylene	22.00	23.3 [20]	1.00
naphthalene	20.00	25.5 [20]	5.00
1,2,3,5-tetramethylbenzene	18.70	27.0 [20]	2.17
1,3,5-triethylbenzene	31.70	31.0 [20]	1.31
cyclohexane	9.88	13.40 [15]	0.74

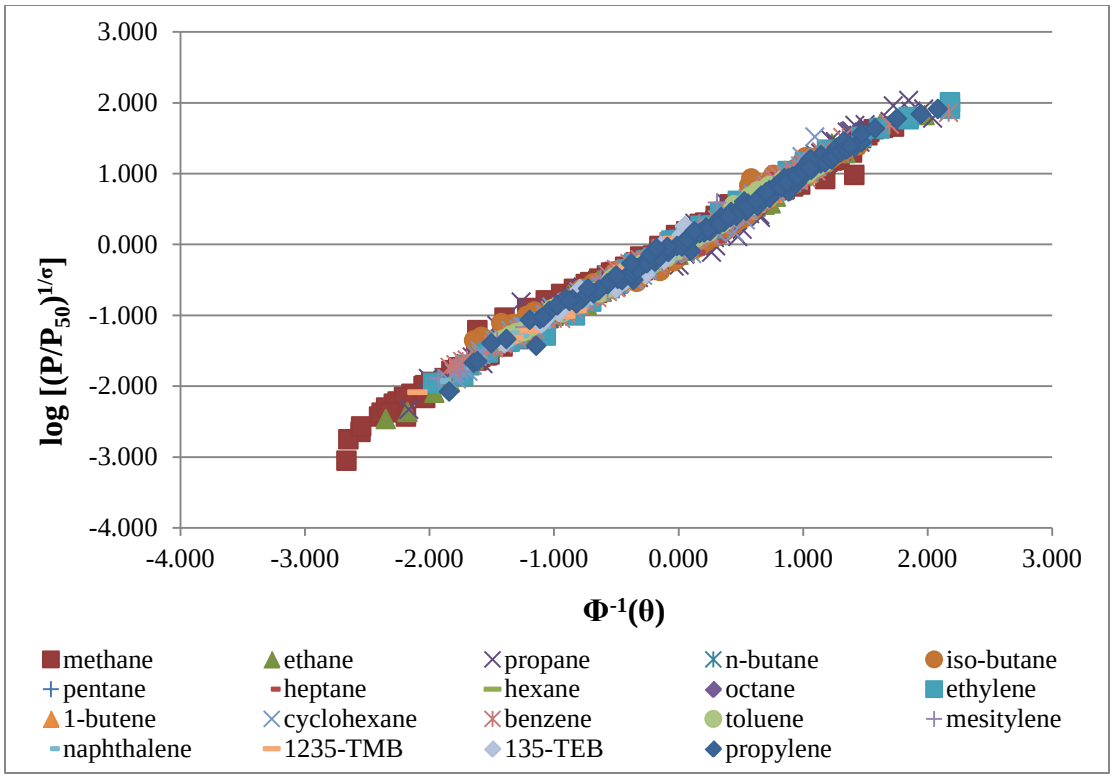

Figure 6.1: Data from 199 hydrocarbon isotherms, overlaid on a single normalized linear graph.

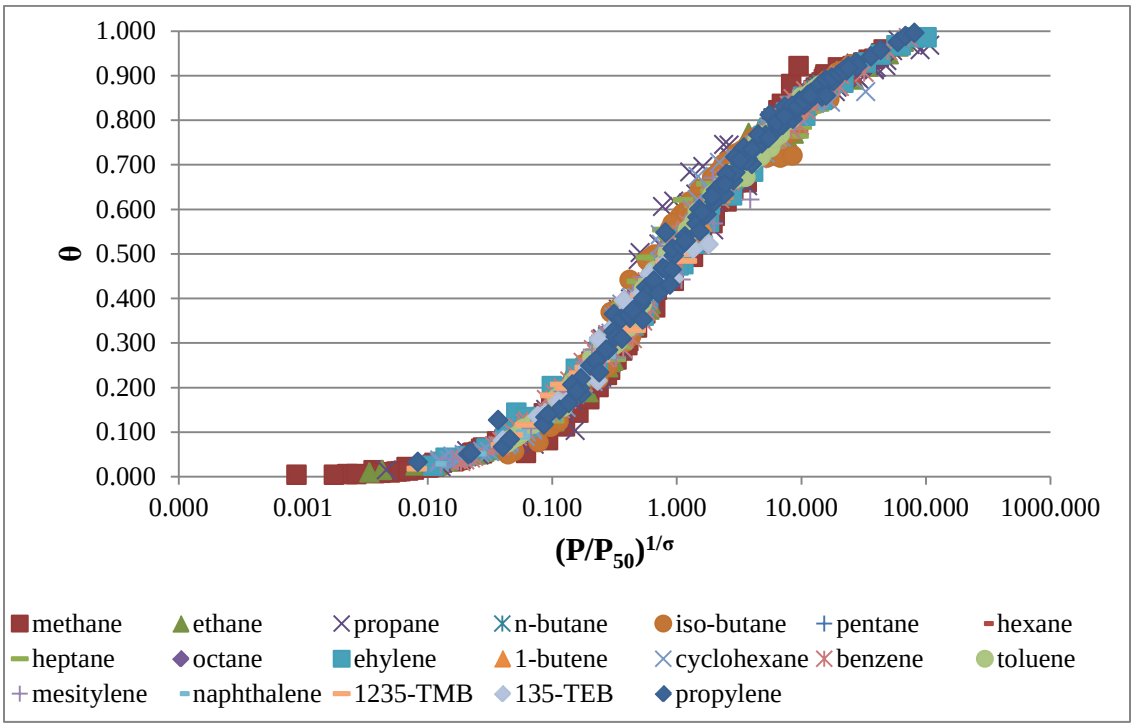

Figure 6.2: Data from 199 hydrocarbon isotherms, overlaid on a single normalized isotherm graph.

REFERENCES

[1] S. Brunauer, The Adsorption of Gases and Vapors:Vol I, London: Princeton University Press, 1943.

[2] C. G. Hill, An Introduction to Chemical Engineering Kinetics and Reactor Design, New York: John Wiley & Sons, 1977.

[3] D. M. Ruthven, "Fundeamentals of adsorption equilibrium and kinetics in microporous solids," *Molecular Sieves,* vol. 7, pp. 1-43, 2008.

[4] S. Brunauer, l. Deming, W. Deming and E. Teller, "Theory of The van Der Waals Adsorption of Gases," *Journal of the American Chemical Society,* vol. 62, pp. 1723-1732, 1940.

[5] D. D. Duong, Adsorption analysis: equilibria and kinetics, London: Imperial College Press, 1998.

[6] B. Crittenden and W. J. Thomas, Adsorption Technology and Design, Elsevier Science & Technology, 1998.

[7] D. M. Ruthven, Principles of adsorption and adsorption processes, New York: John Wiley and sons, Inc., 1984.

[8] G. E. Keller II, R. A. Anderson and C. M. Yon, Handbook pf separation process technology, New York: Wiley-Interscience, 1987.

[9] S. Raseev, Thermal and catalytic processes in petroleum refining, New York: Marcel Dekker, Inc., 2003.

[10] R. Sadeghbeigi, Fluid catalytic cracking handbook, Houston, TX.: Gulf Professional Publishing, 2000.

[11] J. U. Keller and R. Staudt, Gas Adsorption Equilibria: Experimental Methods and Adsorption Isotherms, Boston: Springer Science Inc., 2005.

[12] R. M. Barrer and J. W. Sutherland, "Inclusion complexes of faujasite with paraffins and permanent gases," *Proceedings of The Royal Society A: Mathematical, Physical and Engineering Sciences* , vol. 237, pp. 439-463, 1956.

[13] R. M. Barrer, F. W. Bultitude and J. W. Sutherland, "Structure of faujasite and properties of its inclusion complexeswith hydrocarbons," *Transactions of the Faraday Society,* vol. 53, pp. 1111-1123, 1957.

[14] S. P. Zhdanov, A. V. Kiselev and l. F. Pavlova, "Adsorption of benzene and n-hexane and their liquid solutions by 10X and 13X zeolites," *Kinetika I Kataliz,* vol. 3, no. 3, pp. 445-448, 1962.

[15] D. Ruthven and I. H. Doetsch, "Diffusion of hydrocarbons in 13X zeolites," *The American Institute of Chemical Engineers,* vol. 22, no. 5, pp. 882-886, 1976.

[16] P. D. Rolniak and R. Kobayashi, "Adsorption of methane and several mixtures of ethane and carbon dioxide at elevated pressure near ambient temperatures on 5A and 13X molecular sieves by tracer perturbation chromatography," *The American Institute for Chemical Engineers,* vol. 26, no. 4, pp. 616-623, 1980.

[17] S. H. Hyun and R. P. Danner, "Equilibrium adsorption of ethane, ethylene, isobutane, carbon dioxide, and their binary mixtures on 13X molecular sieves," *Journal of Chemical Engineering Data,* vol. 27, pp. 196-200, 1982.

[18] K. F. Loughlin, H. AbdulRehman and M. A. Hasanain, "Quaternary, ternary, binary and pure component sorption on zeolites. 2. Light alkanes on Linde 5A and 13X zeolites at moderate to high pressures," *Industrial and Engineering Chemistry Research,* vol. 29, pp. 1535-1546, 1990.

[19] D. M. Ruthven and O. H. Tezel, "Sorption of benzene in NaX zeolite: an unusual hysteresis effect," *Journal of Colloid and Interface Science,* vol. 139, no. 2, pp. 581-583, 1990.

[20] D. M. Ruthven and B. K. Kaul, "Adsorption of aromatic hydrocarbons in NaX zeolites. 1.Equilibrium," *Industrial & Engineering Chemistry Research,* vol. 37, pp. 2047-2052, 1993.

[21] M. K. Salem, V. M. Szombathely, B. Braeuer, M. Heuchel, P. Harting and K. Quitzsch, "Thermodynamic of high pressure adsorption of argon, nitrogen and methane on microporous adsorbents," *Langmuir,* vol. 14, pp. 3376-3389, 1998.

[22] F. A. Da Silva and A. E. Rodrigues, "Adsorption equilibria and kinetics for propylene and propane over 13X and 4A zeolite pellets," *Industrial & Engineering Chemistry Research,* vol. 38, pp. 2051-2057, 1999.

[23] C. M. Wang, K. S. Chang and T. W. Chung, "Adsorption equilibria of aromatic compounds on activated carbon, silica gel, and 13X zeolite," *Journal of Chemical & Engineering Data,* vol. 49, pp. 527-531, 2004.

[24] M. L. Pinto, J. Pires, A. P. Carvalho, M. B. de Carvalho and J. C. Bordado, "Characterization of adsorbent materials supported on polyurethane foams by nitrogen and toluene adsorption," *Microporous and Mesoporous Materials,* vol. 80, pp. 253-262, 2005.

[25] N. Lamia, L. Wulff, P. Leflaive, P. Sa' Gomes, C. A. Grande and A. E. Rodrigues, "Propane/ propylene separation by simulated moving bed I. Adsorption of propane, propylene and isobutane in pellets of 13X zeolite," *Separation Science and Technology,* vol. 42, pp. 2539-2566, 2007.

[26] N. Lamia, L. Wulff, P. Leflaive, D. Leinekugel-Le-Cocq, P. Sa' Gomes, C. A. Grande and A. E. Rodrigues, "Equilibrium and fixed bed adsorption of 1-butene, propylene and propane over 13X zeolite pellets," *Separation Science and Technology,* vol. 43, pp. 1142-1156, 2008.

[27] D. Abouelnasr and K. F. Loughlin, "A new Gaussian adsorption model: test data is methane-5A zeolite," *Adsorption,* vol. 16, pp. 93-101, 2010.

[28] T. Nitta, T. Shigetomi, M. Kuro-Oka and T. Katayama, "An adsorption isotherm of muultisite occupancy model for homogenous surface," *Journal of Chemical Engineering of Japan,* vol. 17, pp. 39-45, 1984.

[29] S. Suwanyuen and R. P. Danner, "A gas adsorption isotherm equation based on vacancy solution theory," *The American Institute of Chemical Engineers Journal,* vol. 26, pp. 68-76, 1980.

[30] H. F. Stroud, E. Richards, P. Limchareon and N. G. Parsonage, "Thermodynamic Study of the Linde 5A+ methane system," *Journal of the Chemical Society, Faraday Transactions,* vol. 172, no. 4, pp. 942-954, 1976.

[31] R. E. Walpole, R. H. Myers, S. L. Myers and K. Ye, Probability and statistics for engineers and scientists, Englewood Cliffs: Prentice-Hall, 2002.

[32] J. H. De Boer, The dynamic character of adsorption, London: Oxford University Press, 1968.

[33] K. F. Loughlin, Sorption in 5A zeolite. Ph.D. Dissertation, Fredericton, NB: University of New Brunswick, 1970.

[34] L. Mentasty, R. J. Faccio and G. Zgarblich, "High-pressure methane adsorption in 5A zeolite and the nature of gas-solid interactions," *Adsorption Science and Technology,* vol. 8, no. 2, pp. 105-113, 1991.

[35] J. L. Zeuch, A. L. Hynes and E. D. Sloan, "Methane adsorption on 5A molecular sieve in the pressure range 4 to 690 kPa," *Industrial & Engineering Chemistry Process Design and Development,* vol. 22, no. 1, pp. 172-174, 1983.

[36] K. F. Loughlin and D. Abouelnasr, "Sorbate densities on 5A zeolite above and below the critical conditions: n alkane data evaluation and modeling," *Adsorption,* vol. 15, pp. 521-533, 2009.

[37] C. T. Spencer and R. P. Danner, "Improved equation for prediction of saturated liquid density," *Journal of Chemical & Engineering Data,* vol. 17, no. 2, pp. 236-240, 1972.

[38] K. F. Loughlin and D. Abouelnasr, "Development of predictive criteria for supercritical n alkane adsorption data on 5A zeolite using the Gaussian adsorption isotherm model," *Adsorption,* vol. 151, pp. 368-379, 2012.

[39] S. Cavenati, C. A. Grande and A. E. Rodrigues, "Adsorption equilibrium of methane, carbon dioxide, and nitrogen," *Journal of Chemical Engineering Data,* vol. 49, pp. 1095-1101, 2004.

[40] M. A. Granato, T. J. Vlugt and A. E. Rodrigues, "Molecular simulation of propane-propylene binary adsorption equilibrium in zeolite 13X," *Industrial & Engineering Chemistry Research,* vol. 46, pp. 7239-7245, 2007.

[41] J. Vermesse, D. Vidal and D. Malbrunot, "Gas adsorption on zeolites at high pressure," *Langmuir,* vol. 12, pp. 4190-4196, 1996.

[42] R. H. Perry and D. W. Green, Perry's Chemical Engineers' Handbook (7th edition), New York: McGraw-Hill, 1999.

VITA

Salam Mazen Taji was born on April 4, 1987, in Damascus, Syria. She was educated in private schools in Dubai. She graduated from high school with an average of 98.3 % in 2004. She received her degree with cum laude in Chemical Engineering from the American university of Sharjah in Spring 2007. She was awarded full scholarship from the American University in 2010 to continue her studies in Chemical Engineering.